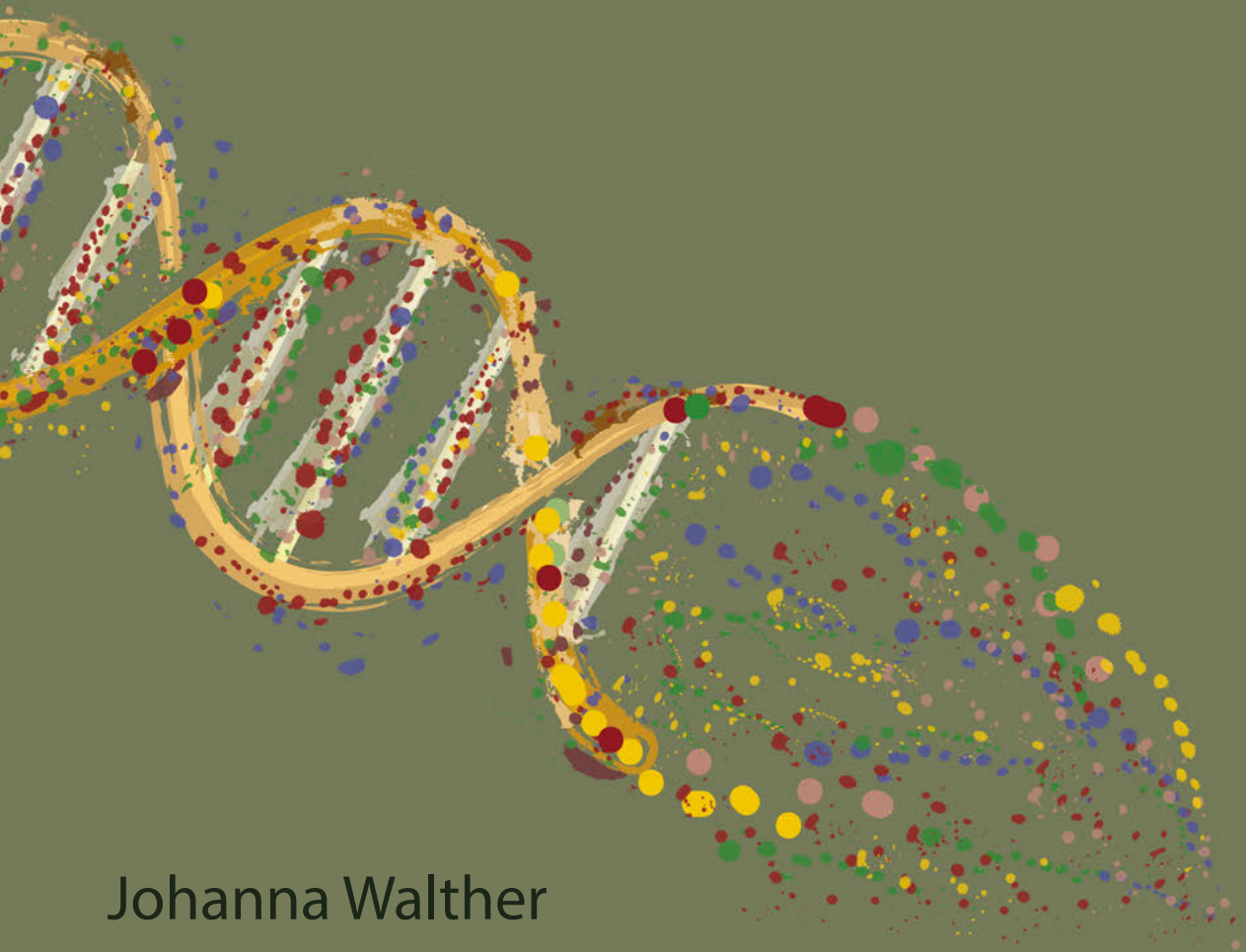# Lipid Nanoparticle-Mediated Delivery of CRISPR-Cas9 for Therapeutic Gene Correction

Johanna Walther

Doctoral thesis

LIPID NANOPARTICLE-MEDIATED DELIVERY OF CRISPR-CAS9 FOR THERAPEUTIC GENE CORRECTION

Johanna Walther

2023

LIPID NANOPARTICLE-MEDIATED DELIVERY OF CRISPR-CAS9 FOR THERAPEUTIC GENE CORRECTION

Afgifte van CRISPR-Cas9 door Lipide Nanodeeltjes voor Therapeutische Gencorrectie
(met een samenvatting in het Nederlands)

Proefschrift

Ter verkrijging van de graad van doctor aan de
Universiteit Utrecht
op gezag van de
rector magnificus, prof. dr. H.R.B.M. Kummeling
ingevolge het besluit van het college voor promoties
in het openbaar te verdedigen op
maandag 4 december 2023 des ochtends te 10.15 uur

door

Johanna Walther

geboren op 8 oktober 1993
te Heidelberg, Duitsland

Promotor
 Prof. Dr. E. Mastrobattista

Copromotor
 Dr. P.J. Bosma

Assessment Committee
 Dr. S.A. Fuchs
 Prof. dr. N. Geijsen
 Prof. dr. O. Merkel
 Prof. dr. R.M. Schiffelers
 Prof. dr. ir. T. Vermonden

Contents

1
General Introduction

There are over 6000 diseases known in human that are caused by mutations in a single gene.[1] The recent advances in molecular biology did not only help gain more knowledge about these diseases, but also led to the development of novel approaches for possible remedies and even cures, by directly targeting the detrimental aberration at the gene level.

The discovery that genes can be modified in their chemical structure, expression levels, or silenced completely laid the ground for the medical field called gene therapy.[2] Within gene therapy, particularly high potential lies in gene editing, such as insertion, deletion, or correction of specific sequences within a gene of interest. The field of gene therapy was revolutionized by discoveries made by Jennifer Doudna and Emmanuelle Charpentier in the early 2010s who demonstrated it was possible to reprogram the bacterial defense mechanism CRISPR-Cas9 into a genome editing tool,[3] which won them the Nobel Prize in Chemistry in 2020. The tens of thousands of scientific publications on this system that since appeared and the rush to commercially capitalize on this technology clearly indicate the great potential of CRISPR-Cas9. The genetic scissors, how the CRISPR-Cas9 system is also being referred to, can precisely edit an organism's DNA and be easily adapted to target seemingly unlimited sequences of the DNA. Therefore, CRISPR-Cas9 has ever since been investigated as a genome editing tool not only in medicine and biotechnology, but also in agriculture.[4–6] Undoubtedly, however, one of the main drivers for scientists to use the gene editing tool is the potential for application in gene therapy. This has now even led to first applications by the companies Vertex and CRISPR Therapeutics for approval by the Food and Drug Administration (FDA) for *ex vivo* cell therapy with CRISPR-Cas9 for sickle cell disease and beta-thalassemia.[7] First clinical studies for usage of CRISPR-Cas9 *in vivo* by the company Intellia Therapeutics show promising results. Introduction of the gene-editing agent NTLA-2001 resulted in 87% gene knock-out of the misfolded protein transthyretin (TTR), implied the cause transthyretin amyloidosis, after a single dose of the therapeutic in patients with the

disease.[8]

The Genome Editing Tool CRISPR-Cas9

Clustered Regularly Interspaced Palindromic Repeats (CRISPR) associated Cas protein is a bacterial RNA-dependent endonuclease discovered for the first time in *E.coli* in 1987.[9] In 2007 scientists discovered that the RNA-dependent endonuclease serves as a bacterial defense mechanism against bacteriophages.[10] By now CRISPR-Cas systems have been divided into two classes based on their compositions, especially of their interference modules, depicted in Fig. 1. Generally, CRISPR loci consist of repeated identical sequences that are interspaced with variable sequences called spacers. These are typically adjacent to Cas genes. In class II systems, Cas genes encode one endonuclease, the Cas protein, with several functional domains including nuclease, helicase, and polymerase domains. The spacers encode CRISPR RNA (crRNA) and originate from foreign DNA of plasmids and phages.[3] Cas proteins of class II require another RNA called transactivating RNA, tracrRNA for functionality. tracrRNA mediates the association between the crRNA and the protein.[11,12] The translated crRNA complexed to the endonuclease via tracrRNA (as a complex called ribonucleoprotein) navigates the complex to the foreign DNA based on Watson-Crick base pairing. After association, the Cas protein cleaves the targeted DNA, leading to the degradation of the foreign DNA. The exact site of cleavage is, however, also determined by a 2-6 base pair sequence located immediately after the DNA sequence complementary to the crRNA. This sequence is called protospacer adjacent motif, PAM.[13,14] Different Cas proteins of class II have varying PAM sequences.[15]
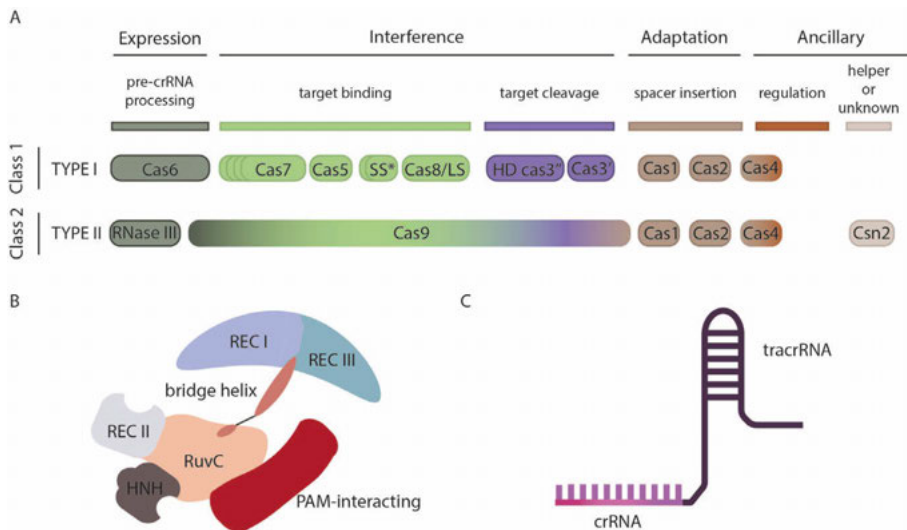
Figure 1: **Architecture of Cas protein and single guide RNA. A)** Exemplary protein architecture of a protein class 1 type I and a protein class 2 type II. An asterisk denotes that the presumed small subunit (SS) protein is fused to Cas8/LS instead. The color gradient in Cas4 and Cas9 indicate that these proteins are involved in the different stages of the CRISPR-Cas response, represented by the same colors of the gradient. Protein names follow the current nomenclature and classification.[16] Scheme adapted from the original work published by Makarova et al.[16] **B)** Protein domains and structure of Cas9 (class II, type II Cas protein). REC I, REC III – involved in association with guide RNA and formation of ribonucleoprotein complex, REC II – not fully clarified yet, bridge helix – binding target DNA and modulates cleavage activity, PAM-interacting domain – recognition of the PAM sequence at the target DNA, HNH and RuvC – cleavage of the complementary DNA strand and non-complementary DNA strand, respectively.[17] Adapted from work published by Cavanagh & Garrity.[18] **C)** Structure of synthetic guide RNA combining both tracrRNA (complexation of guide RNA with Cas9 protein) and crRNA (navigates Cas9 ribonucleoprotein complex via Watson-brick base pairing to target DNA).

Class II CRISPR-systems are subdivided into type II, V, and VI.[16] An example of a type II Cas protein is the Cas9 protein originating from *Streptococcus pyogenes*, called SpCas9. SpCas9 is a commonly used CRISPR-Cas9 system, as it has been extensively studied and optimized, making it highly efficient.   Moreover, SpCas9 has a PAM sequence (5'-NGG-3') commonly found in genomes, therefore compatible with a wide range of organisms.[19] Two to three base pairs upstream of the PAM sequence, SpCas9 generates a blunt-ended double-strand break via the two nuclease domains of the monomer.[20,21] These nuclease domains are HNH and RuvC, which cleave the complementary DNA strand and non-complementary DNA strand, respectively.[20,21] Due to the mechanism of CRISPR-Cas9 and the additional discovery by Jinek et al to generate a synthetic single guide RNA (sgRNA),[22] combining the tracrRNA and crRNA into one RNA, CRISPR-Cas9 has become the promising gene editing tool that it is. Specifically, being able to easily modify the sequence of the sgRNA, and hence determining the targeted DNA, makes CRISPR-Cas9 highly versatile.

Subsequent cellular repair mechanisms are then responsible for the repair of the double-strand break (DSB), generated by CRISPSR-Cas9 (Fig. 2). Most dominating DSB repair mechanisms in eukaryotic cells are classical non-homologous end joining (NHEJ), microhomology-mediated end joining (MMEJ), and homology directed repair (HDR) via double strand DNA template (dsDNA) or single strand DNA templates (ssDNA).[23] While cNHEJ occurs throughout the cell cycle, where DSBs are repaired by direct ligation of the broken ends with minimal DNA end processing, MMEJ is dependent on the S/G2 phase of the cell cycle.[24,25] MMEJ is mediated through microhomologous sequences (5-25 base pairs) near the DSB. The generated 3' ssDNA overhangs are then cleaved off, hence, resulting in loss of genetic information. Knock-out of the edited gene due to the formation of insertions and deletions (INDELs) also occurs during NHEJ. Specific knock-in of a gene at the site of the DSB, called homology directed repair, are generated via repair complementary
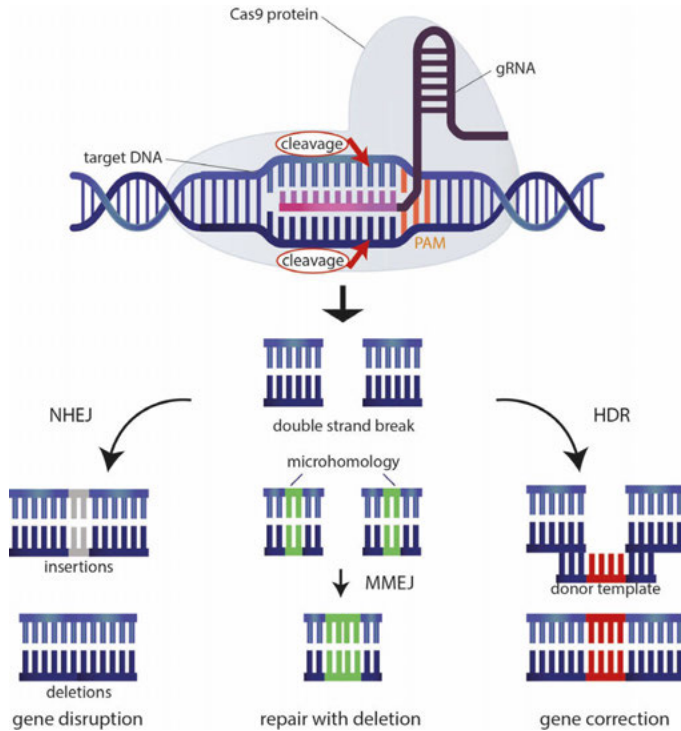
Figure 2: **Schematic representation of gene editing via CRISPR-Cas9.** Cas9 protein forms a complex with the guide RNA (gRNA), which navigates the protein to the complementary sequence on the target DNA. Cas9 protein then introduces a double strand break 2-3 bp upstream of the PAM sequence (5'NGG'3 for SpCas9). Subsequent cellular DNA repair mechanisms, such as non-homologous end joining (NHEJ), microhomology-mediated end joining (MMEJ), and homology directed repair (HDR), repair the double strand break. NHEJ results in gene disruption due to insertions or deletions. MMEJ leads to repair of the DSB however with deletions therefore to gene disruption as well. HDR results in gene correction in the presence of a donor template with homologous sequences flanking the DSB site.

to a template DNA either double- or single-stranded.[26,27] Such DNA templates require two flanking regions complementary to the DSB ends to mediate annealing and additionally contain the corrected gene. Homology directed repair is restricted to S/G2 phase of mitosis, however, it is particularly interesting in the field of gene editing for therapeutic applications.[27]

The Art of Delivery

For effective gene therapy applications, the CRISPR-Cas9 gene editing system needs to be delivered to the respective target cells, tissues, or organs. The development of efficient delivery systems for CRISPR-Cas9 is an ongoing, intensively researched field and crucial for an eventual clinical use of the genome editing tool *in vivo*. Sophisticated delivery systems are required to ensure protection of the cargo from immune recognition and enzymatic degradation, provide extended blood circulation times to enable delivery to target organ or tissue, and to facilitate nuclear uptake of CRISPR-Cas9. Various delivery strategies, either via physical methods, viral vectors, or non-viral particles, are being investigated.[28] CRISPR Therapeutics, a major company dedicated to research on CRISPR-Cas9, are conducting first clinical studies on the bacterial endonuclease for *ex vivo* hematopoietic stem cell therapy of beta thalassemia and severe sickle cell disease.[29] Stem cells are isolated from patients, subsequently administered with the CRISPR-Cas9 gene editing tool via electroporation, and the edited stems cells infused back into patient. Editas Medicine focuses on adeno-associated viral vectors for the delivery of the CRISPR-Cas9 components for retinal degenerative disease, Leber congenital amaurosis, *in vivo*, and treatment of sickle cell disease and transfusion-dependent beta thalassemia (TDT) *ex vivo*.[30,31] And as mentioned above, Intellia Therapeutics has come to show highly promising gene knock-out mediated through lipid nanoparticles delivering CRISPR-Cas9 as an mRNA molecule.[8]

Due to limitations in packaging size of viral vectors and risk of triggering immune responses, thoroughly reviewed in **chapter 2**, lipid-based particles are deemed interesting as delivery vehicles for CRISRP-Cas9.[32,33] Liposomes were first discovered by Alec Bangham and colleagues by observing that certain phospholipids could spontaneously form vesicles with a lipid bilayer structure, mimicking the cell membranes.[34,35] Researchers then started investigating the potential of liposomes as drug delivery vehicles by encapsulating

drugs with the goal to enhance their circulation time and therapeutic effect.[36] Furthermore, the stability of liposomes was significantly improved by introducing the concept of PEGylation in late 1990s, meaning to coat liposomes with polyethylene glycol (PEG), which resulted in reduced immune recognition and clearance.[37] These efforts led to the very first liposomal formulation developed for delivery of doxorubicin, Doxil.[38] Doxil was approved by the U.S. Food and Drug Administration in 1995 and used for the treatment of various cancers, including ovarian cancer, multiple myeloma, and AIDS-related Kaposi's sarcoma. Since then, newer generations of lipids and the discovery of lipid nanoparticles (LNPs) made up of cationic lipids or pH-dependent cationic ionizable lipids that facilitate encapsulation of cargo via electrostatic interactions have advanced the field of drug delivery, especially for RNA therapeutics and gene editing tools such as CRISPR-Ca9.[39,40] In addition to the cationic or ionizable cationic lipids, such as DOTAP, C12-200 or DLin-MC3-DMA, LNPs consist of helper lipids, cholesterol and PEG-modified lipids.[41] Ionizable cationic lipids facilitate the electrostatic interactions between lipid and cargo, however also trigger endosomal escape due to destabilization of the endosomal membrane after protonation in an acidic environment.[42–44] Endosomal escape results in translocation of the nanoparticle's cargo into the cytosol. LNPs have been shown to be taken up via different uptake routes, however particularly via vesicle-mediated intracellular transport through endocytosis by the cell membrane and subsequent fusion with early endosomes.[45–47] Helper lipids are responsible for the stability of the particles. Cholesterol and previously mentioned PEGylation regulate membrane fluidity as well as stability.[41] It has only been five years ago, 2018, that the first LNP carrying a nucleic acid, small interfering RNA, called patisiran (brand name ONPATTRO™, Alnylam), has been approved for treatment of hereditary transthyretin-mediated amyloidosis in adults.[44] Additionally, unique about this formulation was that it was shown to shed PEG in systemic circulation and instead absorb apolipoprotein E on its surface while circulating in the blood stream. This resulted in the nanoparticles being taken up by the

liver, specifically hepatocytes.[44,48] Since this is a general phenomenon of LNPs, the recent study by Cheng et al was highly interesting to expand the options of delivery sites *in vivo*, whereby they showed that adding either cationic or anionic compounds to the LNPs navigate the particles to lungs or spleen, respectively.[49] Another significant milestone for LNPs was achieved in the very recent years, as vaccines developed by BioNTech/Pfizer and Moderna for the COVID-19 outbreak, whereby LNPs delivered modified mRNA encoding a spike protein of SARS CoV-2 to stimulate an immune response and protect against infections.[50,51]

The advancements and clinical breakthroughs achieved with LNPs in the recent years, makes them a prime candidate of delivery vehicles for CRISPR-Cas9. Here, the cargo format can either be the mRNA transcript of Cas9 or Cas9-ribonucleoprotein (Cas9-RNP) directly.[8,52,53] The advantages and disadvantages, and possible nanoparticles for either of the two Cas9 formats have been comprehensively described in reviews, such as by Lin et al.[54] In short, Cas9 mRNA, when used as a delivery cargo, only requires delivery to the cytosol.[55] However, when delivering Cas9 mRNA, both the sgRNA and HDR template need to be packaged within the LNP, and only after translation of the mRNA can the RNP be formed intracellularly as sketched in Fig. 3. Direct delivery of the RNP seems a way to circumvent this and the associated shorter half-life seems promising to reduce risk of off-target effects, but incorporation of the Cas9-RNP in LNPs due to the large size comes with challenges.[56,57]
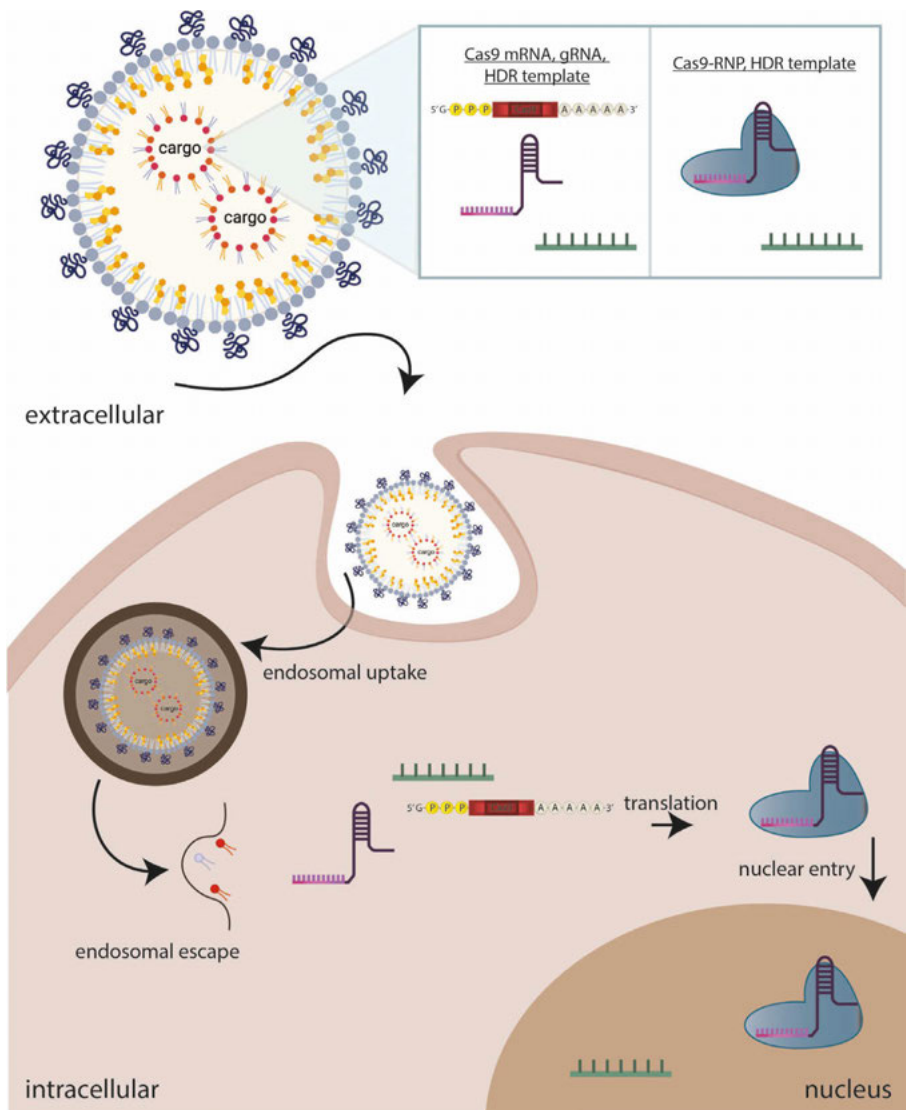
Figure 3: **Schematic representation of lipid nanoparticles carrying either Cas9 mRNA, gRNA and HDR template or directly Cas9-RNP together with HDR template.** These lipid nanoparticles are then taken up via the endosomal pathway. The ionizable lipid mediates endosomal escape of cargo into the cytosol. In the case of delivery of Cas9 mRNA the mRNA needs to be translated to the Cas9 protein in the cytosol first, and can then form the RNP with the gRNA. Direct delivery of the Cas9-RNP can result in entry into the nucleus after release from endosomes into cytosol. The lipid nanoparticle in this figure was created with Biorender.com.

Recent advances in clinical studies with CRISPR-Cas9 have mostly been restricted to *ex vivo* gene editing or gene knock-out. Given the versatility of LNPs in accommodating diverse modalities, they also hold substantial promise for the co-delivery of an HDR template alongside the CRISPR-Cas9 components.   Nevertheless, achieving optimal levels of encapsulation efficiency and the simultaneous packaging of both the HDR template and the CRISPR-Cas9 pose challenges. For gene editing, specifically correction *in vivo*, therefore, several critical questions on sophisticated delivery platforms of the CRISPR/Cas components and HDR template, and subsequent editing efficiency remain to be further optimized.

Avoiding Immune Responses against CRISPR-Cas9

A hurdle to overcome before utilizing the bacterial CRISPR-Cas9 is the immunogenicity of the protein. Due to the abundance of bacteria, such as *Streptococcus pyogenes*, within the human population, it has been reported that humans have formed an adaptive immune response towards SpCas9.[58] The nanoparticles for delivery of CRISPR-Cas9 additionally serve as protection of the cargo from neutralizing antibodies.[59] However, cytotoxic T cells against Cas9 could impact successful gene editing by eliminating cells that took up and have been edited by Cas9 protein.[60,61] Moreover, research on the mRNA vaccines for SARS CoV-2 discovered that LNPs, specifically ionizable lipids, actually boost vaccine effectiveness by stimulating the maturation of dendritic cells upon uptake.[62,63] While this adjuvant effect of LNPs is beneficial in case of vaccines, when delivering CRISPR-Cas9 components this could ignite premature clearance. An approach to avoid premature clearance of the genome editing tool, is to exploit the principles of antigen-specific immune tolerance and to actively accommodate CRISPR-Cas9.

Immune tolerance is mediated by antigen presenting cells, specifically dendritic cells (DCs). Whether DCs mediate tolerance or inflammatory

responses is dependent on their maturation stage and subtype.[64] Immature DCs reside in the blood and peripheral tissues, where they capture antigens. Subsequently, DCs mature into an active state and migrate to lymphoid organs. After an enhanced antigen processing, mature DCs present antigens on major histocompatibility complex (MHC molecules) to naïve T cells. Moreover, mature DCs obtain costimulatory molecules, such as CD40 and CD86, on their surface and produce and secret cytokines.[65] Thereby, mature DCs induce immunity. However, DCs can also induce tolerance through a tolerogenic state of DCs. Tolerogenic DCs are characterized as semi-mature DCs, in which the expression of MHCII, CD40, and CD86 are reduced. Tolerogenic DCs, tolDCs, secrete anti-inflammatory cytokines such as IL-10, transforming growth factor β (TGF-β).[66] TolDCs then initiate immune tolerance, as depicted in Fig. 4, either by T cell anergy, deletion of cytotoxic T cells, and instead induction of regulatory T cells (Tregs).[67] Tregs can be subdivided in different subtypes and can either be CD4$^+$ CD25$^+$ FoxP3$^+$ Tregs or CD4$^+$ Foxp3$^-$ CD49b$^+$ Lag3$^+$ Type 1 Regulatory cells (Tr1s).[67]

It has been discovered that tolDCs can be induced through certain immunomodulators, such as rapamycin or dexamethasone.[68,69] By encapsulating these immunomodulators together with an antigen, such as Cas9 protein, specific tolerance can be induced when nanoparticles are taken up by dendritic cells.[70,71] These nanoparticles have been called tolerogenic nanoparticles and are being investigated as a therapeutic for allergies, autoimmune disease, but also as a pretreatment to better tolerate biologics.[70,72,73] However, tolerogenic nanoparticles have not yet been employed to address the risk of preexisting immunity against SpCas9.
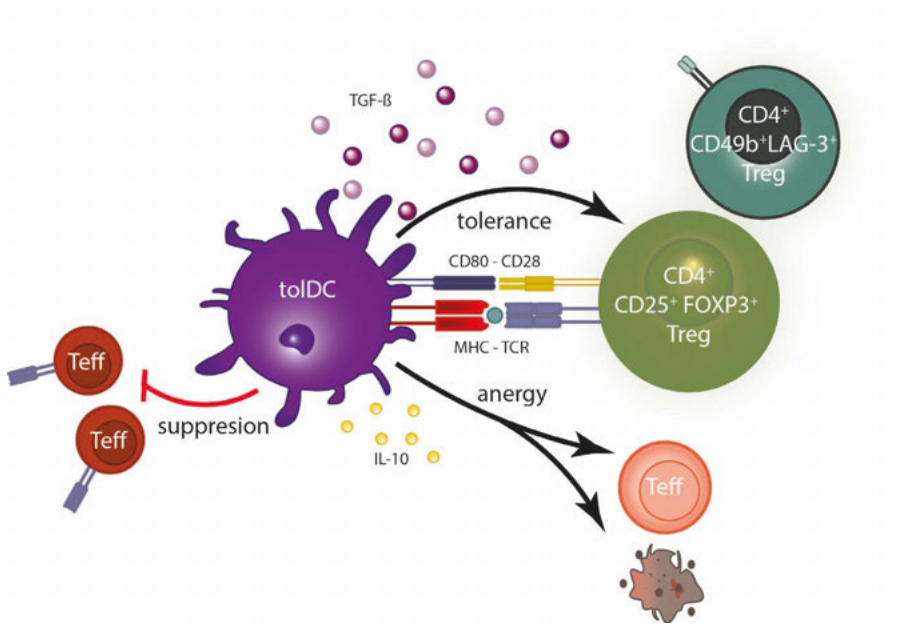
1

13

Figure 4: **Representation of interaction between tolerogenic DCs (tolDCs) with CD4⁺ regulatory T cells (Tregs).** TolDCs play a major role in the establishment of T cell tolerance by inducing anergy or suppression of effector T cells and by stimulating regulatory T cells, e.g. via secretion of anti-inflammatory cytokines such as TGF-β and IL-10.

Gene Therapy of Monogenic Diseases

Ongoing efforts of applying CRISPR-Cas9 as a gene editing tool are for treatment of sickle cell disease, cystic fibrosis, ß-thalassemia, Duchenne muscular dystrophy, and transthyretin amyloidosis.[7,8,74] Another monogenic disease that could be treated via gene therapy with CRISPR-Cas9 is the orphan autosomal recessive condition called Progressive Familial Intrahepatic Cholestasis (PFIC). There are various types of PFIC, type 1, type 2, and type 3, each due to a defect of a gene involved in the metabolism of bile, which results in a reduced functionality of hepatocytes and eventually liver failure.[75] The estimated occurrence of PFIC type 1-3 at birth ranges from 1 in 50,000 to 1 in 100,000 individuals.[76] The cause of type 1 (PFIC1) is a

mutation on chromosome 18q21 in the *ATP8B1* gene which leads to a defective FIC1 protein.[77] Localized at the canalicular membrane of hepatocytes, but also on apical membranes of other epithelial cells in other organs, FIC1 protein acts as a flippase for phosphatidylserine. The liver, as the primary organ responsible for producing and secreting bile, relies on FIC-1 mediated processes. Therefore, when defective, FIC1 protein especially affects the liver and indirectly results in cholestasis.[78]

Studies show that most abundant mutations resulting in PFIC1 are missense mutations such as 380T>C, 863T>C, and 923G>T with the predicted effect L127P, L288S, and G308V, respectively, in the protein.[79] G308V, as a predominant mutation in patients, results in an unfolded conformation of the FIC1 protein.[80] To investigate the underlying disease mechanisms and facilitate the exploration of potential therapeutic interventions, a murine model harboring the G308V mutation has therefore been established. Ongoing investigations, e.g. with ATP8B1$^{G308V/G308V}$ mutant mouse model, study the role of the defective flippase in PFIC1.[78,81,82] Moreover, these mutant mice can additionally be harnessed as a model to study gene correction from tyrosine back to guanine. Up until now, the only treatment of PFIC1 is a liver transplant or medication to ease cholestasis. LNPs co-delivering the Cas9 protein, either as mRNA Cas9 and guide RNA or directly as RNP, and an HDR template could be a therapeutic application to cut out and correct the mutation causing PFIC1.

Aims and Outline of the Thesis

The main aim of this thesis was to develop a system to safely deliver CRISPR-Cas9 gene editing tools together with ssDNA HDR template to hepatocytes via intravenous injection for specific gene correction. To this end, lipid nanoparticles were carefully formulated to entrap and

deliver Cas9, either as mRNA or protein together with sgRNA and ss-DNA HDR template. Additionally, the research presented in this thesis investigated the formulation of tolerogenic nanoparticles to induce tolerance towards Cas9 to circumvent preexisting immune responses and generally the immunogenicity of the protein.

Chapter 2 reviews the aspects and considerations for viral and non-viral delivery vehicles of CRISPR-Cas9, different cargo formats of the gene editing tool, and manipulations on cellular levels to increase ratio between gene correction and gene knock-out, and addresses questions, such as immunogenicity of Cas9, that need to be addressed for use of CRISPR-Cas9 *in vivo*.

In **chapter 3** studies of the design and optimization of formulation parameters for lipid nanoparticles delivering Cas9-RNP are presented. The particles were characterized in size, charge, and stability, and studied on gene editing efficiencies in reporter cell lines in culture. LNPs were additionally optimized for co-delivery of an HDR template for specific gene correction via homology-directed repair and studied on a fluorescent reporter system.

Since CRISPR-Cas9 components can be delivered as different cargo molecules, e.g. Cas9-RNP or mRNA Cas9, **chapter 4** presents a comparison of LNPs delivering Cas9-RNP and HDR template or mRNA Cas9 together with sgRNA and HDR template. The nanoparticles were compared with regards to efficiency of gene correction on two different reporter cell systems and the timing of uptake of Cas9 protein in the nucleus and on-set of gene correction was determined. The chapter also reports the biodistribution of Cy5.5-sgRNA loaded Cas9-LNPs and gene knock-out efficiencies within hepatocytes in Ai9 mice.

Chapter 5 describes a strategy to avoid undesired immune responses against the Cas9 protein by inducing Cas9-specific tolerance *in vivo* via dexamethasone-phosphate and Cas9 loaded liposomes. DPPC-DPPG-cholesterol liposomes are shown to induce tolerogenic phenotype of dendritic cells *in vitro*, however were only determined to decrease anti-Cas9 antibodies minimally *in vivo*.

Besides these chapters, a **supplement** was included to highlight a technical problem that we encountered in the analysis of gene correction in intestinal organoids using droplet digital PCR. Depending on the primers used for digital PCR, it can lead to false positive events due to the prolonged presence of the ssDNA HDR template that is co-amplified. Even though these findings require further investigation, the importance of these preliminary results for other scientists working on new HDR-mediated gene correction strategies warrants inclusion in this thesis.

The findings presented in this thesis are discussed in **chapter 6**, also from the perspective of remaining challenges and further improvements to deliver the gene editing tool, CRISPR-Cas9, in patients and for application as a gene therapy of genetic diseases.

References

1. Gene Map Statistics - OMIM. https://www.omim.org/statistics/geneMap.
2. Esvelt, K. M. & Wang, H. H. Genome-scale engineering for systems and synthetic biology. Mol. Syst. Bio.l **9,** (2013).
3. Doudna, J. A. & Charpentier, E. The new frontier of genome engineering with CRISPR-Cas9. Science **346,** (2014).
4. Zheng, R. et al. Progress and Perspective of CRISPR-Cas9 Technology in Translational Medicine. Adv. Sci. (2023).
5. Zhang, S. et al. Recent Advances of CRISPR/Cas9-Based Genetic Engineering and Transcriptional Regulation in Industrial Biology. Front. Bioeng. Biotechnol. **7,** (2020).
6. Khanna, K., Ohri, P. & Bhardwaj, R. Nanotechnology and CRISPR/Cas9 system for sustainable agriculture. Environ. Sci. Pollut. Res. (2023).
7. Kingwell, K. First CRISPR therapy seeks landmark approval. Nat. Rev. Drug. Discov. **22,** 339–341 (2023).
8. Gillmore, J. D. et al. CRISPR-Cas9 In Vivo Gene Editing for Transthyretin Amyloidosis. N. Engl. J. Med. **385,** 493–502 (2021).
9. Ishino, Y., Shinagawa, H., Makino, K., Amemura, M. & Nakata, A. Nucleotide Sequence of the iap Gene, Responsible for Alkaline Phosphatase Isozyme Conversion in Escherichia coli, and Identification of the Gene Product. J. Bacteriol. (1987).
10. Barrangou, R. et al. CRISPR Provides Acquired Resistance Against Viruses in Prokaryotes. Science (1979) **315,** 1709–1712 (2007).

11. Deltcheva, E. et al. CRISPR RNA maturation by trans-encoded small RNA and host factor RNase III. Nature **471**, 602–607 (2011).

12. Chylinski, K., Le Rhun, A. & Charpentier, E. The tracrRNA and Cas9 families of type II CRISPR-Cas immunity systems. RNA Biol. **10**, 726–737 (2013).

13. Dai, W. J. et al. CRISPR-Cas9 for in vivo Gene Therapy: Promise and Hurdles. Mol. Ther. Nucleic Acids **5**, e349 (2016).

14. Mojica, F. J. M., Díez-Villaseñor, C., García-Martínez, J. & Almendros, C. Short motif sequences determine the targets of the prokaryotic CRISPR defence system. Microbiology (N Y) **155**, 733–740 (2009).

15. Leenay, R. T. & Beisel, C. L. Deciphering, Communicating, and Engineering the CRISPR PAM. J. Mol. Biol. **429**, 177–191 (2017).

16. Makarova, K. S. et al. An updated evolutionary classification of CRISPR-Cas systems. Nat. Rev. Microbiol. **13**, 722–736 (2015).

17. Halat, M., Klimek-Chodacka, M., Orleanska, J., Baranska, M. & Baranski, R. Electronic circular dichroism of the cas9 protein and grna:Cas9 ribonucleoprotein complex. Int. J. Mol. Sci. **22**, 1–14 (2021).

18. Cas9 Mechanism — CRISPR/Cas9. https://sites.tufts.edu/crispr/crispr-mechanism/.

19. Sternberg, S. H., Redding, S., Jinek, M., Greene, E. C. & Doudna, J. A. DNA interrogation by the CRISPR RNA-guided endonuclease Cas9. Nature **507**, 62–67 (2014).

20. Jinek, M. et al. Structures of Cas9 endonucleases reveal RNA-mediated conformational activation. Science **343**, (2014).

21. Zhu, X. et al. Cryo-EM structures reveal coordinated domain motions that govern DNA cleavage by Cas9. Nat. Struct. Mol. Biol. **26**, 679–685 (2019).

22. Jinek, M. et al. A Programmable Dual-RNA – Guided. Science 337, 816–822 (2012).

23. Xue, C. & Greene, E. C. DNA Repair Pathway Choices in CRISPR-Cas9-Mediated Genome Editing. Trends. Genet. **37**, 639–656 (2021).

24. Chang, H. H. Y., Pannunzio, N. R., Adachi, N. & Lieber, M. R. Non-homologous DNA end joining and alternative pathways to double-strand break repair. Nat. Rev. Mol. Cell. Biol. **18**, 495–506 (2017).

25. Sfeir, A. & Symington, L. S. Microhomology-Mediated End Joining: A Back-up Survival Mechanism or Dedicated Pathway? Trends. Biochem. Sci. **40**, 701–714 (2015).

26. Bhargava, R., Onyango, D. O. & Stark, J. M. Regulation of Single-Strand Annealing and its Role in Genome Maintenance. Trends. Genet. **32**, 566–575 (2016).

27. Sung, P. & Klein, H. Mechanism of homologous recombination: mediators and helicases take on regulatory functions. Nat. Rev. Mol. Cell. Biol. **7**, 739–750 (2006).

28. He, Z.-Y. et al. Non-viral and viral delivery systems for CRISPR-Cas9 technology in the biomedical field. Sci. China. Life. Sci. **60**, 458–467 (2017).

29. CRISPR Therapeutics and Vertex Announce New Clinical Data for Investigational Gene-Editing Therapy CTX001TM in Severe Hemoglobinopathies at the 25th Annual European Hematology Association (EHA) Congress-Beta thalassemia: Two patients are transfusion independent at 5 and 15 months after CTX001 infusion; data demonstrate clinical proof-of-concept for CTX001 in transfusion-dependent beta thalassemia. www.crisprtx.com.

30.   De Dreuzy, E. et al. EDIT-301: An Experimental Autologous Cell Therapy Comprising Cas12a-RNP Modified mPB-CD34+ Cells for the Potential Treatment of SCD. Blood **134**, 4636–4636 (2019).

31.   First CRISPR therapy dosed. Nat. Biotechnol. **38**, 382–382 (2020).

32.   Gori, J. L. et al. Delivery and Specificity of CRISPR/Cas9 Genome Editing Technologies for Human Gene Therapy. Hum. Gene. Ther. **26**, 443–451 (2015).

33.   Yin, H., Kauffman, K. J. & Anderson, D. G. Delivery technologies for genome editing. Nat. Rev. Drug. Discov. **16**, 387–399 (2017).

34.   Deamer, D. W. From 'banghasomes' to liposomes: a memoir of Alec Bangham, 1921-2010. FASEB **24**, 1308–1310 (2010).

35.   Trucillo, P., Campardelli, R. & Reverchon, E. Liposomes: From Bangham to Supercritical Fluids. Processes **8**, 1022 (2020).

36.   Laouini, A. et al. Preparation, Characterization and Applications of Liposomes: State of the Art. J. Colloid. Interface. Sci. **1**, 147–168 (2012).

37.   Suzuki, S., Watanabe, S., Masuko, T. & Hashimoto, Y. Preparation of long-circulating immunoliposomes containing adriamycin by a novel method to coat immunoliposomes with poly(ethylene glycol). Biochim. Biophys. Acta. Gen. Subj. **1245**, 9–16 (1995).

38.   Barenholz, Y. (Chezy). Doxil® — The first FDA-approved nano-drug: Lessons learned. J. Control. Release. **160**, 117–134 (2012).

39.   Kulkarni, J. A., Cullis, P. R. & van der Meel, R. Lipid Nanoparticles Enabling Gene Therapies: From Concepts to Clinical Utility. Nucleic Acid Ther. **28**, 146–157 (2018).

40.   Zhang, S., Zhao, B., Jiang, H., Wang, B. & Ma, B. Cationic lipids and polymers mediated vectors for delivery of siRNA. J. Control. Release **123**, 1–10 (2007).

41.   Cheng, X. & Lee, R. J. The role of helper lipids in lipid nanoparticles (LNPs) designed for oligonucleotide delivery. Adv. Drug. Deliv. Rev. **99**, 129–137 (2016).

42.   Hou, X., Zaks, T., Langer, R. & Dong, Y. Lipid nanoparticles for mRNA delivery. Nat. Rev. Mater. **6,** 1078–1094 (2021).

43.   Love, K. T. et al. Lipid-like materials for low-dose, in vivo gene silencing. Proc. Natl. Acad. Sci. USA **107**, 1864–1869 (2010).

44.   Akinc, A. et al. The Onpattro story and the clinical translation of nanomedicines containing nucleic acid-based drugs. Nat. Nanotechnol. **14**, 1084–1087 (2019).

45.   Fröhlich, E. The role of surface charge in cellular uptake and cytotoxicity of medical nanoparticles. Int. J. Nanomedicine **7**, 5577–5591 (2012).

46.   Roger, E., Lagarce, F., Garcion, E. & Benoit, J. P. Lipid nanocarriers improve paclitaxel transport throughout human intestinal epithelial cells by using vesicle-mediated transcytosis. J. Control. Release **140**, 174–181 (2009).

47.   Schmid, S. L. Reciprocal regulation of signaling and endocytosis: Implications for the evolving cancer cell. J. Cell Biol. **216**, 2623–2632 (2017).

48.   Akinc, A. et al. Targeted delivery of RNAi therapeutics with endogenous and exogenous ligand-based mechanisms. Mol. Ther. **18**, 1357–1364 (2010).

49.   Cheng, Q. et al. Selective organ targeting (SORT) nanoparticles for tissue-specific mRNA delivery and CRISPR–Cas gene editing. Nat. Nanotechnol. **15**, 313–320 (2020).

50.   Mahase, E. Covid-19: Moderna vaccine is nearly 95% effective, trial involving high risk and elderly people shows. BMJ m4471 (2020).

51. Chagla, Z. The BNT162b2 (BioNTech/Pfizer) vaccine had 95% efficacy against COVID-19 $\geq 7 days after the 2nd dose. Ann. Intern. Med.$ **174**, $JC15$ (2021).

52. Suzuki, Y. et al. Lipid nanoparticles loaded with ribonucleoprotein–oligonucleotide complexes synthesized using a microfluidic device exhibit robust genome editing and hepatitis B virus inhibition. J. Control. Release **330**, 61–71 (2021).

53. Wei, T., Cheng, Q., Min, Y. L., Olson, E. N. & Siegwart, D. J. Systemic nanoparticle delivery of CRISPR-Cas9 ribonucleoproteins for effective tissue specific genome editing. Nat. Commun. **11**, 1–12 (2020).

54. Lin, Y., Wagner, E. & Lächelt, U. Non-viral delivery of the CRISPR/Cas system: DNA versusRNA versus RNP. Biomater. Sci. **10**, 1166–1192 (2022).

55. Kouranova, E. et al. CRISPRs for optimal targeting: Delivery of CRISPR components as DNA, RNA, and protein into cultured cells and single-cell embryos. Hum. Gene Ther. **27**, 464–475 (2016).

56. Lin, S., Staahl, B. T., Alla, R. K. & Doudna, J. A. Enhanced homology-directed human genome engineering by controlled timing of CRISPR/Cas9 delivery. Elife **3**, e04766 (2014).

57. Khan, O. F. et al. Ionizable amphiphilic dendrimer-based nanomaterials with alkyl-chain-substituted amines for tunable sirna delivery to the liver endothelium in vivo. Angew. Chem. Int. Ed **53**, 14397–14401 (2014).

58. Charlesworth, C. T. et al. Identification of preexisting adaptive immunity to Cas9 proteins in humans. Nat. Med. **25**, 249–254 (2019).

59. Wagner, D. L. et al. High prevalence of Streptococcus pyogenes Cas9-reactive T cells within the adult human population. Nat. Med. **25**, 242–248 (2019).

60. Wagner, D. L., Peter, L. & Schmueck-Henneresse, M. Cas9-directed immune tolerance in humans—a model to evaluate regulatory T cells in gene therapy? Gene Ther. **28**, 549–559 (2021).

61. Li, A. et al. AAV-CRISPR Gene Editing Is Negated by Pre-existing Immunity to Cas9. Mol. Ther. **28**, 1432–1441 (2020).

62. Alameh, M. G. et al. Lipid nanoparticles enhance the efficacy of mRNA and protein subunit vaccines by inducing robust T follicular helper cell and humoral responses. Immunity **54**, 2877-2892.e7 (2021).

63. Connors, J. et al. Lipid nanoparticles (LNP) induce activation and maturation of antigen presenting cells in young and aged individuals. Commun. Biol. **6**, (2023).

64. Castenmiller, C., Keumatio-Doungtsop, B.-C., van Ree, R., de Jong, E. C. & van Kooyk, Y. Tolerogenic Immunotherapy: Targeting DC Surface Receptors to Induce Antigen-Specific Tolerance. Front. Immunol. **12**, (2021).

65. Santambrogio, L. et al. Extracellular antigen processing and presentation by immature dendritic cells. PNAS **26** (1999).

66. Iberg, C. A. & Hawiger, D. Natural and Induced Tolerogenic Dendritic Cells. J. Immunol. **204**, 733–744 (2020).

67. Keijzer, C., Van der Zee, R., Van Eden, W. & Broere, F. Treg inducing adjuvants for therapeutic vaccination against chronic inflammatory diseases. Front. Immunol. **4**, 1–10 (2013).

68. Ozdemir, C. et al. Efficacy of long-term sublingual immunotherapy as an adjunct to pharmacotherapy in house dust mite-allergic children with asthma. Pediatr. Allergy Immunol. Pulmonol., 508–515 (2007).

69.   Gagliani, N. et al. Rapamycin Combined with Anti-CD45RB mAb and IL-10 or with G-CSF Induces Tolerance in a Stringent Mouse Model of Islet Transplantation. PLoS One **6**, e28434 (2011).

70.   Benne, N. et al. Anionic 1,2-distearoyl-sn-glycero-3-phosphoglycerol (DSPG) liposomes induce antigen-specific regulatory T cells and prevent atherosclerosis in mice. J. Control. Release **291**, 135–146 (2018).

71.   Passerini, L. & Gregori, S. Induction of Antigen-Specific Tolerance in T Cell Mediated Diseases. Front. Immunol. **11**, (2020).

72.   Kishimoto, T. K. et al. Improving the efficacy and safety of biologic drugs with tolerogenic nanoparticles. Nat. Nanotechnol. **11**, 890–899 (2016).

73.   Sands, E. et al. Tolerogenic nanoparticles mitigate the formation of anti-drug antibodies against pegylated uricase in patients with hyperuricemia. Nat. Commun. **13**, (2022).

74.   Memi, F., Ntokou, A. & Papangeli, I. CRISPR/Cas9 gene-editing: Research technologies, clinical applications and ethical considerations. Semin. Perinatol. **42**, 487–500 (2018).

75.   Amer. A Comprehensive Review of Progressive Familial Intrahepatic Cholestasis (PFIC): Genetic Disorders of Hepatocanalicular Transporters. Gastroenterology Res (2014). 76. Davit-Spraul, A., Gonzales, E., Baussan, C. & Jacquemin, E. Progressive familial intrahepatic cholestasis. Orphanet J. Rare Dis. **4**, 1 (2009).

77.   Bull, L. N. et al. Genetic and morphological findings in progressive familial intrahepatic cholestasis (Byler disease [PFIC-1] and Byler syndrome): Evidence for heterogeneity. Hepatology **26**, 155–164 (1997).

78.   Naik, J. et al. ATP8B1 and ATP11C: Two lipid flippases important for hepatocyte function. in Dig. Dis. vol. 33 314–318 (S. Karger AG, 2015).

79.   Klomp, L. W. J. et al. Characterization of mutations in ATP8B1 associated with hereditary cholestasis. Hepatology **40**, 27–38 (2004).

80.   Van Der Velden, L. M. et al. Folding defects in P-type ATP 8B1 associated with hereditary cholestasis are ameliorated by 4-phenylbutyrate. Hepatology **51**, 286–296 (2010).

81.   Alam, S. & Lal, B. B. Recent updates on progressive familial intrahepatic cholestasis types 1, 2 and 3: Outcome and therapeutic strategies. World J. Hepatol. **14**, 98–118 (2022).

82.   Pawlikowska, L. et al. A mouse genetic model for familial cholestasis caused by ATP8B1 mutations reveals pertubed bile salt homeostasis but no impairment in bile secretion. Hum. Mol. Genet. **13**, 881–892 (2004).

2

Delivery Aspects of CRISPR/Cas for *In Vivo* Genome Editing

Danny Wilbie, Johanna Walther, Enrico Mastrobattista

Department of Pharmaceutics, Utrecht Institute for Pharmaceutical Sciences (UIPS), Utrecht University, The Netherlands

Abstract

The discovery of CRISPR/Cas has revolutionized the field of genome editing. CRIPSR/Cas components are part of the bacterial immune system and are able to induce double-strand DNA breaks in the genome, which are resolved by endogenous DNA repair mechanisms. The most relevant of these are the error-prone nonhomologous end joining and homology directed repair pathways. The former can lead to gene knockout by introduction of insertions and deletions at the cut site, while the latter can be used for gene correction based on a provided repair template. In this Account, we focus on the delivery aspects of CRISPR/Cas for therapeutic applications *in vivo*. Safe and effective delivery of the CRISPR/Cas components into the nucleus of affected cells is essential for therapeutic gene editing. These components can be delivered in several formats, such as pDNA, viral vectors, or ribonuclear complexes. In the ideal case, the delivery system should address the current limitations of CRISPR gene editing, which are (1) lack of targeting specific tissues or cells, (2) the inability to enter cells, (3) activation of the immune system, and (4) off-target events. To circumvent most of these problems, initial therapeutic applications of CRISPR/Cas were performed on cells *ex vivo* via classical methods (e.g., microinjection or electroporation) and novel methods (e.g., TRIAMF and iTOP). Ideal candidates for such methods are, for example, hematopoietic cells, but not all tissue types are suited for *ex vivo* manipulation. For direct *in vivo* application, however, delivery systems are needed that can target the CRISPR/Cas components to specific tissues or cells in the human body, without causing immune activation or causing high frequencies of off-target effects. Viral systems have been used as a first resort to transduce cells *in vivo*. These systems suffer from problems related to packaging constraints, immunogenicity, and longevity of Cas expression, which favors off-target events. Viral vectors are as such not the best choice for direct *in vivo* delivery of CRISPR/Cas. Synthetic vectors can deliver nucleic acids as well, without the innate disadvantages of viral vectors. They can be classed into lipid, polymeric, and inorganic particles, all of which have been reported in the literature. The advantage of synthetic systems is that they can deliver the CRISPR/Cas system also as a preformed ribonucleoprotein complex. The transient nature of this approach favors low frequencies of off-target events and minimizes the window of immune activation. Moreover, from a pharmaceutical perspective, synthetic delivery systems are much easier to scale up for clinical use compared to viral vectors and can be chemically functionalized with ligands to obtain target cell specificity. The first preclinical results with lipid nanoparticles delivering CRISPR/Cas either as mRNA or ribonucleoproteins are very promising. The goal is translating these CRISPR/Cas therapeutics to a clinical setting as well. Taken together, these current trends seem to favor the use of sgRNA/Cas ribonucleoprotein complexes delivered *in vivo* by synthetic particles.

Introduction

RNA-guided endonucleases derived from the bacterial CRISPR/Cas system have gained tremendous popularity over the use of protein-guided nucleases for genome editing during the past years. This is owed to the ease at which target gene specificity can be changed, enabling precise genome surgery on-targeted diseased cells. This gene surgery method has widespread applications, including crop manipulation, cancer diagnostics, and gene therapy. Preclinical data demonstrate the power of this technology in correcting genetic diseases, and we start to better understand the CRISPR/Cas machinery from a molecular perspective. However, despite CRIPSR/Cas technology slowly moving into the clinic, there remain some critical questions unanswered. One of these questions is whether CRISPR/Cas can be administered safely and effectively to humans via direct intravenous administration. For this, the delivery method being used is critically important and should ideally restrict genome editing to affected target cells only, and thereby avoid gene edits in nontarget cells. In this account, we will address the current status of *in vivo* CRISPR/Cas delivery with both synthetic and viral vectors and will focus on the differences in delivery methods in terms of on-target genome editing efficiency and off-target effects. In addition, we will discuss ways how immunogenicity via bacterial Cas9 in humans can be diminished.[1]

CRISPR/Cas Mechanism of Action and the Minimal Components for Genome Editing

Guide RNA (gRNA) and CRISPR-associated (Cas) proteins are key components of a bacterial defense system based around clustered regularly interspaced palindromic repeats (CRISPR). Together, they enable prokaryotes to develop adaptive immune responses against invading mobile genetic elements, such as bacteriophages. This CRISPR/Cas system has been engineered into a two-part system

to enable therapeutic genome editing in eukaryotic cells: a single guide RNA (sgRNA) and a Cas endonuclease together form the active ribonucleoprotein (RNP) complex. The most commonly used Cas endonuclease is Cas9, although other variants have been discovered for gene editing purposes since then, such as Cpf1.[2] The sgRNA sequence consists of two domains: the spacer sequence, which consists of 20 nucleotides targeting the RNP complex to the DNA, and a backbone sequence anchoring it to the protein.[3]

Therapeutic gene editing is achieved through induction of a double-strand break (DSB) at the DNA locus, directed by the sgRNA. This process requires a specific nucleotide sequence, the protospacer-adjacent motif (PAM), to be present on the target strand in order for the Cas protein to be activated. The active complex cleaves the two DNA strands upstream of the PAM. Different Cas proteins require different PAM sequences, for example 5'-NGG for Cas9 derived from *Streptococcus pyogenes* (spCas9) or 5'-TTTN for Cpf1. Different Cas proteins also have different cleavage patterns. SpCas9, for example, induces a blunt DSB 3 nucleotides upstream of the PAM. A DSB can be induced near any PAM site specific to the chosen Cas protein by changing the 20nt guide RNA sequence. This makes CRISPR/Cas a more appealing method for gene editing than the previously used Zinc-finger nucleases and TAL-effector nucleases, which rely on the engineering of Fok1 endonuclease to induce double-strand breaks.[1,4] Cas9 can also be engineered to induce a single-strand nick (Cas9 nickase, nCas9) or to simply bind the DNA without endonuclease activity (inactive Cas9, dCas9). The latter can be fused to other active regulatory components, such as base-editors.[5,6]

There are several formats in which the sgRNA and Cas protein can be delivered into the cell to achieve therapeutic gene editing. These have been summarized in Fig. 1A. The endonuclease is problematic to deliver, due to the high molecular weight of the protein (158.9 kDa for spCas9) and the gene length (around 4 kb). The gene can be delivered either as an expression plasmid or by viral vectors which need to be imported into the nucleus for transcription. Additionally, it can be de-

livered as mRNA which is directly translated in the cytosol. sgRNA can be delivered as synthetic oligonucleotides, or expressed through plasmids or viral vectors. The combination of Cas protein and gRNA can be delivered as a single plasmid, viral vector(s), or as preformed RNP complexes which only need to localize to the nucleus. An HDR template for specific repair can finally be delivered as single strand DNA (suited for small mutational corrections) or as large DNA plasmids (suited knock-in of large sequences or whole genes). HDR template sequences contain the corrected gene and two flanking homology arms (HA) to improve affinity around the site of the DSB.[1,4,7] After the induction of a DSB, the broken DNA ends are recognized by proteins belonging to the DNA repair machinery, leading to activation of DNA repair. This is achieved through one of several different repair pathways, which are more extensively reviewed elsewhere.[8] The most relevant pathways are nonhomologous end joining (NHEJ), homology directed repair (HDR), and microhomology mediated repair (MMR). NHEJ is imperfect and often leads to small insertions or deletions (indels) in the genome. This can be exploited for gene knockout by introduction of premature STOP-codons or shifts of the genetic reading frame. Gene correction and knock-in can be achieved through HDR, by addition of a template DNA strand, thereby leading to repair complementary to the provided template.[8] These are shown in Fig. 1B.
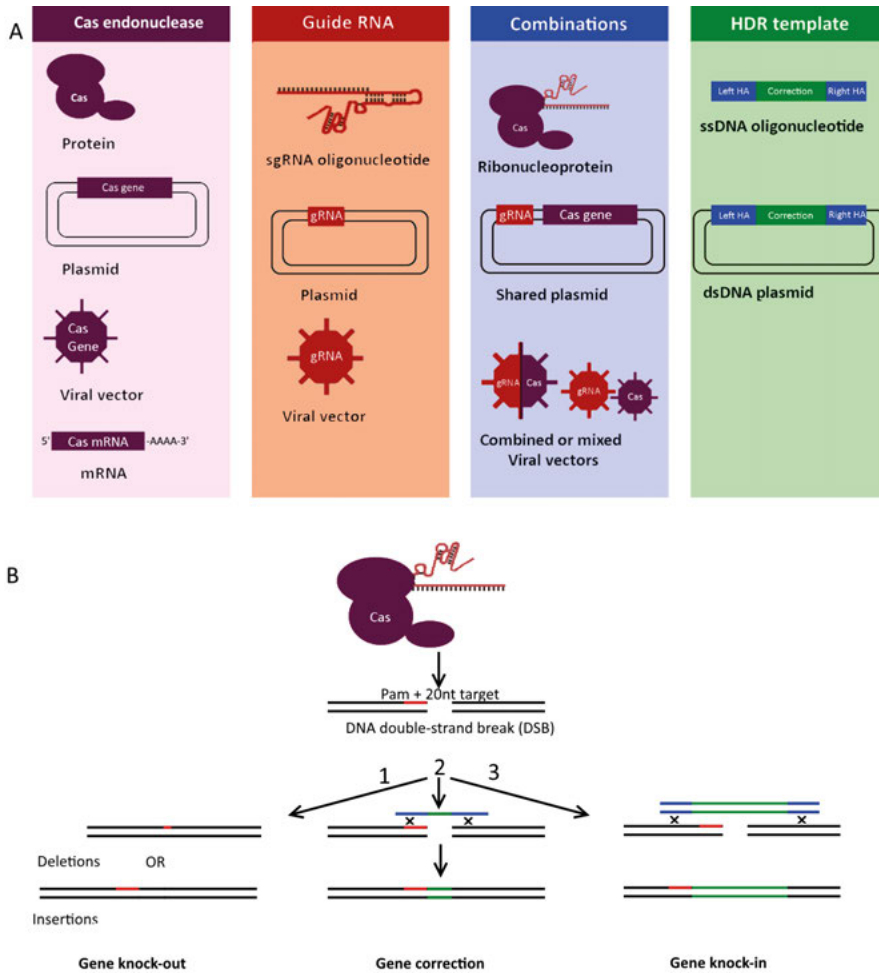
2

Figure 1: **Schematic summary of CRISPR/Cas endonuclease concepts. A)** Different formats in which Cas protein, gRNA and HDR templates can be used to achieve gene editing. **B)** The active RNP complex acts by cleaving 2 DNA strands at the sgRNA target site in the presence of a PAM sequence (red). Three repair mechanisms can occur. 1: NHEJ, which can induce gene knock-out by random indel formation; 2 and 3: HDR using a ssDNA or dsDNA template, respectively.[8]

Direct Delivery of CRISPR/Cas

While CRISPR/Cas mediated therapeutic gene knock-out and correction have many potential applications, the practical execution is not straightforward. Multiple components need to be delivered into the nuclei of target cells for the desired therapeutic effect. Delivery of genetic material or proteins can be done by directly disrupting the barriers between a drug and its target, while barely interacting with the therapeutic cargo. These methods are used extensively *in vitro* to study the effects of CRISPR/Cas systems on the genome because they are economical and often easy to implement on cell lines. While most direct methods of delivery are difficult to utilize *in vivo*, they can be used to introduce CRISPR/Cas components *ex vivo* to cells harvested from patients, before reintroducing them into the patient. Notable examples are hematopoietic cells for treatment of sickle-cell anemia, chimeric antigen receptor (CAR) T cells, and germline cells. The main delivery barriers in these cases are the target cell membrane, potentially endosomal release, and nuclear localization of the active complex.[7,9]

Traditional methods of direct transfection have first been investigated. The main advantage of these techniques is that the uptake mechanism is independent of the cell. Microinjection of single fast-dividing cells has been used to generate a great variety of knock-out and transgenic animals by directly injecting zygotes with CRISPR components into the nucleus. While this technique is very effective, it has the distinct disadvantage of cells requiring individual manipulation.[10] Electroporation, by which pores are formed in cell membranes upon application of a high voltage, can be used to directly transfect cells *ex vivo* as well as some *in vivo* tissues. This has, for example, been used to transfect human B-cells with CRISPR/Cas RNP to induce production of therapeutic proteins, after differentiation into plasma cells.[11] Electroporation can be very toxic, however, due to this technique harming the cell membrane. In some cases this leads to permanent permeabilization of the membrane.[12]

Two novel techniques to deliver CRISPR/Cas RNPs into cells

are through induction of transmembrane internalization assisted
by membrane filtration (TRIAMF) and induced transduction by
osmocytosis and propane betaine (iTOP). In TRIAMF cells are
extruded through a membrane, which has smaller pores than the
cell diameter, thereby inducing transient pore formation in the cell
membrane. This method was used to deliver RNPs in hematopoietic
stem/progenitor cells (HSPCs), which generally exhibit low endocytic
uptake and require more direct methods of transfection.   They
achieved a similar efficiency compared to electroporation techniques,
while observing less cytotoxicity.[13] In iTOP hypertonic sodium
chloride is added to the outside milieu of the cells along with
propane-betaine NDSB-201. These components cause the formation of
endosomes through macropinocytosis, which allow uptake of proteins
and subsequent release by disrupting the endosomal membrane.[14]

While these direct delivery methods are promising to alter specific cells
ex vivo, they are limited in their application as not all tissues are suit-
able for *ex vivo* manipulation. Other delivery methods are therefore
needed to deliver CRISPR/Cas directly *in vivo*. This can be done either
intravenously or through local administration, for example intramus-
cularly for Duchenne's muscular dystrophy. The latter has the distinct
advantage of achieving a high dose in the target tissue and thus a high
likelihood of gene editing.[15] Intravenous administration has the rel-
ative advantage of reaching a wider target, such as whole organs or
systemic targets like vascular endothelium. The optimal route of ad-
ministration needs to be determined for each tissue individually.

Viral Delivery Methods

The ultimate goal in CRISPR therapy is to genetically correct cells di-
rectly in the human body and thereby curing a debilitating genetic
disease. This requires sophisticated carrier systems that ideally target
cells with high specificity, combined with minimal cytotoxicity, and

rapid clearing of the CRISPR system after successful gene modification. However, none of the currently available delivery methods fulfill all of the above criteria. Viral vectors have been used as a first resort to solve the delivery problem of CRISPR/Cas gene editing system. The most widely studied vectors include lentiviral, adeno-associated viral, and adenoviral vectors. A comparison of their main properties is given in table 1.

Adeno-associated viruses (AAV) combine low immunogenicity upon first injection with serotype-related target cell specificity and relatively long expression of the gene without the necessity for genome integration. However, the packaging capacity is limited and, as a consequence, the genetic material encoding the most frequently used spCas9 (4.2 kB) leaves limited space for necessary regulatory elements, such as promoter and polyadenylation signal sequences. This can be solved by splitting spCas9 into two fragments that can recombine inside the cell so that the truncated genes will fit the AAV vector, but this comes at the cost of efficiency in terms of delivery as well as target DNA cutting.[16]

Adenoviral vectors (AV) can easily contain all elements for genome editing due to their high packaging capacity, expressing both the Cas protein as well as one or multiple sgRNAs from a single vector. In addition, large donor DNA sequences to mediate homology-directed repair can be co-delivered as well. The advantage of this is that sgRNA and Cas protein are consistently expressed in the same cell at a fixed ratio and since AV are non-integrating, Cas expression is transient in dividing cells. AV have been successfully used for *in vivo* genome editing in mice, although immune-related toxicities were observed.[17]

Lentiviral vectors (LV) are at present the most widely used viral vectors for clinical gene therapy applications in which long-lasting expression of a gene is required. The advantage of LV is the relatively safe genomic integration of the gene construct and the capacity to transduce both dividing and non-dividing cells with high efficiency. However, the feature that makes this vector suitable for gene delivery

(stable and long-lasting expression) is counterproductive for gene editing purposes. Long-lasting expression of the Cas protein is considered to be unfavorable for the on-target/off-target ratio of indel formation.[18–20] Indeed, a direct comparison of frequencies of indel formation at three potential genomic off-target sites by spCas9 delivered as mRNA, pDNA, RNP, or lentivirus showed highest off-target frequencies with the lentiviral delivery method.[21] To counteract this, self-inactivating constructs have been designed in which the lentiviral vector encodes for Cas9 protein and two sgRNAs: one against the target sequence of choice and one against the Cas9 gene.[22] In this way transient expression of Cas9 from an integrating lentiviral vector can be obtained.

Immunogenicity associated with the use of viral vectors for gene editing is often downplayed by assuming single injections will be enough to obtain gene correction and thereby cure of a disease. As long as pre-existing antibodies are absent, this single-shot approach could indeed be effective in isolated cases. However, for many monogenic diseases a certain threshold of gene-correction is required to revert the disease phenotype. For example, to cure hemophilia B, it is estimated that the levels of FIX activity should be increased from < 2% of normal activity to at least 25-100% (0.25-1.00 IU/ml). Current gene therapy applications can reach levels of 0.12 IU/ml, which is enough to revert severe hemophilia into a mild form, but not enough to completely stop prophylactic FIX treatment.[23] Given the low gene correction efficiencies currently obtained through HDR *in vivo* such a threshold can only be obtained in case multiple injections of the viral vector are feasible to accumulate enough gene corrections to revert the disease. At present, this is not possible as high dose systemic delivery of viral vectors will prime the immune system to generate large quantities of neutralizing antibodies upon concomitant exposure, even under an immunosuppressive regimen.[24]

Table 1: **Comparison of the main properties, advantages and disadvantages of commonly used viral vectors.** References of current examples are given for future reading.

Vector type	Packaging capacity	Diameter	Genome type	Advantages	Disadvantages	Current examples
AAV	$<$ 4.4 kB	20 − 22 nm	ssDNA	Large variety of target tissues, low immuno-genicity on first injection	Low packaging capacity	25
AV	$>$ 8 kB	80 − 100 nm	dsDNA	Large packaging capacity, transient Cas expression	Pre-existing antibodies, high immuno-genicity	26
LV	$<$ 8.5 kB	80 − 120 nm	ssRNA	Large packaging capacity	Potential insertional mutagene-sis	18–21

Non-Viral Delivery Methods

The disadvantages of viral systems, such as a limited packaging capacity and immune activation, have led to the development of synthetic delivery vectors. Synthetic materials are often well characterized and controlled, do not rely on a viral genome and are tunable through chemical modification. Notable properties have been summarized in Fig. 2. Disadvantages include possible problematical biocompatibility and toxicity, immunogenic potential, and problems with therapeutic cargo release. A variety of materials can be used to create these particles and address these problems, some efforts of which will be discussed here.

The simplest synthetic delivery method is by direct conjugation of an excipient molecule to an active substance. This can, for example, be done by conjugation of cell-penetrating peptides (CPPs) to gRNA and Cas protein. By doing so, Ramakrishna et al have shown effective gene editing in HEK293T cells. The conjugation lead to 6.2% editing efficacy for RNP and 7.2% for plasmids, measured by knock-out of a reporter gene. However, it is unlikely that these CPP conjugates will circumvent all delivery barriers outlined in the introduction.[25] Sophisticated delivery platforms such as nanoparticles can be engineered to do just that. Lipid materials are well characterized to create nanocarrier systems. Recent development of liposomal systems has given rise to lipid nanoparticles (LNP) based on ionizable cationic lipids, which exhibit a cationic charge in the lowered pH of late endosomes to induce endosomal escape, because of the tertiary amines in their structure.[26] While these LNPs were initially developed for use with RNA interference (RNAi) components such as Onpattro™, they can also be used for CRISPR/Cas delivery.[27]
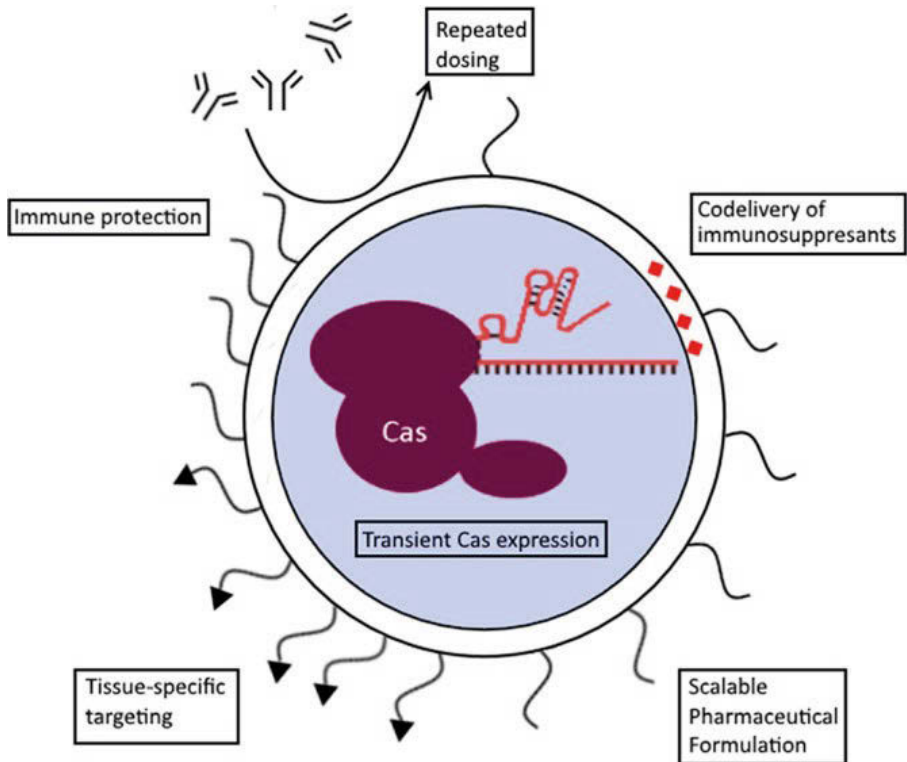
Figure 2: **Advantages of synthetic vectors for CRISPR/Cas delivery using a lipid nanoparticle as example.** The active RNP complex can be encapsulated by synthetic vectors, leading to a transient expression of the Cas protein. Addtionally, there is less risk of immune activation compared to viral vectors which allows for repeated dosing regimens, to potentially achieve cumulative gene editing.[28] Most particles incorporate an inert component which shields the particle from immune detection, such as polyethylene glycol (PEG). These chains can be functionalized to target specific tissues or cells of interest using targeting ligands. Other cargoes can be co-delivered as well, such as immune suppresant drugs. Finally, the chemical nature of the particle formation and modification allows for upscaling of the pharmaceutical production compared to biological production methods for viral particles.

One such application was examined by Wang et al. Briefly they show that using biodegradable cationic lipid nanoparticles, one can deliver CRISPR/Cas RNP into cells and induce effective gene knock-out.[29] The use of a disulfide chain in the lipid would then act as a release mechanism by leading to degradation of the particle in the endosome, which may also contribute to endosomal release.[30] An example of *in vivo* delivery of CRISPR/Cas is the LNP platform developed by Finn et al. They used an ionizable lipid along with cholesterol, DSPC and a PEGylated lipid to create nanoparticles for delivery of Cas9 mRNA and sgRNA to rat livers. They targeted the gene for transthyretin, after which they showed a decrease of >97% of serum transthyretin levels.[28] Interestingly they demonstrated that multiple injections with these LNPs with weekly or monthly intervals led to cumulative gene editing. This will be relevant for correcting genetic defects that require high levels of gene correction in order to revert the disease phenotype. A comparison of the mentioned cationic lipids has been given in Fig. 3.

Polymer based particles can be used for CRISPR/Cas delivery in a similar manner as lipids. Materials which have been used for delivery of other nucleic acids have also been investigated for CRISPR/Cas delivery. Cationic polymers such as polyethyleneimine (PEI) can be complexed to nucleic acids and can induce endosomal uptake and release, similarly to cationic lipids. Zhang et al. have for example formulated particles consisting of PEI-β-cyclodextrin to deliver plasmids coding for sgRNA and Cas9 in HeLa cells, achieving gene knock-out.[31] Sun et al. have also used PEI in their formulation, in which they utilized DNA as a nanomaterial for encapsulation of CRISPR/Cas vectors. These particles were coated by PEI to improve endosomal release. They injected these particles directly into tumors expressing EGFP in mice and found phenotypes exhibiting efficient EGFP knock-out.[32] Dendrimeric structures of poly(amido-amine) (PAMAM) can also be used for transfection. These particles consist of a core, from which the polymer branches and they exhibit cationic primary amines on their surface, which can complex to nucleic acids. Kretzmann et al. for example
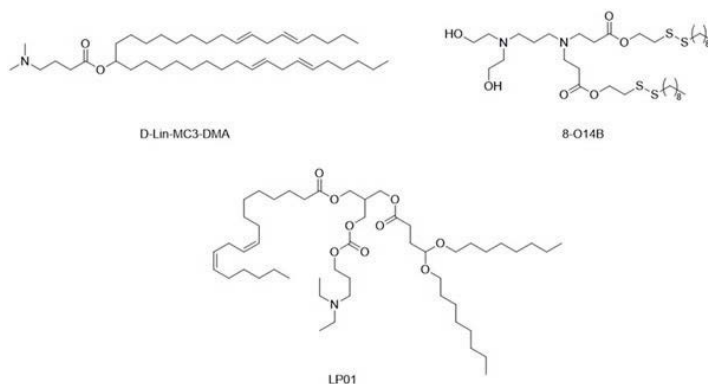
Figure 3: **Key lipid structures of the formulations in the main text.** D-Lin-MC3-DMA and LP01 are ionizable lipids used in Onpattro™ and the formulation of Finn et al respectively.[31] 8-O14B is the biodegradable cationic lipid outlined by Wang et al.[32]

used dendrimers to deliver CRISPR/dCas9 plasmids to MCF-7, a human breast adenocarcinoma cell line. They showed effective transfection while maintaining low cytotoxicity.[33]

Inorganic materials are currently being studied to encapsulate CRISPR/Cas components as well. Alsaiari et al. have for example formulated a network based on zinc to aid crosslinking of imidazole. The low pH of late endosomes would then, after uptake, result in cationic charges due to dissolution of the zeolitic imidazole frameworks (ZIF), after which the CRISPR-Cas components are released into the cytosol. These ZIFs have been used to successfully deliver Cas9-based RNPs into CHO cells. They showed endosomal release of the RNP's and cell viability for at least 12 hours after transfection.[34] Lee et al. showed successful delivery of RNP and HDR template using colloidal gold nanoparticles in a mouse model for the treatment of Duchenne muscular dystrophy. They induced HDR to repair a single nucleotide mutation which caused knock-out of the active dystrophin. They showed that 5.4% of expression was restored compared to the expression in wild-type mice, which was sufficient to

restore the musculature to a healthy phenotype.[35]

The main properties and stage of development of the described formulations have been summarized in table 2. In addition it is poorly understood how an HDR template can be delivered into nuclei using synthetic vectors, especially for slow or nondividing cells where the nuclear envelope is rarely or not disrupted for mitosis. Viral vectors are innately able to do so and often exploit active transport pathways through the nuclear pore complex. A mixture of particles containing different cargo may be used to overcome these issues. One example is the combination of LNPs for delivery of Cas9 mRNA along with an AAV containing both sgRNA and HDR template sequences. The rationale is that the sgRNA and HDR template are needed in the nucleus while the mRNA is needed in the cytosol. Yin et al. showed successful delivery and phenotypic repair in a knock-out mouse model of hereditary tyrosinemia type I.[36] This example shows promise for the utilization of multiple particles *in vivo* for liver targeting. A disadvantage of such an approach is the requirement of uptake of both particles into the same tissue at roughly the same time to ensure intracellular RNP formation and HDR-mediated repair.

For direct *in vivo* application, current trends seem to favor use of synthetic particles to deliver the CRISPR/Cas components either as mRNA or as RNP complexes. Lipid, polymeric, and inorganic particles have all been tested *in vivo* and seem able to deliver CRISPR/Cas components. Of these, LNP based formulations seem the most promising for *in vivo* gene delivery as their low toxicity was already examined for siRNA formulations earlier. Currently the most advanced CRISPR/Cas study has been performed by Finn et al using LNPs in mice, which targets the liver. This tissue exhibits fenestrated capillary endothelia, through which the LNPs can pass. In addition to this passive targeting, these LNPs are opsonized by apolipoprotein E in the bloodstream which then acts as a targeting ligand due to overexpression of the low density lipoprotein receptor on hepatocytes.[37] More research needs to be done examining other

target tissues to confirm if LNP based delivery is more generally applicable and can achieve the desired effects in a clinical setting.

Table 2: **Summary of the specific synthetic delivery systems outlined in the main text.** The cargo formats and some advantages and disadvantages are given.

Particle material	Investigated cargo format	Reported advantages	Reported stage of development	Route of administration	References
Cationic lipids	RNP	High endosomal escape, biodegradable	*In vivo* reporter model in mouse brain	Intravenous	29
Ionizable lipids (LNP)	mRNA	Cumulative gene editing upon repeated dosing *in vivo*	*In vivo* disease model for tyrosinemia	Intravenous	26,28
PEI polyplexes	Plasmid DNA	Easily characterizable	*In vitro*	Not yet applicable	36

Table 2: **Continuation of Table 2.**

Particle material	Investigated cargo format	Reported advantages	Reported stage of development	Route of administration	References
β coated DNA nano-clews	Plasmid DNA	High efficacy upon local administration in a reporter system	*In vivo* reporter model	Intratumoral injection	37
PAMAM dendrimers	Plasmid DNA	High loading efficiency	*In vitro*	Not yet applicable	38
ZIF-8	RNP	High loading capacity, biodegradable	*In vitro*	Not yet applicable	39
CRISPR Gold	RNP	Low immunogenicity locally, *in vivo* proof of concept in relevant disease model (Duchenne's muscular dystrophy)	*In vivo* disease model for Duchenne's muscular dystrophy	Intramuscular	40

Immune Responses and Immunogenicity

Since the CRISPR system is of bacterial origin, an immune reaction against one of its components is likely to occur when it is administered for direct *in vivo* genome editing.38 Moreover, the type of delivery vector used may fortify this immune response and should therefore be carefully chosen. The mode of delivery (e.g., as gene construct, mRNA, or RNP) will also influence the overall immunogenicity of the gene editing system as longevity of Cas protein expression generally favors antigen presentation and thus potential activation of adaptive immune responses.[39,40]

A distinction should be made between innate and adaptive immune responses. Innate immune responses can be triggered by the nucleic acid cargo, especially when formulated in as nanoparticles.[41] It has been reported that exogenous mRNA as well as siRNA delivered by lipid nanoparticles activate innate immune responses through activation of various pattern recognition receptors, specifically toll-like receptors. Pseudouridine modification of the *in vitro* transcribed mRNA or 2'OMe or 2'MOE modifications of the siRNA can ameliorate such responses. Furthermore, CRISPR guide RNAs consist of hairpins that are known to be good activators of such receptors, like TLR3, PKR, and RIG-I. This should be considered when CRISPR/Cas components are delivered as mRNA or ribonucleoproteins. Pharmacological inhibition of these innate immune responses would be an option to prevent undesired immunological effects against CRISPR/Cas.[42–44] For example, toll-like receptor antagonists or drugs inhibiting the downstream signaling pathways (e.g., NfkB or MyD88) could help in dampening innate immune responses against CRISPR/Cas components, although full inhibition of immune responses is most likely difficult to achieve.

Adaptive responses can be directed against the Cas protein or against components of the delivery system. Viral vectors (in particular adenoviral vectors) are immunogenic, especially at the high doses that are often needed for effective transduction in humans.[42–44] Synthetic

vectors can also mount adaptive immune responses. For lipid-based systems with grafted PEG polymers to enhance circulation times, anti-PEG antibodies have been described although clinical effects of such antibodies are under dispute.[45,46] Antivector antibodies may prevent repeated dosing to boost the overall level of gene editing that may be needed for a therapeutic effect.

Adaptive immune responses against the Cas proteins are common. In fact, several studies have demonstrated that both anti-Cas antibodies and Cas-specific cellular responses pre-exist in the human population due to exposure via the microbiome.[47–49] This pre-existing immunity has important implications for clinical applications of CRISPR/Cas as it may influence the effectiveness of the gene editing therapy but may also cause serious safety problems. Antibody-responses can be partly mitigated by mRNA delivery of Cas instead of RNPs or by encapsulation of the Cas RNP into nanocarriers to shield the immunogenic protein from neutralizing antibodies. Conversely, Cas proteins could be immuno-engineered to remove B and T cell epitopes without losing activity or one could revert to Cas variants from microorganisms that are not common to humans, such as the recently discovered CasX.[50] Such strategies would at most lead to reduction rather than elimination of immunogenicity. More troublesome are the cellular responses that could potentially lead to cell killing after gene correction, thereby nullifying the therapeutic effect. Like gene therapy with viral vectors, CRISPR/Cas will most likely require coadministration of immunosuppressants, a proven method to prevent immune responses against often very immunogenic proteins. The downside is that most immunosuppressant regimens are systemic, resulting in an increased vulnerability of the patient against infectious diseases during treatment. Recent developments in antigen-specific tolerization might be further explored to avoid the need of systemic immunosuppression.[51]

Off Target Events and the Influence of Cargo Format

While the on-target efficiency of therapeutic gene editing is important to optimize, we also need to recognize the risk of gene editing outside the target locus. This can potentially lead to gene knockout of other genes. Several bioinformatic tools predict off-target sites based on homology to the target sequence, which can be used to choose sgRNA with minimal off-target effects, for example the Cas-OFFinder tool.[52] Occurred off-target events can be confirmed experimentally in a biased (based on predicted off-target sites) or unbiased (whole genome) manner.[53,54] The variety of techniques can make direct comparisons between experiments difficult, as there are conflicting variables, such as sensitivity and different on-target efficiencies, between experiments. In addition, the choice of Cas protein is significant to reduce off-target events. For example, Shen et al. have shown reduced generation of off-target events using Cas9 nickases in mice, possibly due to the requirement of two cleavage events instead of one.[6] In addition, Anderson et al. have shown, for example, that using higher fidelity Cas proteins significantly reduce the generation of off-target editing events.[55] Guide RNAs can be engineered as well, to improve targeting specificity by chemical or structural modifications and DNA replacements. Modifications such as phosphorothiolates to the ribose-phosphate backbone of gRNA have been shown to improve editing efficiency on-target.[56,57] Internal 2'-O-methyl-3'-phosphonacetate modifications lead to fewer off-target events.[57] Additionally, Yin et al. demonstrated that partial replacement of RNA nucleotides with DNA nucleotides can lead to higher on-target efficiency and reduce off-target cleavage.[58]

To theoretically reduce the risk of off-target events, one can minimize the exposure time to the active RNP complex. This can, for example, be achieved by fusing Cas9 to a FKBP12-like domain, which marks Cas9 for intracellular degradation unless a specific ligand is bound to that domain. This ligand can then be co-delivered, which achieves a period of Cas9 activity while also lowering the half-life.[18,19] Alterna-

tively, the CRISPR/Cas complex can be directly inhibited by the peptide AcrllA4, which is able to bind active RNP complexes and directly compete on the PAM recognition site. Using this inhibitory peptide, Shin et al. have shown that there is an ideal time window for Cas9 with mostly on target cutting in the first 6 h followed by off-target events later on.[59] The exposure time can also be lowered by choosing more transiently active cargo formats. Kim et al. showed that treatment with RNPs reduced the generation of off-target mutations up to 10-fold compared to delivered plasmids coding for Cas9 and sgRNA. They also showed that Cas9 exhibits a maximum activity after 1 day of exposure when delivered as RNP compared to 3 days when delivered as plasmid, proposing that these kinetic differences contribute to the perceived off-target frequencies.60 Kouranova et al. compared Cas9 delivered as protein, DNA vector, or mRNA along with sgRNA in two cell lines. They found the highest on-target efficiency and lowest off-target events in normal cells treated with RNPs or cells stably expressing Cas9 treated with sgRNA.61 Finally, Lattanzi et al. showed by using a deep-sequencing assay on known off-target sites that a lentiviral vector produced more off-target editing compared to mRNA, plasmid, or RNP delivery, while not reaching the same on-target effects as RNP or mRNA delivery.[21]

Based on the current body of data, delivery of RNPs using bioinformatics inspired sgRNA design and an optimized Cas protein seems to be the most rational method to minimize the risk of off-target effects. However, the influence of exposure time and dose-dependency on off-target editing needs further elucidation, preferably using unbiased whole-genome screening. In addition, the main focus in the literature is on the off-target editing events in targeted cells. The unwanted targeting of other cells can also be considered as off-target events, even if the genomic target is correct. This can be caused by usage of viral vectors with an undesired tropism, or by the poor ability of synthetic vectors to target certain cell types. For example, the majority of synthetic vectors are accumulated in the liver and spleen after intravenous injection and this may not be desired if a genetic disease is manifested

outside these organs.

Concluding Remarks

CRISPR/Cas genome editing is less than a decade old but has already reached the stage of clinical development. CTX001 from CRISPR Therapeutics and Vertex Pharma is the first *ex vivo* CRISPR therapy for beta thalassemia in clinical development and more are ongoing in China. These initial applications of CRISPR/Cas in the clinic are treating diseases in which the affected cells are readily accessible and can be edited *ex vivo*. This avoids the ongoing challenge of tissue and cell type specific delivery *in vivo* and mitigates two main hurdles that CRISPR/Cas systems are currently facing: immunogenicity and off-target editing effects. These pioneering clinical trials are being watched with much anticipation but may also reveal some unanticipated side effects. While every effort is being taken to ensure effectiveness and safety, such potential side effects can only be disclosed by performing human trials.

The ultimate goal would be to cure debilitating (mono)genetic diseases with a single injection of CRISPR/Cas. We are still far from this goal and to achieve this several shortcomings of the CRISPR/Cas system need to be addressed.

First, we should have better insights into the frequency and clinical impact of off-target events. Although the algorithms to predict off-target sites are getting better over time, as well as the design of the gRNAs, unbiased whole genome approaches have revealed several sites that have remained under the radar of such algorithms. Additionally, the clinical consequences of such off-target mutagenesis are unclear. Engineering Cas proteins to make them more potent to specific sites or to induce point mutations without the need of introducing double strand breaks are being explored and may in fact be the way forward for safe gene editing. Another approach to increase the on-target/off-target ratio is to reduce exposure time of the genomic DNA to Cas

proteins. Prolonged expression seems to favor increased off-target frequency and strategies to limit or control exposure times are being explored. Moreover, targeted delivery is also crucial to limit unnecessary exposure of nontarget tissue to the Cas nucleases. Although we are still far from such a magic bullet, several delivery systems have been developed that show good targeting to hepatocytes in the liver. As such it is expected that the first applications of direct *in vivo* genome editing will focus on liver diseases in which gene knockout is enough to revert the disease phenotype. With all of these potential reductions of off-target events in mind, it will still be nearly impossible to fully eliminate the probability of off-target events, let alone prove that no off-target events have occurred.

By far the biggest hurdle for widespread *in vivo* application of CRISPR/Cas is the immunogenicity of the CRISPR/Cas components. Although encapsulation of the components in nanocarrier systems might temporarily cause protection against antibody binding and neutralization, eventually the components need to be released to exert their gene editing action. Cellular responses against cells expressing Cas9 have been described, which pose a serious threat to the success and safety of *in vivo* gene editing. Strategies to mitigate such immune responses, including coadministration of immunosuppressive drugs, should therefore be explored.

Despite the challenging tasks ahead, the first steps toward direct *in vivo* application of CRISPR/Cas gene editing have been made and the preclinical results look promising. Intellia Therapeutics has developed a lipid nanoparticle (LNP) platform for the delivery of CRISPR/Cas to the liver, in particular to hepatocytes. With their delivery platform they have reached >97% knock down of serum transthyretin (TTR) levels in healthy mice with a single injection. Moreover, knock down was effective for at least one year.[28]

These encouraging results will spur other *in vivo* applications with CRISPR/Cas. One that might be very interesting is the targeted integration of gene expression constructs for long-term *in situ* expression

of biopharmaceuticals. Increasing numbers of patients require lifelong treatment with biopharmaceuticals that often need frequent injections either i.v. or s.c. Examples are anti-TNF alpha antibody therapies and enzyme replacement therapies. These treatments are expensive and inconvenient for the patient. Targeted insertion of gene constructs in long-lived liver hepatocytes could in principle provide prolonged (up to years) expression without the need of frequent injections. However, this will only become a reality in case we can fully guarantee the safety of *in vivo* genome editing. Whatever the application, it is important to balance the medical benefit with the risks that come from the treatment. With this in mind, it is likely that CRISPR will eventually realize its potential to cure a wide range of diseases.

Acknowledgements

References

1. Doudna, J. A. & Charpentier, E. The new frontier of genome engineering with CRISPR-Cas9. Science **346**, (2014).

2. Zetsche, B. et al. Cpf1 Is a Single RNA-Guided Endonuclease of a Class 2 CRISPR-Cas System. Cell **163**, 759–771 (2015).

3. Ran, F. A. et al. In vivo genome editing using Staphylococcus aureus Cas9. Nature **520**, 186–191 (2015).

4. Oude Blenke, E., Evers, M. J. W., Mastrobattista, E. & van der Oost, J. CRISPR-Cas9 gene editing: Delivery aspects and therapeutic potential. J. Control. Release **244**, 139–148 (2016).

5. Wu, W. Y., Lebbink, J. H. G., Kanaar, R., Geijsen, N. & van der Oost, J. Genome editing by natural and engineered CRISPR-associated nucleases. Nat. Chem. Biol. **14**, 642–651 (2018).

6. Shen, B. et al. Efficient genome modification by CRISPR-Cas9 nickase with minimal off-target effects. Nat. Methods **11**, 399–402 (2014).

7.   Foss, D. V., Hochstrasser, M. L. & Wilson, R. C. Clinical applications of CRISPR-based genome editing and diagnostics. Transfusion **59**, 1389–1399 (2019).

8.   Salsman, J., Masson, J.-Y., Orthwein, A. & Dellaire, G. CRISPR/Cas9 Gene Editing: From Basic Mechanisms to Improved Strategies for Enhanced Genome Engineering In Vivo. Curr. Gene Ther. **17**, (2018).

9.   Sürün, D., von Melchner, H. Schnütgen, F. CRISPR/Cas9 genome engineering in hematopoietic cells. Drug Discov. Today Technol. **28**, 33–39 (2018).

10.   Xu, W. Microinjection and Micromanipulation: A Historical Perspective. in 1–16 (2019).

11.   Hung, K. L. et al. Engineering Protein-Secreting Plasma Cells by Homology-Directed Repair in Primary Human B Cells. Mol. Ther. **26**, 456–467 (2018).

12.   Hui, S.-W. Overview of Drug Delivery and Alternative Methods to Electroporation BT - Electroporation Protocols: Preclinical and Clinical Gene Medicine. In Electroporation Protocols. Methods Mol. Biol. pp 91-107 (2008).

13.   Yen, J. et al. TRIAMF: A New Method for Delivery of Cas9 Ribonucleoprotein Complex to Human Hematopoietic Stem Cells. Sci. Rep. **8**, 16304 (2018).

14.   D'Astolfo, D. S. et al. Efficient Intracellular Delivery of Native Proteins. Cell **161**, 674–690 (2015).

15.   Tabebordbar, M. et al. In vivo gene editing in dystrophic mouse muscle and muscle stem cells. Science **351**, 407–411 (2016).

16.   Zetsche, B., Volz, S. E. & Zhang, F. A split-Cas9 architecture for inducible genome editing and transcription modulation. Nat. Biotechnol. **33**, 139–142 (2015).

17.   Wang, D. et al. Adenovirus-Mediated Somatic Genome Editing of Pten by CRISPR/Cas9 in Mouse Liver in Spite of Cas9-Specific Immune Responses. Hum. Gene Ther. **26**, 432–442 (2015).

18.   Banaszynski, L. A., Chen, L., Maynard-Smith, L. A., Ooi, A. G. L. & Wandless, T. J. A Rapid, Reversible, and Tunable Method to Regulate Protein Function in Living Cells Using Synthetic Small Molecules. Cell **126**, 995–1004 (2006).

19.   Senturk, S. et al. Rapid and tunable method to temporally control gene editing based on conditional Cas9 stabilization. Nat. Commun. **8**, 14370 (2017).

20.   Shin, J., Lee, N., Cho, S. & Cho, B.-K. Targeted Genome Editing Using DNA-Free RNA-Guided Cas9 Ribonucleoprotein for CHO Cell Engineering. in 151–169 (2018).

21.   Lattanzi, A. et al. Optimization of CRISPR/Cas9 Delivery to Human Hematopoietic Stem and Progenitor Cells for Therapeutic Genomic Rearrangements. Mol. Ther. **27**, 137–150 (2019).

22.   Merienne, N. et al. The Self-Inactivating KamiCas9 System for the Editing of CNS Disease Genes. Cell Rep. **20**, 2980–2991 (2017).

23.   Miesbach, W. et al. Gene therapy with adeno-associated virus vector 5–human factor IX in adults with hemophilia B. Blood **131**, 1022–1031 (2018).

24.   van Haasteren, J., Hyde, S. C. & Gill, D. R. Lessons learned from lung and liver in-vivo gene therapy: implications for the future. Expert Opin. Biol. Ther. **18**, 959–972 (2018).

25.   Ramakrishna, S. et al. Gene disruption by cell-penetrating peptide-mediated delivery of Cas9 protein and guide RNA. Genome Res. **24**, 1020–1027 (2014).

26.	Patel, S. et al. Boosting Intracellular Delivery of Lipid Nanoparticle-Encapsulated mRNA. Nano Lett. **17**, 5711–5718 (2017).

27.	Thi, E. P. et al. siRNA rescues nonhuman primates from advanced Marburg and Ravn virus disease. J. Clin. Invest. **127**, 4437–4448 (2017).

28.	Finn, J. D. et al. A Single Administration of CRISPR/Cas9 Lipid Nanoparticles Achieves Robust and Persistent In Vivo Genome Editing. Cell Rep. **22**, 2227–2235 (2018).

29.	Wang, M. et al. Efficient delivery of genome-editing proteins using bioreducible lipid nanoparticles. Proc. Natl. Acad. Sci. **113**, 2868–2873 (2016).

30.	Chang, J. et al. Integrating Combinatorial Lipid Nanoparticle and Chemically Modified Protein for Intracellular Delivery and Genome Editing. Acc. Chem. Res. **52**, 665–675 (2019).

31.	Zhang, Z. et al. Cationic Polymer-Mediated CRISPR/Cas9 Plasmid Delivery for Genome Editing. Macromol. Rapid Commun. **40**, 1800068 (2019).

32.	Sun, W. et al. Self-Assembled DNA Nanoclews for the Efficient Delivery of CRISPR-Cas9 for Genome Editing. Angew. Chemie Int. Ed. **54**, 12029–12033 (2015).

33.	Kretzmann, J. A. et al. Synthetically controlling dendrimer flexibility improves delivery of large plasmid DNA. Chem. Sci. **8**, 2923–2930 (2017).

34.	Alsaiari, S. K. et al. Endosomal Escape and Delivery of CRISPR/Cas9 Genome Editing Machinery Enabled by Nanoscale Zeolitic Imidazolate Framework. J. Am. Chem. Soc. **140**, 143–146 (2018).

35.	Lee, K. et al. Nanoparticle delivery of Cas9 ribonucleoprotein and donor DNA in vivo induces homology-directed DNA repair. Nat. Biomed. Eng. **1**, 889–901 (2017).

36.	Yin, H. et al. Therapeutic genome editing by combined viral and non-viral delivery of CRISPR system components in vivo. Nat. Biotechnol. **34**, 328–333 (2016).

37.	Akinc, A. et al. Targeted delivery of RNAi therapeutics with endogenous and exogenous ligand-based mechanisms. Mol. Ther. **18**, 1357–1364 (2010).

38.	Chew, W. L. Immunity to CRISPR Cas9 and Cas12a therapeutics. Wiley Interdiscip. Rev. Syst. Biol. Med. **10**, 1–23 (2018).

39.	Karikó, K. et al. Incorporation of Pseudouridine Into mRNA Yields Superior Nonimmunogenic Vector With Increased Translational Capacity and Biological Stability. Mol. Ther. **16**, 1833–1840 (2008).

40.	Broering, R. et al. Chemical modifications on siRNAs avoid Toll-like-receptor-mediated activation of the hepatic immune system in vivo and in vitro. Int. Immunol. **26**, 35–46 (2014).

41.	Kedmi, R., Ben-Arie, N. & Peer, D. The systemic toxicity of positively charged lipid nanoparticles and the role of Toll-like receptor 4 in immune activation. Biomaterials **31**, 6867–6875 (2010).

42.	Colamonici, O. R., Domanski, P., Sweitzer, S. M., Larner, A. & Buller, R. M. L. Vaccinia Virus B18R Gene Encodes a Type I Interferon-binding Protein That Blocks Interferon Transmembrane Signaling. J. Biol. Chem. **270**, 15974–15978 (1995).

43.   Kanzler, H., Barrat, F. J., Hessel, E. M. & Coffman, R. L. Therapeutic targeting of innate immunity with Toll-like receptor agonists and antagonists. Nat. Med. **13**, 552–559 (2007).

44.   Bhattacharyya, S. et al. Pharmacological Inhibition of Toll-Like Receptor-4 Signaling by TAK242 Prevents and Induces Regression of Experimental Organ Fibrosis. Front. Immunol. **9**, (2018).

45.   Hsieh, Y.-C. et al. Pre-existing anti-polyethylene glycol antibody reduces the therapeutic efficacy and pharmacokinetics of PEGylated liposomes. Theranostics **8**, 3164–3175 (2018).

46.   Grenier, P., Viana, I. M. de O., Lima, E. M. & Bertrand, N. Anti-polyethylene glycol antibodies alter the protein corona deposited on nanoparticles and the physiological pathways regulating their fate in vivo. J. Control. Release **287**, 121–131 (2018).

47.   Simhadri, V. L. et al. Prevalence of Pre-existing Antibodies to CRISPR-Associated Nuclease Cas9 in the USA Population. Mol. Ther. - Methods Clin. Dev. **10**, 105–112 (2018).

48.   Charlesworth, C. T. et al. Identification of preexisting adaptive immunity to Cas9 proteins in humans. Nat. Med. **25**, 249–254 (2019).

49.   Wagner, D. L. et al. High prevalence of Streptococcus pyogenes Cas9-reactive T cells within the adult human population. Nat. Med. **25**, 242–248 (2019).

50.   Liu, J.-J. et al. CasX enzymes comprise a distinct family of RNA-guided genome editors. Nature **566**, 218–223 (2019).

51.   Lübbers, J., Rodríguez, E. & van Kooyk, Y. Modulation of Immune Tolerance via Siglec-Sialic Acid Interactions. Front. Immunol. **9**, (2018).

52.   Bae, S., Park, J. & Kim, J.-S. Cas-OFFinder: a fast and versatile algorithm that searches for potential off-target sites of Cas9 RNA-guided endonucleases. Bioinformatics **30**, 1473–1475 (2014).

53.   Hendel, A., Fine, E. J., Bao, G. & Porteus, M. H. Quantifying on- and off-target genome editing. Trends Biotechnol. **33**, 132–140 (2015).

54.   Martin, F., Sánchez-Hernández, S., Gutiérrez-Guerrero, A., Pinedo-Gomez, J. & Benabdellah, K. Biased and Unbiased Methods for the Detection of Off-Target Cleavage by CRISPR/Cas9: An Overview. Int. J. Mol. Sci. **17**, 1507 (2016).

55.   Anderson, K. R. et al. CRISPR off-target analysis in genetically engineered rats and mice. Nat. Methods **15**, 512–514 (2018).

56.   Li, B., Zeng, C. & Dong, Y. Design and assessment of engineered CRISPR–Cpf1 and its use for genome editing. Nat. Protoc. **13**, 899–914 (2018).

57.   Ryan, D. E. et al. Improving CRISPR–Cas specificity with chemical modifications in single-guide RNAs. Nucleic Acids Res. **46**, 792–803 (2018).

58.   Yin, H. et al. Partial DNA-guided Cas9 enables genome editing with reduced off-target activity. Nat. Chem. Biol. **14**, 311–316 (2018).

59.   Shin, J. et al. Disabling Cas9 by an anti-CRISPR DNA mimic. Sci. Adv. **3**, (2017).

60.   Kim, S., Kim, D., Cho, S. W., Kim, J. & Kim, J.-S. Highly efficient RNA-guided genome editing in human cells via delivery of purified Cas9 ribonucleoproteins. Genome Res. **24**, 1012–1019 (2014).

61.   Kouranova, E. et al. CRISPRs for Optimal Targeting: Delivery of CRISPR Components as DNA, RNA, and Protein into Cultured Cells and Single-Cell Embryos. Hum. Gene Ther. **27**, 464–475 (2016).

3

Impact of Formulation Conditions on Lipid Nanoparticles Characteristics and Functional Delivery of CRISPR RNP for Gene Knock-Out and Correction

Johanna Walther[*], Danny Wilbie[*], Vincent S. J. Tissingh, Mert Öktem, Heleen van der Veen, Bo Lou, Enrico Mastrobattista

Department of Pharmaceutics, Utrecht Institute for Pharmaceutical Sciences (UIPS), Utrecht University, The Netherlands

[*] equally contributed

Chapter 3.   Impact of Formulation Conditions on Lipid Nanoparticles Characteristics and Functional Delivery of CRISPR RNP for Gene Knock-Out and Correction

Abstract

The CRISPR-Cas9 system is an emerging therapeutic tool with the potential to correct diverse genetic disorders. However, for gene therapy applications, an efficient delivery vehicle is required, capable of delivering the CRISPR-Cas9 components into the cytosol of the intended target cell population. In this study, we optimized the formulation conditions of lipid nanoparticles (LNP) for delivery of ready-made CRISPR-Cas9 ribonucleic protein (RNP). The buffer composition during complexation and relative DOTAP concentrations were varied for LNP encapsulating in-house produced Cas9 RNP alone or Cas9 RNP with additional template DNA for gene correction. The LNP were characterized for size, surface charge, and plasma interaction through asymmetric flow field flow fractionation (AF4). Particles were functionally screened on fluorescent reporter cell lines for gene knock-out and gene correction. This revealed incompatibility of RNP with citrate buffer and PBS. We demonstrated that LNP for gene knock-out did not necessarily require DOTAP, while LNP for gene correction were only active with a low concentration of DOTAP. The AF4 studies additionally revealed that LNP interact with plasma, however, remain stable, whereby HDR template seems to favor stability of LNP. Under optimal formulation conditions, we achieved gene knock-out and gene correction efficiencies as high as 80% and 20%, respectively, at nanomolar concentrations of the CRISPR-Cas9 RNP.

Introduction

The clustered regularly interspaced short palindromic repeats (CRISPR) associated (Cas) endonuclease proteins, such as Cas9, have emerged in recent years as a viable therapeutic option for genetic diseases. The Cas9 endonuclease was first identified as a bacterial defense mechanism against viral infections and has been repurposed into a powerful tool to cleave DNA in an RNA-guided fashion in various cell types. The Cas9 protein, together with a guide RNA molecule, forms an active ribonucleoprotein (RNP) complex.[1] DNA cleavage is mediated by recognition of a 20-nucleotide sequence between the guide RNA and the host DNA, which hybridizes and allow the nuclease to attach to its DNA target. Additionally, the presence of a protospacer-adjacent motif in the host DNA is necessary to facilitate the conformational change in the nuclease to introduce a double strand break in its target.[2] When the genomic DNA is cleaved by the Cas9 enzyme, the host DNA-damage repair response is activated.[3] In mammalian cells, the most prominent pathways are the canonical non-homologous end-joining (c-NHEJ) pathway, the microhomology-mediated end joining (MMEJ) pathway, and homology-directed repair (HDR).[4] C-NHEJ and MMEJ are notably error-prone repair mechanisms, both of which can lead to formation of small insertions and deletions in the target gene. This, in turn, may lead to gene knock-out, which is therapeutically relevant for gene therapy of diseases caused by gain-of-function mutations.[5–7] HDR is mostly active in the G2/S phases of mitosis in dividing cells, and in the presence of a homologous DNA template, this pathway can lead to precise DNA repair of disrupted genes.[8] Especially, the latter signifies potential for gene therapy, thereby curing diseases by editing and correcting the genetic mutations.

Direct *in vivo* gene editing requires the delivery of the CRISPR-Cas9 components into the correct target cells' nuclei.[9] SpCas9, a Cas9 protein derived from *Streptococcus pyogenes*, is currently under clinical investigation for both *ex vivo* and direct *in vivo*

therapeutic applications.[10–12] Examples include subretinal injection of adeno-associated viral vectors encoding the CRISPR-Cas9 components for the treatment of Leber congenital amaurosis, and delivery of CRISPR-Cas9 with non-viral particles such as NTLA-2001 for targeted gene editing of hepatocytes for hereditary amyloid transthyretin amyloidosis.[13,14] Lipid nanoparticles (LNP), which employ cationic or ionizable cationic lipids, serve as particularly promising candidates for delivery of the different cargo formats of the CRISPR-Cas9 components.   Since LNP complex their cargo via electrostatic interactions, they are especially suited to formulate polyanionic DNA or RNA molecules, due to their anionic phosphate backbone.   However, the preassembled RNP complex, with or without co-entrapment of a DNA template to drive homology-directed repair, can also be formulated in LNPs, as was recently demonstrated.[13,15–17]

Direct delivery of the pre-assembled RNP has several advantages over Cas9 expressed from DNA or mRNA templates. Since RNP are pre-assembled, they are directly active once inside the nuclei of target cells as opposed to Cas9 expression from DNA or mRNA templates. First, these need to be translated into the endonuclease in the cytosol, and subsequently, find an intact single guide RNA (sgRNA) within the cell in order to become active.[18] Related to this, direct delivery of RNP assures optimal stoichiometry between Cas9 and sgRNA and protects the sgRNA from rapid degradation within the cell.[19] Finally, RNP are short lived inside cells, with a half-life of approximately one day.[20] This limits the likelihood of off-target gene editing which has been shown to be time dependent.[21,22]

Despite these advantages, delivery of RNP has met with several pharmaceutical challenges. The stability of RNP during LNP formulation is an issue. Solely relying on ionizable cationic lipids to mediate electrostatic interactions with the net negatively charged RNP requires an acidic environment. Acidic conditions can however affect RNP stability.[23,24] Therefore, in this study, formulations already used for siRNA or mRNA delivery with C12-200 ionizable lipid were further

developed for delivery of RNP.[23,25] Specifically, formulation conditions must be optimized to find a good balance between RNP functionality, protection from premature clearance, and timely intracellular release. This work sought to explore several of such often overlooked steps in the pharmaceutical formulation of RNP into LNP, which, as shown here, are often critical in determining gene editing efficiency.[23] This includes buffer composition during formulation, as well as lipid composition of LNP for delivering RNP with or without a single stranded DNA (ssDNA) HDR templates. To understand the effects of these parameters, these LNP were characterized based on their size, surface charge, RNP complexation, and activity. Additionally, their stability in human plasma was studied. Lipid nanoparticles complexing RNP and HDR template were investigated on gene editing capacity in fluorescent reporter cell lines suited to read out gene knock-out and specific gene correction, resulting in promising results for *in vivo* gene correction.

Material and Methods

General Reagents

All reagents and chemicals were acquired from Sigma-Aldrich (Zwijndrecht, The Netherlands) unless otherwise specified. 2' O-methyl and phosphorothioate end-modified sgRNA and template DNA sequences were acquired from Sigma-Aldrich (Haverhill, the United Kingdom, sequences given in Supplementary Tables S1 and S3) and stored in RNAse-free Tris EDTA-buffer pH 7.0 (Thermo Fisher, Landsmeer, The Netherlands). Primers for polymerase chain reaction (PCR) were acquired from Integrated DNA Technologies (IDT, Leuven, Belgium), sequence shown in Supplementary Table S2. In addition, 1,1'-((2-(4-(2-((2-(bis(2-hydroxydodecyl)amino)ethyl)(2-hydroxydodecyl)amino)ethyl)-piperazin-1-yl)ethyl)azanediyl)bis(dodecan-2-ol) (C12-200)25 was acquired from CordonPharma (Plankstadt, Germany), 1,2-dioleoyl-sn-glycero-3-phosphoethanolamine (DOPE) from

Lipoid (Steinhausen, Switzerland), Cholesterol and 1,2-dimyristoyl-rac-glycero-3-methoxypolyethylene glycol-2000 (PEG-DMG) from Sigma-Aldrich (Zwijndrecht, The Netherlands), and 1,2-dioleoyl-3-trimethylammonium-propane (DOTAP) from Merck (Darmstadt, Germany).

SpCas9 Protein Production and Purification

SpCas9 with a nuclear localization signal (NLS) was expressed in the LPS-free Clearcoli™ BL21 strain (Lucigen Corporation, Middleton, WI, USA) using pET15_SpCas9_NLS_His plasmid (Addgene #62731).[26] After growth in LB-Miller medium until the OD600 reached 0.55–0.7, protein production was induced with 0.5 mm isopropyl β-d-1-thiogalactopyranoside (IPTG), followed by overnight fermentation at 18 °C. All bacteria were subsequently pelleted by centrifugation and lysed by tip sonication using a 3 mm tip (Bandelin electronic GmbH & Co. KG, Berlin, Germany), in 50 mL of phosphate buffered saline containing 25 mm imidazole on ice. The lysate was subsequently centrifuged, resuspended in the same buffer, and filtered through a 0.45 μM MiniSart filter (Sartorius, Amersfoort, The Netherlands). Immobilized metal affinity chromatography (IMAC) was performed on this lysate using a 1 mL nickel HisTrap HP column (Cytiva, Medemblik, The Netherlands) in combination with the Äkta PURE chromatography system (Cytiva, Medemblik, The Netherlands). A stepwise gradient of imidazole was applied from 25 mM, going up to 100 mM and ending at 250 mM. After collection of all fractions, the eluted SpCas9 was dialyzed twice against storage buffer (final composition of 300 mM NaCl, 0.1 mM EDTA, 10 mm Tris, pH 7.4) at a 1:1000 ratio of sample to dialysate, followed by addition of 8.3% (w/v) glycerol prior to freezing. The samples were snap-frozen in liquid nitrogen and stored at -80 °C after dialysis.

SpCas9 Characterization and Stability Study

The protein size and protein impurities were assessed using sodium dodecyl sulfate polyacrylamide gel electrophoresis (SDS-PAGE). The samples were treated with Laemmli sample buffer containing 12.5 mM dithiothreitol (DTT). The proteins were separated on 4–12%

Bis-Tris gel (Thermo Fisher, Landsmeer, The Netherlands), after which staining was done using the Pierce silver stain kit (Fischer Scientific, Landsmeer, The Netherlands). Gels were imaged in the ChemiDoc Imaging System (Bio-Rad Laboratories B.V, Veenendaal, The Netherlands). The intensity of the gel bands was quantified by densitometry in ImageJ (version 1.52p), to calculate the protein impurities in the SpCas9 samples over time.[27] This assay was repeated periodically to determine the protein stability during 6 months of storage.

To visualize *in vitro* cleaving activity of SpCas9, an in-house optimized activity assay was performed. SpCas9 was first incubated with sgRNA specific for the EGFP gene (Supplementary Table S1) for 10 min at room temperature, at a molar ratio of 1:1 at a concentration of 1 μM. Subsequently, 2 μL of this RNP was mixed with 3 μL Buffer 3.1 10×, (New England Biolabs, Ipswich, MA, USA), 250 ng linearized plasmid DNA containing the enhanced green fluorescent protein (EGFP) locus (pMJ922, Addgene #78312)28, 1 μL Ribolock R1 RNAse inhibitor (Thermo Fisher, Landsmeer, The Netherlands) and filled to 30 μL with nuclease-free water (Thermo Scientific, Landsmeer, The Netherlands). The reaction was completed in 2 h at 37 °C. The samples were treated with 1 μL proteinase K (Thermo Fisher, Landsmeer, The Netherlands) and filled to 30 μL with nuclease-free water (Thermo Scientific, Landsmeer, The Netherlands), and then separated using agarose gel (1%) electrophoresis and visualized with 5 μL Midori Green (Nippon Genetics, Düren, Germany) staining per 100 mL of agarose. SpCas9 activity was calculated by gel densitometry, by determining the area under the curve in ImageJ, and calculating the relative cleaved fraction. This was repeated over the course of one year to determine the protein stability in storage.

Lipid Nanoparticle Formulation
To formulate LNP for gene knock-out (LNP-RNP), sgRNA and Sp-Cas9 were mixed at a 1:1 molar ratio in different formulation buffers (100 mM citrate buffer (pH 4.0), Dulbecco's phosphate buffered saline (PBS) (pH 7.4), 50 mm HEPES buffer (pH 7.4, LNP-RNP [HEPES]),

or nuclease-free water at an RNP concentration of 0.4 μM. Complexation was performed for 15 min at room temperature. Concurrently, the lipids were mixed in ethanol to achieve a total lipid to sgRNA ratio of 40:1 (w/w), resulting in a total lipid weight of 9.6 μg.[23] The lipid components were C12-200, DOPE, cholesterol, PEG-DMG and DOTAP (molar ratio 35:16:46.5:2.5:variable). Different molar ratios of DOTAP were tested to find the optimal amount for complexation with RNP. The RNP and lipids were mixed by pipetting at a volume ratio of 3:1 (18 μL RNP to 6 μL lipids) and incubating for 15 min at room temperature. Subsequently, the formulation was diluted 4 times with PBS to a final RNP molar concentration of 76.9 nM in 100 μL. The formulation steps with exact volumes are shown in Table S4.

LNP carrying RNP and HDR template (LNP-RNP-HDR) were formulated in the same manner in HEPES buffer or nuclease-free water (LNP-RNP-HDR [HEPES] and LNP-RNP-HDR [H2O], respectively), except that the HDR template was added at varying molar ratios of RNP/HDR template (1:2, 1:3.8, 1:5, 1:10 and 1:20) to the RNP complex, prior to complexation with the lipids.

Physical Characterization of Lipid Nanoparticles
LNP were diluted 1.3 times further in 1 × PBS (pH 7.4) for characterization of size and polydispersity index (PDI) through dynamic light scattering (DLS) using a Zetasizer Nano S (Malvern ALV CGS-3, Malvern, UK) (settings: temperature 25 °C, viscosity 0.8872 cP, RI 1.330). The ζ-potential was determined with a Zetasizer Nano Z (Malvern ALV CGS-3, Malvern, UK) after 9 × dilution in 10 mM HEPES buffer at pH 7.4 (settings: temperature 25 °C, viscosity 0.8872 cP, RI 1.330, dielectric constant 78.5). Each sample was measured in triplicate to determine size and ζ-potential two days after formulation.

Quantification of RNP Complexed with LNP
Complexation efficiencies were determined in LNP prepared in the different formulation conditions. RNP at 1.25 μM and a final formulation volume of 0.47 mL in PBS were used. For determination of SpCas9 complexation, the LNP formulation was additionally dialyzed against

1 × HEPES buffered saline (HBS) with Float-A-Lyzer molecular weight cut-off (MWCO) 300 kDa dialysis chambers (Avantor®, Arnhem, The Netherlands) to remove free SpCas9 from the formulation.

Reversed-phase high performance liquid chromatography (HPLC) (Waters Alliance e2695, Milford, MA, USA) was performed to determine the amount of SpCas9 that was complexed with LNP, using an Xbridge protein BEH C4 300 Å column (Waters #186004505) with a linear acetonitrile gradient, from 5% to 100% in 5 min and back again in 1 min, with 10 min of total elution time. The mobile phase additionally contained 0.1% trifluoroacetic acid. The column was heated at 30 °C. Fluorescence detection was set at ex. 280 nm, em. 350 nm (10 pts/s), and the UV-Vis detection was set at 214 and 280 nm (2 pts/s). Samples were treated with 2% Triton X-100 for 5 min before injection. Samples were injected with an injection volume of 50 μL at a flow rate of 1 mL/min. A calibration curve of empty LNP spiked with SpCas9, with a concentration range of 0–300 nM and treated with 2% Triton X-100, was used to quantify the SpCas9 concentration.

The Quant-iTTM RiboGreen® RNA kit (Fisher Scientific, Landsmeer, The Netherlands) was used to determine the complexation efficiency of sgRNA. The protocol provided by the supplier was followed, except that sgRNA was used instead of the RNA standard to generate a calibration curve in RNAse-free TE buffer. A calibration curve with and without 2% Triton X-100 was made in duplicate. LNP samples and the calibration curve that were not treated with 2% Triton X-100 were treated with the same volume of 1 × RNAse-free TE buffer. Fluorescence signal (ex. 485 nm, em. 520 nm) was determined using a Jasco FP8300 Spectrofluorometer with a microwell plate reader (JASCO Benelux BV, De Meern, The Netherlands).

Stability of Lipid Nanoparticles in Human Plasma
The stability of LNP was determined by asymmetric flow field flow fractionation (AF4) measurements using the AF2000 separation system (Postnova Analytics, Landsberg, Germany). The system is equipped

with a degasser, isocratic pumps, auto samples, fractionation channels, and an in-line DLS detector (Zeta Nano ZS, Malvern Instruments, Malvern, UK). For separation, a FFF channel was used with a 350 μm spacer and a regenerated cellulose membrane with a molecular weight cut-off of 10 kDa. PBS was used as mobile phase.

LNP-RNP [HEPES] and LNP-RNP-HDR [HEPES] or LNP-RNP-HDR [H20] were prepared as described above, with a total lipid concentration of 4.4 mM and RNP concentration of 1.6 μM. In addition, 3 μM HDR template was added to the LNP-RNP-HDR formulation. The LNP formulations were not diluted with PBS as described previously, since high concentrations were needed for the AF4 studies. To verify potential destabilizing effects of blood components on the LNP, the nanoparticles were treated with 20% human plasma (#HMPLCIT, BioIVT, West Sussex, UK) and incubated for 1 h at 37 °C. Subsequently, 20 μL were injected at a flow rate of 0.2 mL/min and focused for 4 min with a crossflow of 1.5 mL/min and a focus flow of 1.8 mL/min. After 1 min transition time, the crossflow was kept consistent at 1.5 mL/min for 5 min before it was decreased with a linear decay of 1 to a final cross-flow of 0.5 mL/min over a span of 25 min. Then, the crossflow was decreased with an exponential decay of 0.3 for 30 min until it reached 0 mL/min, at which it was kept constant for 10 min. During the entire run, the detector flow rate was 0.5 mL/min.

Cell Culture
HEK293T stoplight cells and HEK293T cells with stable EGFP expression were cultured in low-glucose DMEM medium supplemented with 10% fetal bovine serum (FBS), at 37 °C and 5% CO_2. The cell lines were both graciously gifted by Dr. Olivier de Jong and constructed as described previously, using the lentiviral plasmids containing the gene of interest (Stoplight construct[29] or EGFP[30]) in a pHAGE2-EF1a-IRES-PuroR or pHAGE2-EF1a-IRES-NeoR backbone, respectively. Alongside these lentiviral plasmids, HEK293T cells were transfected with pMD2.G plasmid, and PSPAX2 plasmid (Addgene #12259 and #12260, respectively) at a 2:1:1 ratio for lentiviral production. Lentiviral supernatant was then used to transduce HEK293T cells. To prevent multi-

ple integrations of the fluorescent reporter constructs, HEK293T cells were transduced using an MOI < 0.1 and subsequently cultured and expanded with their respective selection antibiotics. After 2 weeks, cells were sorted using a BD FACSAria III cell sorter (Becton Dickinson, Franklin Lakes, NJ, USA), after which they were further expanded in the presence of selection antibiotics.

For subculturing between experiments, 1 mg/mL Gibco® Geneticin® Selective Antibiotic (G418 sulfate, Fischer Scientific, Landsmeer, The Netherlands) was supplemented. Cell culture plastics were acquired from Greiner Bio-One (Alphen aan de Rijn, The Netherlands).

Gene Editing Efficacy Assays
HEK293T stoplight cells were plated at a density of 3×105 cells/cm2 on a 96-well black plate (Greiner CellStar #655090). The following day, the cells were treated with 10 μL of LNP-RNP supplemented with 1% antibiotic/antimycotic solution (Sigma-Aldrich, Zwijndrecht, The Netherlands). Cells were washed after 24 h with 100 μL of low-glucose DMEM medium supplemented with 10% FBS and 1% antibiotic/antimycotic solution. The cells were incubated for another 24 h at 37 °C and 5% CO_2. Following this, the cells were treated with 2 μg/mL Hoechst 33342 in complete cell culture medium for 15 min and imaged using a Yokogawa CV7000 Confocal Microscope (Yokogawa Corporation, Tokyo, Japan). The fluorescence image analysis was performed with the Columbus Software (Perkin Elmer, version 2.7.1), of which the analysis workflow is shown in Supplementary Fig. S18. Gene editing efficiency was defined as the number of cells expressing EGFP divided by the number of cells expressing mCherry, as described previously.[29] LNP formulations were compared to a positive control, consisting of RNP delivered using ProDeliverIN CRISPR (Oz Biosciences, San Diego, CA, USA), as specified by the manufacturer, except that a 3.3 μL:1 μg ratio of reagent to protein was used. The mutation of the EGFP signal to BFP as a measure of gene correction was based on the work of Glaser et al.[31] Briefly, HEK293T-EGFP cells were seeded at a density of 3×105 cells/cm2 in an appropriate cell culture plate. The following day,

medium was supplemented with 1% antibiotic/antimycotic solution and LNP formulations were added to each well, containing a varied concentration of RNP, HDR template, and lipid concentrations. As a positive control, ProDeliverIN CRISPR was used to deliver the RNP and the HDR template in a molar ratio of 15:15:28.5 nM. Cells were washed after 24 h with fresh medium and incubated for two days. Subsequently, they were passaged and expanded for two additional days, leading to a total of five days incubation after transfection. Cells were subsequently harvested, washed twice with PBS, fixed in 1% paraformaldehyde, and transferred to a BD Falcon U-bottom 96-well plate (Becton Dickinson, Franklin Lakes, NJ, USA).

Cell fluorescence was determined by flow cytometry using the BD FACS CANTO II (Becton Dickinson, Franklin Lakes, NJ, USA). BFP was measured using the Pacific Blue channel of the flow cytometer, while EGFP fluorescence was determined in the FITC channel. Data was analyzed with the Flowlogic software (Inivai Technologies, Mentone, Australia, version 7.3). Gene knock-out was defined as a loss in green fluorescent signal, whereas gene correction was defined as a gain in blue fluorescent signal. The gene editing efficiency was determined by the population negative for EGFP and BFP, indicating gene knock-out, as well as the population positive for blue fluorescence, indicating HDR correction using the specified template. A plasmid encoding this BFP plasmid is given in Supplementary Fig. S1, and was acquired from Twist Bioscience (San Francisco, CA, USA). The gating strategy and model validation are presented in Supplementary Fig. S2.

To validate the functional gene-editing readouts, a T7 endonuclease I (T7E1) assay was performed. Genomic DNA was extracted from HEK293T stoplight cells and HEK293T-EGFP cells 2 or 5 days after the transfection with LNP-RNP and LNP-RNP-HDR, respectively, using the PureLink Genomic DNA Mini Kit (Thermo Fisher, Landsmeer, The Netherlands), following the manufacturer's instructions. PCR amplification was performed using primers designed specifically for the target locus (Supplementary Table S2) using Q5® Hot Start

High-Fidelity 2X Master Mix (New England Biolabs, Ipswich, MA, USA). Afterwards, PCR products were purified using a QIAquick PCR Purification kit. The PCR products were denatured at 95 °C for 10 min in the presence of NEBuffer 2 (New England Biolabs, Ipswich, MA, USA) and annealed at -2 °C per second temperature ramp to 85 °C, then, at -0.1 °C per second temperature ramp to 25 °C. Following this, hetero-duplexed sequences were incubated with 5U T7E1 enzyme (New England Biolabs, Ipswich, UK) at 37 °C for 18 min to achieve digestion of mismatched DNA.

Results

SpCas9 Production, Characterization and Stability in Storage
SpCas9 was recombinantly produced by transforming the LPS-free ClearColi™ BL21 strain with plasmid pET15_SpCas9_NLS_His (Addgene #62731). The elution chromatogram of SpCas9, given in Supplementary Fig. S4, shows that the principal protein component elutes at 250 mM imidazole. To study the long-term stability of in-house produced SpCas9, purified SpCas9 from a representative batch was snap frozen in liquid nitrogen and stored in aliquots at -80 °C until needed for analysis of protein size, activity, and for use in LNP formulations. As shown in Fig. 1A, the SpCas9 protein appeared as a clear band on SDS-PAGE at the expected molecular weight of 160 kDa. The relative peak area of the principal SpCas9 band, calculated by SDS-PAGE densitometry, did not deteriorate over time, as shown in Fig. 1B (gel excerpts underlying this graph are given in Supplementary Fig. S5). SpCas9, furthermore, proved to be active at introducing a targeted double strand break in plasmid DNA only when complexed with the cognate sgRNA, as seen in agarose gel electrophoresis in Fig. 1C. This activity was retained over time, as an activity digest after 12 months of storage showed similarly high SpCas9 activity. The activity did not differ significantly from the positive commercial control for each assay performed over time (Supplementary Fig. S3). These results show that the recombinant
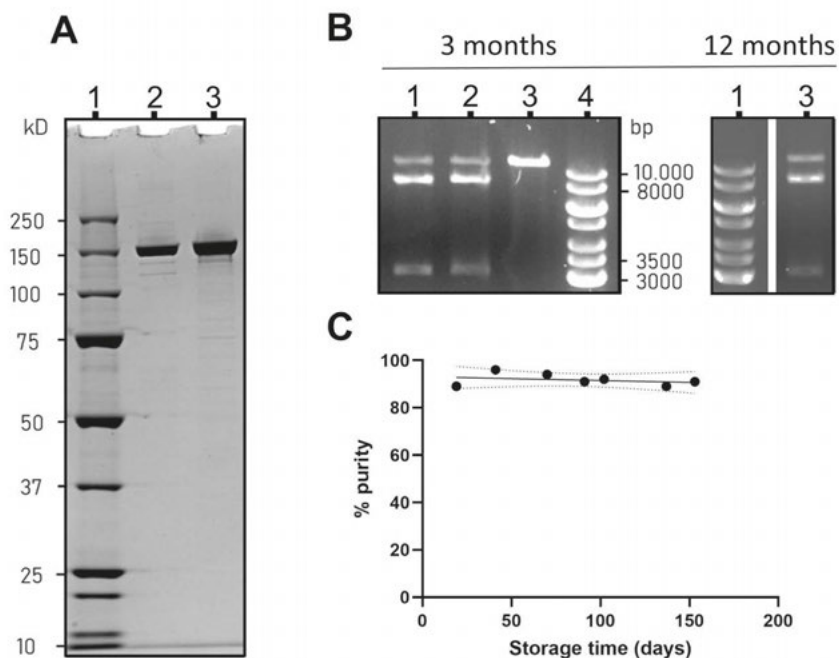
Figure 1: **SpCas9 characterization after purification and extended storage. A)** SDS-PAGE gel of the purified recombinant SpCas9. 1: PageRuler Plus prestained protein ladder. 2: Positive control SpCas9 acquired from Sigma Aldrich. 3: In-house produced SpCas9. **B)** Relative density of the 160 kDa protein band on the SDS-PAGE gels over time, defined as percentage purity. **C)** Activity of the SpCas9 protein (lane 1 left gel, lane 3 right gel) compared to a commercial sample (lane 2, left gel) and a negative control (lane 3, left gel). Generuler 1kB ladder (lane 4 left gel, lane 1 right gel) was used for determining the size of the DNA fragments. The activity is shown for SpCas9 after 3 months and 1 year in storage.

SpCas9, produced and stored with these methods and conditions, was active and stable at least for one year. This recombinant SpCas9 was used in subsequent formulation and gene editing studies.

Characterization and Efficacy of LNP Formulations for Gene Knock-Out (LNP-RNP)

Since pH and ionic strength may influence Cas9 RNP activity as well as RNP complexation during LNP preparation, different LNP formulations for gene knock-out were prepared by varying buffer composition during complexation of RNP with lipids, as well as the total amount of DOTAP in the final LNP-RNP formulations (Fig. 2). LNP consistently showed a particle size between 100 nm and 200 nm and a PDI below 0.2, as well as a ζ-potential between -5 and -20 mV (Fig. 2B,C). Interestingly, the LNP-RNP formulation prepared with nuclease-free water in the complexation phase and containing DOTAP 5 mole% seems to result in a high average particle size and polydispersity index ($\sim$ 1000 nm, PDI 0.8), suggesting this formulation is colloidally unstable, leading to LNP aggregation. A larger polydispersity index was additionally determined for LNP-RNP formulated in nuclease-free water with DOTAP 2 mole%. Quantification of the amount of SpCas9 protein and sgRNA associated with the LNP was done with HPLC and Quant-iTTM RiboGreen® RNA assay, resulting in complexation efficiencies of 63.7% and 68.6% (formulation: DOTAP 5 mole%, 50 mM HEPES buffer for RNP complexation), respectively (Supplementary Fig. S7 and S8). As RNP is a 1:1 complex of sgRNA to SpCas9 protein a similar complexation efficiency to lipid nanoparticles is expected, as validated by studying both SpCas9 and sgRNA.

Thus, complexation of SpCas9 was used in a further study to compare the effect of formulation buffer on RNP complexation in LNP and interestingly no differences could be detected (Supplementary Fig. S9).

To determine LNP-RNP stability under near-physiological conditions, AF4 was applied to detect intact LNP and measure its average size distribution when incubated in 5× diluted human plasma. The formulations tested during the AF4 studies were LNP-RNP [HEPES], containing DOTAP 0 and 5 mole%. Depicted in Fig. 2 are fractograms detected by in-line DLS detectors (Fig. 2D,E). LNP show a retention time around 40 min. The peaks on the DLS fractograms of nanoparticles in-
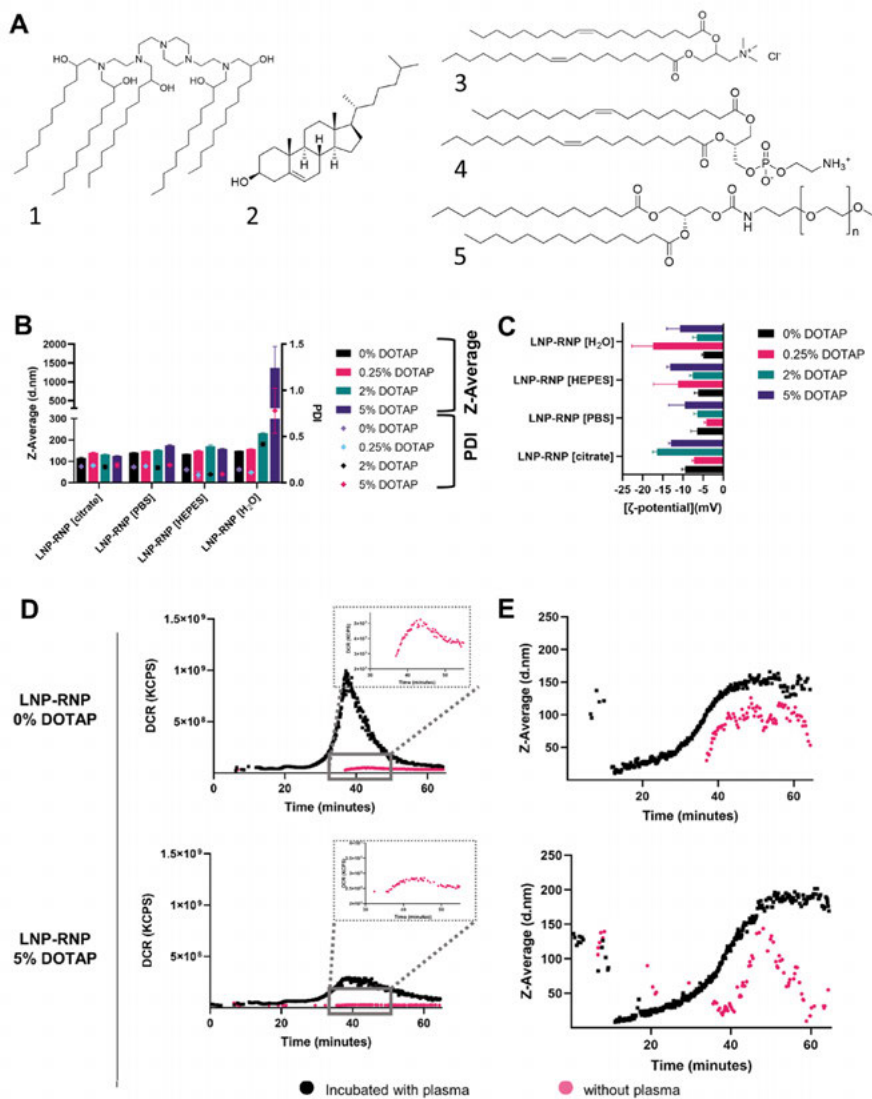
Figure 2: **LNP characterization and plasma stability. A)** Chemical structures of the LNP components in the formulations ((1) C12-200; (2) cholesterol; (3) DOTAP; (4) DOPE; (5) PEG-DMG); **B)** and **C)** LNP-RNP characteristics screened for varying DOTAP concentrations and complexation buffers, **B)** average particle size and PDI in PBS as determined by DLS (measured in triplicate) and **C)** ζ -potential of these formulations in 10 mM HEPES buffer pH 7.4 (measured in triplicate).

Figure 2: Two of these formulations were further characterized on stability in plasma (AF4); **D)** and **E)** AF4 fractograms recorded by DLS detector showing the derived count rate (D) and particle size (E) for LNP-RNP formulated in HEPES buffer with DOTAP 0 and 5 mole%. Inserts show a zoomed-in version of the samples measured without plasma. Detector flow was set to 0.5 mL/min.

cubated with plasma over the range of the retention times between 10 and 20 min are likely to be plasma proteins, suggested by an overlay of the chromatogram of 20% human plasma (Supplementary Fig. S17). LNP-RNP particles show a significantly higher derived count rate after incubation with plasma (Fig. 2D). These results indicate that these LNP do interact with the plasma components, suggesting formation of a protein corona on the surface of the LNP.[32] Based on these findings on particle size, RNP-lipid complexation efficiency and stability, the particles were deemed suitably stable and monodisperse to be tested on reporter cell lines for their gene editing efficiencies.

Determination of Gene Knock-Out Efficiency of Different LNP-RNP Formulations

LNP were applied to the HEK293T stoplight cell line to determine functional delivery of RNP. These cells constitutively express mCherry and, upon introduction of a +1 or +2 frameshift targeted by CRISPR-Cas9 downstream of the mCherry coding sequence, co-expression of EGFP is induced.[29] The influence of buffer composition during RNP formation was first assessed, as acidic buffers were shown to be detrimental in past reports.[17,23] Based on EGFP expression percentages, RNP formed in 50 mM HEPES buffer (pH 7.4) or nuclease-free water resulted in much higher gene editing in comparison to citrate or PBS buffer (Fig. 3A,C). This was confirmed at the genetic level using the T7E1 assay and TIDE analysis (Fig. 3E and Supplementary Fig. S13–S16). An acidic environment clearly has a negative effect on RNP and LNP formation in accordance with the literature.[23] Contrary to these findings, however, limited editing activity was observed in PBS, which is a physiological buffer system. An *in vitro* activity assay was performed to investigate these effects further. These assays showed that complexation in PBS and citrate

leads to irreversible inactivation of the RNP at a DNA-cleavage level (Fig. 3B and Supplementary Fig. S6B). In contrast, RNP mixed at different NaCl concentrations (up to 1 M) did not lose activity (Supplementary Fig. S6B). Taken together these findings indicate that pH or ionic strength alone do not account for the loss of Cas9 activity in the formulations.

The gene knock-out efficiencies determined by flow cytometry were consistently lower than those determined by image analysis (Supplementary Fig. S12C). The higher values obtained with image analysis can be explained by false positives due to difficulties in segmenting individual cells in highly confluent cell images. Nonetheless, flow cytometry confirmed that complexation of the RNP and LNP in HEPES buffer or nuclease-free water are the preferred complexation conditions. As LNP-RNP formulations still have approximately 30–40% of free RNP that was not removed prior to transfection, LNP-RNP transfection efficiencies were compared before and after dialysis overnight against 1 × HBS using a 300 kDa MWCO dialysis membrane to remove free RNP. No difference in gene knock-out efficiency was observed (Supplementary Fig. S12B), indicating that gene editing was primarily caused by the RNP complexed to LNP.

A three-way ANOVA was performed to statistically determine the effect of formulation conditions, experimental repeat, and molar ratio of DOTAP on gene knock-out efficiency. Based on the statistical analysis, the LNP-RNP formulation using nuclease-free water resulted in significantly higher gene editing outcomes as compared with those prepared in HEPES buffer (Supplementary Fig. S17). This result depended on the molar ratio of DOTAP used during nanoparticle formulation as well (Supplementary Fig. S17), indicating that RNP and LNP complexation in HEPES buffer requires higher mole% of DOTAP than in water. The statistical analysis, however, does show batch variation from one experiment to another, especially between formulations with HEPES buffer.
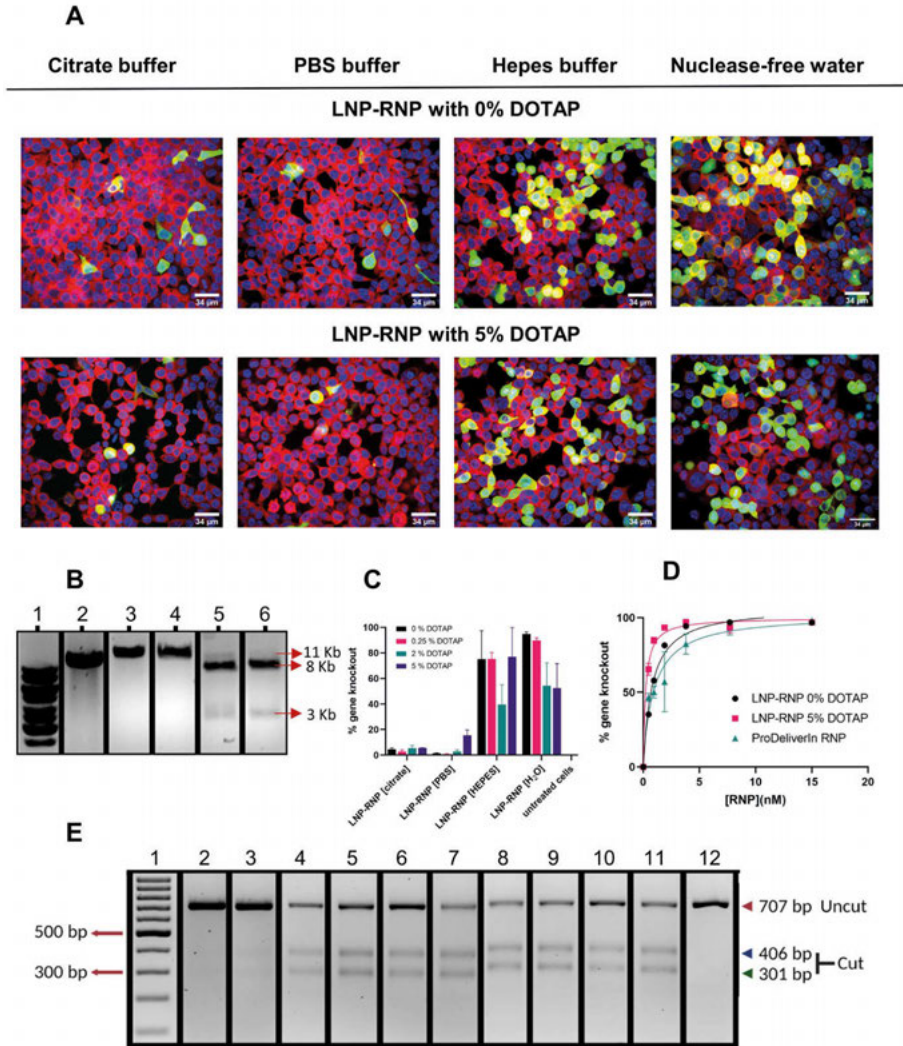
Figure 3: **Determination of gene knock-out efficiency in HEK293T stoplight cells. A)** Confocal microscopy images (60 ×) of HEK293T stoplight cells after treatment with different LNP formulations at a RNP concentration of 7.7 nM (RNP were complexed in different conditions, i.e., 100 mM citrate buffer, PBS buffer, 50 mM Hepes buffer, and nuclease-free water). Red represents mCherry, green represents EGFP (Cas9 gene editing), and blue represents Hoechst (nucleus). Scale bar 34μm. Images were optimized on ImageJ in brightness and contrast for each channel, respectively;

*Chapter 3. Impact of Formulation Conditions on Lipid
Nanoparticles Characteristics and Functional Delivery of CRISPR
RNP for Gene Knock-Out and Correction*

Figure 3: **B)** Cas9 activity *in vitro* using the same buffers as in (A) during RNP complexation. Uncut (11 kB) and cut (8kB and 3kB) DNA are highlighted by arrows. (1) Generuler 1 kB DNA ladder; (2) untreated DNA; (3–6) RNP complexed in citrate (3), PBS (4), HEPES (5), or water (6); **C)** gene knock-out efficiencies for different LNP formulations (with final RNP concentration 7.7 nM) determined by confocal image analysis using Columbus® software (tested in triplicate); **D)** dose-dependent gene knock-out efficiencies of two selected LNP-RNP formulations (0% DOTAP and 5% DOTAP, 50 mM HEPES buffer) as compared with the commercial transfection agent, ProDeliverIN (tested in duplicate); **E)** T7E1 digests performed on the same samples and ordered as in panel (C). (1) DNA ladder; (2) LNP-RNP containing DOTAP 5 mole%, prepared in 100 mM citrate buffer; (3) LNP-RNP containing DOTAP 5 mole%, prepared in PBS; (4–7) LNP-RNP prepared in 50 mM HEPES buffer with DOTAP 0, 0.25, 2 and 5 mole%, respectively; (8–11) LNP-RNP prepared in water with DOTAP 0, 0.25, 2, and 5 mole%, respectively; (12) negative control. The unedited gel is provided in Supplementary Fig. S13A as the order of the lanes was changed for clarity within this figure.

Dose-dependent gene knock-out was studied with two formulations complexed in 50 mM HEPES buffer pH 7.4 and with LNP containing DOTAP 0 or 5 mol% (Fig. 3D). From these results, the concentration to reach 50% of the effect (EC50) was calculated as a measure of gene knock-out efficiency by fitting a dose-response curve (agonist vs. response) using GraphPad PRISM version 9.1 (r2 for LNP-RNP 0% of DOTAP = 0.98, r2 for LNP-RNP 5% of DOTAP = 0.99, and r2 for ProDeliverIN RNP = 0.93). The LNP formulated with DOTAP 0 mole% have a higher EC50 value (0.8 nM) than the formulation with DOTAP 5 mole% (0.2 nM). In comparison, the fit led to an EC50 value of 1 nM for the ProDeliverIN positive control. In conclusion, therefore, LNP-RNP with DOTAP 5 mole% formulated in HEPES buffer seems to be the best performing nanoparticle for gene knock-out. Incubation of HEK293T stoplight cells with LNP-RNP did not result in any cytotoxicity at an RNP concentration around 7.7 nM (Supplementary Fig. S10A). Incubation of cells with 15 nM of LNP-RNP did result in a lower absolute number of cells (Supplementary Fig. S10B).

Characterization of LNP formulations for Gene Correction (LNP-RNP-HDR)
The LNP formulations additionally containing a single stranded DNA template for HDR-mediated gene correction were optimized using a similar rationale as the LNP-RNP formulations.   Water

and HEPES buffer at pH 7.4 were selected as primary formulation conditions following the LNP-RNP screening. Further variables were molar ratio of RNP to HDR template, and mole% of DOTAP in the LNP composition. To determine whether ssDNA HDR template had an effect on size and ζ-potential, these values were determined for formulations prepared in HEPES buffer, as differences amongst formulation conditions were not expected as shown in Fig. 2. Their characteristics were similar to those found for LNP-RNP (Fig. 4A,B), except for the formulation with a 1:1 ratio RNP:HDR, which resulted in a higher polydispersity index. The ζ-potential of these particles was, interestingly, similar to that of the LNP-RNP particles, even though more anionic charges were added to the formulation (up to 10-fold molar excess of template DNA as compared with RNP).

The plasma interaction of these particles was additionally tested using AF4. The results of the LNP-RNP-HDR particle formulated in nuclease-free water, remarkably, do not show a shift in retention time, as opposed to LNP-RNP (Fig. 4C,D). Interestingly, the increased count rate after plasma incubation is less pronounced in particles entrapping HDR template. Moreover, the particles additionally entrapping an HDR template do not change in size (Fig. 4D).[33,34]

3
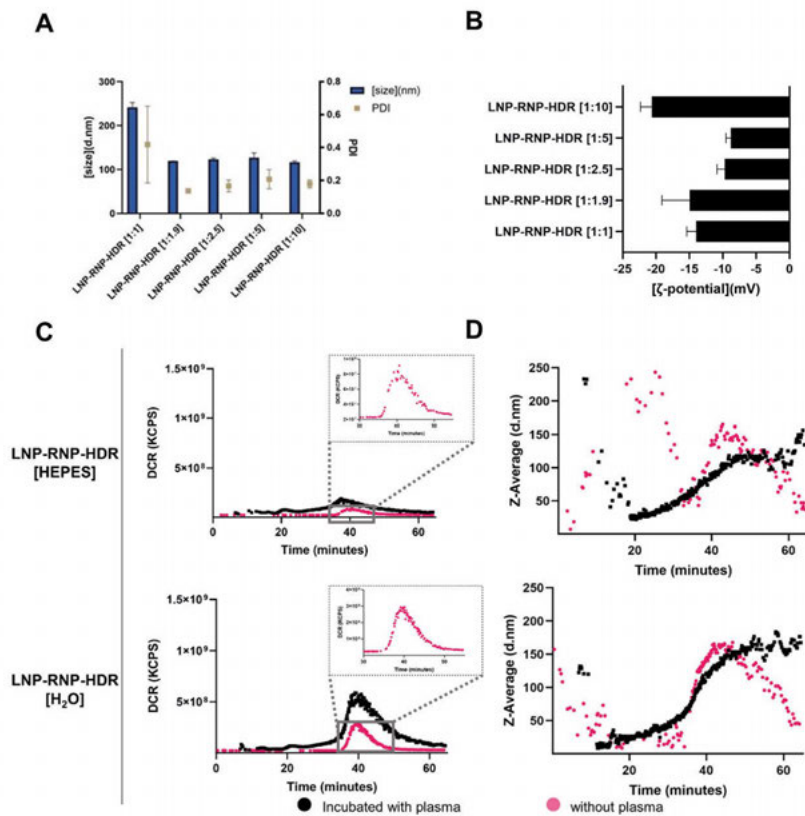
Figure 4: **Characterization of LNP-RNP-HDR formulations. A,B)** Representative LNP-RNP-HDR characteristics screened for varying HDR template concentrations (in molar ratios as compared with RNP) at a fixed complexation buffer (50 mM HEPES) and at a fixed lipid composition (DOTAP 0.25 mole%). (A) Average particle size and PDI as determined by DLS (measure in triplicate) and (B) ζ -potential of these formulations in 10 mM HEPES buffer pH 7.4 (measured in triplicate); **C)** AF4 fractograms recorded by DLS detector showing the derived count rate (DCR) of LNP-RNP-HDR formulations at a fixed HDR template concentration (1:1.9 molar ratio) and DOTAP concentration (0.25 mole%) in varying complexation buffers, with and without plasma incubation; **D)** AF4 fractograms recorded by DLS detector of particle size for LNP-RNP-HDR (same formulations as in (C)). Detector flow was set to 0.5 mL/min.

Determination of Gene Correction Efficiency of Different LNP-RNP-HDR Formulations

LNP-RNP-HDR were tested for their gene editing efficacy on HEK293T cells with constitutive EGFP expression. The loss in EGFP indicates gene knock-out, while a gain in the blue signal indicates gene correction (Supplementary Fig. S2). Several concentrations of HDR template were screened (Fig. 5A,B), as well as DOTAP percentages. Leaving out DOTAP from the formulation led to a significant reduction in the efficiency of gene editing (Supplementary Fig. S20). The formulation that yielded the highest gene correction efficacy was the LNP prepared in water, which contained DOTAP 0.25 mole% at a 1:2 molar ratio of RNP to HDR template. This formulation yielded a gene correction efficacy of 11.4% of the total cell population, as well as a gene knock-out efficacy of 59.6% of the cells at a final RNP concentration of 7.7 nM. For the LNP formed in HEPES buffer, the overall gene correction efficacies were lower. The percentage of HDR events within the total gene editing outcomes is given in Fig. 5B. This percentage is consistently higher for particles complexed in water as compared with HEPES buffer, which indicates that the particles formulated in water were overall more suited for HDR. Another trend is that addition of higher relative concentrations of HDR template is associated with lower gene editing.

A dose-escalation study was performed for LNP-RNP-HDR formulations prepared in water or HEPES buffer with DOTAP 0.25 mole% and a 1:2 ratio of RNP:HDR template, which performed well in the screening. The dose-dependent toxicity of these formulations after one day was assessed by the MTS assay (Fig. 5C). Cell viability decreased slightly over the concentration range but stayed above 90% along the whole concentration range for both formulations. The dose-dependent efficacy was determined by fitting a dose-response curve (agonist vs. response) using Graphpad PRISM version 9.1 for both gene correction (r2 for LNP-RNP-HDR [H2O] = 0.96 and r2 for LNP-RNP-HDR [HEPES] = 0.79) and gene knock-out (r2 for LNP-RNP-HDR [H2O] = 0.97 and r2 for LNP-RNP-HDR [HEPES] = 0.86). These curves showed

that formulations prepared in water exhibited a lower EC50 (7 nM) for gene correction as compared with the particles prepared in HEPES buffer (47 nM). For gene knock-out, the EC50 was lower for all conditions, but the same trend was observed where the water particles showed a lower EC50 (1 nM) than HEPES particles (10 nM) (Fig. 5D). Gene editing was additionally confirmed by the T7E1 assay (Supplementary Fig. S21), indicating that cells in this population contained insertions or deletions in their genome. These data combined showed that LNP-RNP-HDR formulated in water reached a gene correction efficacy of 19.2% at a concentration of 15 nM RNP with good cytocompatibility (95% cell viability).
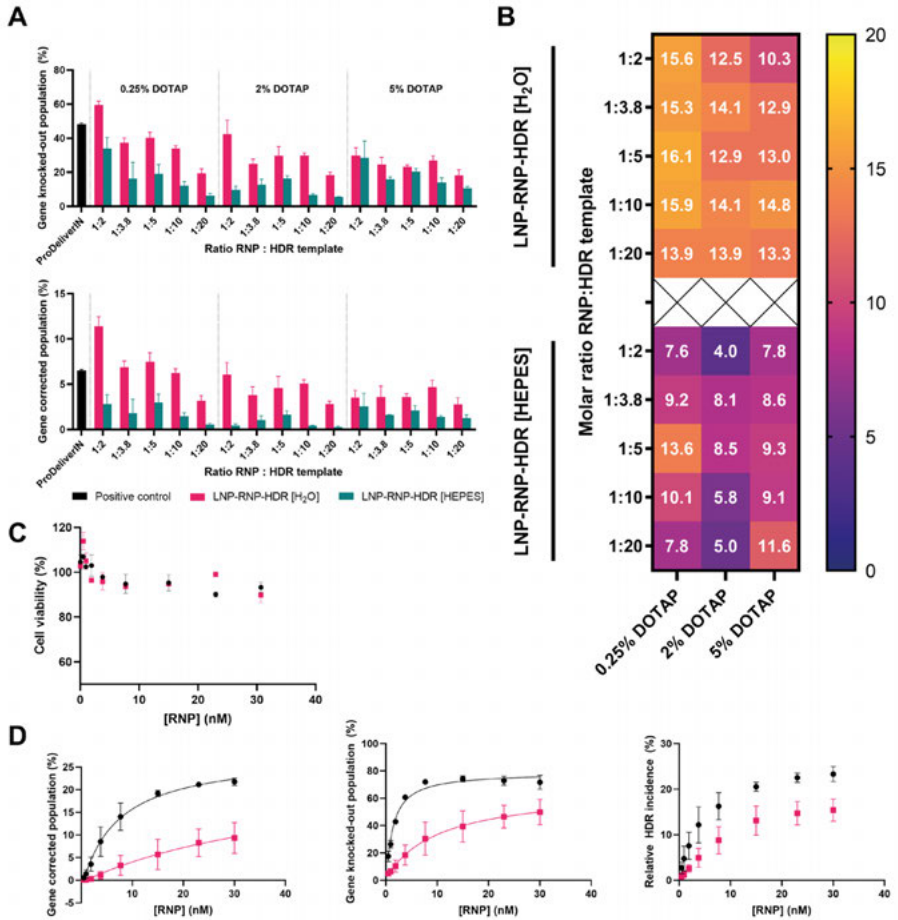
Figure 5: **A)** Formulation optimization to achieve gene correction using LNP at an RNP concentration of 7.7 nM, with varying molar ratios of RNP/HDR template and percentages of DOTAP in the lipid composition (tested in triplicate). Complexation of RNP and lipids was performed in water or HEPES prior to transfection. The concentration of DOTAP and template DNA was varied; **B)** Heatmap representation of the relative gene correction ratio (percentage incidence as compared with the sum of outcomes) within the gene-edited populations of Figure 5A; **C)** MTS cell viability of a dose range of the best performing formulations formed in HEPES buffer (pink) or water (black), containing DOTAP 0.25 mole% and a 1:2 molar ratio of HDR template to RNP (tested in duplicate); **D)** dose escalation study performed with the same formulations in (C) (pooled data from 2 batches, pink represents HEPES buffer and black represents water), represented for the gene correction, gene knock-out, and relative incidence of HDR as percentages within the gene-edited population (tested in duplicate).

Discussion

We based our formulations on previous literature regarding LNP for mRNA delivery as a starting point.[23,35,36] These use ionizable lipids to simultaneously reduce toxicity, as well as facilitate nucleic acid entrapment and endosomal escape in target cells. Our findings support previous reports, showing that for complexation of RNP, the buffer during RNP and lipid nanoparticle complexation and the inclusion of cationic lipid DOTAP are necessary for stable particles.[23] Moreover, the resulting LNP formulations were biocompatible as highlighted in Fig. 5C and Supplementary Fig. S10. We, however, further optimized these conditions for additional complexation of HDR template DNA. Buffer composition during RNP complexation played a major role on its downstream effect on cells. This seems not to be due to Cas9 encapsulation (Supplementary Fig. S9), but rather the Cas9 bioactivity as shown on *in vitro* gel digests (Supplementary Fig. S6B). Whereas the RNP formed in water or HEPES was active, the RNP formed in citrate was not. Citrate, in particular, was tested, as it is used for lipid ionization in reported LNP formulations in the past. To our surprise, *in vitro* activity of SpCas9 RNP in PBS was severely reduced as well. This suggests that the inhibitory effect is not due to pH or ionic strength during complexation, but rather a specific buffer ion interaction. We showed that HEPES, for example, did yield active RNP in our particles. Further investigation of this effect may reveal buffer incompatibilities of Cas9 RNP.

Another interesting finding is the negative ζ-potential. An explanation for the observed negative ζ-potential could be adsorption of excess RNP to the surface of the LNP.[37] Interestingly, the addition of HDR template does not seem to change particle size or shift the ζ-potential further toward negative, indicating that these are not surface bound (Fig. 4A,B).

The efficacy of our optimized particles is in line with the existing literature. Efficiency in gene editing seems to saturate around a concentration of 5–10 nM RNP, thus, higher concentrations of particles would

not be required (Fig. 3D). In comparison, Suzuki et al. showed editing saturation at 1 nM with their lipid nanoparticles, however, formulation conditions were not comparable to the conditions reported in this study.[17] It is interesting to also note that the incidence of NHEJ-based gene knock-out is more efficient in these formulations than HDR-based gene correction. This ratio, indicated in Fig. 5D, needs significant improvement before HDR can be considered for clinical application.

Finally, the AF4 studies show interesting insights with respect to particle stability and potential protein corona formation in the presence of human plasma. More elaborate studies would need to be performed to verify the nature and content of such a protein corona and possibly specify which plasma proteins accumulate on the surface of the particles. Such investigations would be relevant, as a protein corona could mediate specific *in vivo* localization of the LNP, for example, the adsorption of apolipoprotein E to the surface of LNP results in hepatocyte-specific uptake.33,34 Incubation with plasma shifts the retention time of LNP formulated without a ssDNA HDR template to a slightly earlier retention time (Fig. 2D, Fig. 4C and Supplementary Fig. S19). This indicates a change in the particle morphology due to interaction with plasma, which is worth investigating further, and indicates that the HDR template may have a positive influence on particle stability.[38] Previous studies have shown that, in fact, additional anionic charges favor RNP stability in formulations, resulting in better gene editing efficiencies on cells after delivery via electroporation. In any case, these results suggest that the particles are stable for *in vivo* applications and, thus, warrant further *in vivo* experimental studies.

Conclusions

In this study, we set out to find optimized formulation conditions for LNP containing SpCas9 RNP, with and without HDR template. Our main findings are as follows:

i. Preparing RNP for formulation in nuclease-free water or HEPES buffer yielded superior gene editing results as compared with PBS or citrate buffer, due to inadequate formation of an active RNP complex in the latter two buffers. There was no marked difference in encapsulation efficiency of Cas9 between these tested systems.

ii. Incorporation of DOTAP in the LNP-RNP formulation was associated with a high gene-editing efficacy overall, while for LNP-RNP-HDR, a lower concentration was optimal.

iii. High gene knock-out efficacies above 80% were achieved for LNP-RNP prepared in HEPES buffer, with DOTAP 5 mole%, with a clear dose-dependent relationship.

iv. As a highlighted result, 20% gene correction efficacy was achieved with LNP-RNP-HDR formulated in nuclease-free water, DOTAP 0.25 mole%, and a 2:1 ratio of HDR template to RNP, with a clear dose-dependent relationship as well, and high cell viability (>90%).

Moreover, we demonstrated that these LNP formulations remained colloidally stable in the presence of human plasma; however, changes in scattering intensity and average size were detected, which might indicate formation of a protein corona on the particle's surface. Additionally, we provide a protocol for in-house production, purification, and long-term storage of the SpCas9 protein, which can be stored for at least a year at -80 °C without loss of activity. These findings contribute to understand the necessity of optimal formulation conditions to create LNP for direct *in vivo* delivery of CRISPR-Cas9 components.

Acknowledgements

support in statistical analysis by Dirk Walther is appreciated. Finally, we express our gratitude towards Olivier de Jong for providing us with and aiding us in the reporter cell lines.

References

1. Jinek, M. et al. A Programmable Dual-RNA – Guided. Science (80-.). 337, 816–822 (2012).
2. Gasiunas, G., Barrangou, R., Horvath, P. & Siksnys, V. Cas9-crRNA ribonucleoprotein complex mediates specific DNA cleavage for adaptive immunity in bacteria. Proc. Natl. Acad. Sci. U. S. A. 109, 2579–2586 (2012).
3. Doudna, J. A. & Charpentier, E. The new frontier of genome engineering with CRISPR-Cas9. Science (80-.). 346, (2014).
4. Salsman, J., Masson, J.-Y., Orthwein, A. & Dellaire, G. CRISPR/Cas9 Gene Editing: From Basic Mechanisms to Improved Strategies for Enhanced Genome Engineering In Vivo. Curr. Gene Ther. 17, (2018).
5. Yang, H. et al. Methods Favoring Homology-Directed Repair Choice in Response to CRISPR/Cas9 Induced-Double Strand Breaks. Int. J. Mol. Sci. 21, 6461 (2020).
6. Lieber, M. R. The Mechanism of Double-Strand DNA Break Repair by the Nonhomologous DNA End-Joining Pathway. Annu. Rev. Biochem. 79, 181–211 (2010).
7. Chang, H. H. Y., Pannunzio, N. R., Adachi, N. & Lieber, M. R. Nonhomologous DNA end joining and alternative pathways to double-strand break repair. Nat. Rev. Mol. Cell Biol. 18, 495–506 (2017).
8. Gutschner, T., Haemmerle, M., Genovese, G., Draetta, G. F. & Chin, L. Post-translational Regulation of Cas9 during G1 Enhances Homology-Directed Repair. Cell Rep. 14, 1555–1566 (2016).
9. Wilbie, D., Walther, J. & Mastrobattista, E. Delivery Aspects of CRISPR/Cas for in Vivo Genome Editing. Acc. Chem. Res. acs.accounts.9b00106 (2019). doi:10.1021/acs.accounts.9b00106
10. Legut, M., Dolton, G., Mian, A. A., Ottmann, O. G. & Sewell, A. K. CRISPR-mediated TCR replacement generates superior anticancer transgenic T cells. Blood 131, 311–322 (2018).
11. Stadtmauer, E. A. et al. CRISPR-engineered T cells in patients with refractory cancer. Science (80-.). 367, (2020).
12. Lu, Y. et al. Safety and feasibility of CRISPR-edited T cells in patients with refractory non-small-cell lung cancer. Nat. Med. 26, 732–740 (2020).
13. Finn, J. D. et al. A Single Administration of CRISPR/Cas9 Lipid Nanoparticles Achieves Robust and Persistent In Vivo Genome Editing. Cell Rep. 22, 2227–2235 (2018).
14. Ledford, H. CRISPR treatment inserted directly into the body for first time. Nature 579, 185–185 (2020).

3

15. Li, Y. et al. Intracellular delivery and biodistribution study of CRISPR/Cas9 ribonucleoprotein loaded bioreducible lipidoid nanoparticles. Biomater. Sci. **7**, 596–606 (2019).

16. Patel, P., Ibrahim, N. M. & Cheng, K. The Importance of Apparent pKa in the Development of Nanoparticles Encapsulating siRNA and mRNA. Trends Pharmacol. Sci. **42**, 448–460 (2021).

17. Suzuki, Y. et al. Lipid nanoparticles loaded with ribonucleoprotein–oligonucleotide complexes synthesized using a microfluidic device exhibit robust genome editing and hepatitis B virus inhibition. J. Control. Release **330**, 61–71 (2021).

18. Kouranova, E. et al. CRISPRs for Optimal Targeting: Delivery of CRISPR Components as DNA, RNA, and Protein into Cultured Cells and Single-Cell Embryos. Hum. Gene Ther. **27**, 464–475 (2016).

19. Ma, H. et al. CRI SPR-Cas9 nuclear dynamics and target recognition in living cells. J. Cell Biol. **214**, 529–537 (2016).

20. Tu, Z. et al. Promoting Cas9 degradation reduces mosaic mutations in non-human primate embryos. Sci. Rep. **7**, 42081 (2017).

21. Lin, S., Staahl, B. T., Alla, R. K. & Doudna, J. A. Enhanced homology-directed human genome engineering by controlled timing of CRISPR/Cas9 delivery. Elife **3**, (2014).

22. Klein, M., Eslami-Mossallam, B., Arroyo, D. G. & Depken, M. Hybridization Kinetics Explains CRISPR-Cas Off-Targeting Rules. Cell Rep. **22**, 1413–1423 (2018).

23. Wei, T., Cheng, Q., Min, Y. L., Olson, E. N. & Siegwart, D. J. Systemic nanoparticle delivery of CRISPR-Cas9 ribonucleoproteins for effective tissue specific genome editing. Nat. Commun. **11**, 1–12 (2020).

24. Manning, M. C., Chou, D. K., Murphy, B. M., Payne, R. W. & Katayama, D. S. Stability of Protein Pharmaceuticals: An Update. Pharm. Res. **27**, 544–575 (2010).

25. Love, K. T. et al. Lipid-like materials for low-dose, in vivo gene silencing. Proc. Natl. Acad. Sci. U. S. A. **107**, 1864–1869 (2010).

26. D'Astolfo, D. S. et al. Efficient Intracellular Delivery of Native Proteins. Cell **161**, 674–690 (2015).

27. Alonso Villela, S. M. et al. A protocol for recombinant protein quantification by densitometry. Microbiologyopen **9**, 1175–1182 (2020).

28. Burger, A. et al. Maximizing mutagenesis with solubilized CRISPR-Cas9 ribonucleoprotein complexes. Development (2016). doi:10.1242/dev.134809

29. de Jong, O. G. et al. A CRISPR-Cas9-based reporter system for single-cell detection of extracellular vesicle-mediated functional transfer of RNA. Nat. Commun. **11**, 1–13 (2020).

30. Jong, O. G., Balkom, B. W. M., Gremmels, H. & Verhaar, M. C. Exosomes from hypoxic endothelial cells have increased collagen crosslinking activity through up-regulation of lysyl oxidase-like 2. J. Cell. Mol. Med. **20**, 342–350 (2016).

31. Glaser, A., McColl, B. & Vadolas, J. GFP to BFP Conversion: A Versatile Assay for the Quantification of CRISPR/Cas9-mediated Genome Editing. Mol. Ther. - Nucleic Acids **5**, e334 (2016).

32. Hu, Y., Crist, R. M. & Clogston, J. D. The utility of asymmetric flow field-flow fractionation for preclinical characterization of nanomedicines. Anal. Bioanal. Chem. **412**, 425–438 (2020).

33. Liu, Y. et al. Correlation between in vitro stability and pharmacokinetics of poly(-caprolactone)-based micelles loaded with a photosensitizer. J. Control. Release **328**, 942–951 (2020).

34. Caputo, F. et al. Measuring Particle Size Distribution by Asymmetric Flow Field Flow Fractionation: A Powerful Method for the Preclinical Characterization of Lipid-Based Nanoparticles. Mol. Pharm. **16**, 756–767 (2019).

35. Akinc, A. et al. The Onpattro story and the clinical translation of nanomedicines containing nucleic acid-based drugs. Nat. Nanotechnol. **14**, 1084–1087 (2019).

36. Guimaraes, P. P. G. et al. Ionizable lipid nanoparticles encapsulating barcoded mRNA for accelerated in vivo delivery screening. J. Control. Release **316**, 404–417 (2019).

37. Sebastiani, F. et al. Apolipoprotein E Binding Drives Structural and Compositional Rearrangement of mRNA-Containing Lipid Nanoparticles. ACS Nano **15**, 6709–6722 (2021).

38. Nguyen, D. N. et al. Polymer-stabilized Cas9 nanoparticles and modified repair templates increase genome editing efficiency. Nat. Biotechnol. **38**, 44–49 (2020).

3

Supplementary Material for Chapter 3

Synthetic genetic sequences used in this work

Table S1: **Guide RNA spacer sequences used in this work.**

Target	20 nt Spacer Sequence
Stoplight construct	GGACAGUACUCCGCUCGAGU
EGFP construct	GCUGAAGCACUGCACGCCGU

Table S2: **PCR primers used for amplification of the Stoplight and EGFP loci, for T7E1 and TIDE as specified in the primer code.**

Primer Code	Sequence 5′ – 3′
Stoplight (T7E1) Forward	GAAGGGCGAGATCAAGCAGA
Stoplight (T7E1) Reverse	GGTCTTGTAGTTGCCGTCGT
Stoplight (TIDE) Forward	GGACGGCGAGTTCATCTACA
Stoplight (TIDE) Reverse	CTTCATGTGGTCGGGGTAGC
EGFP (T7E1) Forward	CGTAAACGGCCACAAGTTCA
EGFP (T7E1) Reverse	GTCCATGCCGAGAGTGATCC

Table S3: **Template DNA used in the EGFP to BFP mutation assay. DNA mismatches, encoding the mutation, are highlighted green. The PAM sequence, needed for Cas9 activity, is additionally mutated in this sequence.**

86 bp (40bp Homology arms)
CAAGCTGCCCGTGCCCTGGCCCACCCTCGTGACCACCCTGAGCC ACGGCGTGCAGTGCTTCAGCCGCTACCCCGACCACATGAAGC

Model validation using BFP-expressing plasmid transfection

The designed BFP-expressing gene was ordered in a pET17 vector from Twist Biosience. The full plasmid map is given below in Fig. S.1. This gene was transfected into HEK293T cells in a 6-well plate using Lipofectamine CRISPRMax (Thermo Scientific) using the manufacturer's specifications. Cells were grown for 2 days and harvested by trypsinization. Flow cytometry was performed to assess the signal and separation of the signal compared to HEK293T-EGFP cells. Both samples were acquired separately, as well as a mixed sample, to optimize the machine settings and separate the signals.
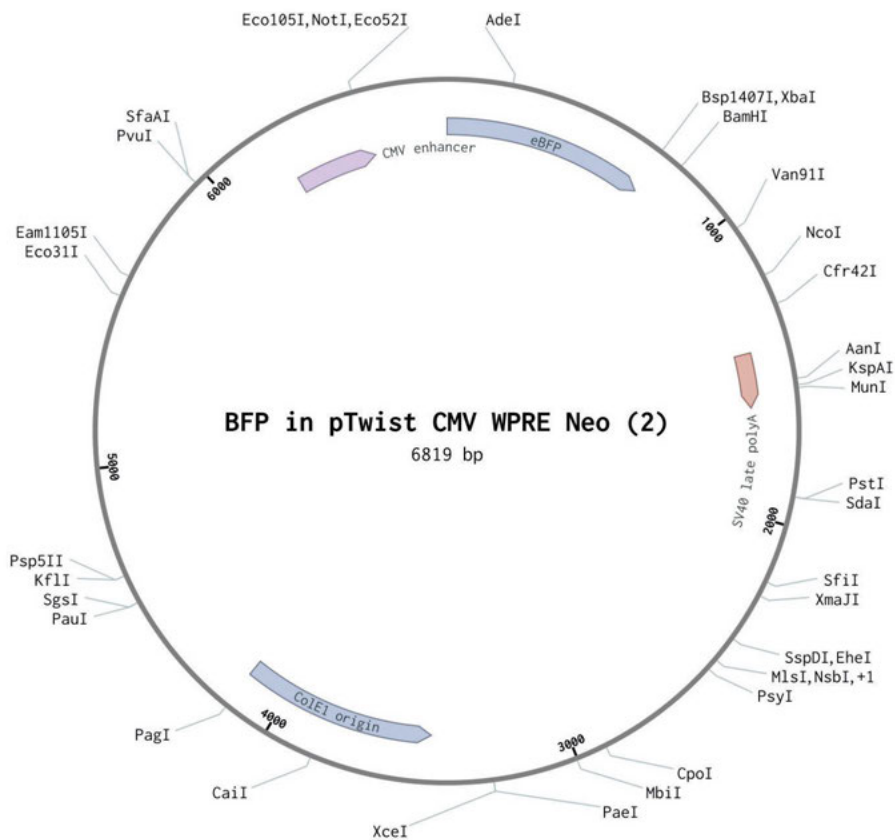
Figure S1: **Plasmid map encoding the mutant EGFP gene, which encodes a blue fluorescent protein.**

Additional information regarding the stability study of SpCas9 protein

The linear plasmid used is 10.930 base pairs long. After cleavage of the EGFP site, two strands of 7926 and 3004 base pairs are formed. The gels were analyzed by densitometry in ImageJ to calculate the cleaving efficiency of the SpCas9 protein. A background subtraction was performed using a rolling ball radius of 50 pixels. Lanes were drawn in the middle of the bands. The areas of each peak were calculated (AUC) and the activity was calculated by dividing the AUC of the digested bands by the AUC of the sum of all bands.

The purity of AF647-Cas9 was determined using SDS-PAGE and measured by fluorescence using the UV/Stain free/Blot free sample tray and the Alexa 647 preset on the Chemidoc imager. Here it is notable that a small fluorescent population is visible under the front of the loading dye, which may correspond to the free AF647 label. This is also seen in the final sample, which contained the crude labeled protein prior to purification. The Cas9 additionally shows up as a fluorescent band high in the gel around 160 kDa, which is expected. The peak area of the free dye (under the front) was approximately 1% as determined by densitometry. Most of the impurities were found to be larger than the original Cas9 molecular weight, which is in contrast to SDS-PAGE of the unlabeled protein as seen in Fig. 1b.

3
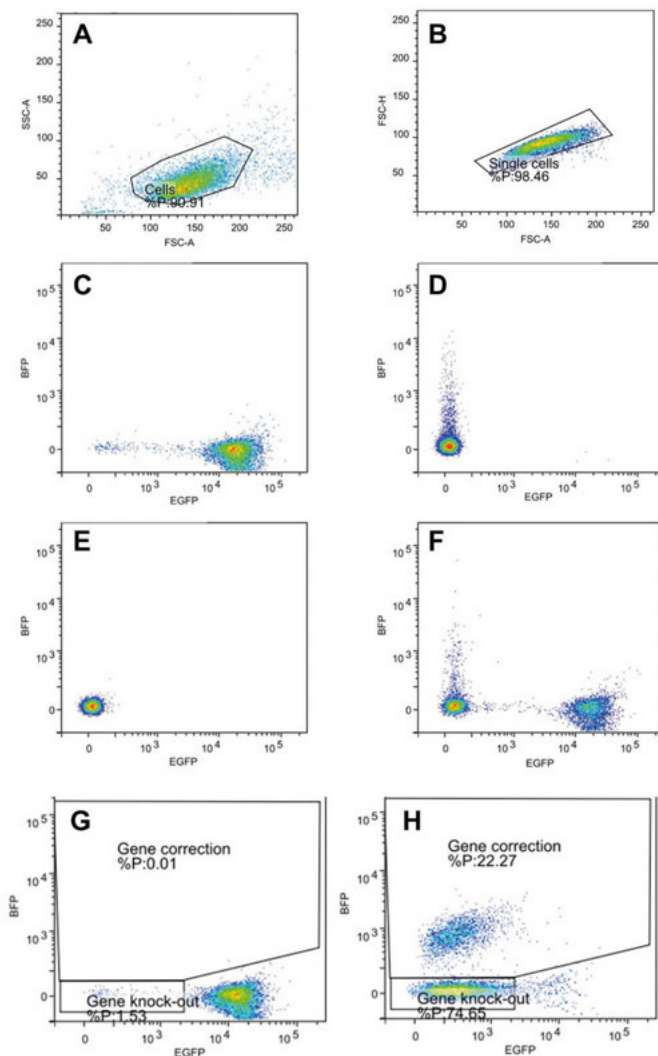
Figure S2: **A and B:** gating strategy to find single cells employed in all flow cytometry experiments using HEK293T cells. **C:** HEK293T cells expressing EGFP. **D:** HEK293T cells transfected with pTwist BFP. **E:** HEK293T cells. **F:** mixed population of C and D to assess the ability to distinguish BFP and EGPF signals. **G:** untreated HEK-EGFP cells from the dose-escalation study presented in Fig. 6 of the main text. H: LNP-RNP-HDR at 0.25% DOTAP, a 1:2 molar ratio of RNP to template DNA and concentration of 30nM of RNP in the well, after formulation in nuclease free water.
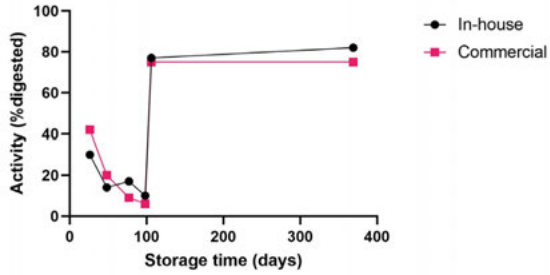
Figure S3: **Calculated *in vitro* SpCas9 activity calculated over a long storage time.** Variation between assays is thought to be due to plasmid quality, which is why the protein was compared to a commercially available control each time.
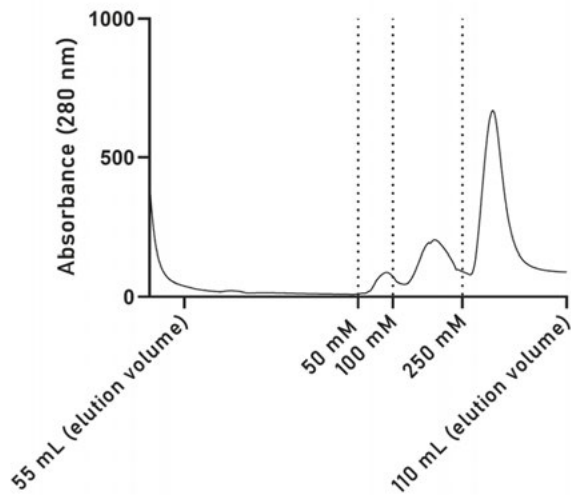
Figure S4: **Elution chromatogram of SpCas9 during His-tag purification.**
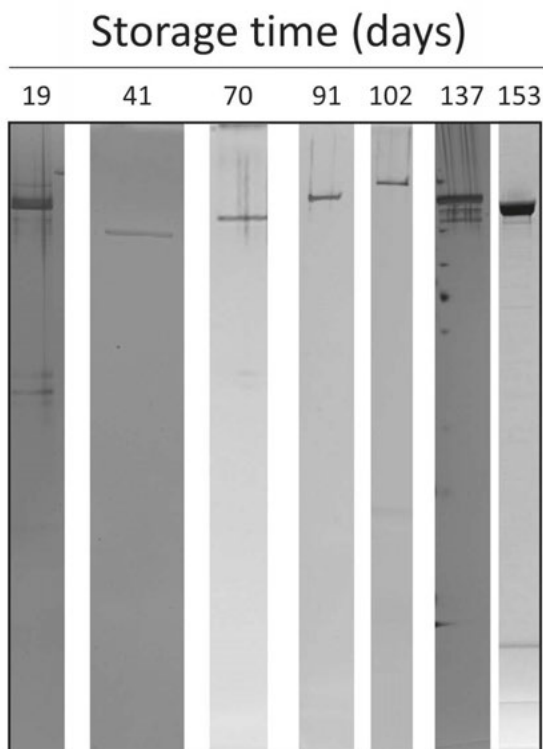
Figure S5: SDS-PAGE gel excerpt used in the gel densitometry stability study [1].

[1]: Alonso Villela, S.M.; Kraïem, H.; Bouhaouala-Zahar, B.; Bideaux, C.; Aceves Lara, C.A.; Fillaudeau, L. A Protocol for Recombinant Protein Quantification by Densitometry. MicrobiologyOpen 2020, 9, 1175–1182, doi:10.1002/mbo3.1027.
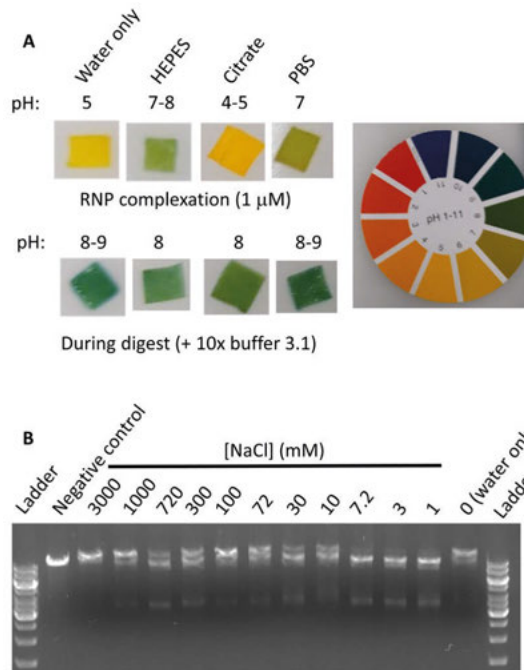
Figure S6: *In vitro* **cleavage activity assay of RNP complexed in various conditions as used during nanopaticle formulation. A)** pH values measured with pH paper of the different conditions. **B)** Agarose gel of the *in vitro* cleavage activity assay with various sodium chloride concentrations.

Additional information regarding lipid nanoparticle formulation

Table S4: **Schematic representation of LNP preparation with the exact volumes for an exemplary LNP-RNP formulation.**

Steps	Description	Volume (μl)
1.	**RNP Complexation**	
	20 μM sgRNA	0.36
	3.75 μM SpCas9	1.92
	*HEPES buffer was added to both gRNA and SpCas9 to a final volume of 9 μl. respectively	
	i. Add 9 μl of 0.8 μM SpCas9 to 9 μl of 0.8 μM sgRNA	
	ii. Incubate for 15 minutes at RT	
2.	**Preparation of Lipid Mixture**	
	20 mM C12-200	0.23
	10 mM DOPE	0.21
	10 mM cholesterol	0.61
	1 mM PEG-DMG	0.33
	7.12 mM DOTAP*	0.09
	(EtOH added to total 6 μl)	
3.	**LNP Formation**	
	i. Add 25.44 μl of RNP to 6 μl of lipids	
	ii. Incubate for 15 minutes at RT	
	iii. Dilute 4x with 1x PBS to final formulation volume of 100 μl	
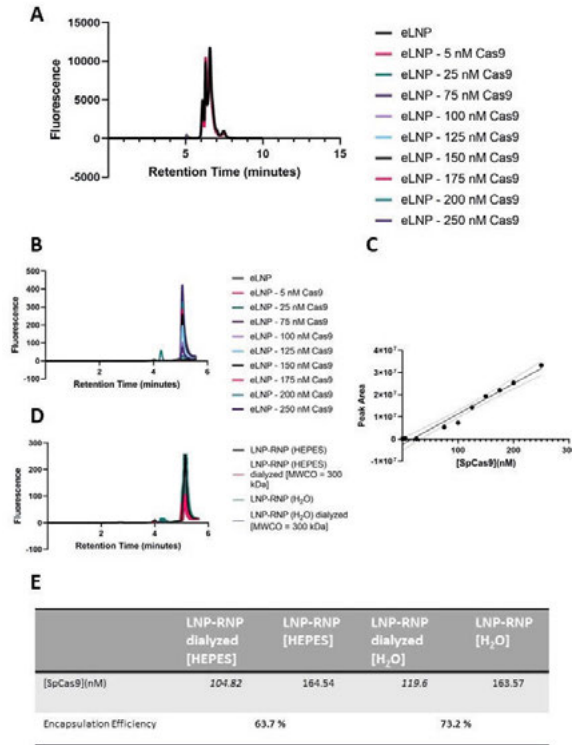
Figure S7: **Determination of complexation efficiency of SpCas9 in LNP. A)** Chromatogram (fluorescent detector; ex. 280 nm, em. 350 nm) of the full HPLC run on the Xbridge protein BEH C4 300Å column of empty LNP spiked with different SpCas9 concentrations for calibration. **B)** Zoomed-in chromatogram of the SpCas9 peak in samples of empty LNP with different SpCas9 concentrations for calibration. **C)** Calibration curve determined with EMPOWER software. (Linear fit equation: $y = 1.35 \times 10^5 x - 1.94 \times 10^6$; $R^2 = 0.970$). **D)** Chromatogram of LNP-RNP where the RNP was formulated in 50 mM HEPES pH 7.35 or nuclease-free water (non-dialyzed vs dialyzed) and with 5 mole% DOTAP. **E)** Overview of the determined molar concentration of SpCas9 in the LNP samples. Complexation efficiency was determined by dividing the concentration of SpCas9 of the dialyzed samples by the non-dialyzed sample, respectively for the two different RNP conditions. Dilution factor of 1.3 was included in the calculations as samples were slightly diluted during dialysis (indicated by italic numbers).
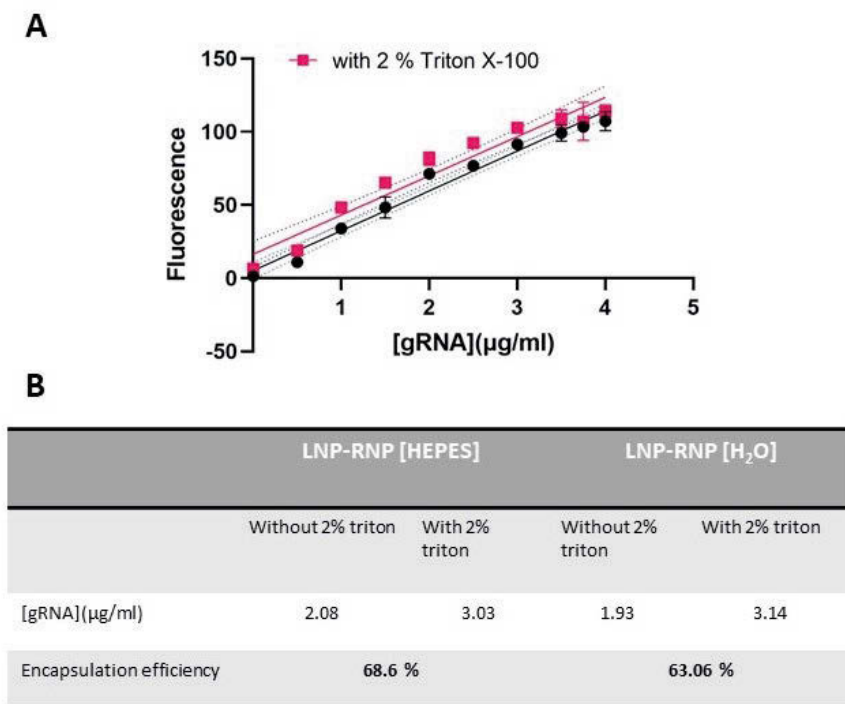
Chapter 3.   Impact of Formulation Conditions on Lipid
Nanoparticles Characteristics and Functional Delivery of CRISPR
RNP for Gene Knock-Out and Correction

Figure S8: **Determination of the complexation efficiency of sgRNA in lipid nanoparticles.**
A) Calibration curve of the fluorescent signal of Quant-iTTM RiboGreen® RNA reagent dependent on gRNA concentration (excitation: 485 nm; emission: 530 nm). Linear fit equation: without 2% Triton X-100 y = 27.24*x + 5.109 (R^2 = 0.972); with 2% Triton X-100 y = 26.78*x + 16.32 (R^2 = 0.936) **B)** Overview of the gRNA concentrations calculated with the linear fit equation in LNP-RNP samples. Two different RNP conditions were compared (50 mM HEPES pH 7.35 buffer and nuclease-free water). Complexation efficiency was determined by dividing LNP samples treated without 2% Triton X-100 with LNP samples treated with 2% Triton X-100.
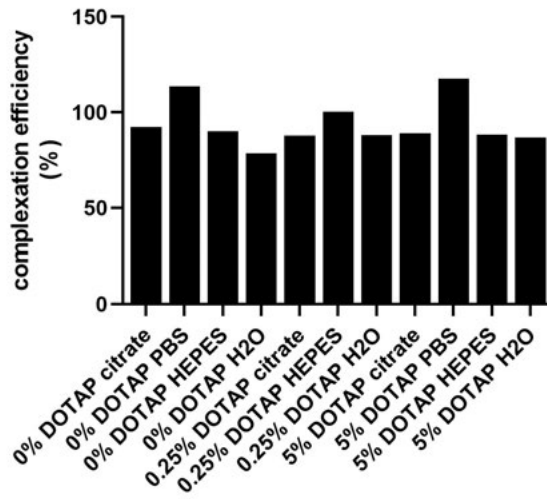
Figure S9: **Complexation efficiency of Cas9 to LNPs in different formulation conditions.**
Complexation efficiency was determined by HPLC as shown in Fig. S7. For each formulation
condition, a LNP-RNP was formulated and run on Xbridge protein BEH C4 300Å column as
a non-dialyzed and dialyzed sample (to remove free SpCas9). Efficiencies were calculated by
dividing the concentration of SpCas9 of the dialyzed samples by the non-dialyzed sample. Con-
centrations of SpCas9 were determined via EMPOWER software based on standard samples of
a calibration curve as depicted in Fig. S7c.

Additional information on LNP-RNP tested on stoplight HEK293T cells
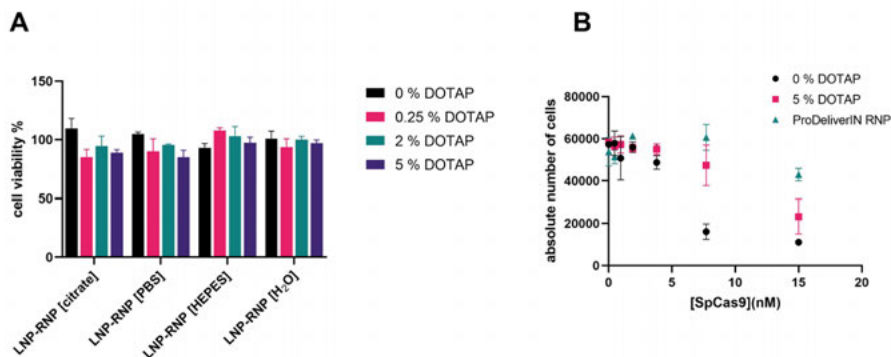
Figure S10: **A)** Cytotoxicity assay to determine cell viability of HEK293T stoplight cells after treatment with lipid nanoparticles with final RNP concentration of 7.7 nM in triplicate. Different LNP-RNP samples with different RNP conditions and molar ratio of DOTAP do not show an effect on cell viability. **B)** Absolute number of stoplight HEK293T cells per well to show cell viability in dependency of dose of LNP-RNP formulations with 0 or 5 mole% DOTAP. Cells were treated in duplicate with nanoparticles. Absolute number of cells treated with LNP were compared to cells treated with commercial transfection agent ProDeliverIN.

Flow cytometry to determine gene knock-out efficiencies in HEK293T stoplight cells

To support the image analysis, gene editing efficiency was also determined by flow cytometry using the BD FACS CANTO II (Becton Dickinson, Franklin Lakes, USA). Cells were harvested off of the Greiner 96-well black plate by trypsinization and transferred to a BD Falcon U-bottom 96 well plate (Becton Dickinson, Franklin Lakes, USA), where the cells were pelleted and washed 2x with 200 μl PBS by centrifugation at 300xg for 5 minutes. The cells were then resuspended and fixed in 1% paraformaldehyde. EGFP fluorescence was measured in the FITC channel, mCherry fluorescence was measured in the PERCP-Cy5 channel. Gene editing efficiency was determined by calculating the parent percentage of EGFP-positive cells in the mCherry-positive cell population using FlowLogic software. Flow cytometry data analysis is represented in Fig. S11 and the results are given in Fig. S12c.
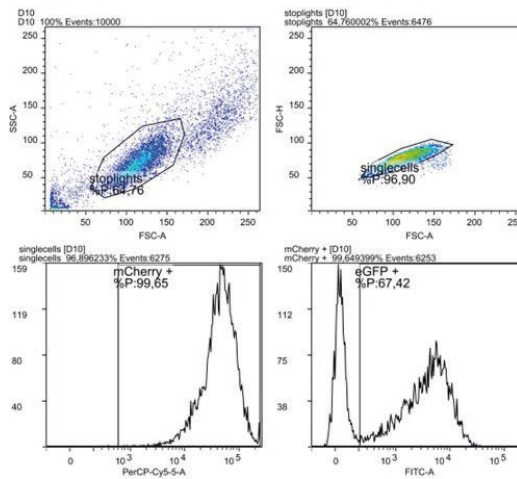

Figure S11: Top panel shows the gating strategy to determine single cells within the HEK293T stoplight cells during flow cytometry studies. Bottom panel shows selection of mCherry population and within that population the EGFP positive selection.
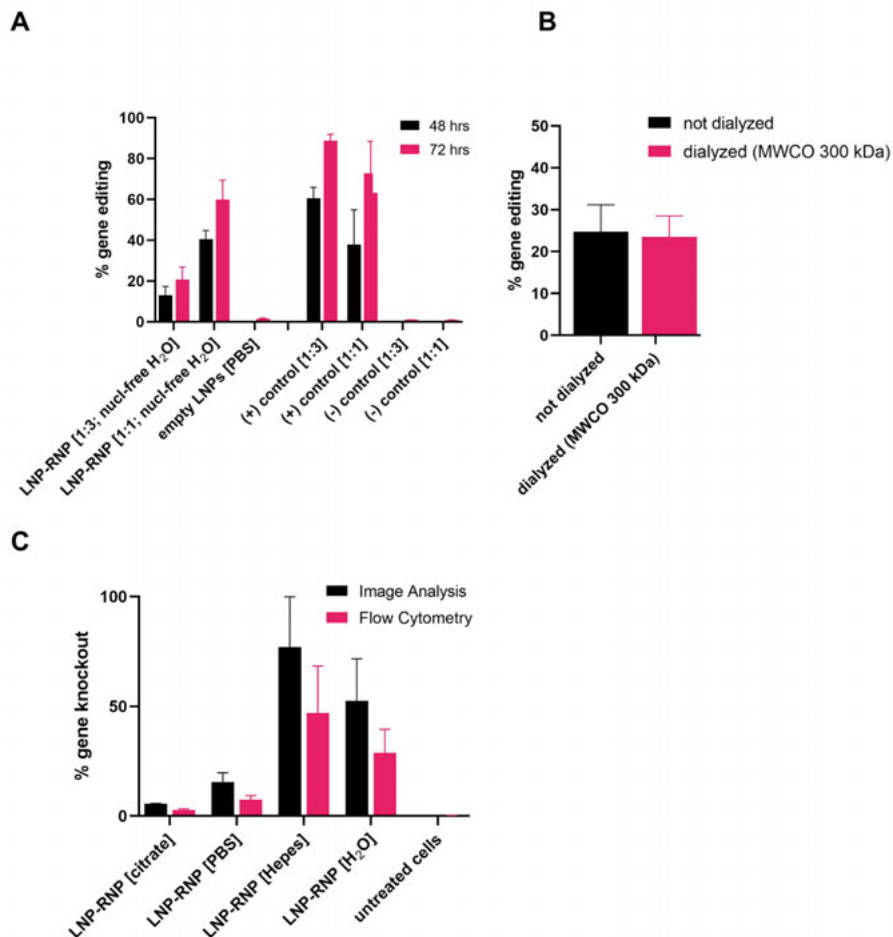
Figure S12: **Optimization of formulation. A)** Optimization of molar ratio between SpCas9 protein and gRNA. Gene editing is depicted after 48 hrs and 72 hrs of treatment of HEK293T stoplight reporter cells with LNP-RNP. The commercial transfection agent RNAiMAX was used as a positive control (following manufacturer's protocol). As a negative control free RNP at same concentration was added to cells. **B)** Dialysis of LNP-RNP against 1x HBS with Float-A-Lyzer MWCO 300 kDa does not result in less gene editing than undialyzed LNP formulation. **C)** Comparison of image analysis and flow cytometry to determine the gene knock-out efficiency of various LNP-RNP formulations. For simplicity, only 5% DOTAP was depicted in this graph. That flow cytometry analysis yields lower gene editing values than image analysis was seen for each complexation condition for RNP and LNP, but the trends follow the same pattern.

Tracking of Indels by Decompossition (TIDE) analysis

TIDE was performed as described by Brinkman et al [2]. In short, genomic DNA was isolated 48h after transfection from HEK293T Stoplight cells using the PureLink Genomic DNA Mini Kit (Thermo Fisher, Landsmeer, the Netherlands) following the manufacturer's instructions. The target region was amplified by PCR, using the sequences given in the supplementary information (S2). The PCR product was purified using QIAquick PCR Purification kit (Qiagen GmbH, Hilden, Germany) and Sanger-sequenced. The forward Sanger sequence chromatogram was used for TIDE analysis, by using the TIDE webtool (http://tide.nki.nl). To determine gene modification frequencies, the sequence chromatogram from untreated cells was used as a reference sequence. The percentage of gene editing was calculated with the indel size range set at 25 and the decomposition window fixed between 300-600 bp.

Brinkman, E.K.; Chen, T.; Amendola, M.; van Steensel, B. Easy Quantitative Assessment of Genome Editing by Sequence Trace Decomposition. Nucleic acids research 2014, 42, e168, doi:10.1093/nar/gku936.
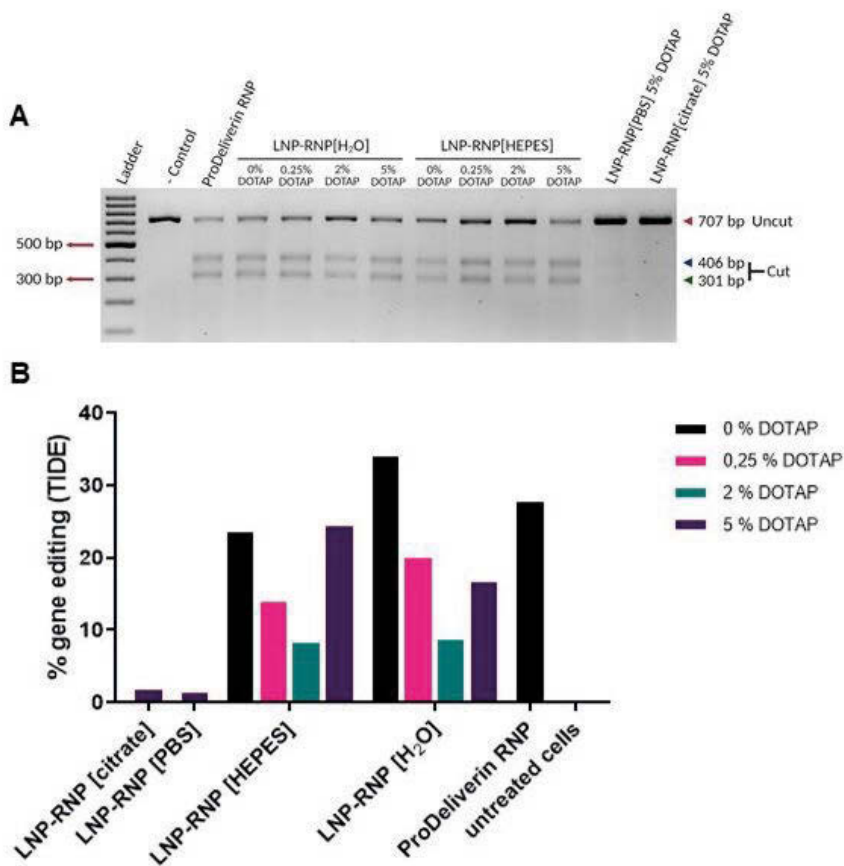
3

Figure S13: **Genetic readouts of gene-editing in the HEK293T-stoplight cells. A:** Original gel of Fig. 3E. **B:** Percentage of gene-edited cells found in TIDE analysis performed on the same samples (n=3). These are in line with the functional data provided in Fig. 3A and 3C.
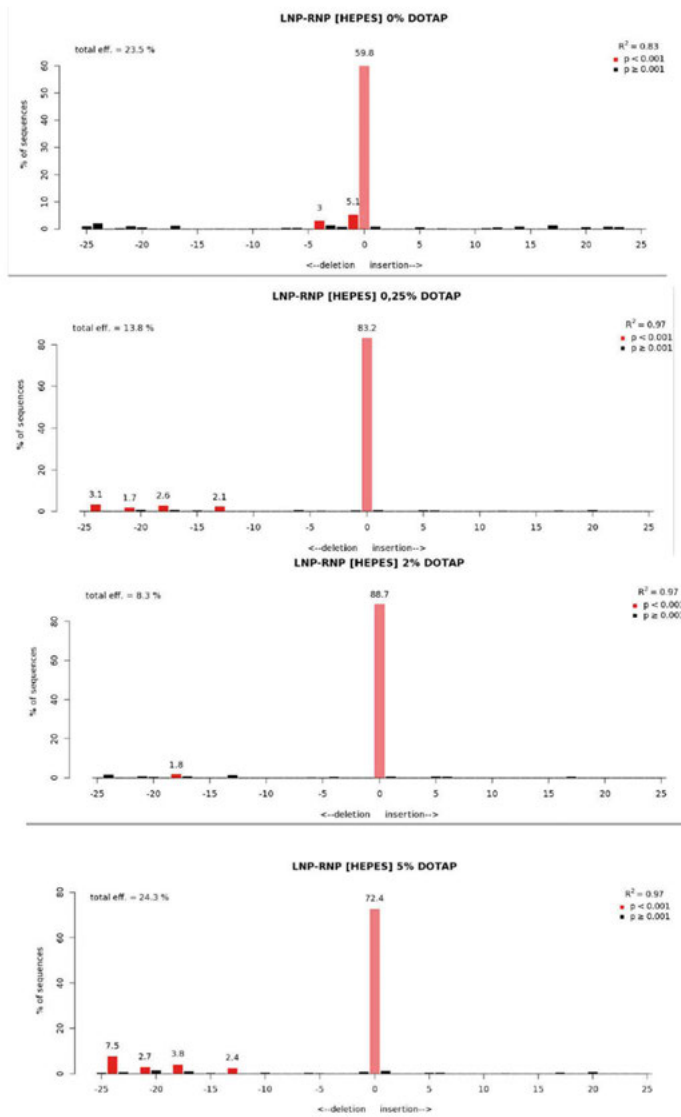
Figure S14: **Raw TIDE data for formulations LNP-RNP complexed in 50 mM HEPES buffer pH 7.35 with DOTAP 0, 0.25, 2, and 5 mole%.**
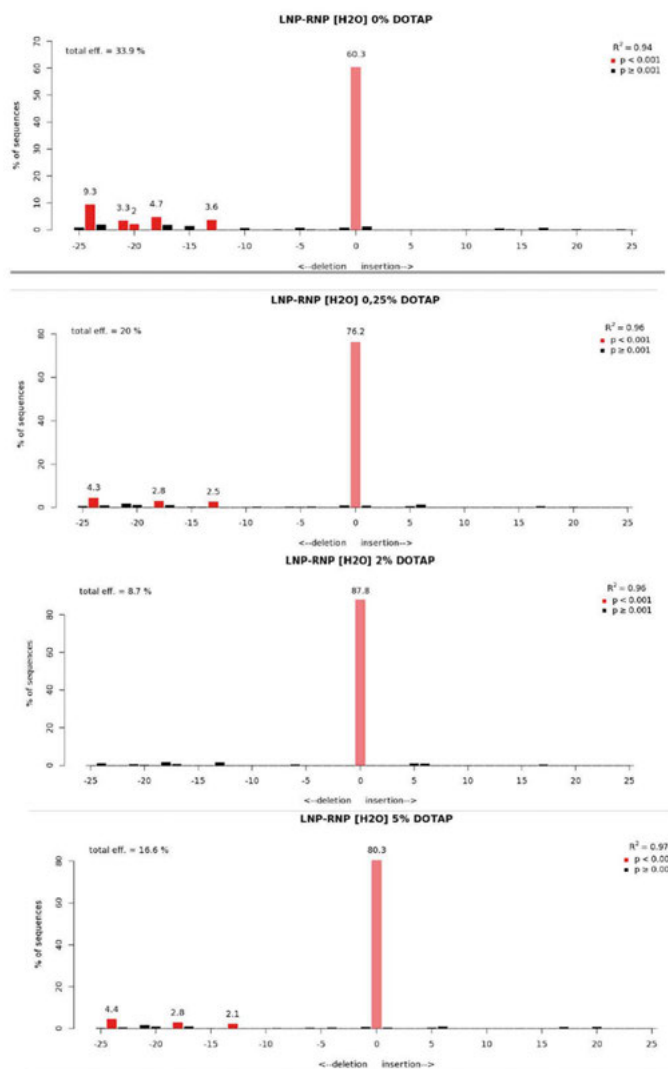
Figure S15: **Raw TIDE data for formulations LNP-RNP complexed in nuclease-free water with DOTAP 0, 0.25, 2, and 5 mole%.**
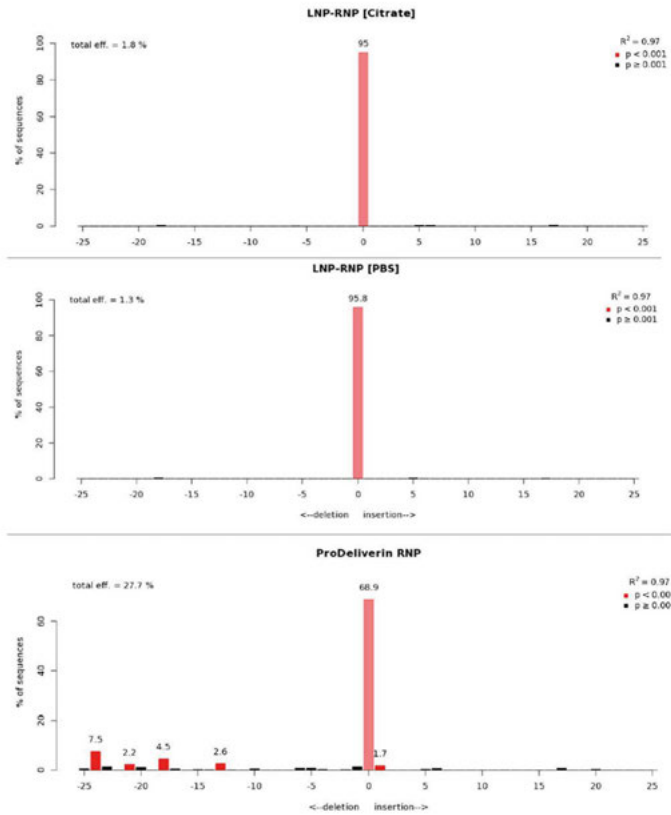
Figure S16: **Raw TIDE data for LNP-RNP formulations complexed in citrate (top) and PBS (middle) with DOTAP 5 mole%. Bottom graph is the raw TIDE data for the positive transfection control, ProDeliverIn RNP.**

Method statistical analysis

To determine the significant effect of formulation condition, molar ratio of DOTAP, or experimental variation on gene editing outcome a three-way ANOVA was performed on R. To illustrate the experimentally observed determinants of editing efficiency, a recursive partitioning and regression tree was generated using the R-package rpart with the minsplit-parameter (minimum number of observations per node to be considered for splitting) set to 10, otherwise default settings were used. Efficiency was regressed based on the parameters: dotap (0%, 0.25%, 2%, 5%), condition (H20 vs. HEPES), and experimental series (E1, E2, or E3). The generated tree was drawn using the R-package partykit (2).

1) Terry Therneau, Beth Atkinson and Brian Ripley (2017). rpart: Recursive Partitioning and Regression Trees. R package version 4.1-11. https://CRAN.R-project.org/package=rpart

2) Torsten Hothorn, Achim Zeileis (2015). partykit: A Modular Toolkit for Recursive Partytioning in R. Journal of Machine Learning Research, 16, 3905-3909. URL http://jmlr.org/papers/v16/hothorn15a.html

Analysis of results of statistical analysis

Statistical analysis shows that nuclease-free water, especially with lower molar ratio of DOTAP, results in higher gene editing outcomes than particles formulated in HEPES buffer. Formulations made in HEPES buffer seem to require a higher molar ratio of DOTAP.
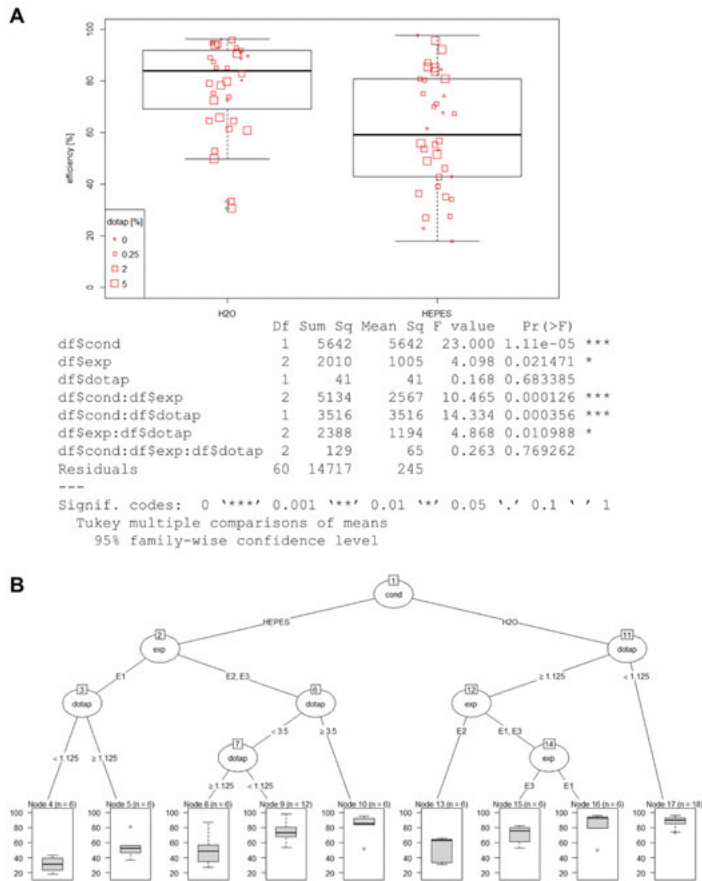
A

```
                       Df Sum Sq Mean Sq  F value   Pr(>F)
df$cond                 1   5642    5642   23.000 1.11e-05 ***
df$exp                  2   2010    1005    4.098 0.021471 *
df$dotap                1     41      41    0.168 0.683385
df$cond:df$exp          2   5134    2567   10.465 0.000126 ***
df$cond:df$dotap        1   3516    3516   14.334 0.000356 ***
df$exp:df$dotap         2   2388    1194    4.868 0.010988 *
df$cond:df$exp:df$dotap 2    129      65    0.263 0.769262
Residuals              60  14717     245
---
Signif. codes:  0 '***' 0.001 '**' 0.01 '*' 0.05 '.' 0.1 ' ' 1
   Tukey multiple comparisons of means
     95% family-wise confidence level
```

B

Figure S17: **Statistical analysis to determine the effect of formulation condition, experimental repeat, and molar ratio of DOTAP on gene knock-out efficiency. A)** Boxplots show range of gene knockout efficiency on HEK293T stoplight cells for the two formulation conditions 50 mM HEPES buffer pH 7.35 and nuclease-free water (H_2O) over the span of three individual experiments and various formulations with different molar ratios of DOTAP (0%, 0.25%, 2%, 5%). The latter is represented with varying square point sizes (smallest – 0% DOTAP, largest square – 5% DOTAP). Statistical significance is indicated with (*). Cond – HEPES buffer or nuclease-free water; exp – three repeats of experiment, dotap – molar ratio of DOTAP in lipid formulation. **B)** Recursive partitioning and regression tree to visualize effect of formulation condition, molar ratio of DOTAP, and experimental repeats on gene editing efficiency.

3

Input Image	**Stack Processing :** Individual Planes **Flatfield Correction :** None		
Find Nuclei	**Channel :** BP445/45 **ROI :** None	**Method :** B Common Threshold : 0.4 Area : > 30 µm² Split Factor : 7.0 Individual Threshold : 0.4 Contrast : > 0.1	Output Population : Nuclei
Select Cell Region	**Population :** Nuclei	**Method :** Resize Region [%] Region Type : Nucleus Region Outer Border : -60 % Inner Border : 100 %	Output Region : Nucleus Region
Calculate Intensity Properties	**Channel :** BP600/37 **Population :** Nuclei **Region :** Nucleus Region	**Method :** Standard Mean	Output Properties : Intensity Nucleus Region BP600/37
Select Population	**Population :** Nuclei	**Method :** Filter by Property Intensity Nucleus Region BP600/37 Mean : > 250	Output Population : mCherry +
Calculate Intensity Properties (2)	**Channel :** BP525/50 **Population :** mCherry + **Region :** Nucleus Region	**Method :** Standard Mean	Output Properties : Intensity Nucleus Region BP525/50
Select Population (2)	**Population :** mCherry +	**Method :** Filter by Property Intensity Nucleus Region BP525/50 Mean : > 200	Output Population : eGFP +
Define Results	**Method :** List of Outputs **Population :** mCherry + Number of Objects Apply to All :		

Figure S18: **Columbus analysis method used to calculate the EGFP-positive population in the Stoplight gene-editing assay.**
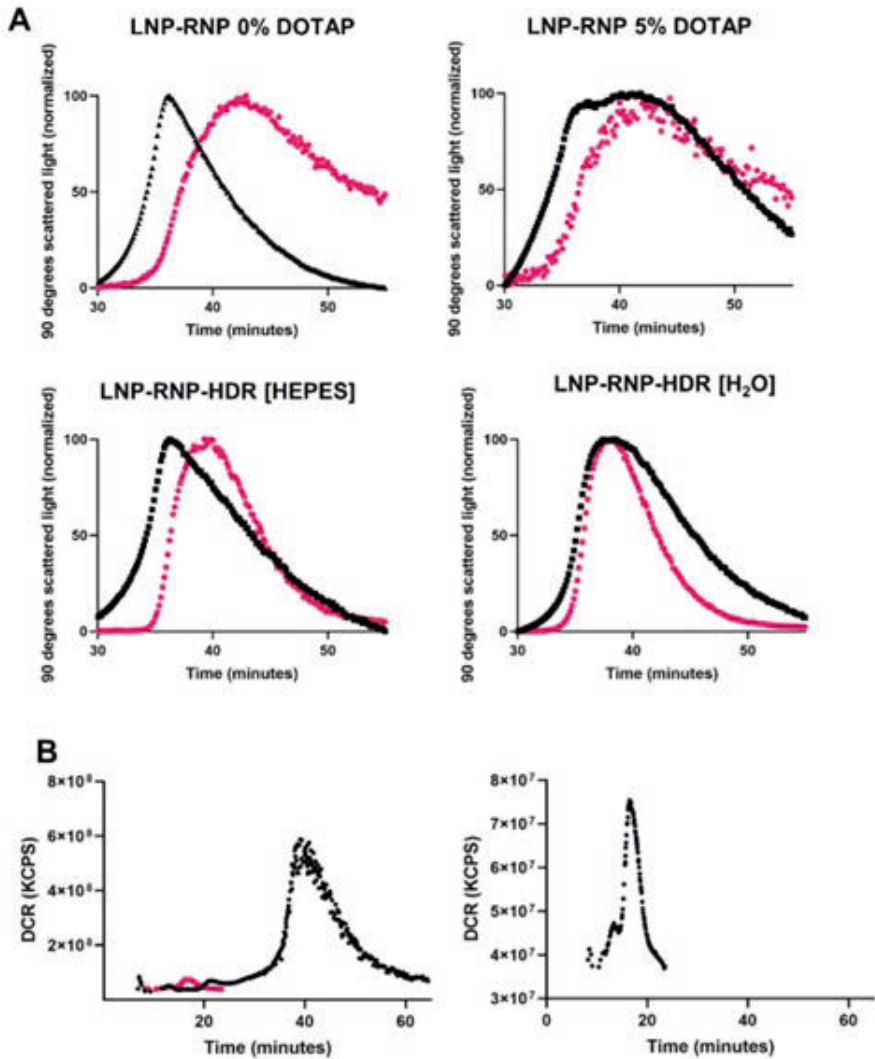
Figure S19: **A:** AF4 fractogram of 90 degrees scattered light (normalized) (lowest signal value corresponds to 0% and highest value corresponds to 100%) to visualize retention time of particles with (black) and without incubation with 20% plasma (pink). **B:** Left panel: Overlay fractogram recorded by DLS detector of LNP-RNP-HDR [H$_2$O] particle incubated with plasma (black) and plasma control (pink). Right panel: MALS fractogram recorded by DLS detector of plasma control sample.
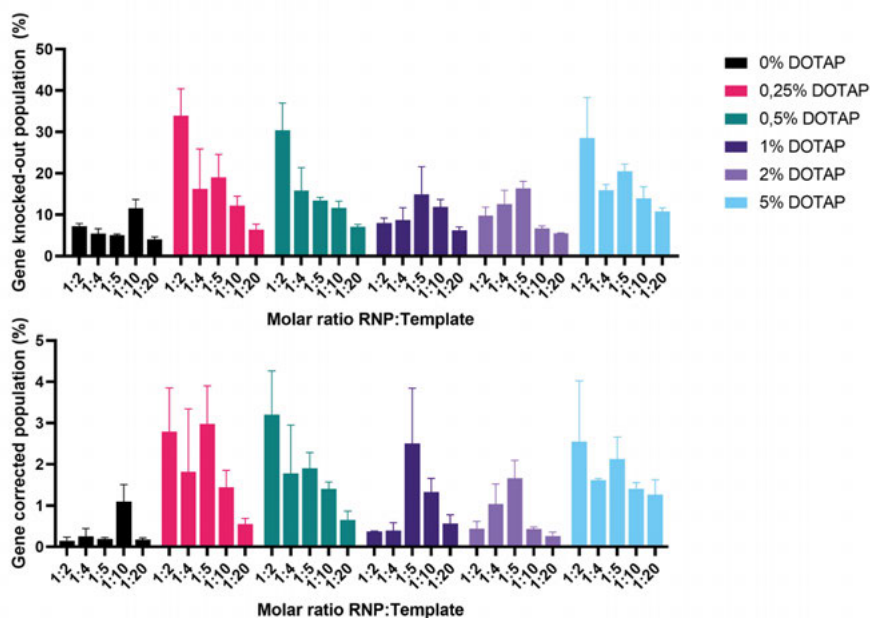
Figure S20: LNP-RNP-HDR [HEPES] optimization study with additional DOTAP concentrations. Removal of DOTAP from the formulation leads to an overall decrease of the editing efficiency.
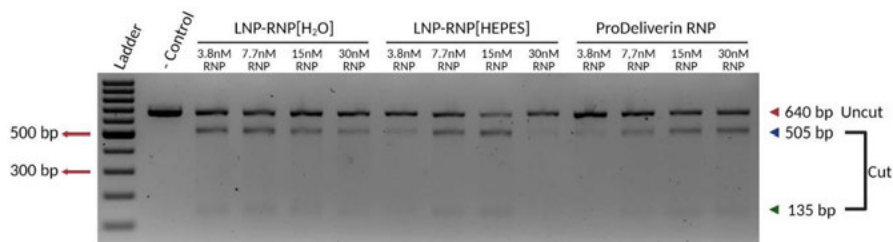

Figure S21: Full T7E1 assay performed on HEK-EGFP treated with ascending dosages of LNP-RNP-HDR with a 1:2 molar ratio of RNP:HDR template and 0.25% DOTAP in the formulation. ProDeliverIN RNP were prepared with an additional 1:1 molar ratio of HDR template. Cells were harvested from the same population as the flow cytometry data presented in Fig. 6.d.

4

Comparative Analysis of Lipid Nanoparticle-Mediated Delivery of CRISPR-Cas9 RNP versus mRNA/sgRNA for Gene Editing *In Vitro* and *In Vivo*

Johanna Walther[1], Deja Porenta[1,2], Danny Wilbie[1], Cornelis Seinen[3], Naomi Benne[2], Qiangbing Yang[3,4], Olivier Gerrit de Jong[1], Zhiyong Lei[3,4], Enrico Mastrobattista[1]

[1]Department of Pharmaceutics, Utrecht Institute for Pharmaceutical Sciences (UIPS), Utrecht University, The Netherlands

[2]Department of Infectious Diseases and immunology, Faculty of Veterinary Medicine, Utrecht University, The Netherlands

[3]CDL Research, University Medical Center Utrecht, The Netherlands

[4]Department of Cardiology, Laboratory of Experimental Cardiology, University Medical Center Utrecht, The Netherlands

Abstract

The discovery that the bacterial defense mechanism, CRISPR-Cas9, can be reprogrammed as a gene editing tool has revolutionized the field of gene editing. CRISPR-Cas9 can introduce a double-strand break at a specific targeted site within the genome. Subsequent intracellular repair mechanisms repair the double strand break that can either lead to gene knock-out (via the non-homologous end-joining pathway) or specific gene correction in the presence of a DNA template via homology-directed repair. With the latter, pathological mutations can be cut out and repaired. Advances are being made to utilize CRISPR-Cas9 in patients by incorporating its components into non-viral delivery vehicles that will protect them from premature degradation and deliver them to the targeted tissues. Herein, CRISPR-Cas9 can be delivered in the form of three different cargos: plasmid DNA, RNA or a ribonucleoprotein complex (RNP). We and others have recently shown that Cas9 RNP can be efficiently formulated in lipid-nanoparticles (LNP) leading to functional delivery *in vitro*. In this study, we compared LNP encapsulating the Cas9 mRNA, sgRNA and HDR template against LNP containing Cas9-RNP and HDR template. Former showed smaller particle sizes, better protection against degrading enzymes and higher gene editing efficiencies on both reporter HEK293T cells and HEPA 1-6 cells in *in vitro* assays. Both formulations were additionally tested in female Ai9 mice on biodistribution and gene editing efficiency after systemic administration. LNP delivering mRNA Cas9 were retained mainly in the liver, with LNP delivering Cas9-RNPs additionally found in the spleen and lungs. Finally, nanoparticles delivering mRNA Cas9 and sgRNA resulted in 60% gene knock-out in hepatocytes in mice. Delivery of mRNA Cas9 as cargo format was thereby concluded to surpass Cas9-RNP for application of CRISPR-Cas9 for gene editing *in vitro* and *in vivo*.

Introduction

Gene therapy is medical technology that modifies or manipulates the expression of a gene for therapeutic use. The discovery of reprogramming Clustered Regularly Interspaced Short Palindromic Repeats (CRISPR) associated (Cas) endonuclease, such as Cas9, as a genome editing tool, will greatly benefit gene therapy.[1] The Cas9 endonuclease forms an active ribonucleoprotein complex (RNP) with a synthetic single-guide RNA (sgRNA) and introduces a double strand break in the genome complementary to the sgRNA.[2] Succeeding cellular DNA repair mechanisms may either lead to gene knock-out by inducing insertions and deletion mutations (indels) via non-homologous end-joining (NHEJ) or repair via homology-directed repair (HDR) making use of exogenous DNA with the correct sequence flanked by homology arms complementary to the targeted genome sequence.[3] Especially the latter is promising for gene therapy as a pathological mutation can be corrected in this manner.

For therapeutic application the CRISPR-Cas9 components require an *in vivo* delivery vehicle that arrives at the targeted cell population and delivers the CRISPR-Cas9 components intracellularly. Different viral and non-viral vectors are being designed for CRISPR-Cas9.[4] Especially non-viral nanoparticles are of great interest due to their relative ease of manufacturing. Moreover, viral vectors face the additional challenge of limitation in cargo size.[5] Amongst non-viral vectors, lipid nanoparticles (LNP), which employ cationic or ionizable cationic lipids, serve as promising candidates for delivery of Cas9 gene editing tool. The benefits of including ionizable cationic lipids in LNP formulations, such as C12-200, are effective encapsulation of cargo via electrostatic interactions, enhanced *in vivo* circulation time and cellular uptake, and endosomal cargo release.[6–8] Therefore, LNPs have been optimized for delivery of negatively charged nucleic acids such as plasmid DNA and mRNA, but also for Cas9-RNP.

Despite the low costs and stability of plasmid DNA, recent efforts focus on delivering the cargo formats Cas9 mRNA or Cas9 RNP via

lipid nanoparticles to reduce the risk of genomic integration and to minimize the delayed onset of gene editing.[14] Unlike plasmid DNA, which requires access to the nucleus for transcription to occur, Cas9 mRNA only needs to be delivered into the cytosol.[15] Delivery of mRNA molecules via LNPs have been shown to trigger Toll-like receptor 4 responses and subsequent immune responses that can then override the translation of mRNA to functional protein.[16] However, advances in chemical modifications such as substitution with pseudouridine, N6-methyladenosine or inosine suppress innate immune responses, and 5′-cap and secondary structures at the 3′-terminus improve the resistance to RNAses.[17,18] The first clinical trials with mRNA Cas9 are on-going and resulting in promising genome editing outcomes, for example NTLA-2001 from Intellia Therapeutics which resulted in 87% gene knock-out of TTR after a single dose of 0.3 mg per kilogram NTLA-2001 in patients.9 In the case of delivery of the mRNA Cas9 the sgRNA needs to additionally be packaged within the LNP. The sgRNA then needs to form the RNP complex intracellularly after translation of the protein to perform gene editing in the nucleus.[19] For direct availability of the RNP, on-going efforts focus on formulating LNPs incorporating the Cas9 RNP.[10,20] It has been reported that the direct delivery of RNP would result in less off-target events as the Cas9-RNP is short-lived.[21] Furthermore, the use of RNPs ensures protection of sgRNA from degradation and at the same time complexation with sgRNA keeps Cas9 in its functional confirmation.[22,23] However, despite the net-negative charge of the Cas9-RNP allowing electrostatic interactions with the lipids, the negative charge is not uniformly distributed over the RNP surface.[24] Additionally, RNP is a large molecule. These attributes can affect the encapsulation of protein and moreover impact the structure, size and charge of LNPs. Due to different cellular membrane permeabilities and thus altering ability to take up LNPs varying in structure, size and charge, LNPs delivering Cas9-RNP may not be deliverable to all types of cells.[25] Just as LNPs delivering mRNA have shown immune activation described above, preexisting immunity against the bacterial protein risk premature clearance or toxicity.[26,27] In both cases, mRNA

Cas9 or Cas9-RNP, a DNA HDR template will have to be packed within the LNP additionally in case of a precise repair strategy based on HDR.

For a better understanding and comparison, delivery of mRNA Cas9 and Cas9-RNP together with an HDR template via LNPs were investigated in this study. The advantages and disadvantages of these two formulations were determined by analyzing the physical characterizations of the formulations, the activity of the LNPs on two different cell types *in vitro*, and the respective activation of inflammatory responses. Furthermore, the LNPs were compared in biodistribution and genome editing efficiencies *in vivo*.

Material and Methods

All reagents and chemicals were commercially obtained from Sigma Aldrich (Zwijndrecht, The Netherlands) unless otherwise specified. SpCas9 was produced in-house via the method described in previous publication.[10] To fluorescently label the SpCas9, Alexa Fluor 647-C2 maleimide (ThermoFisher Scientific, Landsmeer, The Netherlands) was incubated with SpCas9 in a 20:1 molar ratio of dye to protein in Tris buffer pH 7.4 (20 mM Tris, 300 mM NaCl). After overnight incubation at 4 °C, the excess dye was removed by gravity column chromatography using a PD 10 desalting column. After addition of 10% glycerol, the labelled proteins were frozen in liquid nitrogen and stored at -80 °C. 2'O-methyl and phosphorothioate modified sgRNA as well as the Cy5.5-labelled sgRNA and template DNA were bought from Sigma-Aldrich (Haverhill, United Kingdom) and were stored in RNAse-free Tris EDTA buffer pH 7.0 (ThermoFischer Scientific). CleanCap™ mRNA Cas9 (5moU) was acquired from TeBu Bio (Heerhugowaard, The Netherlands). This mRNA was then fluorescently labelled with Cy5 in-house with the Label IT Nucleic Acid Labelling Cy5 Kit from Mirus Bio (Oxford, United Kingdom) following the

manufacturer's protocol. Additionally, mRNA Cas9-GFP was ordered from Horizon Discovery (Waterbeach, United Kingdom). Furthermore, 1,10-((2-(4-(2-((2-(bis(2-hydroxydodecyl)amino)-ethyl)-(2-hydroxydodecyl)amino)ethyl)piperazin-1-yl)ethyl)azanediyl)bis(dodecan-2-ol) (C12-200) was acquired from CordonPharma (Plankstadt, Germany), 1,2-dioleoyl-sn-glycero-3-phospho-ethanolamine (DOPE) from Lipoid (Steinhausen, Switzerland), Cholesterol and 1,2-dimyristoyl-rac-glycero-3-methoxypolyethyleneglycol-2000 (PEG-DMG) from Sigma-Aldrich, and 1,2-dioleoyl-3-trimethylammonium-propane (DOTAP) from Merck (Darmstadt, Germany).

Synthesis of Modified mRNA Cas9

The production of modified mRNA was adapted from Warren et al.[28] Briefly, Cas9 plasmid served as template for PCR to prepare the IVT template. Forward primer used in the PCR was:

5'-TAATACGACTCACTATAAGGAAATAAGAGAGAAAAG -3'

and reverse primer used to introduce 120 polyA tail sequence is:

5'-CTTCCTACTCAGGCTTTATTCAAAGACCA(T)120-3'.

These primers were synthesized by Integrated DNA Technologies (Leuven, Belgium). Reverse primer was synthesized as Ultramer oligos at a 4 nmol scale. The modified mRNA was synthesized with slight modifications as described by Kogut et al.[29] For each 50 μl reaction of the VENI all-in-one mRNA Synthesis Kit with cap1 Analog (Leish Bio, Utrecht, The Netherlands), 2 μg of purified tail PCR product was provided as template. The final nucleotide concentrations in the reaction were 6 mM for the cap1 analog and 7.5 mM for adenosine triphosphate, guanosine triphosphate, cytidine triphosphate and N1-methylpseudouridine triphosphate. The RNA synthesis reaction was incubated at 37 °C for 30 minutes as instructed by the manufacturer. Subsequently, the RNA was purified through LiCL precipitation, dissolved in nuclease-free water, and quantified using Nanodrop (ThermoFisher Scientific). The purified RNA was stored at -20 °C until further use.

Formulation of Lipid Nanoparticles
Cas9-RNP LNPs co-delivering an HDR template (called *p*LNP-HDR for the rest of the manuscript) were formulated as described in a previous publication.[10] In short, Cas9 and sgRNA were mixed together at a 1:1 molar ratio (1.6 μM sgRNA) to formulate the ribonucleoprotein complex. After 15 minutes, an ssODN HDR template was added at a 2:1 molar ratio to the RNP. The CRISPR-Cas9 components were then mixed by pipette-mixing with the lipids at a volume ratio of 3:1 and weight ratio 40:1 (total lipids to sgRNA). The lipid composition is C12-200, DOPE, cholesterol, PEG-DMG, DOTAP with molar ratios of 35:16:46.5:2.5:0.25, respectively. To formulate mRNA Cas9 formulations (named *m*LNP-HDR), the same lipid composition and ratio to sgRNA concentration was used. HDR template concentration was also kept the same. However, as described in literature, mRNA Cas9 was added at a 4:1 weight ratio to the sgRNA.[20]

LNPs used in the animal studies were made with the same properties but at higher concentrations (RNP = 15 μM). mRNA Cas9 used for the formulations for *in vivo* was synthesized as described above. These LNP were made without an HDR template, but only encapsulate the Cas9-RNP (named *p*LNP) or Cas9 mRNA and sgRNA (name *m*LNP). Additionally, the formulations were dialyzed against 1x PBS overnight with Float-A-Lyzer molecular weight cut-off (MWCO) 300 kDA dialysis chambers (Avantor®, Arnhem, The Netherlands).

All sequences of sgRNA and HDR template used in this study are given in Supplementary Table 1.

Physical Characterizations of the Cas9-RNP and mRNA LNPs
The average size and polydispersity index (PDI) of the lipid nanoparticle formulations were determined after a 1.3-fold dilution in 1 X PBS (pH 7.4) by dynamic light scattering using a Zetasizer Nano S (Malvern ALV CGS-3, Malvern, United Kingdom). The Zetasizer Nano Z (Malvern ALV CGS-3, Malvern, United Kingdom) was used to determine the ζ-potential, whereby the formulations had prior to

measurements been diluted 9-fold in 10 mM HEPES buffer at pH 7.4.

Gel Assays

Fluorescently-labelled CRISPR-Cas9 components (Alexa647-SpCas9, Cy5-mRNA Cas9, ATT550-sgRNA, 6-FAM-HDR-template) were complexed with lipids as described above to obtain a Cas9-RNP and an mRNA formulation. Then, 40% glycerol was added to the LNPs to reach a final concentration of 10% glycerol (1:5 v/v). Twenty microliters of the glycerol-treated samples were loaded onto a 2% agarose gel and run at 100 V for 30 minutes in 1 x TAE buffer pH 8 (BioRad Laboratories B.V, Veenendaal, The Netherlands). The gel was then imaged with ChemiDoc Imaging System (Bio-Rad Laboratories B.V) using the channels (Cy5 (protein and mRNA), Alexa488 (HDR template), Alexa467 (sgRNA) to depict the fluorescent signals.

To determine the degree of protection of the CRISPR-Cas9 components provided by the LNP complexation against trypsin and RNase degradation, Alexa647-labelled Cas9-RNP and Cy5-labelled mRNA formulations were treated with different percentages of trypsin and RNase (0, 1, 5, 10, 20, 50%), respectively, for 30 minutes at 37 °C. Twenty microliters of the glycerol-treated samples were loaded onto a 2% agarose gel and run at 100 V for 30 minutes. The gel was then imaged with a ChemiDoc Imaging System (Bio-Rad Laboratories B.V) using the Cy5 channel. The percentage of degradation was quantified by determining the intensity of the gel bands by densitometry in ImageJ (version 1.52p).

Imaging of LNPs with Cryo-TEM

Ten microliter of nanoparticles in suspension in 1x PBS were added to freshly glow-discharged quantifoils and incubated for at least 10 minutes in a humidified environment. Then, the samples were vitrified using a FEI Mark IV Vitrobot (Fei, Hillsboro OR, USA) and subsequently stored in liquid nitrogen until imaging. Samples were imaged on a FEI Tecnai G2 20 TWIN 200kV transmission electron microscope whereby

vitrified quantifoils were loaded in a Gatan 70° tilt cryo-transfer system (pre-cooled using liquid nitrogen) and inserted in the microscope. Samples were imaged at a magnification of 29k and images were acquired by the bottom-mounted FEI High-Sensitive (HS) 4k x 4k Eagle CCD Camera System.

Generation of eGFP Hepa 1-6

To produce hepatocyte cells stably expressing eGFP, lentivirus vectors encoding for eGFP and antibiotic-resistance towards puromycin were used for lentiviral production. Firstly, HEK293T cells (ATCC, Molsheim Cedex, France) were passaged to ensure a 30-50% confluency on the following day in a T25 cell culture flask. After obtaining 30-50% confluency, the HEK293T cells were transfected with a mixture of 2 μg PSPAx2, 2 μg pMD2.G-G, and 4 μg lentiviral transfer plasmid (pHAGE2-EF1a-eGFP-IRES-PuroR-WPRE) in OptiMEM using 3 μg PEI per μg DNA and incubated at 37 °C and 5% CO_2 overnight. The medium was refreshed with 5.5 mL DMEM medium supplemented with 10% FBS (S1810-500, Biowest, VWR International, Amsterdam, The Netherlands) and 1% antimycotic/antibiotic solution and placed back into the cell incubator for 48 hours. Then, the conditioned medium was harvested from the HEK293T cells into a 15 ml falcon tube and centrifuged at 500 x g for 5 minutes. The supernatant was isolated and filtered through a 0.45 μm RC membrane filter (Phenomenex, Utrecht, The Netherlands). To generate eGFP expressing Hepa 1-6 cells, Hepa 1-6 cells (ATCC, CRL-1830, Molsheim Cedex, France) were incubated with the filtered supernatant at 37 °C and 5% CO_2 for 3 days and eGFP-positive cells were selected by culturing in the presence of 2 μg puromycin (InvivoGen, Toulouse, France) per ml DMEM high glucose medium (Sigma, Merck Life Science NV) supplemented with 10% FBS for 3 weeks. Subsequently, eGFP positive cells were sorted using a BD FACSAria III cell sorter and afterwards continuously expanded in the presence of selection antibiotic puromycin.

Cell Culture

eGFP HEK293T cells were cultured at 37 °C and 5% CO_2 in DMEM low

glucose (Sigma, Merck Life Science NV, Amsterdam, The Netherlands) supplemented with 10% FBS (S1810-500, Biowest) and 1 mg/ml geneticin (G418 sulfate, ThermoFischer Scientific).10 eGFP HEPA1-6 cells were cultured as described above. HEK293T cells and HEK293T HDR Stoplight cells were cultured in DMEM low glucose medium supplemented with 10% FBS.30

Gene Editing Efficiency Assay on eGFP HEK293T and eGFP Hepa1-6 Cells

eGFP HEK293T cells or eGFP HEPA1-6 cells were plated with a cell density of 10,000 cells/well onto a clear F-bottom 96-well plate and incubated at 37 °C and 5% CO_2. The following day, the medium was supplemented with antibiotic/antimycotic solution. *p*LNP-HDR or *m*LNP-HDR (using sgGFP and HDR template for GFP -> BFP conversion)[10] were then added to wells in duplicates in different concentrations (0-30 nM sgRNA) and the cells were then incubated for two days at 37 °C and 5% CO_2.[31] Cells were passaged to 12 well plates and expanded for two additional days and then harvested, washed twice and fixed in 1% paraformaldehyde. Cells were transferred to a BD Falcon U-bottom 96-well plate (Becton Dickinson, Franklin Lakes, NJ, USA) for detection of fluorescent signal by flow cytometry using the BD FACS CANTO II (Becton Dickinson). BFP signal was excited by laser with 405 nm wavelength and picked up by filter 450/50 (laser 405 nm) and eGFP fluorescence was excited by laser with wavelength 488 nm and detected in filter 530/30. Data was then analyzed with the Flowlogic software (version 8.6, Inivai Technologies, Mentone, Australia). Cell populations classified as gene knock-out are eGFP negative and BFP negative and cell populations classified as gene correction are eGFP negative and BFP positive.[10]

The experiment was repeated three individual times, whereby in one experiment a positive control was additionally added. ProDeliverIN CRISPR (Oz Biosciences, San Diego, California) was used to deliver the RNP and HDR template in a molar ratio of 15:15:28.5 nM (Cas9:sgRNA:HDR).

Uptake of eGFP-Cas9 RNP vs eGFP-Cas9 mRNA LNPs in HEK293T Cells

HEK293T cells were plated at a cell density of 10,000 cells/well on a flat bottom black 96-well plate and then incubated at 37 °C and 5% CO_2 overnight. Ten microliters (sgRNA concentration = 15 nM) of either eCas9-GFP RNP or eCas9-GFP mRNA LNPs were added to the wells at different timepoints. The wells were then treated collectively with the nuclei stain Hoechst 33342 at a final concentration of 2 μg/ml in Opti-MEM (Gibco TM, Fisher Scientific) for 10 minutes at 37 °C and 5% CO_2. The cells were then imaged with confocal microscopy using the Yokogawa Cell Voyager 7000S (CV7000S) Confocal Microscope (Yokogawa Corporation, Tokyo, Japan). Signal intensities of GFP within the detected nuclei were determined with image analysis using the Columbus Software (Perkin Elmer, version 2.7.1). The analysis method can be found in supplementary Fig. 7.

Timing of Gene Correction on HEK293T HDR Stoplight Cells

To follow the onset of gene correction mediated through pLNP or mLNP, HEK293T HDR Stoplight cells were used.30 These cells continuously express mCherry however, upon introduction of a double strand break downstream of the mCherry coding sequence and subsequent homology directed repair, a stop codon (TAA) is altered to Glutamine (GAA), resulting in eGFP expression.

The cells were plated at a density of 10,000 cells/well in low glucose DMEM medium supplemented with 10% FBS on a flat bottom black 96-well plate (Greiner #955090) and incubated at 37 °C and 5% CO_2. The following day, 10 μl (sgRNA concentration = 15 nM) of either pLNP-HDR or mLNP-HDR were added to the wells at different time-points. After 48 hours, all wells were washed by aspirating off the medium and treated with the nuclear stain Hoechst at a final concentration of 2 μg/ml in OptiMEM for 10 minutes at 37 °C and 5% CO_2. Then, the cells were imaged with confocal microscopy using the Yokogawa CV7000S Confocal Microscope. Gene correction efficiencies (= # GFP positive cells/# mCherry positive cells) were determined by image analysis with Columbus Software (Perkin Elmer, version 2.7.1).

The analysis method can be found in supplementary Fig. 8. Additionally, the mean fluorescent intensity of GFP was calculated for all cells of one microscopy image.

Determination of Cytokine Production via qPCR

Bone marrow isolated from the femurs and tibias of WT BALB/c mice were homogenized and seeded in 6-well plates at a cell density of 450,000 cells/mL in 2 mL IMDM (Gibco, ThermoFisher Scientific, Landsmeer, The Netherlands) supplemented with 10% FCS (Bodinco, Alkmaar, The Netherlands), 100 units/mL of penicillin (Gibco, ThermoFisher Scientific), 100 ug/mL of streptomycin (Gibco, ThermoFisher Scientific) and 0.5 μM β-mercaptoethanol (Gibco, ThermoFisher Scientific). To induce DC differentiation, 20 ng/mL of granulocyte-macrophage colony-stimulating factor (GM-CSF, in-house produced) was added. Cells were cultured at 37°C and 5% CO_2 for a total of 6 days. After 2 days, 2mL of IMDM and 20ng/mL GM-CSF were added to the wells. On day 5 GM-CSF (20ng/mL) was added. On day 6, cells were harvested by scraping. For qPCR cells were plated out at 900,000 cells/well in an F-bottom 12-well plate. The cells were left to adhere for 2 hours. Cells were stimulated with different concentrations pLNP-HDR and mLNP-HDR based on sgRNA molar concentration (30, 15, 7.5 nM). As controls, immature DCs (iDCs) were unstimulated, and mature DCs (mDCs) were stimulated with 10 ng/mL LPS (O111:B4; Sigma-Aldrich). After 24 hours, supernatants were carefully removed, and cells were lysed with RLT buffer (Qiagen Benelux B.V., Venlo, the Netherlands). Total mRNA was immediately extracted using the RNeasy kit (Qiagen) according to the manufacturer's instructions. Transcription of mRNA into cDNA was performed using the iScript™ cDNA Synthesis Kit (Bio-Rad Laboratories B.V.) according to manufacturers' instructions. PCR and Real-Time detection were performed using a Bio-Rad MyiQ iCycler (Bio-Rad). Amplification was performed using IQ™ SYBR Green® Supermix (Bio-Rad) with 0.25 μM final concentrations of primer sets for IL10 (5'-GGT TGC CAA GCC TTA TCG GA-3' and 5'-ACC TGC TCC ACT GCC TTG CT-3'), IL12B (5'-GGA AGC ACG

GCA GCA GAA TA-3′ and 5′-AAC TTG AGG GAG AAG TAG GAA TGG-3′), TNF (5′-CCC TCA CAC TCA GAT CAT CTT CT-3′ and 5′-GCT ACG ACG TGG GCT ACA G-3′), IFNA1 (5′-TAC TCA GCA GAC CTT GAA CCT-3′ and 5′-CAG TCT TGG CAG CAA GTT GAC-3′), TRAF6 (5′-AAA GCG AGA GAT TCT TTC CCT G-3′ and 5′-ACT GGG GAC AAT TCA CTA GAG C-3′), and HPRT (5′-CTG GTG AAA AGG ACC TCT CG-3′ and 5′-TGA AGT ACT CAT TAT AGT CAA GGG CA-3′). The qPCR was performed for 40 cycles using the following settings: denaturation at 95 °C for 20 sec, annealing at 59°C for 30 sec. mRNA expression within each sample was normalized to the detected Ct value of HPRT and expressed relative to the average Ct value of the mDC control.

Animal Studies
Twenty-four female Ai9 mice (B6.Cg-Gt (ROSA) 26Sor tm9 (CAG-tdTomato) Hze/J) were bred at PSP Bilthoven (Bilthoven, The Netherlands) and were 8-12 weeks old at the start of the animal study. Animals were kept under standard conditions of the animal facility (standard chow and water *ad libitum*) and all experiments were approved by the Animal Experiment Committee of Utrecht University and complied with the Dutch Experiments on Animals Act (WOD) under the license AVD10800202115026.

The animal study was split into two parts: 1.) Biodistribution of Cy5.5-labelled sgRNA targeting a stop codon prior to the tdTomato gene construct (Cy5.5-sgTOM) delivered via *p*LNP or *m*LNP in comparison to a non-targeting unlabelled sgRNA targeting nucleotides 200–219 in the eGFP construct (sgGFP) in *p*LNP (see supplementary information table 1 and 2.). Functionality of gene knock-out resulting in tdTomato expression after IV injections of *p*LNP and *m*LNP (both formulations without HDR template). Each experimental group for each part had four mice per group.

Biodistribution
Mice were administered with LNP encapsulating RNP (5% Cy5.5-sgTOM) or mRNA and sgTOM (5% Cy5.5-sgTOM) at a dose

of 20 μg of total sgRNA by tail vein injections. Control mice were administered with LNP encapsulating RNP (unlabelled sgGFP) at the same dose of total sgRNA. After 4 hours, mice were anesthetized with 0.1 mg/kg fentanyl, 10 mg/kg midazolam and 1 mg/kg medetomidine via IP injection, and perfused with PBS via the left ventricle cavity. Liver, kidney, lungs, spleen, heart, ovaries, and brain were harvested for further analysis.

Functionality of gene knock-out

Mice of all three experimental groups (*p*LNP, *m*LNP, and non-targeting *p*LNP) were injected with LNPs at a dose of 20 μg sgTOM via tail vein injections. Seven days later, mice were anesthetized with 0.1 mg/kg fentanyl, 10 mg/kg midazolam and 1 mg/kg medetomidine via IP injection and then perfused with PBS. Liver, kidney, lungs, spleen, heart, ovaries and brain were collected for further analysis.

Biodistribution of Cy5.5-Labelled sgRNA Delivered via LNP RNP or LNP mRNA Cas9 & sgRNA

Harvested organs of mice administered with LNPs as described above were imaged with a Pearl Impulse Imager (LI-COR Biosciences) using channels 700 nm, 800 nm, and white to trace back Cy5.5-labelled sgRNA. All images were further analyzed by Image Studio Lite Software (LI-Cor Biosciences). To quantify the fluorescent signal a region of interest was drawn manually around the separate organs and the total fluorescent intensity was divided by the weight of the imaged organ.

Single Cell Flow Cytometry

One third of the harvested liver was further processed for single cell flow cytometry. The tissue was submerged in 5 ml prewarmed digestion buffer (RPMI-1640 medium supplemented with 1 mg/ml type IV collagenase A (Sigma-Aldrich, Cat. No. C5138)) and minced with surgical blades. The minced tissue was then transferred to a 50 ml falcon tube and another 10 ml of digestion buffer was added and incubated at 37 °C for 30 minutes while gently swirling the mixture every 5 minutes. Then, the digested cell suspension was strained through

a nylon cell strainer (ThermoFisher Scientific). The strained suspension was centrifuged at 70g for 2 minutes to separate the parenchymal and non-parenchymal cells. The supernatant containing the non-parenchymal cells was transferred to a new tube and centrifuged at 500g for 7 minutes at 4 °C and the supernatant was then removed. The cell pellet was resuspended in 2 ml ACK lysis buffer (Gibco, ThermoFisher Scientific) for 3 minutes, and then diluted with cold PBS. Cells were again centrifuged at 500g for 7 minutes at 4 °C. Meanwhile, the parenchymal cells were washed with 10 ml cold PBS and then centrifuged at 70g for 2 minutes at 4 °C. The cells were resuspended in 200 μl of RPMI-1640 medium and transferred to a 96-well V-bottom plate (ThermoFisher Scientific) and stored on ice until further processing. The pelleted non-parenchymal cells were resuspended in 1-5 ml RPMI-1640 medium and plated onto the V-bottom plate with a cell density of 300,000 cells/well. The plate was centrifuged at 175 x g for 5 minutes at 4 °C. Cells were resuspended in 25 μl of FcBlock (2.4G2 monoclonal antibody, produced by Department of Infectious Diseases and Immunology, Utrecht University) and incubated for 5 minutes at 4°C.[32] Seventy-five microliter of antibody staining solution in FACS buffer (2% FCS, 0.005% NaN$_3$ in PBS) was added per well (see table 1 and supplementary table 2) and the stained plate was incubated in the dark for 30 minutes. Cells were washed with PBS three times and then resuspended in 100 μl of FACS buffer and measured on the CytoFlex LX flow cytometer. Data was processed and analyzed in FlowLogic and the gating strategy is shown in Supplementary Fig. 11.

Table 1: **Antibody staining of parenchymal and non-parenchymal liver cells.** For more information about the antibodies see supplementary table 2. As indicated in the table, laser 561 paired with filter 585-42 was used for the detection of PE-labelled MHC-II antibody or tdTomato *in vivo*. Laser 637 paired with filter 712-25 was either used for detection of Cy5.5 fluorescence (biodistribution study) or Alexa700-labelled MHC-II (functionality study).

Laser	Filter	Fluorophore	Marker	Dilution of antibody
405	450-45(405)	eFluor 450	CD11b	1:800
	525-40(405)	BV510	CD31	1:200
			B220	1:200
488	525-40(488)	Alexa488	CD45	1:400
561	585-42(561)	PE (biodistribution) or tdTomato	MHC-II (biodistribution) or gene editing	1:800
	763-43(561)	PE-Vio770	CD11c	1:400
637	660-10(637)	APC	F4/80	1:200
	712-25(637)	Cy5.5 or Alexa700 (functionality)	LNP or MHC-II (functionality)	1:400
808	885-40(808)	Viakrome	Live/dead	1:1000

Results

Physical Characterization of Lipid Nanoparticles Encapsulating pLNP-HDR and mLNP-HDR

Nanoparticles were formulated as described in previous publication in the presence of 0.25 mole% DOTAP to mediate electrostatic interactions between lipid and cargo in nuclease-free water.[10] The characterization of the formulations encapsulating Cas9-mRNA (named *m*LNP-HDR) or Cas9-RNP (named *p*LNP-HDR) was performed as described. *m*LNP-HDR are smaller in their average size and more monodisperse than *p*LNP-HDR (150 nm vs 245 nm and PDI 0.12 vs 0.26, respectively) as shown in Fig. 1A. Cryo-TEM images displayed in Fig. 1B show that both *p*LNP-HDR and *m*LNP-HDR take the shape of lipoplexes and spheres. *p*LNP and *m*LNP without HDR templates were additionally characterized as spherical particles via cryo-TEM (see Supplementary Fig. 1).
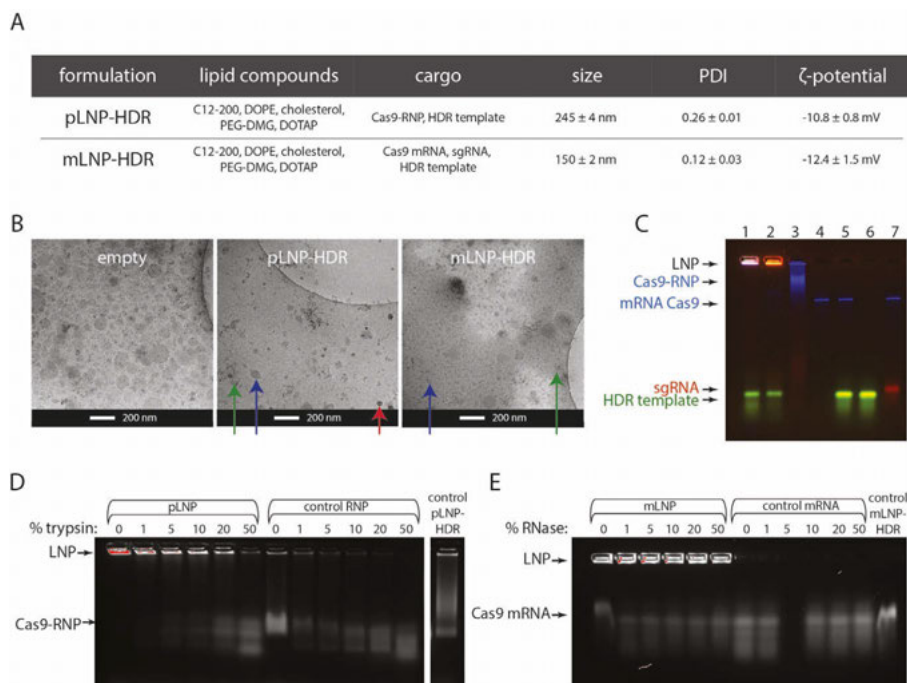
Figure 1: **Physical characterizations of *p*LNP-HDR and *m*LNP-HDR. A)** Overview of the formulation's lipid compounds, cargo, size, polydispersity index (PDI) and charge. **B)** Cryo-TEM images of empty LNPs and *p*LNP-HDR and *m*LNP-HDR. Scale bar represents 200 nm. Green arrows indicate lipoplex structures, blue arrows point to spherical particles, and red arrows indicate dense particles. **C)** Gel retardation assay of labelled CRISPR-Cas9 components for determination of entrapment of cargo in LNPs. SpCas9 – Alexa647 (blue), mRNA – Cy5 (blue), sgRNA – ATTO550 (red), HDR template – 6FAM (green). Gel lanes: 1 – *p*LNP, 2 – *m*LNP, 3 – control Cas9-RNP, 4 – control mRNA Cas9, 5 – control mRNA Cas9 & HDR template, 6 – control HDR template, 7 – control mRNA Cas9 & sgRNA. Pink indicates overlap of mainly blue (Cas9) and red (sgRNA) signal but also green (HDR template). Orange color indicates overlap of blue (mRNA Cas9), red (sgRNA), and green (HDR template). **D)** Agarose gel of a trypzination assay to determine protection and localization of Alexa647-Cas9-RNP in *p*LNP-HDR. Control *p*LNP-HDR (from a separate gel) was treated with final concentration of 2% triton to disrupt lipids. The lowest band on the gel was assigned for calculation of percentage of degradation via trypsin as shown in Supplementary Fig. 3. **E)** Agarose gel of an RNAse assay to determine protection and localization of Cy5-mRNA Cas9 in *m*LNP-HDR. Control *m*LNP-HDR was treated with final concentration of 2% triton to disrupt lipids.

Within the cryo-TEM images of *p*LNP-HDR, however, more dense structures were observed compared to *m*LNP-HDR (Fig.1B, middle). Gel retardation assays with fluorescently-labelled CRISPR-Cas9 components showed that Cas9-RNP and HDR template and Cas9-mRNA, sgRNA, and HDR template remain retained within *p*LNP-HDR and *m*LNP-HDR, respectively (Fig. 2C). Some non-complexed HDR template was detected in both *p*LNP-HDR and *m*LNP-HDR (Fig. 2C lane 1,2). The lipid nanoparticles provide protection against trypsin, an endopeptidase, and RNAse indicating that the Cas9 protein or mRNA are incorporated in a lipid core (Fig. 2D,E). At higher percentages of trypsin, Cas9 eventually does degrade and degradation was quantified to a percentage of 20% after 30 minutes incubation with 50% trypsin as can be seen in Supplementary Fig. 3.

Timing of Gene Editing and Gene Editing Efficiencies of pLNP and mLNP In Vitro

After physical characterization, *p*LNP-HDR and *m*LNP-HDR were compared in terms of kinetics of gene correction and gene editing efficiencies on eGFP reporter cell lines in culture. Delivery of the CRISPR-Cas9 components as RNP or mRNA via *p*LNP-HDR and *m*LNP-HDR, respectively, resulted in gene editing efficiencies comparable or higher to the commercial transfection agent ProDeliverIN CRISPR (Fig. 2A). *m*LNP-HDR however resulted in about a 5-fold higher efficiency than *p*LNP-HDR: 80% gene knock-out and 15% gene correction at 30 nM sgGFP versus to 24% gene knock-out and 5% gene correction via *p*LNP-HDR (Fig. 2A). Interestingly, gene editing efficiencies of eGFP construct were higher in HEK293T cells than in hepatoma cells, wherein especially gene correction did not exceed over 2% for *p*LNP-HDR nor for *m*LNP-HDR (Fig. 2A). *m*LNP-HDR resulted in saturation of gene knock-out on eGFP HEK293T cells already at a final concentration of 3.8 nM sgGFP. The relative gene corrections (determined as fraction of total edits), however, were similar between the two different formulations on eGFP HEK293T cells, but higher for *p*LNP-HDR on eGFP HEPA1-6

cells as shown in Fig. 2B.

Cellular toxicity assays shown in supplementary Fig. 4C indicate that *p*LNP-HDR show higher cytotoxicity with eGFP HEK293T cells than *m*LNP-HDR, while both *p*LNP-HDR and *m*LNP-HDR do not result in toxicity on eGFP HEPA1-6 cells. Over time, both formulations lose functionality, but do not change in size (Supplementary Fig. 4A,B). However, notably, *p*LNP-HDR aggregated and sedimented over time (Supplementary Fig. 5).

To gain insight in the timing of delivery of Cas9 protein to the cytosol and subsequently the nucleus, the presence of eGFP-Cas9 fusion protein was measured by fluorescence confocal microscopy in HEK293T cells. Cas9 protein was located within the cytosol and nucleus within 30 minutes after transfection of cells with *p*LNP-HDR (Fig. 2C). When delivered as mRNA, eGFP-Cas9 fusion protein was first detected in the cytosol and nucleus after 4 hours (2C). Furthermore, it is interesting to highlight that the eGFP-Cas9 fusion protein signal within HEK293T cells differs in intensity between *p*LNP and *m*LNP-mediated delivery (images shown in Supplementary Fig. 6). Despite the earlier delivery of Cas9 in the nucleus via *p*LNP, gene correction became apparent after 22 hours in HEK293T HDR Stoplight cells, reporter cells in which gene correction results in a GFP signal (Fig. 2D), treated with *m*LNP-HDR (Fig. 2E) and saturating after 30 hours. Onset of gene correction detected in the cells treated with *p*LNP-HDR occurred around 24 hours but was determined to still increase until the end of the experiment (48hours).

LNPs encapsulating Cas9-RNP or mRNA Cas9 were compared on stimulation of inflammatory cytokines after treatment of DCs with LNPs via qPCR. *m*LNP-HDR triggered 13-fold higher expression of IFN-α to mDCs while *p*LNP-HDR resulted in a 5-fold expression at 30 nM sgRNA (Fig. 2F). Cytokines TRAF6 and TNF-α were only expressed 3-fold and 5-fold, respectively, higher than mDCs after treatment with *p*LNP-HDR, while *m*LNP-HDR upregulated expression of IL-12 and IL-10.
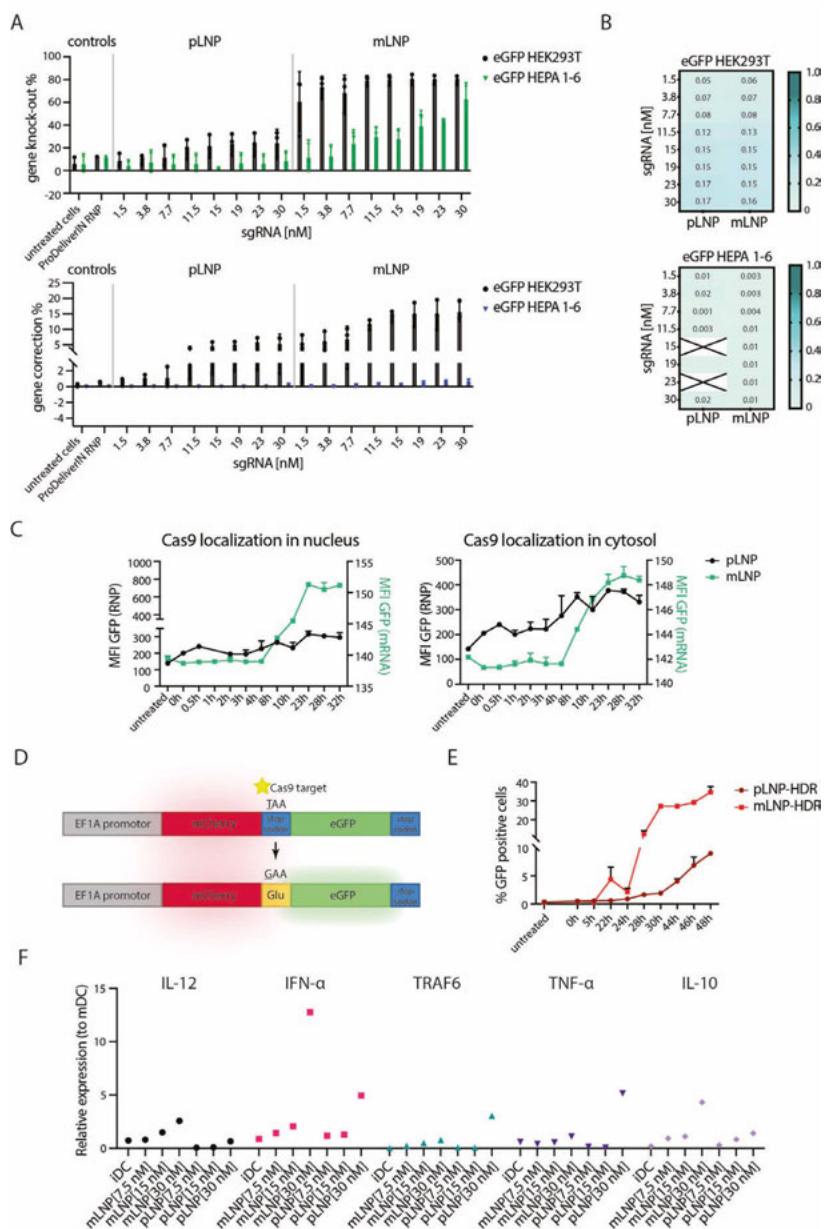
Figure 2: **Comparison of *p*LNP and *m*LNP on intracellular delivery of Cas9, gene editing efficiency and timing of HDR on-set.**

Figure 2: **A)** Gene knock-out (top) of eGFP fluorescence and gene correction (bottom) of eGFP to BFP fluorescence in eGFP HEK293T and eGFP HEPA1-6 cells mediated through different concentrations of *p*LNP and *m*LNP (n=3). sgGFP and HDR template for GFP reporter system used in this experiment (see supplementary table 1). **B)** Heatmaps of relative gene correction between *p*LNP and *m*LNP in eGFP HEK293T (top) and eGFP HEPA1-6 (bottom) cells. **C)** Uptake of eGFP-Cas9 fusion protein delivered as RNP or as mRNA via LNP in nucleus (left) and cytosol (right) of HEK293T cells over time. MFI of eGFP-Cas9 was determined by image analysis of confocal microscopy images with the Columbus software. **D)** Scheme of HEK293T HDR Stoplight cells: gene editing of a stop codon (TAA-¿GAA) via HDR results in expression of eGFP. **E)** Onset of homology-directed repair in HEK293T HDR Stoplight cells. Percentage of GFP positive cells was determined as GFP positive cells within mCherry positive cells by image analysis of confocal microscopy images with the Columbus software. sgSTOP and HDR template for HDR Stoplight system were used in this experiment. **F)** Expression of cytokines (IL-10, IFN-α, TRAF6, TNF-α, IL-10) relative to LPS-stimulated matured mature dendritic cells (expression of 1) of dendritic cells treated with *p*LNP-HDR or *m*LNP-HDR measured via qPCR. Immature dendritic cells (iDCs) are plotted as control values.

In Vivo Biodistribution and Gene Knock-Out Efficiencies of pLNP and mLNP

After *in vitro* characterization, the *p*LNP and *m*LNP formulations were compared in biodistribution and gene editing functionality, specifically gene knock-out, in female Ai9 mice as shown in the schematic representation in Fig. 3A. Both formulations were larger in particle size with a higher PDI at these concentrations than the formulations for *in vitro* work described above (Supplementary Fig. 10B). Four hours after administration intravenously, *p*LNP were detected in the liver, spleen and lungs while Cy5.5-sgTOM via *m*LNP was detected in the liver, lungs, and kidneys (Fig. 3B,C,D). The biodistribution study had been split into two separate runs. In the first run, the signal of Cy5.5-sgTOM via *p*LNP was higher in the lungs than in the second run (Supplementary Fig. 13). Notably, in general the fluorescent signal of Cy5.5-sgTOM is stronger in organs of mice treated with *p*LNP. On closer look at the liver, Fig. 3E shows that Cy5.5-sgTOM delivered via *p*LNP was mainly detected in liver sinusoidal endothelial cells (LSEC) (71% of cells positive for Cy5.5 signal) and additionally in dendritic cells (14%) and hepatocytes (12%). Cy5.5-sgTOM delivered by *m*LNP also resulted in uptake mainly in LSEC (46%), and in dendritic cells (13%) and hepatocytes (41%). One mouse that received control formulation (*p*LNP with

irrelevant sgRNA) within the biodistribution study died after IV injection. To investigate the gene knock-out efficiency of the stop codon resulting in the expression of tdTomato, female Ai9 mice were injected intravenously with *p*LNP and *m*LNP. Within 20 hours all mice treated with *p*LNP died and only *m*LNP-treated mice lived until the end of the experiment. Within the liver, *m*LNP were found to result in 60% tdTomato-positive hepatocytes, hence successful gene knock-out (Fig. 3F). tdTomato-positive cells were not detected in LSEC, myeloid cells, Kupffer cells or dendritic cells.
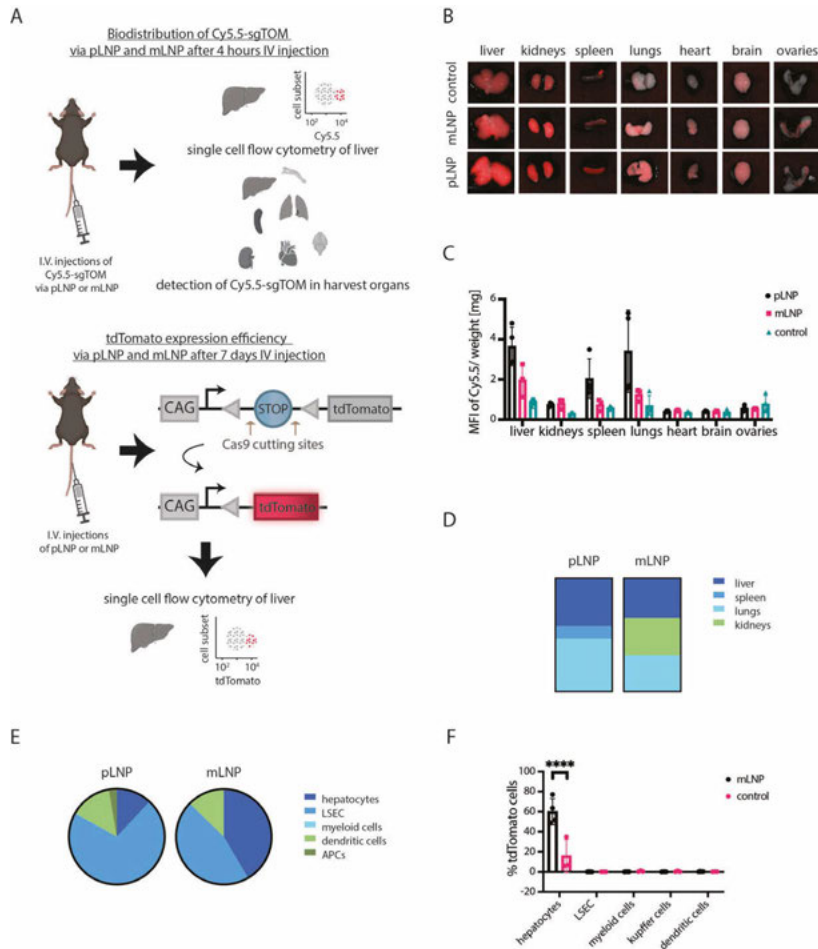
Figure 3: **Biodistribution of Cy5-5-sgTOM and gene editing efficiencies of *p*LNP and *m*LNP *in vivo*. A)** Schematic representation of biodistribution and functionality studies of *p*LNP and *m*LNP in Ai9 female mice. Scheme was partially created with Biorender.com. **B)** Images taken with Pearl Impulse Imager of organs harvested from mice treated with *p*LNP and *m*LNP and control LNP. **C)** Biodistribution of Cy5.5-sgTOM after 4 hours IV injection of *p*LNP and *m*LNP plotted as MFI per weight of organ. MFI was determined by drawing area of interest around scanned image of organs with Image Studio Lite Software. 4 mice for *p*LNP, 3 mice for *m*LNP (as one injection was not successful), 4 mice for control. **D)** Relative distribution of Cy5.5-sgTOM per mice (MFI for each organ divided by cumulative MFI of all organs). Percentage of Cy5.5-sgTOM in mouse organs treated with *p*LNP: 42% liver, 46% lungs, 11% spleen and *m*LNP: 35% liver, 33% kidney, 32% lungs. 4 mice per experimental group (3 mice for *m*LNP as one injection was not successful).

Figure 3: **E)** Distribution of Cy5.5-sgTOM in cell subsets of liver in mice treated with pLNP or mLNP by single cell flow cytometry. Gating strategies and markers defining each cell subset are shown in Supplementary Fig. 11 and table 3, respectively. Percentage of Cy5.5-sgTOM in individual liver cell subsets of the entire signal: pLNP: 12% - hepatocytes, 71% -LSEC, 0.11% myeloid cells, 14% - dendritic cells, 2.66% APCs and mLNP: 41% - hepatocytes, 46% - LSEC, 13% dendritic cells. 4 mice per experimental group (3 mice for mLNP as one injection was not successful). **F)** Gene knock-out efficiency given as percentage of tdTomato-positive cells in cell subsets in liver of four mice treated with mLNP and three untreated mice (control). Two-way ANOVA was performed via GraphPad Prism 9 (version 9.0) (p-value **** < 0.0001). Gating strategies are shown in Supplementary Fig. 12.

Discussion

This study shows a comparison of lipid nanoparticles delivering CRISPR-Cas9 components either as single molecules, mRNA Cas9 and sgRNA, or directly as ribonucleoprotein complex. The formulation of pLNP-HDR was based on our previous publication.[10] The same formulation conditions were used for mLNP-HDR, except that mRNA Cas9 was added to sgRNA at a 4:1 weight ratio prior to complexation with lipids. mLNP-HDR were found to be more monodisperse (PDI 0.12) in their size (150 nm) than pLNP-HDR and additionally the lipids seem to protect the mRNA Cas9 more efficiently against higher concentrations of degrading enzymes (Fig. 1). From this result we conclude that mRNA Cas9 is better incorporated into the core of LNPs, while the Cas9-RNP is partially associated to the outside surface. While the Cas9-RNP has a net-negative charge, the distribution of anions has been shown to not be equally distributed across the surface of the RNP. This might affect the incorporation of the Cas9-RNP into the core of LNPs, which can additionally explain the difference in size of particles.[24] Nonetheless, gel retardation studies (Fig. 1C) showed that both pLNP-HDR and mLNP-HDR formulations retained the Cas9-RNP or mRNA Cas9 and sgRNA, respectively. HDR template was also retained in both formulations, though gel assay also showed uncomplexed HDR template. Additional studies, such as single-particle analysis by a dedicated flow cytometer, e.g. nanoFCM, should be performed to confirm that each CRISPR-Cas9 component is entrapped within

4

one nanoparticle. Furthermore, taking a look at the structure of the nanoparticles, cryo-TEM images reveal both lipoplex and spherical particles for *m*LNP-HDR and *p*LNP-HDR (Fig. 1B). Self-assembly particles have been previously studied by Ianiro et al to be in an equilibrium between lipoplexes and spheres.[33] In comparison to cryo-TEM images of LNPs with HDR template less lipoplex formation are detected in formulations without HDR template. This might suggest that in the presence of an HDR template sub-complexes between lipids and HDR template are formed. At closer look, cryo-TEM images of *p*LNP-HDR also reveal darker, hence denser, structures, which might be RNP aggregates.[34] *p*LNP-HDR particles were found to start aggregating and sediment over time or at higher concentrations within the *in vivo* study as shown in Supplementary Fig. 5 and 10.

It is of great importance to note that all mice treated with *p*LNP unexpectedly died within 20 hours after tail-vein injections while *m*LNP-treated mice remained alive and showed no effects to their well-being. Death of mice may have been due to particle aggregates. *p*LNP were discovered to aggregate and sediment at these higher concentrations (RNP = 15 μM) shown in Supplementary Fig. 10A. Together with the gel retardation assay on protection from degrading enzymes and cryo-TEM images revealing darker spheres for *p*LNP-HDR, LNPs entrapping Cas9-RNP deem less stable than mRNA Cas9-loaded nanoparticles, possibly due to coating of Cas9-RNP on the surface of LNPs (Fig. 1). Another reason for death of mice could be contaminations of Cas9 protein with endotoxins. Cas9 protein was produced in LPS-free ClearColi™ BL21 strain, however during purification contaminations might have been introduced which was not assessed in this study. It has been reported that young mice (7-9) weeks have a LD50 (50% lethal dose) of 601 microgram per mouse resulting in lethality due to high levels of IL-10.[35] In contrast, *m*LNP interestingly lead to higher expression of inflammatory cytokines *in vitro* than LNPs containing Cas9-RNP (Fig. 2F).

The differences in particle aggregates and general particle size can ex-

plain the observed uptake of *p*LNP in tissue and cell subsets. Alongside high uptake in the liver, *p*LNP was highly retained in the lungs and spleen (Fig. 3B,C). The data shown here supports that aggregating particles are known to be taken up by the lungs as uptake was especially high for *p*LNP. Uptake by the lung could also be due to incorporation of DOTAP in LNPs, as shown by Cheng et al that cationic lipids selectively sort particles to lungs. However, ideal molar percentage of DOTAP for delivery to the lungs was found to be at least 50% and in this study DOTAP composition was set to a mole% of 0.25%.[36]

LNPs have been characterized in previous studies to migrate to the liver after intravenous injections due to protein corona formation consisting of mainly apolipoprotein E.[37,38] Incubating *m*LNP and *p*LNP with 50% serum showed increase in size of nanoparticles suggesting an accumulation of serum proteins on the surface of particles (Supplementary Fig. 10B). Therefore, single cell flow cytometry was performed in this study to investigate both distribution of Cy5.5-sgTOM and gene knock-out efficiencies in liver cell subsets. Herein, Cy5.5-sgTOM via both *p*LNP and *m*LNP was found back in the same cell subsets: mainly LSECs followed by dendritic cells and hepatocytes. *m*LNP-delivered Cy5.5-sgTOM showed higher uptake in hepatocytes than *p*LNPs (Fig. 3D). However, total fluorescent signal of Cy5.5-sgTOM was stronger in the organs of mice treated with *p*LNP, despite similar fluorescent signal within injected formulations (Supplementary Fig. 9), suggesting premature degradation or clearance of sgRNA in non-complexed form. Noteworthily, gene knock-out mediated through CRISPR-Cas9 delivered via *m*LNP was only detected in hepatocytes (60%) despite delivery of Cy5.5-sgTOM to other cell subsets via single cell flow cytometry. Further validation methods and investigation on gene editing efficiencies in other organs of treated mice are still required.

Moreover, *m*LNP-HDR surpass *p*LNP-HDR in gene editing efficiencies *in vitro* on both reporter HEK293T and HEPA1-6 cells (Fig. 2). Gene editing efficiencies were generally higher on HEK293T cells than on hepatoma cells (Fig. 2A,B). Perhaps internalization

of lipid nanoparticles is less efficient in HEPA1-6 cells *in vitro*, an indication for that also being higher cytocompatibility of particles with hepatoma cells (Supplementary Fig. 4C) and internalization resulting in gene knock-out confirmed in hepatocytes in Ai9 mice (Fig. 3 E,F). Further studies such as uptake of fluorescently labelled lipids within LNPs could help investigate internalization and difference between the formulations. On the other hand, gene editing is dependent on cell-cycle and cell differentiation. Cells in a prolonged G1 phase have been shown to favor NHEJ over HDR as HDR only occurs during S/G2 phase.[39,40] HEK293T cells have been studied to induce higher HDR efficiencies than other cell lines such as HeLa and iPSCs.[41] Remarkably, onset of gene correction occurred earlier in cells treated with *m*LNP-HDR despite Cas9 protein localizing significantly later in the nucleus (Fig 2.C,E). While onset of gene correction only starts around 24 hours after transfection with *p*LNP-HDR, eGFP positive cells (HDR) were detected after 22 hours after treatment with *m*LNP-HDR (Fig. 2E). Moreover, while cells treated with *m*LNP-HDR plateau in HDR around 30 hours, HDR in cells treated with *p*LNP-HDR was found to still increase up until the end of the experiment. This may indicate that mRNA delivery results in a higher amount of Cas9 protein at a faster rate.[42] It would be interesting to determine the amount of protein present in cells at various timepoints of gene editing. Another observation is that despite Cas9 being present in the nucleus within a few hours, detection of eGFP in HDR Stoplight reporter cells is only 20 hours later (Fig. 2C,E). However, fluorescent proteins have a long half-life probably delaying the detection of eGFP. Studies such as TIDE-R could help determine the exact time of gene correction. The finding of a later onset of gene correction after delivery of the Cas9-RNP could nonetheless be relevant for ongoing studies to optimize the ratio HDR to NHEJ through chemical or genetic disruption of the NHEJ pathway.[43]

In conclusion, this study investigated the delivery of CRISPR-Cas9 via lipid nanoparticles as mRNA Cas9 versus Cas9-RNP for gene editing *in vitro* and *in vivo*. Ongoing studies on design of delivery vehicles for

CRISPR-Cas9 focus on either cargo format and a comparative analysis of mRNA Cas9 vs RNP has not been studied. Under tested conditions in our study, we conclude that mRNA Cas9 seems a better cargo format for delivery of CRISPR-Cas9 for gene editing via LNPs, resulting not only smaller sized nanoparticles but also in higher gene editing *in vitro* and delivery of functional CRISPR-Cas9 to hepatocytes *in vivo*.

Acknowledgements

4

References

1. Jinek, M. et al. A Programmable Dual-RNA – Guided. Science (80-.). 337, 816–822 (2012).
2. Gasiunas, G., Barrangou, R., Horvath, P. & Siksnys, V. Cas9-crRNA ribonucleoprotein complex mediates specific DNA cleavage for adaptive immunity in bacteria. Proc. Natl. Acad. Sci. U. S. A. 109, 2579–2586 (2012).
3. Zaboikin, M., Zaboikina, T., Freter, C. & Srinivasakumar, N. Non-homologous end joining and homology directed DNA repair frequency of double-stranded breaks introduced by genome editing reagents. PLoS ONE 12, (2017).
4. Cheng, H., Zhang, F. & Ding, Y. Crispr/cas9 delivery system engineering for genome editing in therapeutic applications. Pharmaceutics 13, 1–23 (2021).
5. Asmamaw Mengstie, M. Viral Vectors for the in Vivo Delivery of CRISPR Components: Advances and Challenges. Front. Bioeng. Biotechnol. 10, 1–6 (2022).
6. Hou, X., Zaks, T., Langer, R. & Dong, Y. Lipid nanoparticles for mRNA delivery. Nat. Rev. Mater. 6, 1078–1094 (2021).

7. Semple, S. C. et al. Rational design of cationic lipids for siRNA delivery. Nat. Biotechnol. **28**, 172–176 (2010).
8. Love, K. T. et al. Lipid-like materials for low-dose, in vivo gene silencing. Proc. Natl. Acad. Sci. U. S. A. **107**, 1864–1869 (2010).
9. Gillmore, J. D. et al. CRISPR-Cas9 In Vivo Gene Editing for Transthyretin Amyloidosis. N. Engl. J. Med. **385**, 493–502 (2021).
10. Walther, J. et al. Impact of Formulation Conditions on Lipid Nanoparticle Characteristics and Functional Delivery of CRISPR RNP for Gene Knock-Out and Correction. Pharmaceutics **14**, (2022).
11. Wei, T., Cheng, Q., Min, Y. L., Olson, E. N. & Siegwart, D. J. Systemic nanoparticle delivery of CRISPR-Cas9 ribonucleoproteins for effective tissue specific genome editing. Nat. Commun. **11**, 1–12 (2020).
12. Yi, J. et al. Co-delivery of Cas9 mRNA and guide RNAs edits hepatitis B virus episomal and integration DNA in mouse and tree shrew models. Antiviral Res. **215**, 105618 (2023).
13. Suzuki, Y. et al. Lipid nanoparticles loaded with ribonucleoprotein–oligonucleotide complexes synthesized using a microfluidic device exhibit robust genome editing and hepatitis B virus inhibition. J. Control. Release **330**, 61–71 (2021).
14. Chen, F., Alphonse, M. & Liu, Q. Strategies for nonviral nanoparticle-based delivery of CRISPR/Cas9 therapeutics. Wiley Interdiscip. Rev. Nanomedicine Nanobiotechnology **12**, 1–14 (2020).
15. Lin, Y., Wagner, E. & Lächelt, U. Non-viral delivery of the CRISPR/Cas system: DNA versus RNA versus RNP. Biomater. Sci. **10**, 1166–1192 (2022).
16. Lokugamage, M. P. et al. Mild Innate Immune Activation Overrides Efficient Nanoparticle-Mediated RNA Delivery. Adv. Mater. **32**, 1–9 (2020).
17. Vaidyanathan, S. et al. Uridine Depletion and Chemical Modification Increase Cas9 mRNA Activity and Reduce Immunogenicity without HPLC Purification. Mol. Ther. - Nucleic Acids **12**, 530–542 (2018).
18. Boo, S. H. & Kim, Y. K. The emerging role of RNA modifications in the regulation of mRNA stability. Exp. Mol. Med. **52**, 400–408 (2020).
19. Kouranova, E. et al. CRISPRs for optimal targeting: Delivery of CRISPR components as DNA, RNA, and protein into cultured cells and single-cell embryos. Hum. Gene Ther. **27**, 464–475 (2016).
20. Liu, S. et al. Membrane-destabilizing ionizable phospholipids for organ-selective mRNA delivery and CRISPR–Cas gene editing. Nat. Mater. **20**, (2021).
21. Lin, S., Staahl, B. T., Alla, R. K. & Doudna, J. A. Enhanced homology-directed human genome engineering by controlled timing of CRISPR/Cas9 delivery. Elife **3**, e04766 (2014).
22. Ma, H. et al. CRI SPR-Cas9 nuclear dynamics and target recognition in living cells. J. Cell Biol. **214**, 529–537 (2016).
23. Lim, Y. et al. Structural roles of guide RNAs in the nuclease activity of Cas9 endonuclease. Nat. Commun. **7**, 1–8 (2016).
24. Chen, G. et al. A biodegradable nanocapsule delivers a Cas9 ribonucleoprotein complex for in vivo genome editing. Nat. Nanotechnol. **14**, 974–980 (2019).
25. Khan, O. F. et al. Ionizable amphiphilic dendrimer-based nanomaterials with alkyl-chain-substituted amines for tunable sirna delivery to the liver endothelium in vivo. Angew. Chemie - Int. Ed. **53**, 14397–14401 (2014).

26.   Charlesworth, C. T. et al. Identification of preexisting adaptive immunity to Cas9 proteins in humans. Nat. Med. **25**, 249–254 (2019).

27.   Li, A. et al. AAV-CRISPR Gene Editing Is Negated by Pre-existing Immunity to Cas9. Mol. Ther. **28**, 1432–1441 (2020).

28.   Warren, L. et al. Highly efficient reprogramming to pluripotency and directed differentiation of human cells with synthetic modified mRNA. Cell Stem Cell **7**, 618–630 (2010).

29.   Kogut, I. et al. High-efficiency RNA-based reprogramming of human primary fibroblasts. Nat. Commun. **9**, (2018).

30.   Jong, O. G. De, Mastrobattista, E. & Scholar, G. An Amphipathic Cell-Penetrating Peptide-Aided De- livery of Cas9 RNP for Gene Editing and Correction. (2023).

31.   Glaser, A., McColl, B. & Vadolas, J. GFP to BFP Conversion: A Versatile Assay for the Quantification of CRISPR/Cas9-mediated Genome Editing. Mol. Ther. - Nucleic Acids **5**, e334 (2016).

32.   Braake, D. Ter, Benne, N., Lau, C. Y. J., Mastrobattista, E. & Broere, F. Retinoic acid-containing liposomes for the induction of antigen-specific regulatory T cells as a treatment for autoimmune diseases. Pharmaceutics 13, (2021).

33.   Ianiro, A. et al. Liquid–liquid phase separation during amphiphilic self-assembly. Nat. Chem. **11**, 320–328 (2019).

34.   Tan, Z. et al. Block Polymer Micelles Enable CRISPR/Cas9 Ribonucleoprotein Delivery: Physicochemical Properties Affect Packaging Mechanisms and Gene Editing Efficiency. Macromolecules **52**, 8197–8206 (2019).

35.   Tateda, K., Matsumoto, T., Miyazaki, S. & Yamaguchi, K. Lipopolysaccharide-induced lethality and cytokine production in aged mice. Infect. Immun. **64**, 769–774 (1996).

36.   Cheng, Q. et al. Selective organ targeting (SORT) nanoparticles for tissue-specific mRNA delivery and CRISPR–Cas gene editing. Nat. Nanotechnol. **15**, 313–320 (2020).

37.   Akinc, A. et al. Targeted delivery of RNAi therapeutics with endogenous and exogenous ligand-based mechanisms. Mol. Ther. **18**, 1357–1364 (2010).

38.   Sabnis, S. et al. A Novel Amino Lipid Series for mRNA Delivery: Improved Endosomal Escape and Sustained Pharmacology and Safety in Non-human Primates. Mol. Ther. **26**, 1509–1519 (2018).

39.   Dodsworth, B. T., Hatje, K., Meyer, C. A., Flynn, R. & Cowley, S. A. Rates of homology directed repair of CRISPR-Cas9 induced double strand breaks are lower in naïve compared to primed human pluripotent stem cells. Stem Cell Res. **46**, 101852 (2020).

40.   Mao, Z., Bozzella, M., Seluanov, A. & Gorbunova, V. DNA repair by non-homologous end joining and homologous recombination during cell cycle in human cells. Cell Cycle **7**, 2902–2906 (2008).

41.   Miyaoka, Y. et al. Systematic quantification of HDR and NHEJ reveals effects of locus, nuclease, and cell type on genome-editing. Sci. Rep. **6**, 1–12 (2016).

42.   Schwanhüusser, B. et al. Global quantification of mammalian gene expression control. Nature **473**, 337–342 (2011).

43.   Schimmel, J. et al. Modulating mutational outcomes and improving precise gene editing at CRISPR-Cas9-induced breaks by chemical inhibition of end-joining pathways. Cell Rep. **42**, (2023).

4

Supplementary Material for Chapter 4

Sequences of sgRNA and HDR template

Table S1: **Sequences of sgRNA and HDR template used in this study.** HDR sequence designed to additionally silence-mutate the PAM sequence. The edited nucleotides are indicated by small letters.

Target	20 nt Spacer Sequence
sgRNA for eGFP reporter cells (`sgGFP`)	GCUGAAGCACUGCACGCCGU
sgRNA for HEK293T HDR Stoplight cells (`sgSTOP`)	GCUUACUUGUACAGCCGUCC
sgRNA for Ai9 mouse study (`sgTOM`)	AAGUAAAACCUCUACAAAUG
Cy5.5-sgRNA for Ai9 study (`Cy5.5-sgTOM`)	[Cyanin5.5]AAGUAAAACCUCUACAAAUG
HDR template for eGFP reporter	CAAGCTGCCCGTGCCCTGGCCCACCCTCGTGACCACCCTGAg CcACGGCGTGCAGTGCTTCAGCCGCTACCCCGAC CACATGAAGC
HDR template for HDR Stoplight reporter	ACGACGCCCGTGAAAAGCTCTTCACCCTTAGACACGGCTTg CTTGTACAGCTCGTCCAaGCCGCCCGTAGAATGCCTGCCT

Antibodies used for flow cytometry

Table S2: **Antibodies used for single cell flow cytometry.**

Feature	Clone	Isotype	Fluorophore	Company	Cell Subset
CD45	30-F11	Rat IgG2b, , mono-clonal	Alexa Fluor 488	Biolegend	Hemato-poietic cells (immune cells)
CD31 (PECAM-1)	MEC 13.3	Rat Lewis IgG2a,	BV510	BD Bio-sciences	Endothelial cells (LSEC)
CD11b	M1/70	Rat IgG2b,	eFluor 450	Invitrogen	Myeloid cells (macro-phages, mono-cytes, some dendritic cells)
CD11c	N418	Hamster IgG	PE-Vio770	Miltenyi Biotec	Dendritic cells
MHC II (I-A/I-E)	M5/114.15.2	Rat IgG2b,	PE	BD Bio-sciences	Antigen presenta-tion

Table S2: **Continuation of Table S2.**

Feature	Clone	Isotype	Fluorophore	Company	Cell Subset
F4/80	BM8	Rat IgG2a	APC	eBio-science	Macro-phages /Kupffer cells
Viability	-	-	Viakrome 808, Fixable Viability Dye	Beckman Coulter	Viability

Determination markers of specific cell subset in liver

Table S3: **Gating of specific markers to determine the different cell subsets in liver: LSEC, hepatocytes, myeloid cells, dendritic cells, kupffer cells.**

Markers	Cell Subset
CD45-CD31-	Hepatocytes
CD45-CD31+	LSEC
CD45+CD11b+	Myeloid Cells
CD45+CD11c+	Dendritic Cells
CD45+F4/80+	Kupffer Cells

Cryo-TEM images of LNPs encapsulating RNP or mRNA Cas9 without HDR template
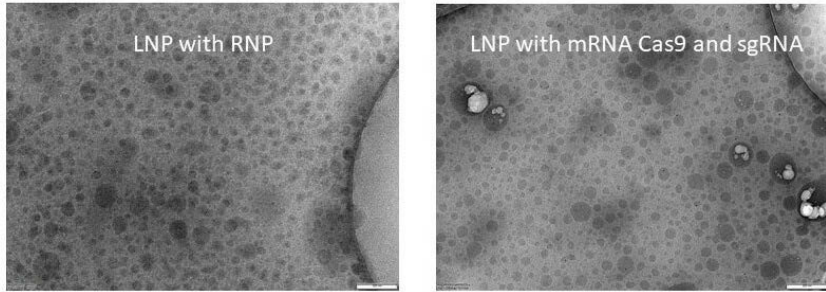
Figure S1: **Cryo-TEM images of LNPs encapsulating Cas9-RNP (left) or mRNA Cas9 and sgRNA (right) with the addition of an HDR template.** White spots on right cryo-TEM images are boiling artifacts. Size of the error bars are 200 nm.

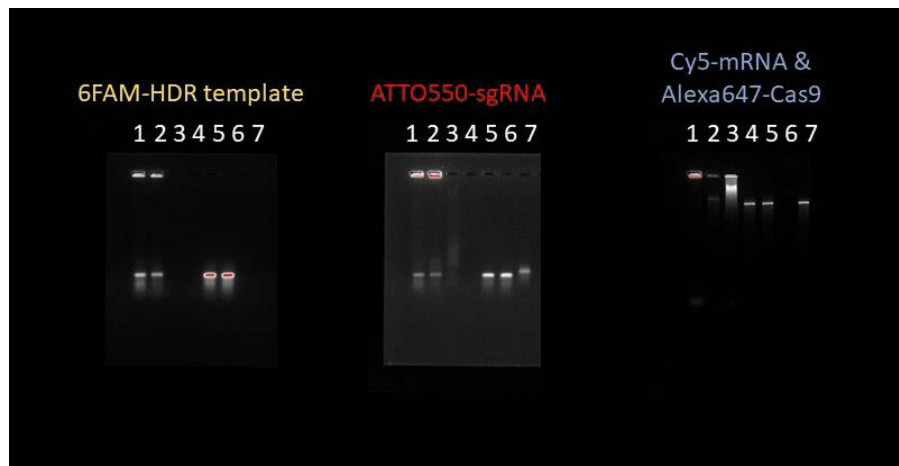## Gel retardation assay to determine entrapment of CRISPR-Cas9 components

Figure S2: **Gel retardation assay to determine entrapment of CRISPR-Cas9 components in *p*LNP and *m*LNP.** Depicted here are the separate channels to show the individual bands of 6FAM-labelled HDR template (left), ATTO550-labelled sgRNA (middle), and Cy5-labelled mRNA and Alexa647-labelled Cas9 (right). Gel lanes: 1 – *p*LNP, 2 – *m*LNP, 3 – control Cas9-RNP, 4 – control mRNA Cas9, 5 – control mRNA Cas9 HDR template, 6 – control HDR template, 7 – control mRNA Cas9 sgRNA.

Determination of degradation of RNP or mRNA during trypsin and RNase digestion assay
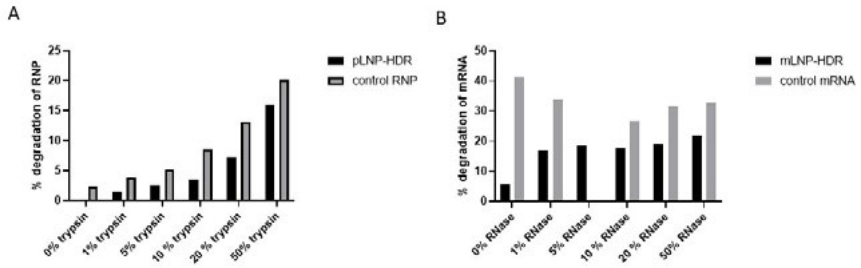
Figure S3: **Degradation efficiencies of trypsin and RNase in degradation assays. A)** Percentage of degradation of RNP in /textitpLNP-HDR vs control RNP samples with increasing percentage of trypsin. **B)** Percentage of degradation of mRNA in *m*LNP-HDR vs control mRNA with increasing percentage of RNase.
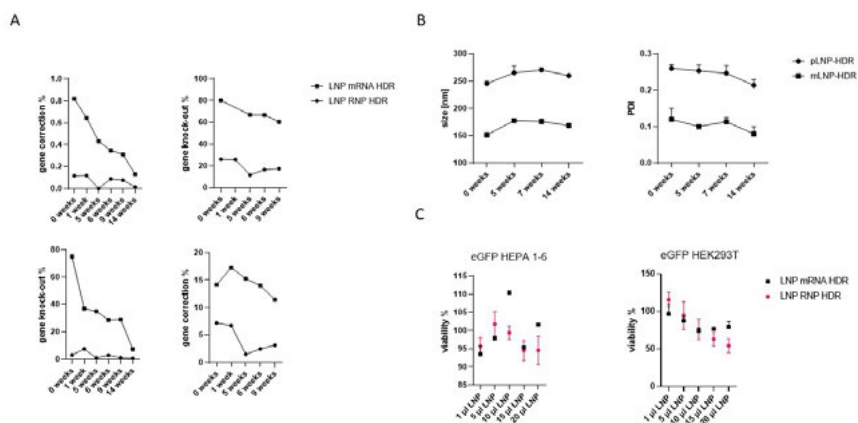
Stability of *p*LNP and *m*LNP over storage at 4°C for 14 weeks

Figure S4: **Stability and cytotoxicity studies of pLNP and mLNP on eGFP HEK293T and eGFP HEPA1-6 cells. A)** Stability in gene editing knock-out (top) and gene correction (bottom) of *p*LNP and *m*LNP on eGFP HEPA1-6 cells (left) and eGFP HEK293T cells (right). **B)** Size and PDI of formulations over time. **C)** Cell viability of eGFP HEK293T and eGFP HEPA1-6 cells after treatment with *p*LNP and *m*LNP determined with an MTS assay.

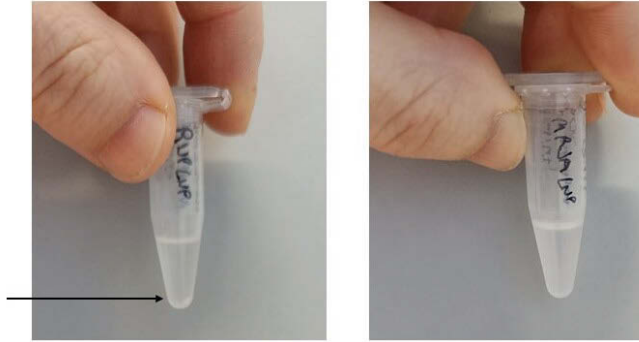## Aggregation and sedimentation of pLNP-HDR

Figure S5: **Images of Eppendorf tubes containing LNP formulation.** Images of pLNP-HDR and mLNP-HDR, respectively, were taken at 14 weeks storage at 4°C. Both formulations were formulated with 1.6 μM sgRNA. LEFT: LNP formulation with Cas9-RNP and HDR template as cargo; RIGHT: LNP formulation with mRNA Cas9, sgRNA, and HDR template as cargo. Arrow indicates the visible sedimented pellet of aggregated particles.

4

Microscopy images of GFP-Cas9 inHEK293T cells delivered via *p*LNP and *m*LNP
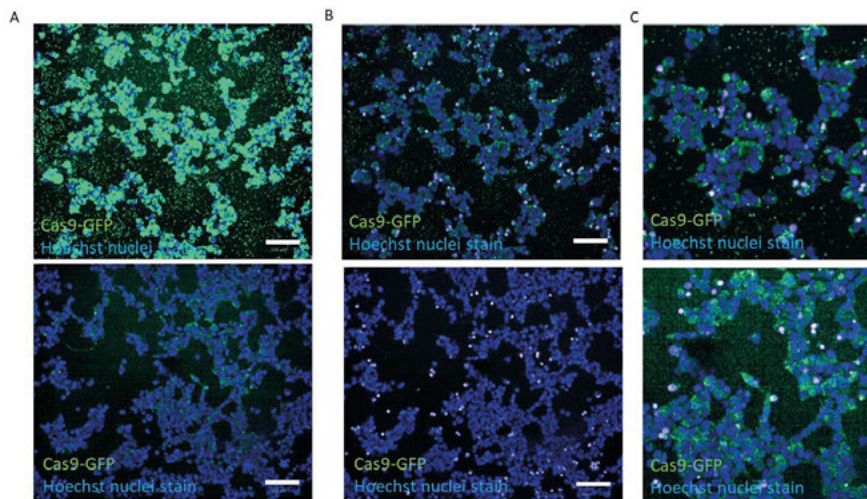

Figure S6: **Confocal microscopy images of HEK293T cells treated with *p*LNP delivering eGFP-Cas9 or *m*LNP delivering mRNA eGFP-Cas9. A)** Confocal microscopy image of HEK293T after 32 hours treatment with *p*LNP (top) and *m*LNP (bottom). Channel for eGFP signal was set to optimal settings for *m*LNP-treated cells, resulting in oversaturation of eGFP signal in cells treated with *p*LNP. **B)** Confocal microscopy image of HEK293T after 32 hours treatment with *p*LNP (top) and *m*LNP (bottom). Microscopy image with eGFP-channel set to optimal setting for *p*LNP, resulting in underexposure of eGFP signal in cells treated with *m*LNP. Green signal is eGFP-Cas9 protein. Blue signal is nuclear stain, Hoechst 33342. Images were taken at 20x magnification. Scale bar represents 100 μm. **C)** Zoom-in on the images with auto-optimal settings for eGFP signal for *p*LNP-treated (top) and *m*LNP-treated (bottom) HEK293T cells.

Confocal microscopy analysis script of Cas9 localization in nucleus and onset of genecorrection

Figure S7: **Image Analysis script on Columbus software of eGFP-Cas9 localization in nucleus and cytosol after treatment with** *p*LNP or *m*LNP.

Figure S8: **Image analysis script on Columbus software of onset of gene correction in HEK293T HDR Stoplight cells after treatment with *p*LNP-HDR or *m*LNP-HDR.**

Gel with labelled sgRNA to confirm it is complexed in LNPs

Figure S9: **Confirmation of entrapment of Cy5.5-sgTOM in *p*LNP and *m*LNP formulation for the biodistribution study *in vivo*.**

Aggregation and sedimentation of *in vivo* formulation with Cas9-RNP

formulation	size	PDI	1h incubation with 50% plasma at 37 °C	
			size	PDI
*p*LNP	238 ± 7 nm	0.3 ± 0.05	282 ± 4 nm	0.2 ± 0.01
*m*LNP	204 ± 4 nm	0.06 ± 0.003	293 ± 2 nm	0.2 ± 0.02
control *p*LNP	243 ± 12 nm	0.3 ± 0.03		
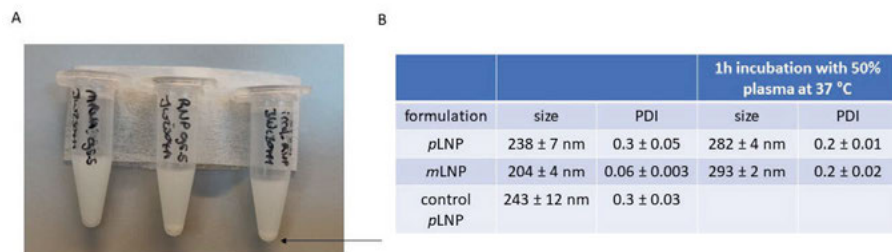
Figure S10: **Images of eppendorf tubes containing formulations for biodistribution study *in vivo*. A)** Image showing an eppendorf tube containing *m*LNP with Cy5.5-sgTOM (left), an eppendorf tube containing *p*LNP with Cy5.5-sgTOM (middle) and an eppendorf tube containing *p*LNP with non-targeting and unlabelled sgGFP (right). Both formulations were found to be turbid. Arrow indicates the pellet of aggregated particles. **B)** Particle size and PDI of *p*LNP, *m*LNP and control *p*LNP formulated for *in vivo* study. *p*LNP and *m*LNP were incubated with 50% mouse serum at 37°C and 300 rpm for 1h and then measured in size and PDI. Formulation were diluted 1:20 in 1x PBS prior to DLS measurements and measured 3 times.

Gating Single Cell Flow Cytometry of Liver
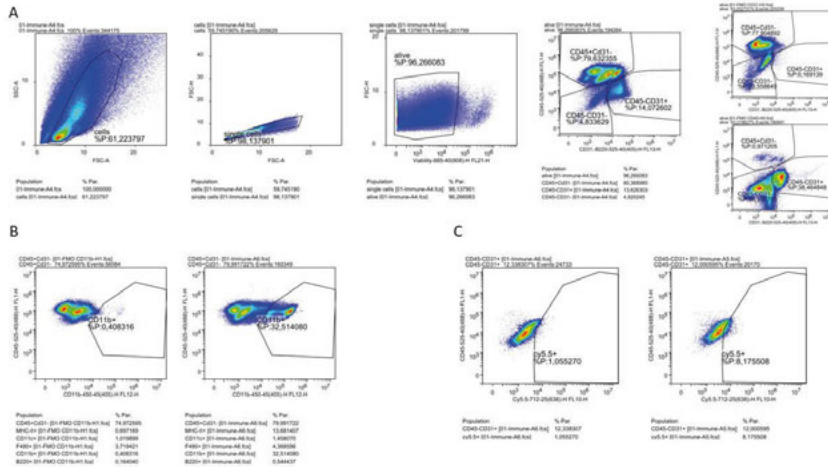
Figure S11: **Gating strategy of single cell flow cytometry of liver samples to determine biodistribution of Cy5.5-sgTOM.** The markers that defined each cell subset are listed in supplementary table 3. **A)** From left to right: gating of cells, gating of single cells, gating of living cells, gating of CD45 vs CD31 positive cells based on Fluoresence Minus One (FMO) controls CD31 (top) and FMO (bottom). **B)** Gating strategy to differentiate CD45$^+$ cells into subsets (myeloid cells, kupffer cells, dendritic cells). Example shows gating for CD11b$^+$ cells. **C)** Gating strategy example on LSEC to determine cells positive for Cy5.5, indicating uptake of Cy5.5-sgTOM.
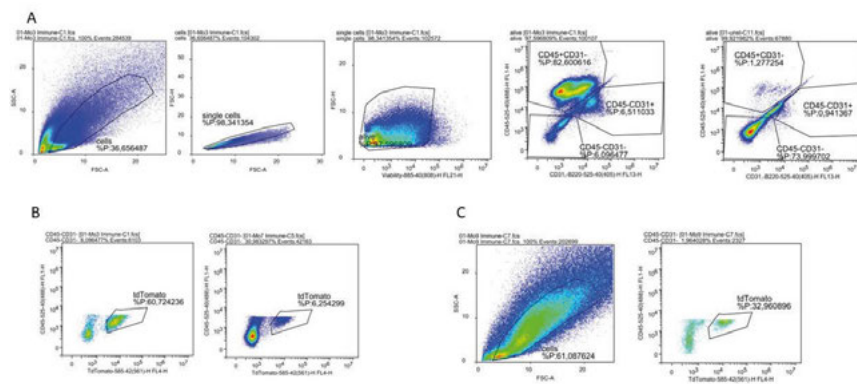
Figure S12: **Gating strategy of single cell flow cytometry of liver samples to determine expression of tdTomato in cell subsets.** The markers that defined each cell subset are listed in supplementary table 3. **A)** From left to right: gating strategy to determine liver cells, single cells, living cells, CD45+ and CD31+ and CD45-CD31- cell populations. **B)** tdTomato gating in CD45-CD31- cells (hepatocytes) in *m*LNP-treated mice (left) and control mice (right). **C)** Applied gating on control mouse that was found to have a different FSC and SSC scattering plot than the other mice in this study (left). tdTomato positive cells were higher in this particular mouse as well (right).

Biodistribution study of Cy5.5-sgTOM via IV injections of *p*LNP and *m*LNP in female Ai9 mice
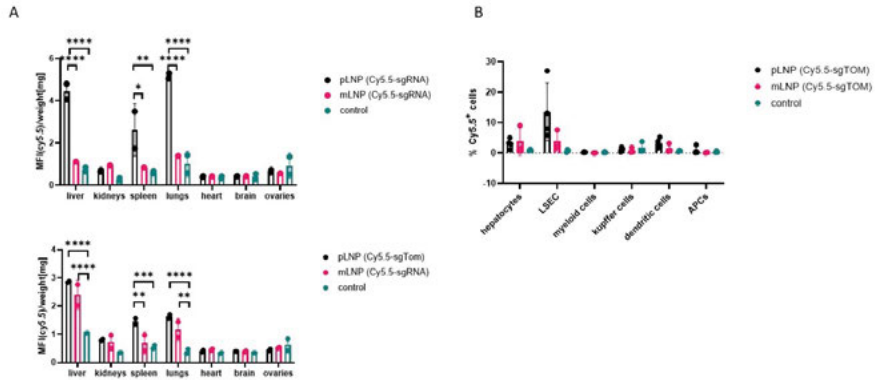
Figure S13: **Biodistribution study of Cy5.5-sgTOM via IV injections of *p*LNP and *m*LNP in female Ai9 mice. A)** Top graph shows the mean fluorescent intensity of Cy5.5 per weight of the organ of the first run-through of the biodistribution study. Thereby, one mouse of the control group died. Organs were harvested immediately and incorporated in the follow up studies. One mouse of *m*LNP group excluded as full injection was not successful. Bottom graph shows the data of the second run through. Control mice were administered with untargeted and unlabelled LNPs. **B)** Bar graph of the single cell flow cytometry showing the percentage of Cy5.5+ cells in each cell subset for the three experimental groups of the merged data set. Control mice were administered with untargeted and unlabelled LNPs.

5

Dexamethasone-Phosphate and Antigen-Carrying Liposomes for the Induction of Antigen-Specific Tolerance to SpCas9

Johanna Walther[1*], Daniëlle ter Braake[2*], Deja Porenta[1,2], Vasilis Papamoschou[1], Bonne Keijer[1], Cornelis Seinen[3], Naomi Benne[2], Femke Broere[2], Enrico Mastrobattista[1]

[1]Department of Pharmaceutics, Utrecht Institute for Pharmaceutical Sciences (UIPS), Utrecht University, The Netherlands
[2]Department of Infectious Diseases and immunology, Faculty of Veterinary Medicine, Utrecht University, The Netherlands
[3]CDL Research, University Medical Center Utrecht, The Netherlands
[*] equally contributed

Abstract

CRISPR-Cas9 technology is considered one of the most promising gene editing tools currently available for application as therapy for several genetic disorders, as the technique allows for introducing specific double-stranded breaks at targeted sites within the genome. However, the bacterial origin of SpCas9 may hinder the efficiency in patients since pre-existing immunity towards the SpCas9 protein could result in the systemic clearance of the complex resulting in subsequent elimination of its gene editing features or clearance of cells modified with the CRISPR-Cas9 components. To avoid such adaptive immune responses against SpCas9 protein, it is vital to induce tolerance towards the bacterial components. To achieve this, anionic liposomes were formulated for the co-delivery of the SpCas9 protein alongside the immunomodulator prodrug dexamethasone disodium phosphate (DexPhos). Immunomodulators, such as DexPhos, induce a tolerogenic state in dendritic cells. Tolerogenic dendritic cells play a major role in the establishment of T cell tolerance by e.g. T cell anergy and stimulation of suppressive regulatory T cells. *In vitro*, we show that our DexPhos liposomes are efficiently taken up by DCs, leading to a tolerogenic phenotype, also when co-encapsulating SpCas9. *In vivo*, these DexPhos-SpCas9 liposomes migrate to the spleen and liver and can slightly decrease the formation of SpCas9-specific antibodies.

Introduction

Clustered Regularly Interspaced Palindromic Sequences (CRISPR)-Cas9 is a bacterial defense mechanism that has been reprogrammed as a tool for specific gene editing and correction. The CRISPR-Cas9 system is a complex between an endonuclease and a short synthetic guide RNA, which directs the protein to a specific location within the DNA where it introduces a double-strand break.[1] Subsequent DNA-repair mechanisms can repair the double-strand breaks by various mechanisms, amongst them homology-directed repair where disrupted genes can be specifically repaired in the presence of a homologous DNA template.[2] Therefore, ongoing efforts are investigating how to deliver the CRISPR-Cas9 components using non-viral particles such as exosomes or lipid nanoparticles for clinical application *in vivo*.[3–5]

A major drawback is, however, that the CRISPR-Cas9 components originate from bacteria. The Cas9 protein ortholog, SpCas9, originates from *S. pyogenes* which is a known human commensal that can also be pathogenic. Therefore, due to the abundance of bacteria within the human population, such as *S.pyogenes*, it has been reported that humans are routinely exposed to SpCas9 and have generated SpCas9-specific antibodies. Charlesworth et al. and Simhadri et al. reported seropositivity for SpCas9 and another ortholog, SaCas9 from *S. aureus*.[6,7] While direct delivery via non-viral vectors such as lipid nanoparticles can overcome the risk of neutralizing antibodies to SpCas9, the additional finding of pre-existing effector T cells specific for SpCas9 is cause for more concern. The presence of the nuclease in correctly targeted cells would be expected to result in presentation on major histocompatibility complex (MHC) molecules, specifically MHC-I, potentially attracting the attention of cytotoxic T cells.[6,8] Therefore, the presence of preexisting immunity may counteract the efficacious use of CRISPR-Cas9 or cause systemic inflammatory reactions when treating patients with the CRISPR-Cas9 system. Hence, an approach to overcome neutralization or clearance

of CRISPR-Cas9 is to exploit the principles of immune tolerance and actively accommodate the foreign gene editing components.[9,10]

Dendritic cells (DCs) are antigen-presenting cells (APCs) with a variety of functions in the immune system, both adaptive and innate immune responses, and are pivotal regulators of immunity as well as tolerance.[11,12] The function of DCs is dependent on their maturation stage and subtype.[13] DCs can be converted to a tolerogenic state using dexamethasone disodium phosphate (DexPhos), a prodrug of the immunomodulator and anti-inflammatory drug dexamethasone.[14,15] Tolerogenic DCs (tolDCs) are characterized by a semi-mature state with reduced expression of MHCII, CD40 and CD86, decreased secretion of inflammatory cytokines such as IL-1, IL-6, and IFN-γ and instead an increased release of anti-inflammatory cytokines such as IL-10 and transforming growth factor β (TGF-β) in comparison to their mature state.[16] Due to this change in DC state, these cells can present antigens whilst inducing regulatory T cells (Tregs) and inhibiting the proliferation of effector T cells.[17,18] Tregs can be subdivided into different subtypes, including the conventional CD4$^+$ CD25$^+$ FoxP3$^+$ Tregs and CD4$^+$ Foxp3$^-$CD49b$^+$ Lag3$^+$ Type 1 Regulatory cells (Tr1s).

To utilize immunomodulators for induction of specific tolerance towards biologic drugs or self-antigens, ongoing efforts focus on polymeric or lipid nanoparticles as tolerogenic nanoparticles (tolNP).[19–21] Kim et al. report that poly(lactic-co-glycolic-acid) polymeric particles co-delivering dexamethasone and ovalbumin protein result in suppression of Ova-specific IgG and cytotoxic T cells, while Tregs were induced.[22] Liposomes entrapping rapamycin with CD22-ligand and ovalbumin conjugated to PEGylated lipid-reduced antibodies targeting ovalbumin *in vivo* after intravenous injections.[23] Furthermore, liposomes have been reported to be delivered to the liver and spleen *in vivo*, key organs in immune responses and tolerance.[24] However, to our knowledge no studies have yet investigated using tolNP as adjunctive therapy for gene therapy with CRISPR-Cas9.

In this study, we therefore hypothesize that DPPC:DPPG:cholesterol liposomes encapsulating the SpCas9 protein and DexPhos is a potent delivery system for induction of SpCas9 tolerance *in vivo*. We investigate the physical characteristics and stability of the liposomes and study the induction of tolerance both *in vitro* and *in vivo*.

Material and Methods

Materials
All reagents and chemicals used in this study were acquired from Sigma-Aldrich (Zwijndrecht, The Netherlands) unless mentioned differently. sgRNA (sequence: 5'-GCUGAAGCACUGCACGCCGU-3') was purchased from Sigma-Aldrich (Haverhill, UK). The lipids 1,2-dipalmitoyl-sn-glycero-3-phosphocholine (DPPC) and 1,2-dipalmitoyl-sn-glycero-3-phospho-(1'- rac-glycerol) (sodium salt) (DPPG) were acquired from Lipoid (Steinhausen, Switzerland. 1,10-((2-(4-(2-((2-(bis(2-hydroxydodecyl)-amino)ethyl)(2-hydroxydodecyl)-amino)ethyl)piperazine-1yl)ethyl)azanediyl)bis(dodecane-2-ol) (C12-200) was bought from CordonPharma (Plankstadt, Germany), 1,2-dioleoyl-sn-glycero-3-phosphoethanolamine (DOPE) from Lipoid, Cholesterol and 1,2-dimyristoyl-rac-glycero-3-methoxypolyethyleneglycol-2000 (PEG-DMG) from Sigma-Aldrich and 1,2-dioleoyl-3-trimethylammonium-propane (DOTAP) from Merck (Darmstadt, Germany). 1,1'-Dioctadecyl-3,3,3',3'-Tetramethylindodicarbocyanine, 4-Chlorobenzenesulfonate Salt (DiD) was acquired from Invitrogen (Thermo Fisher Scientific, Landsmeer, The Netherlands).

Formulation of Liposomes Encapsulating Dexamethasone-Phosphate and SpCas9 Protein
Liposomes were produced via the thin film lipid hydration method. DPPC, DPPG, and cholesterol were weighed and dissolved at a molar ratio of 47.4/0.6/52 and a final total molar concentration of 50 mM in 3 mL chloroform:methanol at a v/v ratio of 9:1. The lipid film was

obtained by evaporation of the organic solvents at full rotation speed and 60 °C for 5 minutes with a rotavapor and then dried further under mild nitrogen flow for 10 minutes. Afterwards, the lipid film was rehydrated with 500 μl of 50 mg/mL dexamethasone-phosphate (Dex-Phos; Duchefa Biochemie, Haarlem, The Netherlands) resuspended in formulation buffer (5 mM HEPES, 15 mM NaCl, 5% w/v D-Glucose, pH 7.4) while rotating at 60 °C for 15 minutes. In the case of formulating empty liposomes or only loading with SpCas9, the lipid film was rehydrated with 500 μl formulation buffer solely. Subsequently, the liposomes were extruded with the mini hand extruder (Avanti Polar Lipids, Inc, Alabaster, AL, USA) at 60 °C through two drain disks (Whatman 10MM PE 230300) and two 200 nm membranes (Whatman Nucleopore Track-Etch Membrane PC MB 19MM 0.2μm) 15 times. To encapsulate SpCas9 protein (recombinantly produced in Clearcoli™ in-house) 3.6 mg/ml SpCas9 was added to the formulation at a v/v ratio of 1:9 and then freeze-thawed three times.25 Finally, the formulation was ultracentrifuged twice at 40,000 rpm and 4 °C using a Beckman Coulter Optima L-90K Ultracentrifuge with a 70.1Ti rotor to remove any free dexamethasone-phosphate or SpCas9. The liposome pellet was resuspended in 500 μL of formulation buffer and stored at 4 °C.

To follow the biodistribution of tolerogenic liposomes *in vitro* and *in vivo*, empty liposomes were formulated as described above. However, before making the lipid film 1,1'-Dioctadecyl-3,3,3',3'-Tetramethylindodicarbocyanine, 4-Chlorobenzenesulfonate Salt (DiD) was added to the lipids dissolved in chloroform:MeOH at a mole% of 0.02 of the total lipids, resulting in a final molar concentration of 0.01 mM.

For the formulation of liposomes for *in vivo* studies, a commercially available endotoxin-free SpCas9, Alt-R SpCas9 nuclease V3 (IDT-DNA, Leuven, Belgium) was used. Additionally, a formulation encapsulating DexPhos and ovalbumin (v/v 1:9 ovalbumin:lipids) instead of SpCas9 were formulated. Each formulation was diluted 16.6 times to maintain < 1.44 mg total lipids (tolerated amount

determined from previous intravenous injections in mice at animal facility in Utrecht) for safety precautions when injecting in mice.

Formulation of Lipid Nanoparticles Complexing SpCas9-Ribonucleoprotein Complex (RNP)

Lipid nanoparticles (LNPs) complexating SpCas9-RNP were formulated as previously described.[25] Briefly, RNP complexation occurred in a 1:1 ratio of sgRNA to SpCas9 in nuclease-free water and incubated for 15 minutes at RT. Meanwhile, a lipid mixture of 40x more total lipid weight than sgRNA with the following lipids was prepared: C12-200, DOPE, cholesterol, PEG-DMG, and DOTAP (molar ratio: 35:16:46.5:2.5:0.25). Then, the RNP was mixed in a volume ratio of 3:1 with the lipid mixture and incubated for 15 minutes at RT. LNPs were formulated to ensure a final amount of 2 μg of SpCas9 in 200 μl LNPs.

Physical Characterization of Liposomes

For the determination of the average size and polydispersity index (PDI) of the nanoparticles dynamic light scattering on a Zetasizer nano-s (Malvern ALV CGS-3, Malvern, UK) was used. To determine the ζ-potential, the formulations were diluted 1:100 in 10 mM HEPES buffer pH 7.4 and measured using a dip cell cuvette on the zetasizer nano-z (Malvern ALV CGS-3).

Determine Encapsulation of Dexamethasone-Phosphate and SpCas9 in Liposomes (and SpCas9 in Lipid Nanoparticles)

Encapsulation of DexPhos in DPPC:DPPG:cholesterol liposomes was determined via reversed-phase high-performance liquid chromatography (HPLC) analysis. Samples were run over an XBridge protein BEH C4 300 Å column (3.5 μm, 4.6 mm X 150 mm, serial no 0166312161884, Waters Alliance e2695, Milford, MA, USA) attached to an XBridge protein BEH C4 300 Å sentry guard cartridge (Waters Alliance, 3.5 μm, 4.6 mm X 20 mm, 2/pk) and with a linear acetonitrile gradient from 5% to 100% in 5 min and back again in 1 min. Starting conditions were then equilibrated for another 4 minutes before injection of the next sample. The mobile phase additionally contained 0.1% trifluoroacetic

acid. UV-Vis detection was set to 214 and 280 nm (2pts/s). Before injection samples were treated with 1% triton X-100 and injected with a volume of 50 μl at a flow rate of 1 ml/min. A calibration curve of dexamethasone-phosphate diluted to a concentration range of 0-400 μg/ml in formulation buffer was prepared to determine the concentration of encapsulated DexPhos. Encapsulation efficiency was then determined by dividing the concentration of encapsulated DexPhos in ultracentrifuged liposomes by the concentration of the total amount of DexPhos in non-ultracentrifuged liposomes via the EMPOWER software. Verification of encapsulation of SpCas9 in lipid nanoparticles complexating the SpCas9-RNP was performed as above with slight differences and described in a previous publication.[25] Briefly, SpCas9-RNP loaded LNPs were injected onto the same column and same mobile phase as above. However, detection was with fluorescence signal and the detector was set at ex. 280 nm, em. 350 nm. Prior to injection were treated with 2% triton X-100. Entrapment of SpCas9 in LNPs was calculated by dividing the concentration of encapsulated SpCas9 in dialyzed (MWCO 300kDa) LNPs by the concentration of total amount of SpCas9 in non-dialyzed LNPs.

Cryo-TEM Liposome Imaging
For Cryo-TEM imaging, 10 μl of dispersed nanoparticles were added to freshly glow-discharged Quantifoils and incubated for at least 10 minutes in a humidified environment and then vitrified using an FEI Mark IV Vitrobot (Fei, Hillsboro OR, USA). After vitrification samples were stored in liquid nitrogen until imaging. Samples were imaged on an FEI Tecnai G2 20 TWIN 200kV transmission electron microscope. Vitrified Quantifoils were loaded in a Gatan 70° tilt cryo-transfer system which was pre-cooled using liquid nitrogen and inserted in the microscope. Samples were imaged at a magnification of 29k and images were acquired by the bottom-mounted FEI High-Sensitive (HS) 4k x 4k Eagle CCD Camera System.

Release Assay of Dexamethasone-Phosphate at 37 °C and 4 °C
Liposomes encapsulating dexamethasone-phosphate and SpCas9 protein were formulated as described above. The formulation was stored

in aliquots of 50 μl in the fridge at 4 °C or in an incubator at 37 °C for different time points (0, 1h, 4h, 7h, 24h, 48h, 120h, 168h, 240h, 336h, 504h, 672h). Per timepoint, 2 aliquots were assigned at both 4 °C and 37 °C. At each given time, one of the aliquots was diluted in formulation buffer to a final volume of 12 ml and ultracentrifuged for 1 hour at 40,000 x g at 4 °C. The supernatant was removed and the liposome pellet was resuspended overnight in 50 μl of fresh formulation buffer. Resuspended samples were then stored in the fridge until all time points were collected. Subsequently, the samples were treated with a volume ratio 10% triton-X100 (v/v 10:1). In parallel, the other aliquot was not ultracentrifuged and instead immediately treated with 10% triton-X100 (v/v 10:1) as a control for the total amount of Dex-Phos (released and still entrapped). All samples were analyzed with reversed-phase high-performance liquid chromatography as described above. Afterwards, the peak area of the DexPhos peaks on the chromatograms was integrated into the EMPOWER software and a release ratio was calculated by dividing the peak area of samples that were centrifuged (equivalent to entrapped DexPhos) by the mean peak area of non-centrifugated samples of all timepoints (equivalent to total Dex-Phos).

$$\text{release ratio} = \frac{A(DexPhos)_t}{A(mean((totalDexPhos)_{t1\text{-}to})))} \tag{5.1}$$

DexPhos = entrapped DexPhos (centrifuged sample)
Total DexPhos = non-centrifuged sample
t = timepoint x
t1 = 0 hours
to = 672 hours

Mice

Wildtype Balbc/cANCrl mice (female) at 8 weeks old were purchased from Charles River laboratories as a source for bone marrow-derived dendritic cell cultures. For the *in vivo* study, 18 Balb/cAnNCrl mice were purchased from Charles River Laboratory to be 6 weeks old at the start of the study. Mice were given one week of acclimatization and housed under standard conditions at the animal facility facility (standard chow and water *ad libitum*). Mice were randomized into experimental groups based on weight using RandoMice. All

experiments were approved by the Animal Experiment Committee of Utrecht University (AVD10800202115687 (*in vitro* experiments) & AVD10800202115026 (*in vivo* experiments)).   Humane end points considered for immediate euthanasia were: no food intake for 24 hours (result in 10% weight loss), stop of normal activity or inability to stand up or walk, and clear evidence of discomfort such as piloerection.

Induction of Tolerogenic Dendritic Cells on Bone Marrow-Derived Dendritic Cells (BMDCs)

Murine femurs and tibias were flushed with a 21G needle.   Bone marrow was homogenized and seeded in 6-well plates at a cell density of 450,000 cells/mL in 2 mL IMDM (Gibco, Thermo Fisher Scientific, Landsmeer, The Netherlands), supplemented with 10% FCS (Bodinco, Alkmaar, The Netherlands), 100 units/mL of penicillin (Gibco, ThermoFisher Scientific100 ug/mL of streptomycin (Gibco, ThermoFisher Scientific and 0.5 μM β-mercaptoethanol (Gibco, ThermoFisher Scientific).   Cells were cultured at 37°C and 5% CO_2 in the presence of 20 ng/mL of granulocyte-macrophage colony-stimulating factor (GM-CSF, in-house produced) for 7 days.   On the second day, 2 mL of complete IMDM and 20ng/mL GM-CSF were added to the wells.   Extra GM-CSF (20ng/mL) was supplemented on day 5.   Cells were matured by 10 ng/mL lipopolysaccharide (LPS, O111:B4) and simultaneously treated with 1μM free Dex (D4902; Sigma Aldrich), 1μM free DexPhos, 12.5nM SpCas9 or differentially generated liposomes on day 7.   After 16 h, DCs were harvested for phenotypic characterization by flow cytometry.

Flow Cytometry for Tolerance Induction in BMDCs

For all flow cytometry experiments, cells were resuspended in a 96-well round bottom plate (Corning) at a concentration of 200,000 cells/mL in 200 μl FACS buffer. The suspensions were first blocked for 15 minutes with 10ug/mL Fc Block (clone 2.4G2, in-house produced) to prevent non-specific antibody binding.   Extracellular staining was performed using a cocktail of antibodies, consisting of CD11c-APC

(N418, eBioscience, Thermo Fisher Scientific), MHCII-eFluor450 (M5/114.15.2, eBioscience, Thermo Fisher Scientific), CD40-PE (3/23, BD Biosciences, Franklin Lakes, NJ, USA), CD86-FITC (GL-1, BD Biosciences) and ViaKrome808 (Beckman Coulter, Indianapolis, IN, USA) in FACS Buffer (1X PBS supplemented with 2% FCS). For all flow cytometric analyses, appropriate single-stain and fluorescence minus one controls were taken along. Flow cytometry was performed using the Beckman Coulter Cytoflex LX at the Flow Cytometry and Cell Sorting Facility located at the Faculty of Veterinary Medicine at Utrecht University. Acquired data were analyzed using FlowJo Software v.10.7 (FlowJo LLC, Ashland, OR, USA).

In Vitro Uptake Studies of DiD-Labelled Liposomes
DC2.4 cells (ATCC) were cultured at 80% cell density in RPMI-1640 medium supplemented with 10% FCS, 10 μM β-mercaptoethanol, 1x HEPES, 1x Glutamax, and 1x MEM non-essential amino acids at 37 °C and 5% CO_2. Twelve microliters of DiD-labelled empty liposomes were added to LPS-matured DC2.4 cells (LPS; E. coli O127:B8; 20 μg/mL LPS for 30 minutes) seeded on 24-well plate at a 50000 cells/well density for 1h, 7h, and 24h before analysis and incubated at 37 °C and 5% CO_2. Cells were harvested and transferred onto a BD FALCON U-bottom 96-well plate (Becton Dickinson, Franklin Lakes, NJ, USA) for flow cytometry. Cells were washed 3 times with PBS. After washing the cells with PBS again, the cells were fixated in 1% PFA before measuring the DiD signal on the FACS CANTO II. Additionally, 10,000 cells per well were harvested and transferred to a black 96-well imaging plate for confocal microscopy. Cells were washed with PBS and then the cell pellet was resuspended in 100 μl of 2 μg/ml Hoechst 33342 and incubated for 10 minutes at 37 °C and 5% CO_2. Then, the cells were imaged on the Confocal spinning disc microscope Cell Voyager 70005 (Yokogawa, Yokogawa Corporation, Tokyo, Japan), whereby Hoechst was excited by the 405 nm laser and DiD was excited with the 640 nm laser.

In Vivo Assessment of Tolerance Induction by tolNPs
Eighteen female naïve Balb/c mice were randomly assigned to the

three experimental groups (6 mice per group) according to weight. On day 0, each mouse of each experimental group was treated with 200 μl of liposome formulations (group 1 – DexPhos-SpCas9 liposomes, group 2 – DexPhos-Ova liposomes, group 3 – SpCas9 liposomes) with a final amount of 46.8 μg DexPhos and 2 μg SpCas9. Seven days later, the mice were injected with the same formulations and same concentrations dependent on their assigned experimental group. On day 15, blood samples were collected for each mouse via cheek punctures into z-serum separation tubes (Greiner Bio-One, Kremsmünster, Austria). Serum was separated from red blood cells by centrifuging the blood samples at 10,000 x g for 5 minutes at 4 °C and collected into separate tubes and stored at -20 °C. On day 17, all mice were challenged with SpCas9 via lipid nanoparticles complexing SpCas9-RNP at a final amount of 2 μg SpCas9 and a volume of 200 μl per injection. The challenge was repeated one week later on day 24. Before the second challenge, blood samples were collected and serum stored as described above. One week later, on day 31, blood samples were collected again via cheek punctures and serum was stored, and the mice were sacrificed. Spleens were collected from each mouse for flow cytometry analysis.

Biodistribution of DiD-Labelled Liposomes In Vivo

DiD-labelled empty liposomes were injected in three selected mice (one of each experimental group) 1h before sacrifice. After sacrificing the mouse, liver, spleens, lungs, kidneys, heart, ovaries and bones were harvested from the mice injected with DiD-labelled liposomes and three control mice (again one from each experimental group). The organs were weighed and then snap-frozen in liquid nitrogen and stored at -80 °C until imaging. The organs were imaged on the Odyssey scanner (LI-COR Biosciences, Lincoln, NE, USA) with the following settings to determine uptake of DiD-labelled empty liposomes: channel 700 nm, resolution 169 μm, intensity 1, quality high. The mean fluorescent intensity of each organ area on the image was determined with the Image Studio software. The mean fluorescent intensity was divided by the weight of the organ to

determine the MFI/weight of each organ.

Determination of SpCas9-Antibody Levels in Mouse Serum
The ELISA protocol described by Charlesworth et al. was used in this study.6 96-well ELISA well plates were coated with 1 μg/well Sp-Cas9 in 100 μl 1x coating solution (ELITech, Group B.V., Spankeren, The Netherlands) overnight at 4°C. The following day, the wells were washed three times with 100 μl 1x wash buffer for 5 minutes at 200 rpm at RT and then blocked with 100 μl 1% BSA blocking solution (ELITech Group B.V.) for 2 hours at RT. Meanwhile, the serum samples were prepared in serial dilutions ranging from 1:500 – 1:1,000,000 (diluted in 1% BSA blocking solution). Additionally, commercial antibodies against SpCas9 (Sanbio B.V., Uden, The Netherlands) and ovalbumin (Merck) were serial diluted 1:1,000 – 1:10,000,000 in 1% BSA blocking solution. After blocking the wells, the serum samples (100 μl) and commercial antibodies (100 μl) were added to the wells and incubated for 5 hours at 4 °C and shaking at 200 rpm. Then, the wells were washed again three times with 100 μl 1x wash buffer and shaken at 200 rpm for 5 minutes. Next, the wells were incubated with 100 μl HRP-labelled goat anti-mouse IgG1 (BD Biosciences, Vianen, The Netherlands) (1:1,000 diluted in 1% BSA blocking solution) for 1 hour at RT and then washed four times. The wells were then treated with 100 μl of ABTS ELISA HRP (Abcam, Amsterdam, The Netherlands) substrate for 15 minutes. The reaction was stopped with 1% SDS and then measured on the SpectraMax for absorbance at 405 nm.

Flow Cytometry Analysis of Splenocytes at t=0 after In Vivo Study
Spleens were collected from each mouse, mashed through a 70 μm filter (Falcon, Corning, New York, USA) and erythrocytes were lysed using Ammonium–Chloride–Potassium (ACK) lysis buffer (0.15 M NH4Cl, 1 mM KHCO3, 0.1 mM Na2EDTA; pH 7.3). Cells were seeded in a round bottom 96-well plate (Falcon, Corning, New York, USA) at 1,000,000 cells/well. Before staining, cell suspensions were blocked for 15 min with Fc Block (2.4G2, in-house produced). Cells were stained at t=0 with a monoclonal antibody mix of CD4-BV785 (RM4-5, BioLegend, USA), Lag3-PE (C9B7W, eBioscience, Thermo

Fisher Scientific, USA), CD49b-APC (DX5, Biolegend, USA) and CD25-PerCPCy5.5 (PC61.5, eBioscience, Thermo Fisher Scientific, USA) and ViaKrome808 (Beckman Coulter, Indianapolis, IN, USA) in FACS Buffer. After 30 min incubation at 4°C in the dark, cells were washed with PBS, fixed, and permeabilized using the FoxP3 transcription factor staining set (eBioscience, San Diego, CA, USA). Subsequently, cells were stained intracellularly according to the manufacturer's instructions with FoxP3-eFluor450 (FJK-16s, eBioscience, San Diego, CA, USA). Finally, cells were washed and resuspended in 100 μL PBS for measurement. To ensure correct analysis, relevant single-stain and fluorescence minus one (FMO) controls were used. Samples were measured on a Beckman Coulter Cytoflex LX at the Flow Cytometry and Cell Sorting Facility at the Faculty of Veterinary Medicine at Utrecht University. Acquired data were analyzed using FlowJo Software v.10.7 (FlowJo LLC, Ashland, OR, USA).

Restimulation of Splenocytes for Cytokine Measurement after the In Vivo Study

Splenocytes were seeded in a 96-well round bottom plate (Falcon, Corning, USA) at 1,000,000 cells/well and restimulated with medium, SpCas9 (20 μg/mL), Ova protein (20 μg/mL) and PMA (50ng/mL) /Ionomycin (1 μg/mL) for 6 hours at 37°C and 5% CO_2. After 2 hours, cells were supplemented with 1ug/mL Brefaldin A. Cells were stained with CD4-BV785 (RM4-5, BioLegend, USA), LAP-PE (TW7-16B4, eBioscience, San Diego, CA, USA), ViaKrome808 (Beckman Coulter, Indianapolis, IN, USA), IL-10-APC (JES5-16E3, BD Biosciences, Franklin Lakes, NJ, USA), FoxP3-eFluor450 (FJK-16s, eBioscience, San Diego, CA, USA) and IFNy-FITC (XMG1.2, BD Biosciences, Franklin Lakes, NJ, USA) using the protocol described above and the FoxP3 transcription factor staining set (eBioscience, San Diego, CA, USA). For all experiments, cells were washed and resuspended in 100 uL PBS for measurement. To ensure correct analysis, relevant single-stain and fluorescence minus one (FMO) controls were used. Samples were measured on a Beckman Coulter

Cytoflex LX at the Flow Cytometry and Cell Sorting Facility at the Faculty of Veterinary Medicine at Utrecht University. Acquired data were analyzed using FlowJo Software v.10.7 (FlowJo LLC, Ashland, OR, USA).

Restimulation of Splenocytes for Immune Cell Analysis
Splenocytes were labeled with carboxyfluorescein succinimidyl ester (CFSE, 0.5 nM) according to the manufacturer's protocol (ThermoFisher) and seeded in a 96-well flat bottom plate (Falcon, Corning, USA) at 1,000,000 cells/well and restimulated with medium, SpCas9 (20ug/mL), Ova protein (20 μg/mL), Ova peptide (323-339; 20 μg/mL) and ConA (10 μg/mL) for 3 days at 37°C and 5% CO_2. Cells were transferred to a 96-well round bottom plate, blocked with FcBlock (2.4G2, in-house produced), and stained with CD4-BV785 (RM4-5, BioLegend, USA) and Viakrome808 (Beckman Coulter, Indianapolis, IN, USA) using the protocol described above. To ensure correct analysis, relevant single-stain and FMO controls were used. Samples were measured on a Beckman Coulter Cytoflex LX at the Flow Cytometry and Cell Sorting Facility at the Faculty of Veterinary Medicine at Utrecht University. Acquired data were analyzed using FlowJo Software v.10.7 (FlowJo LLC, Ashland, OR, USA).

Results

Physical Characterizations of DexPhos-SpCas9 Liposomes
Liposomes, empty or loaded with either DexPhos or SpCas9, or encapsulating both DexPhos and SpCas9 were produced via the thin film lipid hydration and extrusion method.[26] All formulations were on average approximately 200 nm in size with a variation of less than 10% (Fig. 1A). The formulation containing both SpCas9 and DexPhos had a higher polydispersity index. The determined ζ-potential ranged from -4.2 mV for SpCas9-loaded liposomes to -8.3 mV for SpCas9&DexPhos-loaded liposomes. The formulations remained stable (defined as only

slight fluctuations in size, PDI and charge) for over one month. Interestingly, after one week a slight decrease in particle size for all formulations was found which however then remained stable over time, as shown in Fig. 1D. Furthermore, the four different formulations were characterized to be stable in the presence of 25% human plasma up to 24 hours incubation at 37 °C (see supplementary info Fig. 2). Cryo-TEM images show clear spherical bilayer membrane structures, typical for liposomes. However, the cryo-TEM images additionally indicate that multilamellar liposomes and spherical particles were formed during the formulation (Fig. 1B). The encapsulation efficiency of Dex-Phos and SpCas9 was determined to be 10% and 55% via HPLC and SDS Page analysis, respectively, shown in Fig. 1A, and HPLC chromatograms and SDS PAGEs are depicted in Supplementary Fig. 1. It was additionally found through a release study that the ratio of entrapped DexPhos to total DexPhos remained rather consistent over the time span of one month during storage at 4 °C or 37 °C (Fig. 1C).

Figure S1: **Physical characterizations of empty and various cargo-loaded DPPC:DPPG:cholesterol liposomes.** **A)** An overview table that shows the encapsulation efficiencies of the different cargos, size, polydispersity index, and ζ-potential of the formulations. **B)** Cryo-TEM images at 29k magnification of empty, SpCas9-loaded, DexPhos-loaded, and SpCas9-DexPhos-loaded liposomes. Depicted scale bar represents 200 nm. **C)** Release of DexPhos at 4 °C and 37 °C for 1 month from SpCas9-DexPhos-loaded liposomes (same batch, one-time experiment) given as the ratio of DexPhos entrapped in particle vs mean total DexPhos (equation 1 in Material and Methods). Mean total DexPhos is the mean peak area of total DexPhos at each time point: 4°C: 901146 ± 228854, Pearson correlation $r^2 = 0.2$; 37°C: 1247651 ± 873731, Pearson correlation $r^2 = 0.08$.

Figure S1: **D)** Stability study of empty, SpCas9-loaded, DexPhos-loaded and SpCas9-DexPhos-loaded liposomes over 4 weeks. The left graph depicts the size, the middle graph depicts the polydispersity index, and the right graph depicts the ζ-potential of the formulations. Data depicts 3 replicates within each DLS and zeta-potential measurement.

Uptake of DiD-Labelled Liposomes In Vitro in DC2.4 Cells
DC2.4 cells treated with DiD-labelled empty liposomes show uptake of liposomes after 1 hour (MFI = 4000) already and significantly higher uptake after 24 hours (MFI 20000) as confirmed by microscopy and flow cytometry (Fig. 2A,B).

Induction of Tolerogenic BMDCs after Treatment with DexPhos-SpCas9 Liposomes
To determine whether tolNPs induce tolerogenic dendritic cells *in vitro*, BMDCs were treated with PBS or LPS alone and in combination with free Dex, free DexPhos, free SpCas9, or differentially generated liposomes and analyzed for the expression of co-stimulatory molecules CD40 and CD86 on their cell surface. A significant lack of expression of CD40 (Fig. 2C) and CD86 (Fig. 2D) in comparison to mature BMDCs was observed in cells treated with free Dex or DexPhos and in cells treated with formulations encapsulating DexPhos at a final concentration of 1 μM (DexPhos-SpCas9- and DexPhos-loaded liposomes). BMDCs treated with empty or SpCas9-loaded liposomes did not induce a change in CD40 and CD86 surface marker expression. Expression levels of surface marker MHC-II did decrease in the presence of free or encapsulated DexPhos, however maturation with LPS did not upregulate MHC-II (see supplementary Fig. 4).
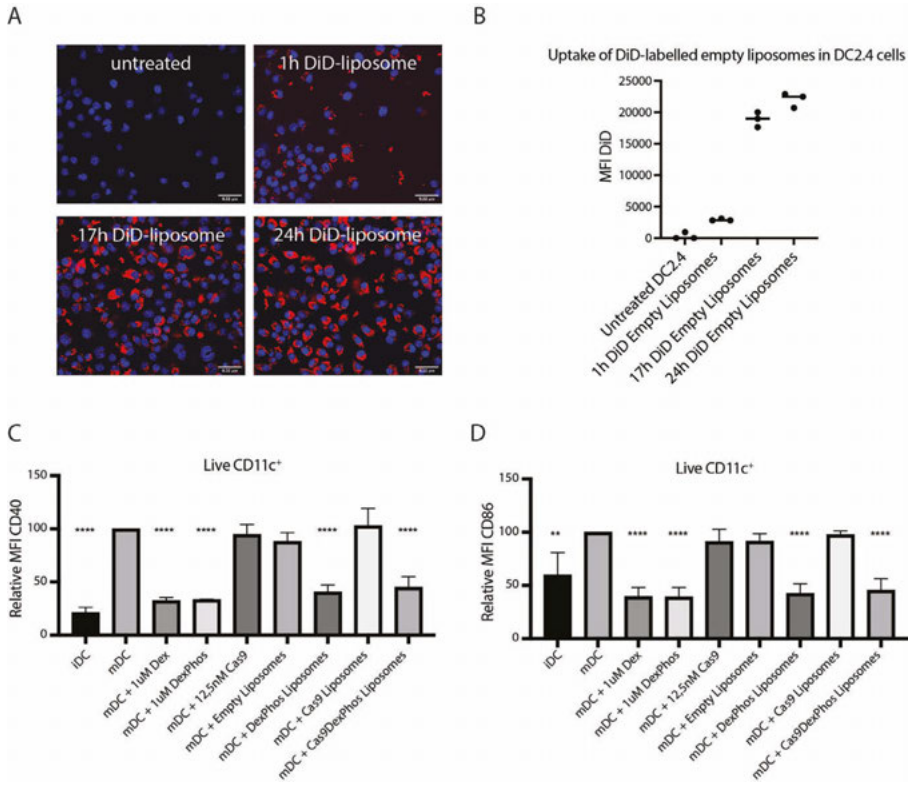
Figure S2: *In vitro* **characterizations of DPPC:DPPG:cholesterol liposomes. A)** Confocal microscopy of DC2.4 cells treated with DiD-labelled empty liposomes (red signal) for 1h, 17h, and 24h. Before microscopy cells were treated with $2\mu g/ml$ Hoechst 33342 to stain the nuclei (blue signal). Scale bars indicate $0.22\mu m$. Experiment was performed in triplo. **B)** Quantification of MFI of DiD in DC2.4 cells via flow cytometry. **C, D)** Expression of surface markers depicted in relative MFI compared to mDC (%) of the antibody staining CD40 and CD86, respectively (n=3). BMDCs were matured with 10 ng/ml LPS (derived from O111:B4 E.coli) and then treated with $1\mu M$ free dexamethasone and DexPhos or with liposomes. Gating strategies are shown in Supplementary Fig. 3.

DiD-Labelled Liposomes are observed in the Liver and Spleen of Balb/c Mice

Next, to analyze the uptake of DiD-labelled liposomes in DC2.4 cells *in vivo*, DiD-labelled liposomes were injected intravenously in
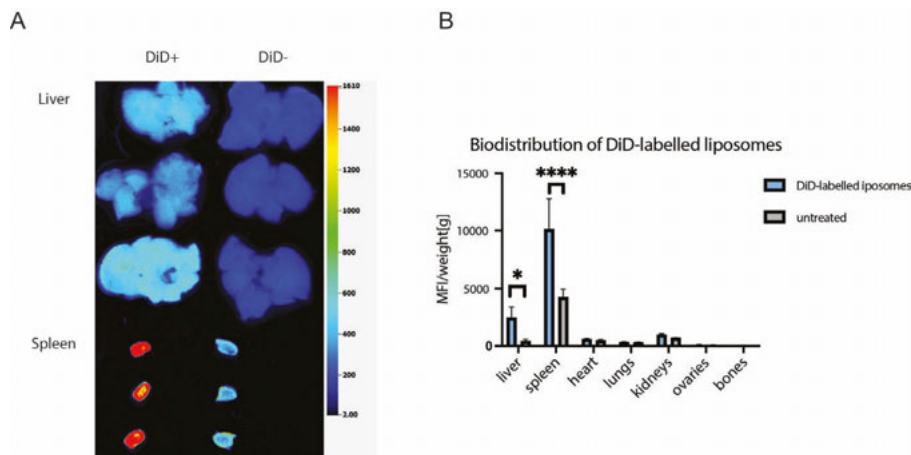
Figure S3: **Biodistribution of DiD-labelled empty liposomes in Balb/c mice. A)** Images of livers and segments of spleen treated with and without DiD-labelled liposomes. Images were obtained on the Odyssey scanner (channel 700 nm, resolution 169μm, intensity level) to depict the fluorescent signal of DiD. The scale bar on the right indicates that dark blue represents the lowest signal intensities (2.00) and red represents the highest signal intensities (1610). Images of all other organs (heart, lungs, kidneys, ovaries, bones) are in Supplementary Fig. 5. **B)** Mean fluorescent intensity of DiD per weight of liver, spleen, heart, lungs, kidneys, ovaries, and bones of 3 mice treated with and 3 mice treated without DiD-labelled empty liposomes 1h before sacrifice. A 2-way Anova via GraphPhad determined significant effects: * - p = 0.02, **** - p = < 0.0001. The scanned images of the heart, lungs, kidneys, ovaries, and bones are shown in the supplementary information.

Balb/c mice. Analysis using the Odyssey scanner revealed liposomal localization to the liver and spleen, as shown by the significantly higher weight-corrected MFI compared to untreated mice (Fig. 3; SI Fig. 6).

Induction of SpCas9-Specific Tolerance in Balb/c Mice

To study whether the described SpCas9-DexPhos liposomes would induce SpCas9-specific tolerance *in vivo*, female Balb/c mice were tolerized with SpCas9-DexPhos-, Ova-DexPhos- or SpCas9-liposomes, and then challenged with SpCas9-LNPs (Fig. 4A). Subsequently, SpCas9-specific IgG levels were measured in serum as well as levels of CD4$^+$ FoxP3$^+$ CD25$^+$ Tregs was measured in the spleens of mice (Fig. 4C). Mice tolerized with SpCas9-DexPhos liposomes show a

tendency of slightly (non-significant) lower SpCas9-specific IgG titer after challenge with SpCas9-RNP loaded LNP, in comparison to mice treated with aspecific antigen (Ova-DexPhos liposomes), as depicted in Fig. 4B and additionally supported by the calculated area under the absorbance curve resulting in 8.5 ± 1.2 , 7.8 ± 0.7 , and 8.3 ± 0.6 for Ova-DexPhos, SpCas9-DexPhos and SpCas9 treated groups, respectively (Supplementary Fig.6B). Mean IgG titer in mice treated with SpCas9-liposomes did not change value before or after challenge (Fig. 4B). Through sinusoidal fitting of the standard antibody titer curve (see Supplementary Fig. 6C), the concentration of the SpCas9-specific IgG in mice tolerized with tolNPs and after challenge with SpCas9-RNP LNPs was interpolated to be 0.03 ± 0.03 μg/ml at a 1:2000 serum dilution shown in Supplementary Fig. 6D. In comparison, though again non-significantly, the concentration of SpCas9-specific IgG for mice treated with a-specific antigen (Ova-DexPhos liposomes) and mice treated with SpCas9-liposomes resulted in 0.08 ± 0.13 μg/ml and 0.04 ± 0.04 μg/ml, respectively (Supplementary Fig. 6D).

Directly after tolerization, mice treated with SpCas9-liposomes have started developing more antibodies than mice treated with SpCas9-DexPhos tolNP or liposomes encapsulating Ovalbumin and DexPhos (Supplementary Fig. 6D). Understandably, mice treated with the Ova-DexPhos formulation do not have any SpCas9-specific IgG present in their serum, but those levels noteworthily increase over time to the overall highest concentration of antibodies of all experimental groups (Supplementary Fig. 6D).

It was confirmed that the ELISA was specific for SpCas9 by primary treatment with commercially available anti-SpCas9 antibody and anti-Ova antibody (Supplementary Fig. 6A). Furthermore, Balb/c mice were confirmed to have no prior existing antibodies towards SpCas9 (Supplementary Fig. 6A)
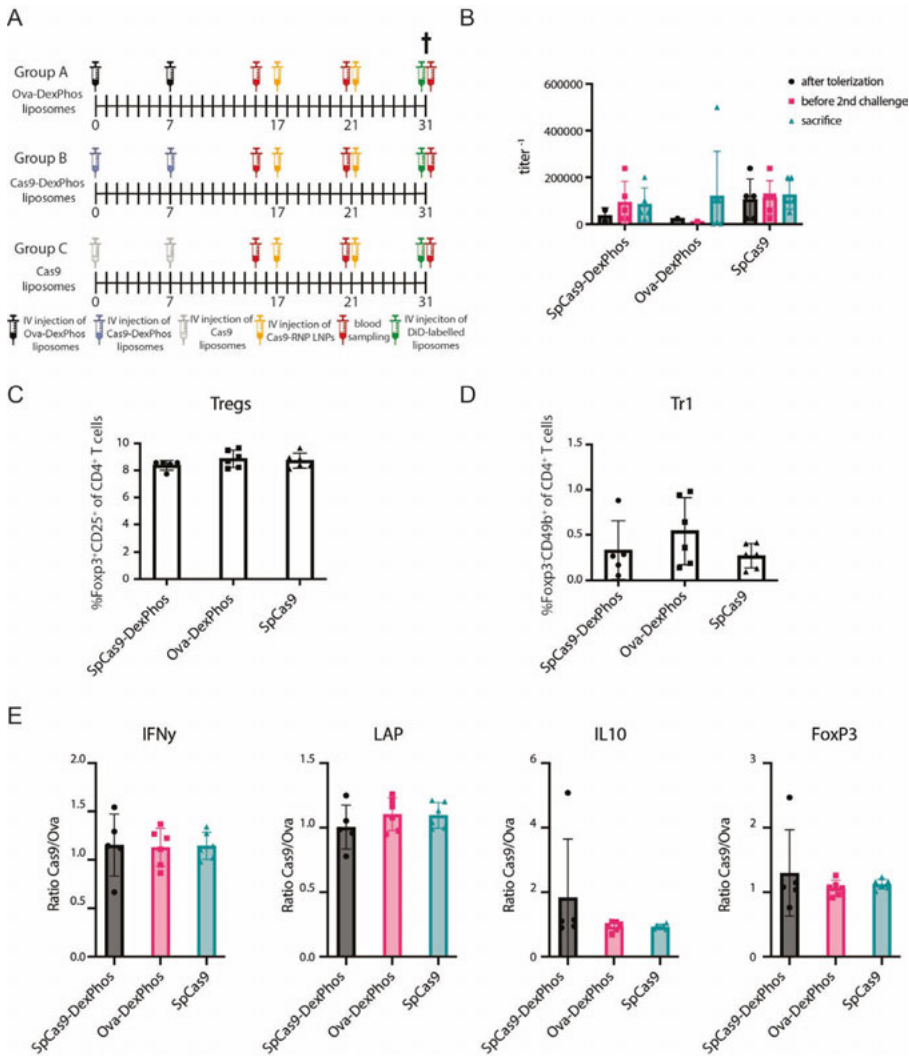
Figure S4: **Induction of tolerance towards SpCas9 protein *in vivo*. A)** Schematic representation of the *in vivo* study showing the three different experimental groups and the time points of tolerization and challenge and serum collection. **B)** SpCas9-specific IgG titers in mouse serum. Antibody titers were determined by selecting serum dilution at which absorbance of ABTS HRP substrate was at least 2-fold higher than the background. **C, D)** Mice were sacrificed and spleens were processed, stained, and analyzed using flow cytometry for CD4^{+} FoxP3^{+} CD25^{+} Tregs and CD4^{+} CD49b^{+} Lag3^{+} Tr1s, respectively. **E)** Splenocytes were restimulated with SpCas9 and Ova and incubated for 6 hours, of which 4 were in the presence of Brefaldin A. Cells were gated for live CD4^{+} single cells.

Tolerizing Mice with SpCas9-DexPhos Liposomes does not affect CD4+ Regulatory T Cells in the Spleen

Using flow cytometry to assess the spleens of liposome-treated mice for the presence of conventional CD4$^+$ FoxP3$^+$ CD25$^+$ Tregs and CD4$^+$ CD49b$^+$ Lag3$^+$ Tr1s revealed no significant differences in non-antigen specific regulatory T cells in the spleen (Fig. 4C&D).

Tolerizing Mice with SpCas9-DexPhos Liposomes does not affect Cytokine Production in the Spleen

To assess antigen-specific T-cell responses, splenocytes were isolated and restimulated with SpCas9 and Ova. Intracellular cytokines were measured after 6 hours. The final 4h of incubation were in the presence of the Golgi-stop Brefeldin A. No significant differences were found in cytokine production between the different restimulations (Fig. 4E).

Restimulation of Splenocytes from Tolerized Mice with SpCas9 for Three Days does not Induce a CD4+ T Cell Response

Next, we hypothesized that the restimulation time might be too short or that the whole protein restimulations might be affecting the efficiency of our restimulation experiments. Here, splenocytes obtained from untreated, SpCas9-liposome or Ova-DexPhos-liposome treated mice were restimulated for 3 days with medium, SpCas9 (protein), Ova (protein & peptide) or ConA. Restimulation with ConA resulted in an average of 40% T cell proliferation, characterized by a lack of CFSE signal, in all splenocyte groups (Fig. 5), however, splenocytes restimulated with SpCas9 protein, Ova protein, or Ova peptide did not show changes in proliferation, suggesting a lack of CD4$^+$ T cell responses to both SpCas9 and Ova antigens.

5
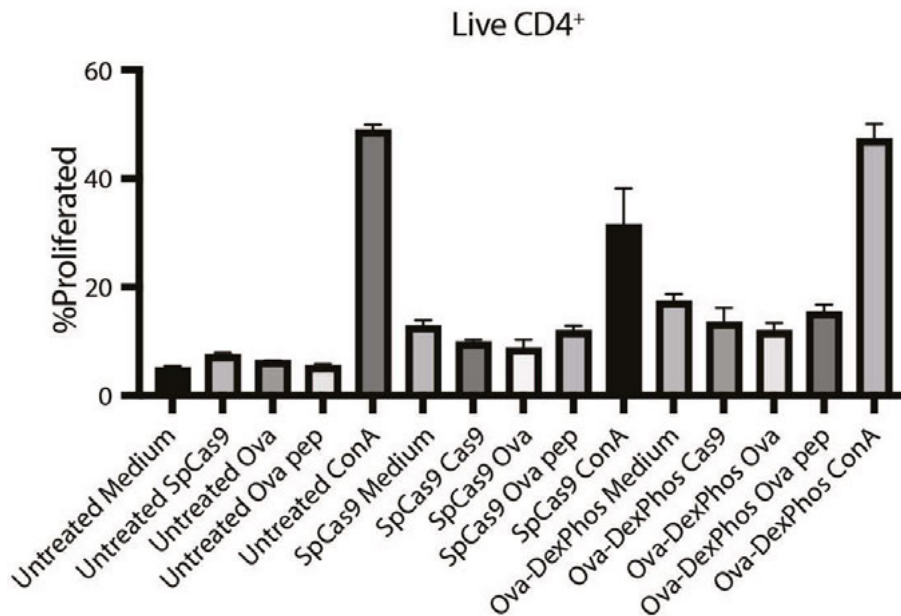
Figure S5: **Three-day restimulation of splenocytes with SpCas9 does not change CD4+ T cell proliferation.** Untreated, SpCas9-liposome-treated or Ova-DexPhos-liposome-treated splenocytes were each restimulated with medium, SpCas9, Ova (protein or peptide (indicated with pep) or ConA and incubated for 3 days as shown in the overview plot. Restimulation with proteins SpCas9 and Ova did not affect CD4+ T cell proliferation, assessed by a lack of CFSE signal, in untreated, SpCas9-liposome-treated or Ova-DexPhos-liposome-treated mice.

Discussion

Inducing immune tolerance at the site of SpCas9 release is essential to avoid elimination of CRISPR-Cas9-edited cells *in vivo*. Currently very little is known about SpCas9-encapsulating nanoparticles for the tolerization towards components of CRISPR-Cas9 gene therapy. Here we show that tolerogenic nanoparticles encapsulating both DexPhos and SpCas9 efficiently reduce a pro-inflammatory phenotype *in vitro* (Fig. 2) and are taken up in the spleen and liver *in vivo* (Fig. 3), organs generally associated with tolerance induction.

The liposomal formulations described in this study are stable in size,

monodispersity, and charge (Fig. 1D) and were even found to remain stable in the presence of human plasma (Supplementary Fig. 2). Using these liposomes in an *in vitro* culture of matured BMDCs, we observed reduction in the expression of costimulatory surface markers CD40 (Fig. 2A) and CD86 (Fig. 2B). Liposomes solely encapsulating SpCas9 did not reduce the expression levels of CD86 and CD40 on matured BMDCs, highlighting the maturation-inhibiting effect of Dex-Phos encapsulation (Fig. 2). Fluorescently labeling these liposomes with DiD shows that they are efficiently taken up by DC2.4 cells (Fig. 2C,D), indicating they might be good delivery vehicles for SpCas9 and DexPhos. Previous reports show that particles larger or equal to 200 nm (Fig. 1) are mainly taken up via phagocytosis by APCs, commonly mediated through targeting of scavenger receptors which are predominantly expressed by phagocytes.[19,27,28]

The observed *in vitro* efficacy of the liposomes lead us to study the liposomes *in vivo* for SpCas9 tolerization. However, our hypothesis was not met and SpCas9-specific tolerance could not be measured *in vivo*. Mice tolerized with DexPhos-SpCas9-loaded nanoparticles and then challenged with SpCas9-RNP LNPs only had slightly lower, but non-significant levels in SpCas9-specific IgG than the DexPhos-Ova- or SpCas9-liposome controls (Fig. 4). The high immunogenicity of the SpCas9 protein that we observed has been reported before, as 2 injections of 2 μg of SpCas9 resulted in a high amount of SpCas9-specific IgG (Supplementary Fig. 6D).[29] Furthermore, the described liposomes did not induce differences in conventional CD4$^+$ CD25$^+$ FoxP3$^+$ Tregs and CD4$^+$ CD49b$^+$ Lag3$^+$ Tr1s in the spleen, nor differences in levels of inflammatory and non-inflammatory cytokines between treatment groups (Fig. 4 C,D,E). Based on *in vitro* studies on DCs showing transformation to tolDCs after treatment with tolNPs (Fig. 2), we expected tolDCs to obtain a tolerogenic phenotype, characterized by reduced expression of CD40 and CD86 on their cell surface, and to secrete anti-inflammatory cytokines, enabling them to stimulate CD4$^+$ Tregs. Further analysis of antigen-specific immune responses by restimulating splenocytes with SpCas9 for 3 days revealed again no differences in

immune responses to SpCas9 between the groups (Fig. 5). A reason for this could be that the APCs in the spleen have only seen limited amounts of SpCas9, for example, due to a lack of liposome uptake or protein presentation, or that T cells in the spleen do not have sufficient T cell receptors (TCRs) to bring about a measurable response to Sp-Cas9. Despite the uptake of liposomes in DC2.4 cells *in vitro*, *in vivo* uptake by APCs might have been less efficient. Incorporating targeting ligands, such as DC-Sign, that allow liposomes to be specifically taken up by dendritic cells might be able to ensure DC uptake.[30] On the other hand, Zheng et al. reported a depletion of DCs and an increase in tolerogenic macrophages in a dose-dependent matter from 0 - 4.5 mg/kg of dexamethasone.[31] The dose of dexamethasone-phosphate used in this study lies within that range (2.6 mg/kg) which could indicate that a DC depletion has occurred in this model as well, however, further research is needed to confirm this hypothesis. Further studies on the release profile of DexPhos should be conducted as well. Though release was barely detected in liposomes over time *in vitro* (Fig. 1C), no conclusions can be drawn regarding the premature release of DexPhos *in vivo*.

It needs to be noted that one mouse died during IV injection of DexPhos-Cas9 liposomes. However, no specific conclusions could be drawn that that was related to formulation and most likely response to intravenous injections or shock.

Another strategy would be to explore transient immune suppression using glucocorticoids or rapamycin,[32,33] where patients are treated with the immunomodulator on the same day as SpCas9-LNP administration. The rationale behind using the co-encapsulation of DexPhos and SpCas9 in liposomes laid out in this manuscript is based on a multitude of factors. Firstly, the described approach would avoid dexamethasone-mediated systemic immune suppression, assuming dexamethasone does not leak from liposomes.[34] Secondly, incorporating dexamethasone in liposomes has been shown to increase its half-life.[35] SpCas9 has been determined to have a half-life of 24 hours in cells.[36] The increased half-life of liposomal

encapsulated dexamethasone would ensure immune suppression in liposome-targeted organs and cells during exposure to SpCas9. Inducing long-lasting antigen-specific tolerance towards SpCas9 would allow for the potential need of multiple injections of SpCas9-LNPs to sustain gene editing efficiency. The use of LNPs removes the added risk of immune activation observed when viral vectors, such as AAV vectors, are used[37], rendering them safe for repeated administration for cumulative gene editing. Pre-tolerization, mediated through liposomes co-encapsulating DexPhos and SpCas9, in patients selected for CRISPR-Cas9 gene therapy reduces the need for repeated dexamethasone treatments and thereby circumvents the unwanted side-effects observed with systemic dexamethasone treatment.[38]

Conclusively, we show that liposomes encapsulating DexPhos with or without co-delivery of the antigen SpCas9 can reduce the upregulation of the costimulatory molecules CD40 and CD86 on DCs and thereby convert them into tolDCs *in vitro*. *In vivo*, these liposomes are localized in the liver and spleen and if even at all only minorly decrease the amount of anti-SpCas9 antibodies formulated after challenging mice with SpCas9-RNP loaded lipid nanoparticles, whilst not affecting CD4$^+$ T cell responses. Despite the data indicating the need for further optimizations of the liposomes, this study nonetheless provides leads on a strategy to induce SpCas9-specific tolerance for better applicability of the gene editing tool for gene therapy, a currently unexplored frontier.

Acknowledgements

References

1.   Zhang, F., Wen, Y. & Guo, X. CRISPR/Cas9 for genome editing: Progress, implications and challenges. Hum. Mol. Genet. **23**, 40–46 (2014).

2.   Xue, C. & Greene, E. C. DNA Repair Pathway Choices in CRISPR-Cas9-Mediated Genome Editing. Trends Genet. **37**, 639–656 (2021).

3.   Gee, P. et al. Extracellular nanovesicles for packaging of CRISPR-Cas9 protein and sgRNA to induce therapeutic exon skipping. Nat. Commun. **11**, 1334 (2020).

4.   Wei, T., Cheng, Q., Min, Y. L., Olson, E. N. & Siegwart, D. J. Systemic nanoparticle delivery of CRISPR-Cas9 ribonucleoproteins for effective tissue specific genome editing. Nat. Commun. **11**, 1–12 (2020).

5.   Duan, L. et al. Nanoparticle Delivery of CRISPR/Cas9 for Genome Editing. Front. Genet. **12**, (2021).

6.   Charlesworth, C. T. et al. Identification of preexisting adaptive immunity to Cas9 proteins in humans. Nat. Med. **25**, 249–254 (2019).

7.   Simhadri, V. L. et al. Prevalence of Pre-existing Antibodies to CRISPR-Associated Nuclease Cas9 in the USA Population. Mol. Ther. - Methods Clin. Dev. **10**, 105–112 (2018).

8.   Wagner, D. L. et al. High prevalence of Streptococcus pyogenes Cas9-reactive T cells within the adult human population. Nat. Med. **25**, 242–248 (2019).

9.   Crudele, J. M. & Chamberlain, J. S. Cas9 immunity creates challenges for CRISPR gene editing therapies. Nat. Commun. **9**, 9–11 (2018).

10.   Wignakumar, T. & Fairchild, P. J. Evasion of Pre-Existing Immunity to Cas9: a Prerequisite for Successful Genome Editing In Vivo? Curr. Transplant. Reports **6**, 127–133 (2019).

11.   Audiger, C., Rahman, M. J., Yun, T. J., Tarbell, K. V. & Lesage, S. The Importance of Dendritic Cells in Maintaining Immune Tolerance. J. Immunol. **198**, 2223–2231 (2017).

12.   Banchereau, J. et al. Immunobiology of Dendritic Cells. Annu. Rev. Immunol. **18**, 767–811 (2000).

13.   Castenmiller, C., Keumatio-Doungtsop, B.-C., van Ree, R., de Jong, E. C. & van Kooyk, Y. Tolerogenic Immunotherapy: Targeting DC Surface Receptors to Induce Antigen-Specific Tolerance. Front. Immunol. **12**, (2021).

14. Cauwels, A. & Tavernier, J. Tolerizing Strategies for the Treatment of Autoimmune Diseases: From ex vivo to in vivo Strategies. Front. Immunol. **11**, (2020).

15. Hackstein, H., Thomson, A. W. & Starzl, T. E. Dendritic Cells: Emerging Pharmacological Targets of Immunosuppresive Drugs. 4, 24–34 (2004).

16. Iberg, C. A. & Hawiger, D. Natural and Induced Tolerogenic Dendritic Cells. J. Immunol. **204**, 733–744 (2020).

17. Sakaguchi, S., Yamaguchi, T., Nomura, T. & Ono, M. Regulatory T Cells and Immune Tolerance. Cell **133**, 775–787 (2008).

18. Keijzer, C., Van der Zee, R., Van Eden, W. & Broere, F. Treg inducing adjuvants for therapeutic vaccination against chronic inflammatory diseases. Front. Immunol. **4**, 1–10 (2013).

19. Dangkoub, F., Sankian, M., Tafaghodi, M., Jaafari, M. R. & Badiee, A. The impact of nanocarriers in the induction of antigen-specific immunotolerance in autoimmune diseases. J. Control. Release **339**, 274–283 (2021).

20. Li, H., Yang, Y. G. & Sun, T. Nanoparticle-Based Drug Delivery Systems for Induction of Tolerance and Treatment of Autoimmune Diseases. Front. Bioeng. Biotechnol. **10**, 1–14 (2022).

21. Kishimoto, T. K. et al. Improving the efficacy and safety of biologic drugs with tolerogenic nanoparticles. Nat. Nanotechnol. **11**, 890–899 (2016).

22. Kim, S. H. et al. Induction of antigen-specific immune tolerance using biodegradable nanoparticles containing antigen and dexamethasone. Int. J. Nanomedicine **14**, 5229–5242 (2019).

23. Pang, L., Macauley, M. S., Arlian, B. M., Nycholat, C. M. & Paulson, J. C. Encapsulating an Immunosuppressant Enhances Tolerance Induction by Siglec-Engaging Tolerogenic Liposomes. ChemBioChem **18**, 1226–1233 (2017).

24. Bozzuto, G. & Molinari, A. Liposomes as nanomedical devices. Int. J. Nanomedicine **10**, 975–999 (2015).

25. Walther, J. et al. Impact of Formulation Conditions on Lipid Nanoparticle Characteristics and Functional Delivery of CRISPR RNP for Gene Knock-Out and Correction. Pharmaceutics **14**, (2022).

26. Olson, F., Hunt, C. A., Szoka, F. C., Vail, W. J. & Papahadjopoulos, D. Preparation of liposomes of defined size distribution by extrusion through polycarbonate membranes. Biochim. Biophys. Acta - Biomembr. **557**, 9–23 (1979).

27. Kishimoto, T. K. & Maldonado, R. A. Nanoparticles for the induction of antigen-specific immunological tolerance. Front. Immunol. **9**, (2018).

28. Benne, N., ter Braake, D., Stoppelenburg, A. J. & Broere, F. Nanoparticles for Inducing Antigen-Specific T Cell Tolerance in Autoimmune Diseases. Front. Immunol. **13**, 1–15 (2022).

29. Toral, M. A. et al. Investigation of Cas9 antibodies in the human eye. Nat. Commun. **13**, 1–9 (2022).

30. Du, J., Zhang, Y. S., Hobson, D. & Hydbring, P. Nanoparticles for immune system targeting. Drug Discov. Today **22**, 1295–1301 (2017).

31. Zheng, G. et al. Dexamethasone promotes tolerance in vivo by enriching CD11c lo CD40 lo tolerogenic macrophages. 219–227 (2013).

32. Seregin, S. S. et al. Transient pretreatment with glucocorticoid ablates innate toxicity of systemically delivered adenoviral vectors without reducing efficacy. Mol. Ther. **17**, 685–696 (2009).

33. Xiang, Z. et al. The Effect of Rapamycin and Ibrutinib on Antibody Responses to Adeno-Associated Virus Vector-Mediated Gene Transfer. Hum. Gene Ther. **33**, 614–624 (2022).

34.   Giles, A. J. et al. Dexamethasone-induced immunosuppression: Mechanisms and implications for immunotherapy. J. Immunother. Cancer **6**, 1–13 (2018).
35.   Metselaar, J. et al. A phase I first-in-man study to investigate the pharmacokinetics and safety of liposomal dexamethasone in patients with progressive multiple myeloma. Drug Deliv. Transl. Res. **13**, 915–923 (2023).
36.   Tu, Z. et al. Promoting Cas9 degradation reduces mosaic mutations in non-human primate embryos. Sci. Rep. **7**, 1–11 (2017).
37.   Wilbie, D., Walther, J. & Mastrobattista, E. Delivery Aspects of CRISPR/Cas for in Vivo Genome Editing. Acc. Chem. Res. **52**, 1555–1564 (2019).
38.   Madamsetty, V. S. et al. Dexamethasone: Insights into Pharmacological Aspects, Therapeutic Mechanisms, and Delivery Systems. ACS Biomater. Sci. Eng. (2022).
39.   Gagnon, R. C. & Peterson, J. J. Estimation of confidence intervals for area under the curve from destructively obtained pharmacokinetic data. J. Pharmacokinet. Biopharm. **26**, 87–102 (1998).

Supplementary Material for Chapter 5

Encapsulation of DexPhos and SpCas9 in DPPC:DPPG:cholesterol liposomes
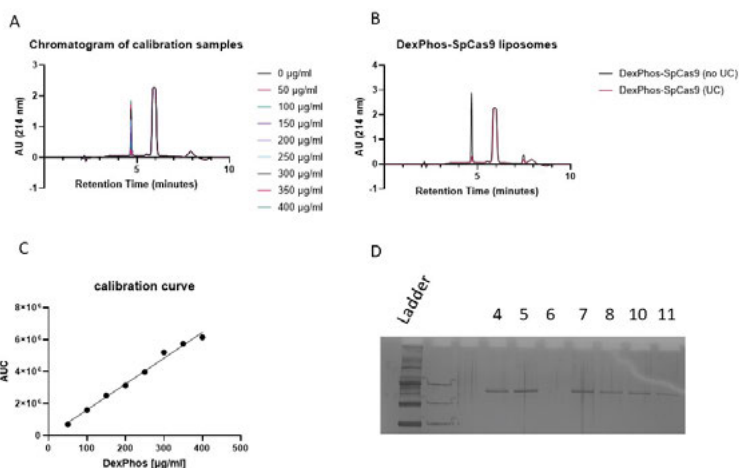
Figure S1: **Determination of encapsulation efficiency of DexPhos and SpCas9 in DPPC:DPPG:cholesterol liposomes. A)** Chromatogram (UV detector 214 nm) of the calibration samples (DexPhos resuspended at different concentrations in formulation buffer) run on Xbridge protein BEH C4 300Å column. **B)** Chromatogram of DexPhos-SpCas9 liposomes were free Dex-Phos and SpCas9 were removed by ultracentrifugation compared to the chromatogram of liposomes not centrifuged (=total amount of DexPhos). **C)** Calibration curve determined with EM-POWER software (linear fit equation: y=16142x+521.4). **D)** SDS-PAGE of SpCas9 and DexPhos-SpCas9 samples to determine encapsulation efficiency of SpCas9 via gel densitometry. Lane 4 – SpCas9, lane 5 – SpCas9 treated with 1% triton-X100, lane 6 – empty liposomes, lane 7 - DexPhos-SpCas9 liposomes (total amount), lane 8 – DexPhos-SpCas9 liposome ultracentrifuged to show encapsulated SpCas9, lane 9&10 – sterile-filtered DexPhos-SpCas9 liposomes non-centrifuged and ultracentrifuged, respectively. Encapsulation efficiency via gel densitometry was estimated to be 55%.

Stability of liposomes in the presence of 25% human plasma via asymmetric flow field flow fractionation

The stability of liposomes in the presence of human plasma was measured by asymmetric flow field flow fractionation (AF4) using

the AF2000 separation system (Postnova Analytics, Landsberg, Germany). The system is equipped with a degasser, isocratic pumps, auto samples, an in-line MALS detector, and an in-line DLS detector (Zeta Nano ZS, Malvern Instruments, Malvern, UK). A FFF channel with 350 μm spacer and regenerated cellulose membrane with molecular weight cut-off of 10 kDa was used for particle separation. The mobile phase was PBS. Liposomes were incubated with 25% human plasma at 37 °C and 300 rpm for 0, 3, 8, and 24 hours. Then, particles were diluted 20x in a HEPES buffer with the same concentration as the formulation (5 mM HEPES, 15 mM NaCl) and injected at a flow rate of 0.2 ml/min, and focused for 4 minutes with a cross-flow of 2 ml/min and a focused flow of 2.30 ml/min. Then, over 60 minutes the cross flow was decreased with an exponential decay of 0.03 and then kept consistent at 0 ml/min for another 40 minutes. There, the detector flow rate was set to 0.5 ml/min throughout the entire run.
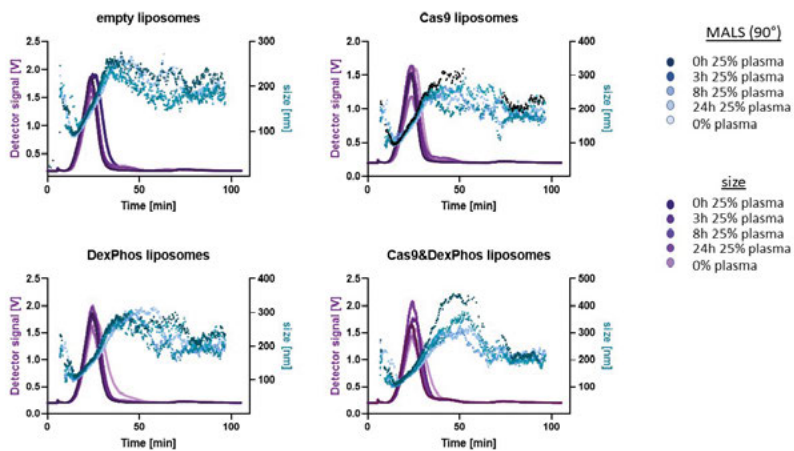
Figure S2: **Stability of liposomes in the presence of 25% human plasma via AF4.** Liposomes were incubated at 37 °C and 300 rpm for 0h, 3h, 8h, and 24h and then characterized via AF4 studies on size stability and light scattering at an angle of 90°. AF4 fractograms recorded by the MALS detector and DLS detector show the light scattering signal (purple) and particle size (blue) for empty (top left), SpCas9-loaded (top right), DexPhos-loaded (bottom left), and SpCas9-DexPhos-loaded (bottom right) liposomes.

Gating strategies for BMDCs
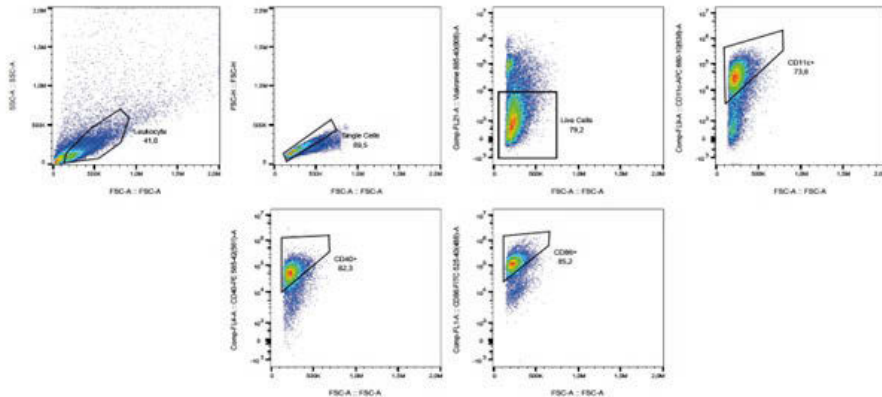
Figure S3: **Gating strategy BMDCs. Balb/c BMDCs were cultured in the presence of GM-CSF for 7 days.** LPS and free Dex, free DexPhos, free SpCas9, or liposomes were added and cells were incubated for another 16 hours. Cells were gated for leukocytes, single cells, and live cells. Subsequently, in the CD11c^{+} population, cells were analyzed for expression of CD40 and CD86.

Downregulation of MHC-II on BMDCs
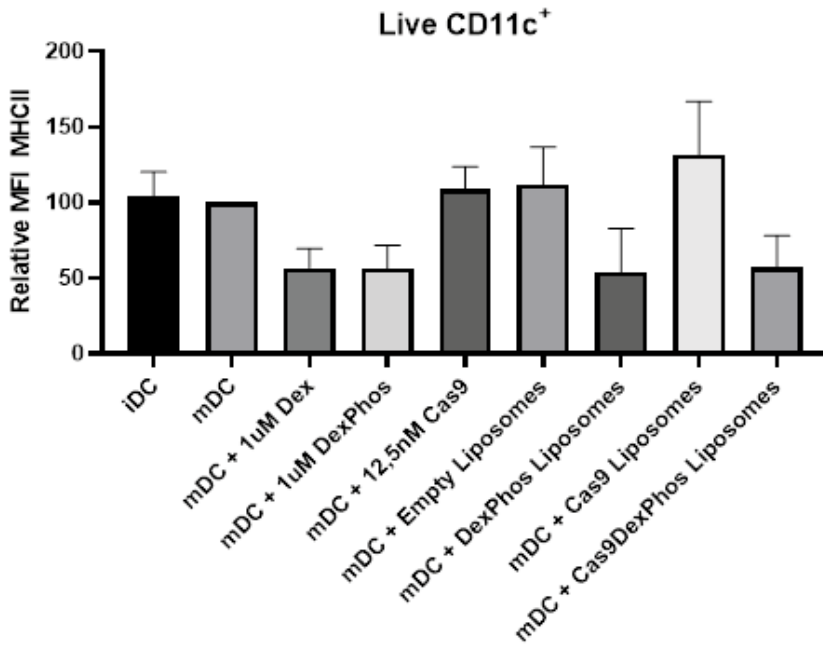
Figure S4: Expression of surface markers depicted in MFI of the antibody staining MHC-II. BMDCs were matured with 10 ng/ml LPS (derived from O111:B4 E.coli) and then treated with 1 μM free dexamethasone and DexPhos or with liposomes.

In vivo biodistribution of DID-labelled liposomes
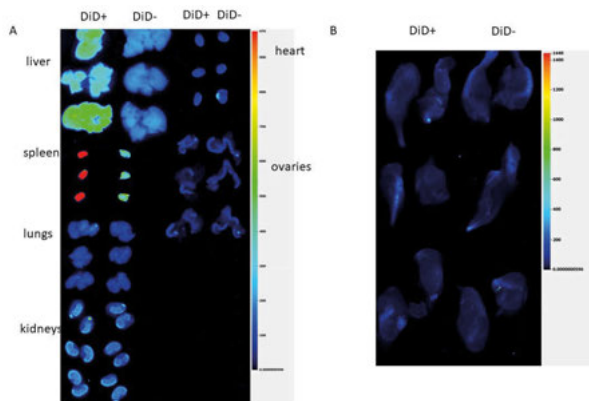
Figure S5: **Images of all organs studied in the biodistribution study of DiD-labelled liposomes *in vivo*. A)** Images of liver, spleen, lungs, kidneys, heart, and ovaries harvested from DiD-labelled liposome treated mice (DiD+) and control mice (DiD-). **B)** Bones of hindlegs of mice treated with DiD-labelled liposomes (DiD+) and control mice (DiD-).

Specificty of ELISAs and interpolation of AB concentration at different absorbance values
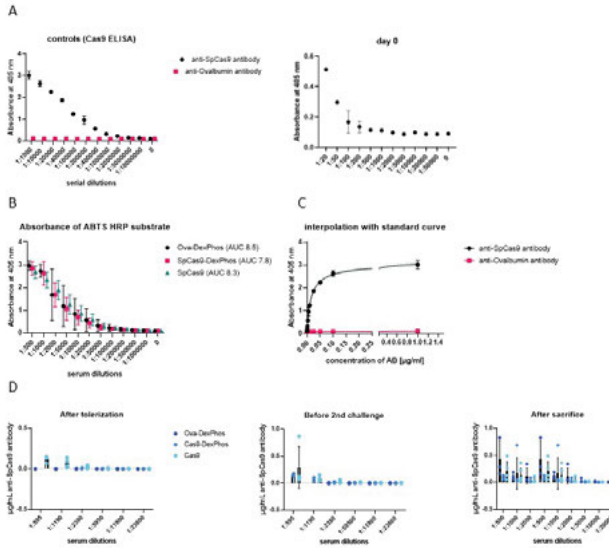
Figure S6: **Additional graphs from the ELISA study to determine antibody levels in mouse serum. A)** Absorbance levels of HRP ABTS substrate after primary treatment of well coated with SpCas9 with commercial anti-SpCas9 antibody and anti-Ova antibody as control of SpCas9 (left) and absorbance levels of HRP ABTS substrate. Collective serum sample of all mice before the start of *in vivo* study (right). **B)** Absorbance values of HRP substrate after treatment of SpCas9-coated ELISA plate with serial serum dilution of all mice serum (n=6, except for experimental group SpCas9-DexPhos n=5) for each experimental group. The area under the curve (AUC) was calculated based on the mean and SD at each dilution for each experimental group via GraphPad.[39] The resulting confidence intervals are: Ova-DexPhos – 8.5 ± 1.2; SpCas9-DexPhos – 7.8 ± 0.7; SpCas9 – 8.3 ± 0.6. **C)** Calibration curve of absorbance at 405 nm of HRP ABTS substrate in correlation to the antibody concentration of the commercial anti-SpCas9 antibody. **D)** Concentration of SpCas9-specific IgG for each experimental group after tolerization (left), before 2nd challenge (middle), and after the *in vivo* study (right). Not all absorbances could be interpolated into concentration of antibodies as they laid outside of the calibration curve.

6
Discussion and Perspectives

The discovery of CRISPR-Cas9 as a genome editing tool has sparked an impressive amount of research in utilizing the tool in agriculture, biotechnology, and medicine. Already 10 years after the discovery, first requests for approval by the FDA for using CRISPR-Cas9 *ex vivo* have been filed by Vertex and CRISPR Therapeutics for treatment of sickle cell disease and beta-thalassemia, respectively.[1] For direct *in vivo* application first clinical trials of the lipid nanoparticles carrying Cas9 mRNA together with a single guideRNA are showing highly promising results of successful gene knock-out.[2] These advances are truly awe-inspiring. The scope of this thesis was to contribute to the design of delivery vehicles that can carry CRISPR-Cas9 components, however with an additional DNA template to enable therapeutic gene correction. This thesis also investigated an approach to induce specific immune tolerance to avoid premature clearance via pre-existing immune response towards the bacterial Cas9 protein.

Summary of Key-Findings

In this thesis lipid nanoparticles (LNPs) were chosen as a delivery vehicle for CRISPR-Cas9 for eventual therapeutic gene correction *in vivo*. As reviewed in **chapter 2**, viral or non-viral vectors can serve as and are being investigated as delivery vehicles for CRISPR-Cas9. However, viral vectors are limited in packaging size, and additionally, pose the risk of vector-induced innate and adoptive immune responses.[3] Especially the latter would undermine repeated dosing for higher gene editing efficiencies. Therefore, LNPs are particularly promising vectors due to their versatility in entrapping different nucleic acid as well as protein-based cargo and high transfection efficiencies.[4] Hence, LNPs are possible delivery vehicles for the different formats in which CRISPR-Cas9 can be delivered but also for co-delivery of a DNA template for homology-directed repair (HDR). Furthermore, LNPs have been thoroughly investigated to passively target the liver due to the tissue exhibiting fenestrated capillary endothelia, but also form a protein corona made up of apolipoprotein

6

E which then actively targets the low density lipoprotein receptor on hepatocytes in the liver.[5] As the aim of the thesis was to design a therapy for a liver disease, we can take advantage of the passive and active targeting to the liver and set off to design LNPs that encapsulate the CRISPR-Cas9 components.

Originally, LNPs are based on the electrostatic interactions between an ionizable cationic lipid and a negative mRNA or siRNA molecule. Hence, complexation between lipids and cargo can occur in an acidic environment for protonation of the ionizable lipid. However, in the case of the direct delivery of the Cas9 ribonucleoprotein complex (RNP), the formulation parameters needed to be optimized as the acidic environment below pH 5.9 is irreversibly detrimental for RNP activity.[6,7] **Chapter 3** concluded that HEPES buffer pH 7.4 or nuclease-free water resulted in superior gene editing and that co-delivery of an HDR template was most efficient at 0.25 mole% DOTAP and a 2:1 molar ratio of HDR to RNP. The optimized LNP formulation co-delivering Cas9-RNP and HDR template was found to be stable in presence of human plasma and resulted in 20 % gene correction at 30 nM RNP in eGFP HEK293T reporter cells. Furthermore, in **chapter 3**, a protocol was described for the in-house production, purification, and storage of the endonuclease, which can be stored for at least one year at -80°C without loss of activity.

Since CRISPR-Cas9 can be delivered as mRNA or RNP complexes (**chapter 2**), a head-to-head comparison of these two modalities, when co-delivered with HDR template via LNPs, was described in **chapter 4**. The formulation parameters optimized for the LNPs (Cas9-RNP and HDR template) in **chapter 3** were maintained for both RNP and mRNA formulations described in this chapter. Hence, formulation occurred in nuclease-free water, with 0.25 mole% DOTAP and the same HDR and sgRNA concentrations. The ratio of mRNA added to the formulation was based on literature, 4:1 molar ratio mRNA to sgRNA.[8] Strikingly, **chapter 4** proved mRNA-Cas9 as the better cargo format for LNPs than Cas9-RNP, resulting in earlier onset of gene correction, but generally also higher gene editing efficiencies. LNPs

encapsulating mRNA Cas9 instead of Cas9-RNP were determined to be smaller in size and LNPs were shown to protect mRNA fully against degrading enzymes. Possibly these differences in formulation allow mRNA Cas9 loaded LNPs to be taken up more efficiently by cells or result in increased endosomal escape. Another explanation for earlier onset of editing may be that mRNA Cas9 results in higher concentration of Cas9 protein at a faster rate than when administered as Cas9-RNP. Administration of LNPs delivering mRNA Cas9 in Ai9 mice resulted in gene knock-out in 60 % of the hepatocytes as measured by the appearance of tdTomato fluorescence. Unexpected was the finding that the intravenous injections of LNPs loaded with Cas9-RNP resulted in death of all mice in that treatment group. The Cas9-RNP LNPs were found to aggregate at higher formulation concentrations. These formulation concentrations had not been studied in **chapter 3** and therefore aggregation was something that had not yet been observed. The concentrations used for formulation of LNPs for *in vivo* studies (70-fold high sgRNA amount than for *in vitro* studies) were based on literature.[6,8,9] Toxicity in mice was not mentioned in those reports. Ndeupen et al. showed in their study, however, that intradermal and intramuscular inoculation with LNPs induced inflammation and mortality dependent on dose of LNPs in mice.[10] It therefore raises the question what caused the mice to die. Was it the concentration of injected LNPs? However, the formulation of LNPs delivering mRNA Cas9 or Cas9-RNP were based on the same dose of sgRNA and lipids, respectively. Or was it caused by LNP aggregation (and what exactly caused nanoparticles to aggregate)? Then again, if aggregation was the cause we would have expected to see signs of difficult breathing in mice quite shortly after administration of Cas9-RNP LNPs, which was not observed. Perhaps the Cas9 protein itself induced sepsis, or mortality was caused by immunotoxicity due to traces of endotoxins. Until these aspects will have been addressed, LNPs delivering the Cas9-RNP are not ready for use *in vivo*.

Besides the optimization of LNPs as a delivery vehicle for the

CRISPR-Cas9 technology, **chapter 5** focuses on a way to avoid clearance of edited cells due to a pre-existing cellular immunity against the bacterial Cas9 protein. The pursued strategy is based on inducing Cas9-specific tolerance by introducing Cas9-specific regulatory T cells via liposomes entrapping an immunomodulator, dexamethasone phosphate, and Cas9 protein. These liposomes would be administered as a tolerization treatment prior to LNPs delivering CRISPR-Cas9 for gene editing. In **chapter 5**, the liposomes were shown to reduce a pro-inflammatory phenotype of bone marrow derived dendritic cells in *in vitro* assays. Subsequently, these dendritic cells would then stimulate regulatory T cells and inhibit effector T cells *in vivo*. However, in BALB/c mice tolerization and then challenge with Cas9 did not result in differences of regulatory T cells. If anything, mice tolerized with DexPhos-Cas9-loaded liposomes showed only a tendency to minimally reduce Cas9-specific antibodies in comparison to aspecific-antigen tolerized mice or mice administered with Cas9-loaded liposomes. Importantly, mice administered with the same LNPs loaded with Cas9-RNP as in chapter 4 did not harm the well-being of the mice in this study. Protein concentrations for injections were almost 100-fold lower than in the LNPs formulated for intravenous injections in mice described in **chapter 4**. However, it needs to be noted that the Cas-RNP LNPs in **chapter 5** were formulated with a commercial endotoxin-free SpCas9.

Improvements to the Delivery Vehicle

On account of research on LNPs as delivery vehicles mainly for nucleic acids, numerous technological advancements in the field are taking place. Newer generations of ionizable lipids are optimized to ensure cytocompatibility, prolonged circulation time, targeting of various tissues, or enhanced endosomal escape after cellular uptake. Unsaturated, multi-tail, polymeric, biodegradable, and branched-tail ionizable lipids provide a diverse catalogue of options.[11] For example,

Liu et al. formulated LNPs with a membrane-destabilizing ionizable multi-tail phospholipid that was shown to enhance endosomal escape.[8] Not only new ionizable lipids but also altering the construction of LNPs is being studied to improve LNPs. The research group led by Siegwart is working on dendrimer-based LNPs to encapsulate mRNA Cas9, sgRNA, and ssDNA as an HDR template for precise gene editing *in vivo*.[12] Pieter Cullis' lab investigates effects of nanoparticle structure or incorporation of sphingomyelin in LNPs to improve transfection potency or protein expression, respectively.[13,14] However, the discovery of anti-PEG antibodies introduces the risk of premature clearance, immune activation, altered biodistribution and limits repeated dosing.[15] The focus in this thesis was to deliver CRISPR-Cas9 to the liver, specifically to hepatocytes. However, in case of targeting other organs, modifications to the formulation with cationic or anionic lipids as studied by Cheng et al. could help steer to lungs and spleen, for example.[16] Moving forward with LNPs for delivery of CRISPR-Cas9 it would therefore be interesting to investigate alternative surface modifications other than PEG, continue to improve the formulation parameters, and screen various ionizable lipids to enhance gene editing outcomes.

High throughput screening of newer generations of ionizable lipids could not only help finding formulations for better gene editing outcomes, but hopefully higher efficiencies at lower dosages. LNPs have been determined to unfortunately lead to dose-limiting toxicities.[10,17] As mentioned above, the 100-fold higher dosage of Cas9-RNP loaded LNPs led to the deaths of mice in the *in vivo* study in Ai9 mice (**chapter 4**). A lower dosage of Cas9-RNP loaded LNPs, though also formulated with a commercial endotoxin-free SpCas9, did not seem to affect the well-being of mice in the tolerance study in BALB/c mice (**chapter 5**). While ONPATTRO are tolerated in non-tumor-bearing mice at a dose of 15 mg/kg, Jackson et al. showed that already at 5 mg/kg ONPATTRO triggered lethal toxicities in cancer mouse models.[17,18] These results raise the questions which factors of LNPs should additionally be optimized besides ionizable lipids to avoid unrealized or under-

6

studied toxicities in the future.[17]

A major bottleneck for the delivery of drug cargo is endosomal escape. Studies have shown that frequently often only 1 % of cargo is released from endosomes.[19] It would therefore certainly be of interest to learn more about the biology of endosomal escape to find targeted strategies to increase endosomal escape. Ongoing efforts to enhance endosomal escape include, for example, incorporation of small-molecule endolytics, such as chloroquine or use of endolytic peptides.[19,20] Jackson et al. discovered that platelet activating factor (PAF) from Kupffer cells play an essential role in toxicity of LNPs.[17] They reported a strategy to circumvent toxicities via pre-treatment of mice with ABT-491, an inhibitor of the PAF receptor. Additional investigations of key players at the cellular level, and which components of LNPs are involved in LNP-triggered toxicities, should be performed to improve the delivery vehicles for a safe and efficient application.

On another note, LNPs are commonly synthesized via microfluidic mixing as microfluid devices allow quick upscaling of reproducible nanoparticles.[21,22] For the eventual clinical application of the nanoparticles described in this thesis, LNPs were also prepared by microfluidic mixing and determined to be functional in delivery of CRISPR-Cas9 components in *in vitro* reporter cells (data not shown). However, as microfluidics requires a minimal volume and, hence, a minimal amount of components for complexation of particles, we opted to continue with pipette-mixing for the screening stage of the study.[23] Further investigations and optimizations of using microfluidics would help improve reproducibility and particle size (larger/smaller and uniformity), though, and possibly could have circumvented the negative outcome in the animal study reported in **chapter 4**. Therefore, formulation with microfluidics may be essential for translation to the clinic.

Translation from the Lab Bench to *In Vivo*

The work presented in this thesis showed that translation of outcomes observed in *in vitro* assays do not necessarily correlate with outcomes in vivo. Even though LNPs delivering the Cas9-RNP were found to be more cytotoxic in *in vitro* assays than LNPs delivering mRNA, surprisingly LNPs delivering Cas9-mRNA resulted in an increased release of pro-inflammatory cytokines (**chapter 4**). *In vivo*, however, injections of Cas9-RNP loaded LNPs unfortunately resulted in the death of mice, while LNPs delivering mRNA resulted in gene knock-out in 60% of the hepatocytes and mice showing no signs of any adverse effects. Furthermore, the liposomes described in **chapter 5** to induce specific tolerance against Cas9 were demonstrated to successfully induce a tolerogenic phenotype of dendritic cells in culture. It was hypothesized that induction of tolDCs via these liposomes would upregulate regulatory T cells and downregulate Cas9-specific antibodies in mice. Only with further investigations will we be able to understand the translation of a functional *in vitro* application to a dysfunctional approach *in vivo*.

Using animals for experiments is highly debated ethically, but also due to lack of knowledge of translation of *in vitro* to animal models and subsequent clinical trials in humans. Advancements in human tissue and their reconstruction *in vitro* are promising emerging alternatives for animal testing. For instance bioprinting, organ-on-chip bioengineering and organoids facilitate a wide range of options to test new drug molecules or therapeutic applications.[24–26] In this thesis, *in vitro* assays with reporter cells served as main proof of mechanism. These reporter cells are convenient for screening and optimization of particles, as shown in **chapter 3 and 4**, whereby **chapter 4** incorporates a direct comparison of two different reporter cell systems. eGFP Hepa 1-6 were purposefully generated to study whether LNPs function on different cell types, but especially to determine gene editing efficiencies in hepatocytes, even if hepatoma cells in culture. It was interesting to see the difference in gene editing efficiencies between two different cell types, HEK293T and hepatoma cells. However, 2D culturing can

6

only give us an insight in functionality. Examining the uptake and functionality of LNPs in 3D cultures such as organoids will help interpret the outcomes *in vivo*, though interactions within the bloodstream of a living organism are still missing in these models. Regardless, the studies with intestinal organoids in the **Supplement** were promising as administration of LNPs did not show signs of toxicity. However, efficiency of LNP-mediated CRISPR-Cas9 HDR strategy to correct a mutation in intestinal organoids remains an open question due to inconclusive droplet digital PCR (ddPCR) data. False positive occurrences may arise depending on the primers used for ddPCR, attributed to the prolonged presence of the ssDNA HDR template and then coamplified during ddPCR. Therefore, testing the LNPs as gene therapy for the autosomal recessive disorder Progressive Familial Intrahepatic Cholestasis type 1 could unfortunately not be thoroughly studied in this thesis.

These alternatives to animal studies still come with shortcomings and challenges ahead. For instance, responses of the immune system entail highly complex interactions between many different cell types, molecules and organs. **Chapter 5** demonstrated that the induction of tolerogenic dendritic cells *in vitro* with liposomes containing antigen, Cas9 protein, and the anti-inflammatory prodrug dexamethasone phosphate could not be reproduced *in vivo*. To understand why tolerance was not induced in mice, thorough investigations of the formulation characteristics *in vivo* and interactions between immunological key players will be required. Tolerogenic nanoparticles were studied to remain stable in size and polydispersity index (PDI) over a time span of one month and stable in the presence of 20% human serum. Release of DexPhos was minimal at both 4 °C and 37 °C in *in vitro* assays, however we cannot conclude that the formulation was leaky *in vivo* resulting in premature release of DexPhos. It would therefore be of interest to study release profiles of DexPhos and Cas9 protein *in vivo*. An alternative to animal studies could be the recent development of a microfluidic immune system on a chip to study the interactions

between immunological cells.[27–29] These microfluidic chips could be coated with dendritic cells, then introduced to liposomes entrapping Cas9 protein and dexamethasone phosphate in a flow of cell culture medium. Afterwards, immune cells such as B-cells and T-cells could be brought in, and Cas9-presentation on dendritic cells and interactions with B-cells and T-cells studied.[27] However, inside an organism, the immune system interacts with other organ systems to orchestrate the essential actions required for inducing processes such as tolerance. These complex interactions will remain a challenge to be reproduced in petri dishes.

In both animal studies presented in this thesis, the nanoparticles were found to distribute to the specific tissues and cells of interest. Tolerogenic nanoparticles were taken up by the liver and spleen (**chapter 5**). LNPs delivering mRNA Cas9 showed gene editing in hepatocytes after intravenous injection in mice (**chapter 4**). Next studies would ideally not only investigate gene knock-out, but also focus on specific gene correction of mutations or deletions via homology-directed repair, such as mutations in ATP8B1 resulting in PFIC type 1 in ATP8B1^{G308V} mice.

Steering DNA Repair towards Homology Repair

Homology directed repair (HDR) is the desired type of cellular repair mechanisms for correction of specific genetic disorder mutations. After Cas9-induced double strand breaks both non-homologous end joining (NHEJ) and HDR compete for and act upon the same cleaved DNA site. Eukaryotic cells, however, rather employ NHEJ over HDR. NHEJ is active throughout the cell cycle and is not restricted to the S/G2 phase, but additionally NHEJ represses HDR through various mechanisms.[30,31] Therefore, the frequency of HDR is significantly lower than NHEJ as shown in the studies on precise gene correction in this thesis (**chapter 3,4**). The efficiency of gene correction could be confirmed to not only be cell cycle dependent, but also differ between

cell types and reporter models. While the same LNPs resulted in roughly 20% gene correction in reporter HEK293T cells (**chapter 3,4**), only 0.7% correction was found in reporter hepatoma cells (**chapter 4**).

While the data in this thesis proves a promising functional co-delivery of HDR template via LNPs, **chapter 4** shows that HDR template was not completely retained by LNPs entrapping Cas9-RNP or Cas9 mRNA. The ssDNA templates studied in this thesis had a short base pair length of either 86 base pairs (**chapter 3,4**) and 125 base pairs (in the **Supplement**) in accordance with other lipid-based delivery vehicles for co-delivery of an HDR template.[12,32] Co-delivery of an HDR template via LNPs will most likely limit the length of an HDR template, thus limit the length of DNA repair sequences possible via this method, as probably the encapsulation efficiencies of the additional modality will decrease with size of the DNA template. In the case of knock-in of larger sequences or whole genes even, the HDR template would need to be co-delivered via a different delivery vehicle. Lee et al. showed successful gene knock-in mediated through co-administration of LNPs entrapping Cas9 mRNA and sgRNA together with AAVs directly delivering an HDR template to the nucleus.[33] However, co-administration of the HDR template via AAV vectors would not allow for repeated injections for cumulative gene editing to increase HDR.[34]

Tipping the mode of action towards homology repair instead of NHEJ will be essential for clinical applications. In-depth research on understanding the cell's choice of repair mechanism has led to numerous approaches to increase the frequency of HDR. For instance, HDR can be promoted by either suppressing the key factors inducing NHEJ, using HDR agonists, or synchronization of cells to HDR-permissive cell cycle phase while editing with Cas9.[31,35] Favoring HDR could also be done by modulating various pathways, such as cell cycle progression.[36,37] A study by Tsuji et al. showed enhancement of HDR by inhibiting ribonucleotide reductase via co-administration of fludarabine with AAV-mediated delivery of

CRISPR-Cas9 together with an HDR template in mice.36 A recent screen by my colleague Danny Wilbie showed that alisertib, an Aurora Kinase 1 inhibitor, led to HDR becoming the dominant repair pathway in HEK293T cells and enhanced the pathway more than four-fold in Hepa 1-6 cells (to be published). Initial studies combining the LNPs described in this thesis together with alisertib showed enhancement of HDR in HEK293T cells. It would be interesting to continue studying these effects, also with other methods to enhance HDR. However, suppression of NHEJ or synchronization of cells may also come with safety issues, as NHEJ is nonetheless critical for genome stability and suppression thereof may lead to toxicity.31 Furthermore, majority of the research to enhance HDR occurs in in vitro assays and therefore translation to *in vivo* still needs to be thoroughly investigated.

Another approach to favor HDR is based on modifications of the CRISPR-Cas components directly. For instance, researchers are focusing on ensuring availability of donor templates at the time of Cas9-induced DNA cleavage. Ligating a ssDNA template to the sgRNA via streptavidin-biotin interactions or generation of RNP-ssDNA complexes have been shown to increase HDR by 18-fold and 24-fold, respectively, in comparison to unlinked components.[38,39] Moreover, modifications to the Cas protein itself to solely introduce nicks, single-strand breaks, result in higher HDR.[40–43] Nicked DNA has been studied to be an incompatible template for NHEJ, hence invoking repair based on homologous recombination.[44] Chen et al. reported on in trans paired nicking of genomic DNA via Cas9 nickases and additionally on template DNA for HDR, resulting in HDR of large genetic payloads at higher rates than compared to double strand breaks via CRISPR-Cas9.[42] Tran et al. also utilize the Cas9 nickase, where they created two nicks using two guideRNAs to target specific sequences on opposite strands.[43] They carefully designed the guideRNA to generate nicks at an optimal distance to maintain effective HDR while minimizing NHEJ events. Modifications of the Cas9 protein has additionally ignited the engineering of newer CRISPR-based genome editing tools for more on-target specificity and

favoring specific gene correction.

The Emerging "Next Best Thing"

The landmark discovery and great potential of the RNA-dependent endonuclease has already sparked the creation of next generation gene editing tools in the last few years. Protein engineering has allowed to modify the Cas9 protein for more on-target specificity or favor homology-directed repair as reviewed by Huang et al.[45] David Liu's lab engineered the CRISPR base editor and prime editor. In short, CRISPR base editor can convert nucleotides to other nucleotides, , e.g. CG to TA, via point mutations by being a catalytically impaired Cas nuclease fused to a deaminase yet once again navigated to a DNA target via a guideRNA.[46] Prime editors on the other hand have been developed to allow precise modifications at the single-nucleotide level, insertions, deletions and combinations thereof with minimized INDEL byproducts, mediated through Cas9 nickase domain fused to a reverse transcriptase, this time navigated by a guideRNA that additionally acts as a template DNA, called the primer editing guide RNA (pegRNA).[47] Meanwhile, prime editors are being investigated as a twin prime editor (twinPE) strategy within the David Liu's lab to expand the size of edited insertions.[48] The idea behind twinPE is to use two primer editors however targeting different genomic targets via two different pegRNA. The two pegRNA generate 3' flap that are complementary to each other and would then anneal generating a replacement of the original DNA with an edited DNA sequence.[48] Another recent addition to gene editing tools, PASTE (Programmable Addition via Site-Specific Targeting Elements), uses a Cas nickase fused to both reverse transcriptase and serine integrase to "drag-and-drop" DNA insertions without double strand breaks.[49] Alongside base editor, primer editor and PASTE, Integra Therapeutics and Tessera Therapeutics designed gene writers to create specific gene insertions via mobile genetic elements, such as piggyBac transposase, for kilobase-scale double strand break-free and HDR-independent

editing technologies.[50–52] These developments show the momentum with which the field of gene therapy is expanding and improving, but also raise the question whether CRISPR-Cas9 and subsequent and (inefficient) HDR are already outdated.

The emerging technologies face challenges as well, however. The main challenge will again be in design of delivery vehicles to expand from *ex vivo* applications to *in vivo*.[46,53,54] These newer gene editing molecular components are even larger than CRISPR-Cas9, which could result in larger nanoparticles and thereby more challenges in delivery, circulation, and tissue and cellular uptake. Additionally, studies investigating the risk of off-target events need to be performed and ethical concerns need to be addressed.

Are we Tinkering Too Much with Nature?

Critical voices argue that gene therapy, such as mediated through CRISPR-Cas9, may excessively tinker with nature. The concerns revolve around the risks associated with making permanent alterations to our DNA, which serves as the blueprint of our bodies. It is crucial for scientists in this field to be mindful of these concerns throughout their research. For instance, any editing of germline are and should remain strictly forbidden.[55,56] This ensures that any modifications via CRISPR-Cas9 affect only the individual undergoing treatment and are not hereditary. In fact, a recent study presented by Dr. Kubikova (University of Oxford) at 39th annual meeting of the European Society of Human Reproduction and Embryology warns that the CRISPR-Cas9 technology has to be avoided for use on human embryos. Her research discovered that human embryos are unable to repair damage to their DNA mediated through CRISPR-Cas9.[57] The presence of unrepaired DNA strands ultimately results in the formation of significant chromosome abnormalities, greatly impacting the viability of embryos. In the event of embryo transfer to the uterus, these abnormalities can pose a significant risk of severe congenital

abnormalities in the resulting babies.   Taking this severe risk is moreover not needed, when embryo selection would already offer a safe and functional strategy to determine the qualities of fertilized embryos and selection for transfer or cryopreservation.[58]

Concerns are not only about the directed repair mediated by CRISPR-Cas9, but also about unintended wrongful target genomic alterations (inversions, translocations, etc.) and the risk of off-target events.   The ongoing efforts to favor HDR and the newer gene editing tools should help to achieve target-directed repairs.   To really understand what the risks of these genomic alterations can be, long-term clinical studies will be required. To put the possible alterations and off-target events into perspective, spontaneous double strand breaks and subsequent repair occur at a frequency of 50 per cell per cell cycle.[59] The degree of specificity of CRIPSR-Cas9 seems to mainly arise from the sgRNAs.[60,61] With advancements in computational predictions, but also assays for *in vitro* screening and whole genome sequencing, design of sgRNA has been greatly improved to be highly specific instead of promiscuous.[60,62] Ideally, these methods on screening and optimizing on-target specificity of sgRNA leads to trustworthy sgRNA that do not need to be tested on off-targets eventually, as that would make CRISPR-Cas9 a highly expensive tool.   Nonetheless, differences in number of off-targets has additionally been associated to the endonuclease-of-choice, Cas9 derived from *S.aureus* that seems to induce less off-targets than the Cas9 derived from *S.pyogenes*.[63] Ongoing efforts are engineering the endonucleases to be more target-specific.[64] In a slight different manner, Dilliard and Siegwart show that co-delivery of oligonucleotides alongside CRISPR-Cas9 components can reduce off-target editing in the liver.[65]

A genome editing tool such as CRISPR-Cas9 also raises the questions of designer babies and when and what limitations need to be set. Personally, I believe, the consensus should be to only utilize the tool for therapies of diseases, as for example PFIC type 1. Additionally, I believe that the question of designing human phenotypes at will also

needs to be tied closely with ethical, philosophical, and sociological debates. Also, we have to accept differences and ensure equality a the same time. In The Netherlands, leading on societal debates is the Rathenau Institute. Through organized public dialogues the Rathenau Institute discusses use of gene editing by raising socio-economic questions and future scenarios on germline editing and the reproductive industry.[66] Addressing these moral debates and public concerns needs to remain strictly connected to research on CRISPR-Cas9. If the application of gene editing tools are found to pose substantial risks, scientists should diligently report their findings and reassess the usage of CRISPR-Cas9 in gene therapy. By carefully navigating ethical considerations, researchers and public dialogues can foster a safer and more responsible approach to the development and implementation of CRISPR-Cas9 gene editing techniques.

LNPs in Times of COVID-19 Pandemic

The work presented in this thesis was conducted during the global COVID-19 pandemic. A peculiar time of social distancing, lockdowns and quarantines, but also a unique time for research on and implementation of LNPs. By the time of the pandemic, research on incorporating mRNA in LNPs was already quite advanced, as mRNA-loaded LNPs started being investigated for cancer vaccines as means of antitumor immunotherapy. mRNA vaccines are greatly reviewed by Deng et al in Frontiers in Immunology with a list of ongoing clinical trials with mRNA vaccines.[67] BNT111 from the BioNTech FixVac platform has entered phase II of clinical trials after showing tolerability and immunity against the vaccine antigens in phase I in patients with advanced melanoma.[68] The research on mRNA vaccines and clinical studies allowed an enormously fast adaptation for a vaccine for COVID-19 and approval by the U.S. American Food and Drug Administration (FDA) and the European Medicines Agency (EMA). Notwithstanding the official approval, there was skepticism in the general public towards the vaccines,

caused both fear over the mechanisms of the vaccines or suspicion about the necessity of using them in the first place.   While the nanoparticles have been studied and the mRNA COVID-19 vaccines were approved for general use, still, anyone injected with a vaccine for COVID-19 is part of an unparalleled, global clinical trial.   These first commercialized LNPs together with the very first approved LNP patisiran (brand name ONPATTRO™, Alnylam), will prove to be greatly beneficial for the ongoing research by learning more about the mechanisms and the possible side-effects.[5]

Conclusion

In conclusion, the work described in this thesis demonstrated the design of LNPs that can deliver CRISPR-Cas9 components with or without an HDR-template intracellularly *in vitro* and *in vivo*.   The thesis highlights the necessity to optimize formulation parameters for the cargo-of-interest.   Against our hypothesis, the thesis concluded that, for now, mRNA Cas9 is the better cargo format in comparison to the direct delivery of Cas-RNP when delivered with LNPs.   Additionally, first attempts to protect the CRISPR-Cas9 components and edited cells from an immune response were described, to our knowledge a field not yet otherwise investigated. Meanwhile, advances on gene editing tools remained a fast-developing field. Therefore, the next steps in this field of research should include the design of delivery vehicles for the newer gene editing tools, and, hopefully, the work described in this thesis contributed towards their successful development.   Nonetheless, the investigations on favoring HDR after CRISPR-Cas9-induced-double-strand breaks hold great promises that should be continued and combined with LNPs for co-administration *in vivo*. By developing a range of editing approaches, researchers can generate a gene editing tool box to choose from, depending on the editing task in question. It remains an open question, why an induction of tolerance via tolerogenic nanoparticles was not successful. Future studies will hopefully shed light on the reasons and then result in a functioning approach.

Despite the challenges, incorporating CRISPR-Cas9 in LNPs as a gene editing tool holds a great potential and, while simultaneously keeping ethical concerns in mind, may lead to major breakthroughs in the therapy of genetic diseases.

References

1. Kingwell, K. First CRISPR therapy seeks landmark approval. Nat. Rev. Drug Discov. **22**, 339–341 (2023).
2. Gillmore, J. D. et al. CRISPR-Cas9 In Vivo Gene Editing for Transthyretin Amyloidosis. N. Engl. J. Med. **385**, 493–502 (2021).
3. Asmamaw Mengstie, M. Viral Vectors for the in Vivo Delivery of CRISPR Components: Advances and Challenges. Front. Bioeng. Biotechnol. **10**, 1–6 (2022).
4. Hald Albertsen, C. et al. The role of lipid components in lipid nanoparticles for vaccines and gene therapy. Adv. Drug Deliv. Rev. **188**, 114416 (2022).
5. Akinc, A. et al. The Onpattro story and the clinical translation of nanomedicines containing nucleic acid-based drugs. Nat. Nanotechnol. **14**, 1084–1087 (2019).
6. Wei, T., Cheng, Q., Min, Y. L., Olson, E. N. & Siegwart, D. J. Systemic nanoparticle delivery of CRISPR-Cas9 ribonucleoproteins for effective tissue specific genome editing. Nat. Commun. **11**, 1–12 (2020).
7. Wang, S. R. et al. Conditional control of RNA-guided nucleic acid cleavage and gene editing. Nat. Commun. **11**, (2020).
8. Liu, S. et al. Membrane-destabilizing ionizable phospholipids for organ-selective mRNA delivery and CRISPR–Cas gene editing. Nat. Mater. **20**, (2021).
9. Noureddine, A. et al. Engineering of monosized lipid-coated mesoporous silica nanoparticles for CRISPR delivery. Acta Biomater. **114**, 358–368 (2020).
10. Ndeupen, S. et al. The mRNA-LNP platform's lipid nanoparticle component used in preclinical vaccine studies is highly inflammatory. iScience **24**, (2021).
11. Han, X. et al. An ionizable lipid toolbox for RNA delivery. Nat. Commun. 8–13 (2021).
12. Farbiak, L. et al. All-In-One Dendrimer-Based Lipid Nanoparticles Enable Precise HDR-Mediated Gene Editing In Vivo. Adv. Mater. **33**, 1–8 (2021).
13. Cheng, M. H. Y. et al. Induction of Bleb Structures in Lipid Nanoparticle Formulations of mRNA Leads to Improved Transfection Potency. Adv. Mater. **2303370**, e2303370 (2023).
14. Chi, Y., Yang, P., Ren, S. & Yang, J. Jo ur na l P re of. Sci. Total Environ. **138954** (2020).
15. Estapé Senti, M. et al. Anti-PEG antibodies compromise the integrity of PEGylated lipid-based nanoparticles via complement. J. Control. Release **341**, 475–486 (2022).

6

16. Cheng, Q. et al. Selective organ targeting (SORT) nanoparticles for tissue-specific mRNA delivery and CRISPR–Cas gene editing. Nat. Nanotechnol. **15**, 313–320 (2020).

17. Jackson, M. A. et al. Kupffer cell release of platelet activating factor drives dose limiting toxicities of nucleic acid nanocarriers. Biomaterials **268**, 120528 (2021).

18. FDA. CENTER FOR DRUG EVALUATION AND MULTI-DISCIPLINE REVIEW Summary Review Office Director Clinical Statistical Clinical Pharmacology. Acalabrutinib NDA (2016).

19. Dowdy, S. F., Setten, R. L., Cui, X. S. & Jadhav, S. G. Delivery of RNA Therapeutics: The Great Endosomal Escape! Nucleic Acid Ther. **32**, 361–368 (2022).

20. Pei, D. & Buyanova, M. Overcoming Endosomal Entrapment in Drug Delivery. Bioconjug. Chem. **30**, 273–283 (2019).

21. Leung, A. K. K., Tam, Y. Y. C., Chen, S., Hafez, I. M. & Cullis, P. R. Microfluidic Mixing: A General Method for Encapsulating Macromolecules in Lipid Nanoparticle Systems. J. Phys. Chem. B **119**, 8698–8706 (2015).

22. Tomeh, M. A. & Zhao, X. Recent Advances in Microfluidics for the Preparation of Drug and Gene Delivery Systems. Mol. Pharm. (2020).

23. Cheng, Q. et al. Selective organ targeting (SORT) nanoparticles for tissue-specific mRNA delivery and CRISPR–Cas gene editing. Nat. Nanotechnol. **15**, 313–320 (2020).

24. Daly, A. C., Prendergast, M. E., Hughes, A. J. & Burdick, J. A. Bioprinting for the Biologist. Cell **184**, 18–32 (2021).

25. Azizipour, N., Avazpour, R., Rosenzweig, D. H., Sawan, M. & Ajji, A. Evolution of biochip technology: A review from lab-on-a-chip to organ-on-a-chip. Micromachines **11**, 1–15 (2020).

26. Hofer, M. & Lutolf, M. P. Engineering organoids. Nat. Rev. Mater. **6**, 402–420 (2021).

27. Goyal, G. et al. Ectopic Lymphoid Follicle Formation and Human Seasonal Influenza Vaccination Responses Recapitulated in an Organ-on-a-Chip. Adv. Sci. **2103241**, 1–15 (2022).

28. Sasserath, T. et al. Differential Monocyte Actuation in a Three-Organ Functional Innate Immune System-on-a-Chip. Adv. Sci. **2000323**, 1–19 (2020).

29. Koyilot, M. C. et al. Breakthroughs and Applications of Organ-on-a-Chip Technology. (2022).

30. Mao, Z., Bozzella, M., Seluanov, A. & Gorbunova, V. DNA repair by non-homologous end joining and homologous recombination during cell cycle in human cells. Cell Cycle **7**, 2902–2906 (2008).

31. Yang, H. et al. Methods favoring homology-directed repair choice in response to crispr/cas9 induced-double strand breaks. Int. J. Mol. Sci. **21**, 1–20 (2020).

32. Suzuki, Y. et al. Lipid nanoparticles loaded with ribonucleoprotein–oligonucleotide complexes synthesized using a microfluidic device exhibit robust genome editing and hepatitis B virus inhibition. J. Control. Release **330**, 61–71 (2021).

33. Lee, J. H. et al. In vivo genome editing for hemophilia B therapy by the combination of rebalancing and therapeutic gene knockin using a viral and non-viral vector. Mol. Ther. - Nucleic Acids **32**, 161–172 (2023).

34. Wilbie, D., Walther, J. & Mastrobattista, E. Delivery Aspects of CRISPR/Cas for in Vivo Genome Editing. Acc. Chem. Res. **52**, 1555–1564 (2019).

35. Shams, F. et al. Advance trends in targeting homology-directed repair for accurate gene editing: An inclusive review of small molecules and modified CRISPR-Cas9 systems. BioImpacts **12**, 371–391 (2022).

36. Tsuji, S. et al. Fludarabine increases nuclease-free AAV- and CRISPR/Cas9-mediated homologous recombination in mice. Nat. Biotechnol. **40**, 1285–1294 (2022).

37. Maurissen, T. L. & Woltjen, K. Synergistic gene editing in human iPS cells via cell cycle and DNA repair modulation. Nat. Commun. **11**, (2020).

38. Carlson-Stevermer, J. et al. Assembly of CRISPR ribonucleoproteins with bi-otinylated oligonucleotides via an RNA aptamer for precise gene editing. Nat. Commun. **8**, (2017).

39. Savic, N. et al. Covalent linkage of the DNA repair template to the CRISPR-Cas9 nuclease enhances homology-directed repair. Elife **7**, 1–18 (2018).

40. Roy, S. et al. Cas9/Nickase-induced allelic conversion by homologous chromosome-templated repair in Drosophila somatic cells. Sci. Adv. **8**, (2022).

41. Rees, H. A., Yeh, W. H. & Liu, D. R. Development of hRad51–Cas9 nickase fusions that mediate HDR without double-stranded breaks. Nat. Commun. **10**, (2019).

42. Chen, X. et al. In trans paired nicking triggers seamless genome editing without double-stranded DNA cutting. Nat. Commun. **8**, (2017).

43. Tran, N. T. et al. Precise CRISPR-Cas–mediated gene repair with minimal off-target and unintended on-target mutations in human hematopoietic stem cells. Sci. Adv. **8**, (2022).

44. Davis, L. & Maizels, N. DNA nicks promote efficient and safe targeted gene correction. PLoS One **6**, 1–7 (2011).

45. Huang, X., Yang, D., Zhang, J., Xu, J. & Chen, Y. E. Recent Advances in Improving Gene-Editing Specificity through CRISPR–Cas9 Nuclease Engineering. Cells **11**, (2022).

46. Rees, H. A. & Liu, D. R. Base editing: precision chemistry on the genome and transcriptome of living cells. Nat. Rev. Genet. **19**, 770–788 (2018).

47. Anzalone, A. V. et al. Search-and-replace genome editing without double-strand breaks or donor DNA. Nature **576**, 149–157 (2019).

48. Anzalone, A. V. et al. Programmable deletion, replacement, integration and inversion of large DNA sequences with twin prime editing. Nat. Biotechnol. **40**, 731–740 (2022).

49. Yarnall, M. T. N. et al. Drag-and-drop genome insertion of large sequences without double-strand DNA cleavage using CRISPR-directed integrases. Nat. Biotechnol. **41**, (2022).

50. Pallarès-Masmitjà, M. et al. Find and cut-and-transfer (FiCAT) mammalian genome engineering. Nat. Commun. **12**, 1–9 (2021).

51. Tou, C. J. & Kleinstiver, B. P. Recent Advances in Double-Strand Break-Free Kilobase-Scale Genome Editing Technologies. Biochemistry (2022).

52. Robitzski, D. Can 'Gene Writing' Deliver What Gene Editing Can't? — TS Digest — The Scientist. (2022).

6

53.   Chen, P. J. & Liu, D. R. Prime editing for precise and highly versatile genome manipulation. Nat. Rev. Genet. **24**, 161–177 (2023).

54.   Raguram, A., Banskota, S. & Liu, D. R. Therapeutic in vivo delivery of gene editing agents. Cell **185**, 2806–2827 (2022).

55.   Baltimore, D. et al. A prudent path forward for genomic engineering and germline gene modification. Science **348**, 36–38 (2015).

56.   On, R. European Group on Ethics in Science and New Technologies (EGE) Statement on Gene Editing. Jahrb. für Wiss. und Ethik **21**, (2017).

57.   Cooke, E. CRISPR gene editing on human embroys may have dangerous consequences, says new study. (2023).

58.   Kumar, A. et al. Whole-genome risk prediction of common diseases in human preimplantation embryos. Nat. Med. **28**, 513–516 (2022).

59.   Vilenchik, M. M. & Knudson, A. G. Endogenous DNA double-strand breaks: Production, fidelity of repair, and induction of cancer. Proc. Natl. Acad. Sci. U. S. A. **100**, 12871–12876 (2003).

60.   Geen, H. O., Yu, A. S. & Segal, D. J. ScienceDirect How specific is CRISPR / Cas9 really? Curr. Opin. Chem. Biol. **29**, 72–78 (2015).

61.   Li, L. H. Y. & Wang, Y. Controlling CRISPR-Cas9 by guide RNA engineering. Wiley Interdiscip. Rev. RNA 1–16 (2023).

62.   Liu, X. S. et al. Sequence determinants of improved CRISPR sgRNA design. Genome Res. **25**, 1147–1157 (2015).

63.   Kriz, A. J., Zetsche, B., Shalem, O., Wu, X. & Kira, S. In vivo genome editing using Staphylococcus aureus Cas9. Nature **520**, 186–191 (2015).

64.   Slaymaker, I. M. et al. Rationally engineered Cas9 nucleases with improved specificity. Science **351**, 84–89 (2016).

65.   Dilliard, S. A. & Siegwart, D. J. Disrupting off-target Cas9 activity in the liver. Nat. Biomed. Eng. **6**, 106–107 (2022).

66.   Van Baalen, S., Gouman, J. & Verhoef, P. Discussing the modification of heritable DNA in embryos. (2019).

67.   Deng, Z., Tian, Y., Song, J., An, G. & Yang, P. mRNA Vaccines: The Dawn of a New Era of Cancer Immunotherapy. Front. Immunol. **13**, (2022).

68.   Sahin, U. et al. An RNA vaccine drives immunity in checkpoint-inhibitor-treated melanoma. Nature **585**, 107–112 (2020).

Appendices

Supplement
Technical Challenges when Determining Single-Base Gene Correction in Organoids: Lessons Learned

Johanna Walther[1], Lysbeth ten Bloemendaal[2], Yue Chen[2], Danny Wilbie[1], Piter J. Bosma[2], Enrico Mastrobattista[1]

[1]Department of Pharmaceutics, Utrecht Institute for Pharmaceutical Sciences (UIPS), Utrecht University, The Netherlands

[2]Tytgat Institute for Liver and Intestinal research, Amsterdam Gastroenterology and Metabolism, Amsterdam University Medical Center, University of Amsterdam, Amsterdam, The Netherlands

Abstract

CRISPR-Cas9 is a promising tool for therapeutic application of monogenic diseases, such as the rare infantile hereditary disease Progressive Familial Intrahepatic Cholestasis Type 1 (PFIC1). CRISPR-Cas9 introduces a double strand break at a specific DNA site homologous to the sgRNA of the Cas9-ribonucleoprotein complex. In the presence of a DNA template, subsequent cellular repair mechanism homology-directed repair (HDR) can result in specific gene correction. This therefore could be an approach to correct mutations or small deletions of the ATP8B1 gene, encoding a flippase for phospholipids, causing PFIC1. However, to be able to utilize the Cas9-RNP together with a DNA template for HDR the components require a sophisticated delivery vehicle. Therefore, we investigate the delivery of Cas9, either as mRNA or protein together with sgRNA and single strand DNA template via lipid nanoparticles in ATP8B1$^{G308V/G308V}$ murine intestinal organoids as a disease model. Unfortunately, it seems that the HDR template remained present in organoids even after three weeks of culturing and was faultily detected via ddPCR resulting in false-positive gene correction efficiencies.

Introduction

Gene therapy mediated through CRISPR-Cas9 could potentially be a therapeutic application for Progressive Familial Intrahepatic Cholestasis (PFIC). PFIC results in impaired bile flow with concomitant toxic accumulation of bile acids in the liver and eventually liver failure.[1] Individuals diagnosed with either of the three types of PFIC (PFIC1, PFIC2, and PFIC3) experience severe itching, jaundice, failure to gain weight and grow at the expected rate, and enlarged liver and spleen. Clinical symptoms of PFIC1 expand to extrahepatic symptoms such as deafness, diarrhea, inflammation of the pancreas, low levels of fat-soluble vitamins (vitamins A, D, E, and K).[2] Hepatic and extrahepatic symptoms are due to the faulty expression of FIC1 protein on the canalicular membrane of hepatocytes and other epithelial cells of small intestine, kidney, and pancreas, respectively, due to mutations of the ATP8B1 gene.[3] The liver, as the primary organ responsible for producing and secreting bile, remains nonetheless the organ mainly severely affected, as FIC1 protein is a flippase of phospholipids.[4] Individuals affected by PFIC1 typically develop liver failure before adulthood.[2]

Various mutations have been determined that result in PFIC1.[3,5,6] Klomp et al. report on 10 mutations anticipated to interfere with splicing, 6 nonsense mutation, 11 mutations involved in small insertions or deletions, 1 instance of a large genomic deletion, 2 small in-frame deletions, and 24 missense mutations.[6] Most abundant mutations of PFIC1 are missense mutations that result in loss-of-function of FIC1. Most common amongst the missense mutations are 380T>C, 863T>C, and 923G>T with the predicted effect L127P, L288S, and G308V.[6] The missense mutation G308V, for example, results in an unfolded flippase, which can indirectly interfere with the secretion of biliary bile acids, which results in cholestasis.[7] Current therapeutic strategies are drugs to treat cholestasis or liver transplantations in severe cases.[8] However, gene therapy would be a more promising therapeutic strategy by precisely addressing the detrimental anomaly on the genetic level.

CRISPR-Cas9 could be installed for the repair of the nonsense mutations, small insertions and deletions, in-frame deletions and the missense mutations listed above, assuming that the mutated site is located near a PAM sequence. Therefore, the LNPs designed in this thesis entrapping CRISPR-Cas9 components together with an HDR template were tested on PFIC1 murine intestinal organoids to determine their therapeutic applicability of a monogenic disease. Additionally, the ATP8B1[G308V] murine intestinal organoids served as an interesting model to test the LNPs in a 3D cell culture model as a better transitional model towards the clinical situation. Both LNPs delivering Cas9, either as mRNA/sgRNA or ribonucleoprotein complex, together with an HDR template were studied on organoids to continue the comparative analysis of the two different LNPs.

HDR-mediated single base gene correction can be detected via droplet digital polymerase chain reaction (ddPCR) with great sensitivity.[9,10] To differentiate between corrected and unmodified DNA sequences, two different fluorescently-labelled probes can be installed to detect and amplify the DNA according to the respective probe. In the standard PCR, the DNA would be amplified in bulk, however, and therefore the fluorescent signal of the more dominant DNA strand would outcompete a low percentage of HDR-mediated gene correction, for instance. ddPCR allows for partitioning of the DNA samples into microdroplets prior to PCR amplification with primer-probe pairs.[11] The DNA molecules are then randomly distributed in a large number of partitions, resulting in either empty droplets, DNA sequences with the specific correction, unmodified DNA sequences, or a combination of corrected and unmodified DNA sequences. This allows for a limited number of molecules per droplet and therefore a fluorescent signature is generated within each partition according to its DNA content. Subsequently, the rate of HDR-mediated gene correction can be calculated by counting the number of HDR-positive droplets in comparison to unmodified DNA sequences.

Here, we report the unfortunate and surprising discovery that the HDR template delivered together with the CRISPR-Cas9 components

via LNPs remained present in ATP8B1^{G308V} organoids longer than anticipated. Moreover, the HDR template was faultily detected via ddPCR resulting in false-positive gene correction results.

Material and Methods

Materials
All material and chemicals listed in this work were obtained from Sigma Aldrich (Zwijndrecht, The Netherlands) unless otherwise specified. Primers were bought from Integrated DNA Technologies (IDT, Leuven, Belgium). The lipids were obtained from: 1,10-((2-(4-(2-((2-(bis(2-hydroxydodecyl)amino)ethyl)(2hydroxydodecyl)amino)ethyl)piperazin-1yl)ethyl)azanediyl)bis(dodecan-2-ol) (C12-200) from CordonPharma (Plankstadt, Germany), 1,2-dioleoyl-sn-glycero-3-phosphoethanolamine (DOPE) from Lipoid (Steinhausen, Switzerland), Cholesterol and 1,2-dimyristoyl-rac-glycero-3-methoxypolyethyleneglycol-2000 (PEG-DMG) from Sigma-Aldrich, and 1,2-dioleoyl-3-trimethylammonium-propane (DOTAP) from Merck (Darmstadt, Germany). SpCas9 protein was produced in our labs as previously described (chapter 3).[12] CleanCap mRNA Cas9 (5moU) was acquired from TeBu Bio (Heerhugowaard, The Netherlands).

Formulation of Lipid Nanoparticles Complexing CRISPR-Cas9 RNP and HDR Template
Lipid nanoparticles delivering Cas9 either as mRNA or protein together with sgRNA and HDR template were formulated as described in this thesis (**chapter 4**).

Table S1: **Sequences of sgRNA and HDR template for ATP8B1 organoids.** Small and high-lighted yellow letter 'g' in the HDR sequence indicates the correct base pair G within the ATP8B1 sequence for gene correction of T->G. Small and highlighted green letter 'a' indicates that after HDR the PAM sequence is altered with a silent mutation.

	5′-3′ Sequence Data
sgRNA	TTATCACACAACCTCGTAAC
HDR template	TTTGGAAGAACCAAAGCTTTCCTTTGGATGCTGAT AAAATaCTGTTACGAGGTTGTGTGATAAGGAACAC CGATGTCTGCCATGgCCTGGTCATTTTTGCAGGTAC TTCCCAAATGTGCTTCGAG

Figure S1: **Scheme of DNA sequence of a segment of *ATP8B1* gene showing exon 10 and subsequent intron of PFIC1 patients.** The sgRNA to target the cutting site is indicated by purple letters. The site of mutation is indicated by red letters. The yellow bar above the DNA sequence represents the HDR template and it's targeting within the *ATP8B1* gene.

ATP8B1$^{G308V/G308V}$ Mice

ATP8B1^{G308V} mice were generated and bred as described by Pawlikowska et al. at the ARIA Amsterdam institute.[5] Mice were housed at ARIA Amsterdam under standard conditions with chow diet *ad libitum*. All animal procedures complied with the guidelines of the EU and were approved by the Animal Welfare Body (ALC102556).

ATP8B1$^{G308V/G308V}$ *Organoids*

Intestinal organoids were generated as reported by Sato et al.[13] Intestines were harvested from ATP8B1$^{G308V/G308V}$ mice and the intestinal crypt isolated. The intestinal crypt were washed with 10 ml ice cold PBS 20 times. Then, 25 ml of 2mM EDTA in PBS were added to the intestinal crypt and left on ice for 30 minutes while constantly shaking. Subsequently, the intestinal crypt were treated with 10 ml of ice cold PBS/10% FBS 5 times and eventually the supernatant was collected. Cells were collected by passing the supernatant through a sterile 70 μm cell strainer (BD/VWR) in a 50 ml tube (Greiner, Alphen aan de Rijn, The Netherlands). Cells were spun down at 800 rpm for 5 minutes and then resuspended in 10 ml of Advanced DMEM/F12 medium (Ad-DF+++, Capricorn Scientific GmbH, Leusden, The Netherlands) supplemented with 10% FCS (Capricorn Scientific GmbH, 1x Glutamax (Invitrogen, Thermo Fischer Scientific, Landsmeer, The Netherlands), 0.1M HEPES and 1x Pen/Strep (Invitrogen). Again, cells were spun down at 800 rpm for 5 minutes and the cell pellet was resuspended carefully to prevent forming of air bubbles resuspend in matrigel (Corning, Amsterdam, The Netherlands) with 20μl/well (BD, Amsterdam, The Netherlands). Twenty microliters of cells mixed in matrigel were added per well of a 48-well plate (Corning) and placed into an incubator (37 °C, 5% CO_2) for 15 minutes. Then, 250 μl of complete growth medium (ENR-Medium: AD-DF+++ supplemented with Supplement B27 (Invitrogen), Supplement N2 (Invitrogen), 1.8 mM n-Acetylcysteine, 5.7 % mNoggin, mEGF, and 1.4 x Rspondin) was added per well and the plates were incubated at 37 °C, 5% CO_2, refreshing the medium every 2-3 days. The outgrown crypt were passaged after 7 days by transferring the organoids, medium and matrigel via pipetting to a 15 ml conical tube where the suspension was diluted up to 2 ml with Ad-DF+++ medium. Via a narrowed and sterilized Pasteur pipet the organoids were broken down into small pieces by pipetting up and down. Another 2 ml of Ad-DF+++ was added and the suspension was centrifuged at 700 rpm for 5 minutes. The pellet was resuspended in 2 ml of ice cold Ad-DF+++ and mixed again with a Pasteur pipette and centrifuged. The supernatant were removed and the cell

pellets were resuspended in matrigel with 20 μl/well and 20 μl of the cell-matrigel suspension are transferred to each well of a 48-well plate. The plates were incubated at 37 °C, 5% CO_2 and after 15 minutes 250 μl of ENR-Medium was added to the wells and continuously incubated at 37 °C and 5% CO_2. Medium was refreshed every 2-3 days until the next passaging.

Treatment of ATP8B1$^{G308V/G308V}$ Organoids with LNPs

ATP8B1$^{G308V/G308V}$ organoids were treated with either mRNA Cas9 LNPs or Cas9-RNP LNPs, both formulation co-delivering the HDR template as well. First, the matrigel containing the organoids in medium was dissociated by pipetting with a Pasteur pipet up and down for 20 times. The dissociated organoids were then centrifuged at 700 rpm for 5 minutes and the supernatant was removed. Subsequently, the dissociated organoids were resuspended in ENR-medium and LNPs were added at a final sgRNA concentration of 77nM. The organoids were incubated with the LNPs for 4 hours at 37 °C and 5% CO_2. Subsequently, the organoids were washed with Ad-DF+++ and transferred to a sterile Eppendorf cup and centrifuged at 3000 rpm for 5 minutes. The organoids were resuspended in matrigel (20 μl/well) and plated on 48-well plates. After 15 minutes 250 μl of ENR-medium was added to the wells. Every 2-3 days the medium was refreshed until the organoids were processed for subsequent procedures after a week of administration of LNPs.

Enrichment of Wildtype Intestinal Organoids

To increase the percentage of corrected cells, one week after transduction the organoids were harvested as above and subsequently treated with trypsin to generate single cells. Since only stem cells can form organoids again and the percentage of stem cells in WT organoids is higher than in ATP8B1^{G308V} organoids, this will enhance the percentage of corrected cells. To split organoids into single cells, organoids are harvested and resuspended with a Pasteur pipet and collected into a 15 ml conical tube and centrifuged at 700 rpm for 5 minutes. Then, the cell pellet is incubated with 500 μl of trypsin (Capricorn Scientific GmbH) in a 37 °C water bath for 3 minutes. Trypsin was inactivated

with 1 ml ENR-medium containing FCS. Then, the cells are centrifuged at 1200 rpm for 5 minutes. The cells were plated on 48-well plates in 20 μl/well matrigel and grown out to organoids for 3 weeks.

Determination of Gene Correction Efficiency via Droplet Digital PCR (ddPCR)

To determine the efficiency of gene correction, organoids were harvested after one week and after three weeks (enrichment) after administration of LNPs, respectively. The organoids were then processed for analysis with digital droplet PCR (ddPCR). Organoids were harvested by scratching the matrigel and transferring everything to a 15 ml canonical tube. The mixture was then spun down via centrifugation at 700 rpm for 5 minutes. The pellet was washed with PBS and then resuspended in 200 μl PBS. Then, DNA was isolated from organoids with DNAeasy® Blood & Tissue Kit from Qiagen (Venlo, The Netherlands) by following the manufacturer's protocol. 4 μl isolated DNA samples were then further processed for ddPCR by mixing samples with 10 μl master mix, primers for specific sequence amplification, 1 μl ddPCR mutation detection assay mix (Bio-Rad Laboratories, Veenendaal, The Netherlands) containing the primers for sequence amplification and Hex- and Fam-labelled probes to determine HDR-mediated gene corrected DNA sequences and unmodified ATP8B1^{G308V} DNA sequences, respectively, 1 μl restriction enzyme mix (1:5 Mse1 restriction enzyme:CutSmart buffer), and 5 μl water. The restriction enzyme ensures accessibility of the targeted region by fragmenting the genomic DNA. ddPCR was performed at the Core Facility AUMC located at the Amsterdam University Medical Centre. The ddPCR was run with the standard protocol given by Bio-Rad: enzyme activation at 95°C for 10 minutes, denaturation at 94°C for 30 seconds and annealing at 55 °C for 1 minute, denaturation and annealing repeated 39 times, and subsequently enzyme deactivation at 98 °C for 10 minutes with a final hold on 4 °C. The raw data was processed in the software QuantaSoft program (version 1.7.4.0917; Bio-Rad) to gate the four different channels (both positive, WT positive, ATP8B1 positive, empty). The efficiency of gene correction is calculated with the following equation:

$$\text{Gene correction efficiency} = \frac{both\,positive + WT\,positive}{both\,positive + WT\,positive + ATP8B1\,positive} \cdot 100 \quad (1)$$

Results and Discussion

To determine the efficiency of gene correction of G308V mutation in the ATP8B1 gene, ATP8B1^{G308V} organoids were administered with LNPs delivering Cas9, either as mRNA or protein, together with sgRNA and HDR, called *m*LNP-HDR and *p*LNP-HDR, respectively. Organoids were incubated for a total of 4 hours with the LNP formulations, washed and subsequently cultured for 1 or 3 weeks before DNA was harvested and gene correction was determined by ddPCR (for details see M&M section). ddPCR detected 99.8% in both ATP8B1^{G308V} organoids treated with *p*LNP-HDR and *m*LNP-HDR, and 2%, and 10% WT sequence in, untreated ATP8B1^{G308V} organoids and control 10% WT sample, respectively, before splitting organoids into single cells. After splitting into single cells and regrowing the organoids as described in the method section, ddPCR detected 61% and 84% WT sequence in *p*LNP-HDR and *m*LNP-HDR treated organoids.

Unfortunately, instead of determining gene correction, it seems that the HDR template remained stable and present in the ATP8B1^{G308V} organoids after delivery via LNPs and was detected via the ddPCR up to 3 weeks after organoid culturing. Even though direct proof for HDR template amplification is at present lacking, we are confident that HDR template amplification is causing these unexpected results based on the high dilutions required of the genomic DNA for successful ddPCR and the detection of 99.8% WT sequence after treatment with LNPs delivering CRISPR-Cas9 either as mRNA or Cas9 protein (Fig. 2). Furthermore, after re-growing organoids from organoids split into single cells, successfully modified organoids, with a WT phenotype, were expected to be enriched over ATP8B1^{G308V} organoids. Conversely, the data presented in Fig. 2 shows less percentage of WT sequence than before single cell splitting. This might suggest that with further culturing of the organoids the HDR template was washed out or degraded more over time.
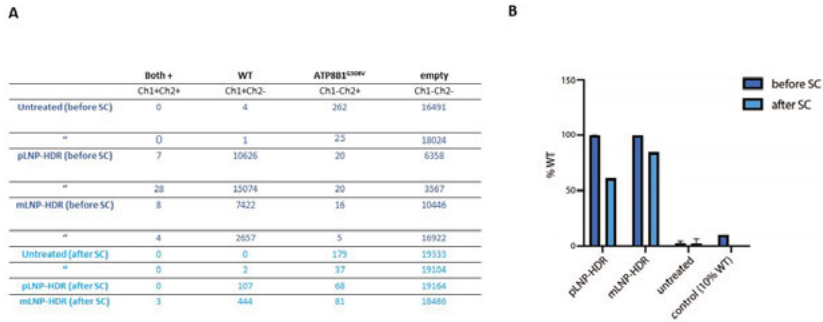
	Both + Ch1+Ch2+	WT Ch1+Ch2-	ATP8B1^{G308V} Ch1-Ch2+	empty Ch1-Ch2-
Untreated (before SC)	0	4	262	16491
"	0	1	25	18024
pLNP-HDR (before SC)	7	10626	20	6358
"	28	15074	20	3567
mLNP-HDR (before SC)	8	7422	16	10446
"	4	2657	5	16922
Untreated (after SC)	0	0	179	19333
"	0	2	37	19104
pLNP-HDR (after SC)	0	107	68	19164
mLNP-HDR (after SC)	3	444	81	18486

Figure S2: **Percentage of WT intestinal organoids after administration with *p*LNP-HDR and *m*LNP-HDR. A)** Raw data retrieved from the ddPCR. Dark blue indicates the DNA samples harvested from ATP8B1^{G308V} organoids retrieved before enriching the organoids for WT positive organoids after successful HDR-mediated gene correction. **B)** Plotted ddPCR data as percentage of detected WT organoids (calculated via equation 1 with data in Fig. 2A) after administration of *p*LNP-HDR or *m*LNP-HDR to ATP8B1^{G308V} organoids in comparison to untreated organoids. The control sample was a mix of genomic DNA isolated from WT organoids (10%) and ATP8B1^{G308V} organoids (90%).

Therefore, the data is inconclusive and predictions on HDR-mediated single-base gene correction investigated in this study cannot be made. It was promising, nonetheless, to note that toxicity induced by the LNPs could not be detected based on morphology of the ATP8B1^{G308V} organoids (data not shown). Possibly, however, that suggests a lack of uptake of LNPs in organoids. To investigate whether LNPs are taken up, uptake studies with fluorescently-labelled LNPs would be interesting to perform. Moreover, seeing that cells rather employ non-homologous end joining over homology directed repair,[14] determining gene knock-out of a surface marker, for example, mediated through CRISPR-Cas9 delivered by LNPs might be a first step to study the functionality of LNPs in organoids prior to single-base gene correction studies.

The detection of the ssDNA template via ddPCR resulted in false-positive results for gene correction. Therefore, the ddPCR requires optimizations to be used for detection of single-base corrections such as the G308V mutation in FIC1 protein. While the probes were seemingly synthesized to be specific for the repaired and mutated (G308V) sequence, as both sequences can be detected, a technical flaw of this study appears to have been in the design of the primers for ddPCR, overlapping and therefore amplifying the ssDNA HDR template as well. The primers need to be optimized to solely amplify the inserted HDR template within the genome, by ensuring that the primer sequences are outside of the region homologous to the ssDNA template. Even if one of the primers already overlaps with the ssDNA sequence the risk of chimeric PCR products in multi-templated PCRs and thus false-positive increases.[15–17]

Nonetheless, the detection of the ssDNA via ddPCR lead to the finding that ssDNA is still present in cells even after weeks of culturing of organoids. This surprising stability of ssDNA upon LNP delivery has not been reported before. As this risk of contamination of amplicon samples, and therefore can lead to false-positive results in determination of gene correction efficiencies, purifying genomic DNA samples and removing ssDNA prior to ddPCR seems wise. Column purifications of the extracted DNA from cells could separate the ssDNA from the genomic DNA. The genomic DNA could also be isolated via gel electrophoresis and subsequently excised from the gel and purified for ddPCR. Moreover, the ssDNA contaminations could be removed via enzymatic digestion through ssDNA-specific enzymes such as exonuclease VII (both 5'-3' and 3'-5' ssDNA) or exonuclease I (only 3'-5'ssDNA). Adding at least one of these steps to the preparations of genomic DNA for ddPCR would ensure specific detection of HDR-mediated gene correction.

To conclude, ATP8B1^{G308V} organoids served as an interesting model to test functionality of LNPs in a more physiologically relevant environment, 3D cell cultures. Via ddPCR we hoped to determine the HDR-mediated single-base gene correction efficiencies of the missense

mutation causing PFIC type 1. However, in our hands the experiments resulted in inconclusive data. Instead, we discovered that the ssDNA template for HDR remained present in organoids even after 3 weeks of culturing, resulting in faulty detection of the template instead of specific repair via ddPCR. Technical optimizations of the experimental design of ddPCR and administration of LNPs to organoids will be required first before continuing with ATP8B1^{G308V} organoids to test LNP-mediated delivery of CRISPR-Cas9 and subsequent HDR-mediated gene correction for therapeutic application of PFIC type 1.

Acknowledgements

References

1. Davit-Spraul, A., Gonzales, E., Baussan, C. & Jacquemin, E. Progressive familial intrahepatic cholestasis. Orphanet J. Rare Dis. **4**, 1–12 (2009).
2. Srivastava, A. Progressive familial intrahepatic cholestasis. J. Clin. Exp. Hepatol. **4**, 25–36 (2014).
3. Naik, J. et al. ATP8B1 and ATP11C: Two lipid flippases important for hepatocyte function. Dig. Dis. **33**, 314–318 (S. Karger AG, 2015).
4. Eppens, E. F. et al. FIC1, the protein affected in two forms of hereditary cholestasis, is localized in the cholangiocyte and the canalicular membrane of the hepatocyte. J. Hepatol. **35**, 436–443 (2001).
5. Pawlikowska, L. et al. A mouse genetic model for familial cholestasis caused by ATP8B1 mutations reveals pertubed bile salt homeostasis but no impairment in bile secretion. Hum. Mol. Genet. **13**, 881–892 (2004).

6. Klomp, L. W. J. et al. Characterization of mutations in ATP8B1 associated with hereditary cholestasis. Hepatology **40**, 27–38 (2004).

7. Van Der Velden, L. M. et al. Folding defects in P-type ATP 8B1 associated with hereditary cholestasis are ameliorated by 4-phenylbutyrate. Hepatology **51**, 286–296 (2010).

8. Alam, S. & Lal, B. B. Recent updates on progressive familial intrahepatic cholestasis types 1, 2 and 3: Outcome and therapeutic strategies. World J. Hepatol. **14**, 98–118 (2022).

9. Überbacher, C. et al. Application of CRISPR/Cas9 editing and digital droplet PCR in human iPSCs to generate novel knock-in reporter lines to visualize dopaminergic neurons. Stem Cell Res. **41**, 101656 (2019).

10. Miyaoka, Y. et al. Systematic quantification of HDR and NHEJ reveals effects of locus, nuclease, and cell type on genome-editing. Sci. Rep. **6**, 1–12 (2016).

11. Hindson, C. M. et al. Absolute quantification by droplet digital PCR versus analog real-time PCR. Nat. Methods **10**, 1003–1005 (2013).

12. Walther, J. et al. Impact of Formulation Conditions on Lipid Nanoparticle Characteristics and Functional Delivery of CRISPR RNP for Gene Knock-Out and Correction. Pharmaceutics **14**, (2022).

13. Sato, T. et al. Paneth cells constitute the niche for Lgr5 stem cells in intestinal crypts. Nature **469**, 415–418 (2011).

14. Mao, Z., Bozzella, M., Seluanov, A. & Gorbunova, V. DNA repair by non-homologous end joining and homologous recombination during cell cycle in human cells. Cell Cycle **7**, 2902–2906 (2008).

15. Kanagawa, T. Bias and artifacts in multitemplate polymerase chain reactions (PCR). J. Biosci. Bioeng. **96**, 317–323 (2003).

16. Shuldiner, A. R., Nirula, A. & Roth, J. Hybrid DNA artifact from PCR of closely related target sequences. Nucleic Acids Res. **17**, 4409–4409 (1989).

17. Wintzingerode, F. V., Göbel, U. B. & Stackebrandt, E. Determination of microbial diversity in environmental samples: Pitfalls of PCR-based rRNA analysis. FEMS Microbiol. Rev. **21**, 213–229 (1997).

Nederlandse samenvatting

CRISPR-Cas9, oorspronkelijk een bacterieel afweermechanisme, is gemodificeerd tot een hulpmiddel voor het nauwkeurig bewerken van genen in elk organisme. De werking van CRISPR-Cas9 wordt ook wel vergeleken met een schaar, omdat deze techniek voor het bewerken van genen ons genoom op precieze locaties kan knippen. Na de snede wordt het DNA hersteld door de afgeknipte uiteinden willekeurig te combineren of door nauwkeurig een specifieke DNA-sequentie in te voegen op basis van een sjabloon van bijvoorbeeld enkelstrengs DNA (ssDNA). De mogelijkheid om het gen permanent te bewerken via CRISPR-Cas9 maakt dit tot een veelbelovende techniek voor de behandeling van genetische ziekten. Voor gebruik bij patiënten moet CRISPR-Cas9 echter worden verpakt in een transportmiddel ter grootte van een virus, zodat CRISPR-Cas9 naar de zieke cellen kan worden gebracht, deze kan binnendringen en het DNA kan snijden en repareren. Het doel van dit proefschrift is om een transportmiddel te ontwerpen dat CRISPR-Cas9 veilig naar hepatocyten, een subset van cellen in de lever, kan brengen voor de behandeling van erfelijke leverziekten. Omdat CRISPR-Cas9 afkomstig is van bacteriën, is in dit proefschrift ook een methode onderzocht om tolerantie te induceren in plaats van een immuunrespons om voortijdige klaring van CRISPR-Cas9 te voorkomen.

CRISPR-Cas9 is gemaakt van een eiwit, Cas9, dat de knip in het DNA genereert. Om op een specifieke positie te knippen vormt Cas9 een complex met een RNA-molecuul dat Cas9 naar een DNA-sequentie leidt die complementair is aan het RNA, genaamd guideRNA (gRNA). Zoals hierboven vermeld, is voor specifieke reparatie een sjabloon nodig. Dit kan ssDNA zijn dat, indien aanwezig op het moment van DNA-reparatie, in de plaats van de DNA-snede wordt ingebracht. Cas9 kan samen met het gRNA en ssDNA worden geleverd voor gebruik in patiënten met een genetische ziekte. Hierbij

kan Cas9 rechtsreeks als een eiwitmolecuul of als messenger RNA (mRNA), dat zich na succesvolle levering vertaalt naar een eiwit in het cytosol van cellen, geleverd worden.

Er zijn verschillende soorten transportmiddelen die worden onderzocht voor de levering van CRISPR-Cas9. **Hoofstuk 2** van dit proefschrift bespreekt virale en niet-virale opties. Aangezien virale vectoren gebaseerd zijn op virussen, is het risico met deze vectoren inductie van een immuunrespons. Bovendien is de verpakkingsgrootte in virale deeltjes beperkt. Daarom is in de review ook gekeken naar niet-virale vectoren zoals lipide nanodeeltjes. Lipide nanodeeltjes (LNPs) zijn samengesteld uit lipiden en cholesterol, biologische moleculen. Een van de lipidemoleculen is een ioniseerbaar kationisch lipide dat het insluiten van nucleïnezuren of op eiwitten gebaseerde lading via elektrostatische interacties vergemakkelijkt. Ioniseerbare lipiden zijn bovendien bestudeerd om endosomale afgifte van de lading te induceren na door vesikels gemedieerde cellulaire opname van de LNPs. Daarom werden LNPs in dit proefschrift verder onderzocht om CRISPR-Cas9 te vangen en uiteindelijk af te geven aan hepatocyten in levers.

Aangezien ioniseerbare lipiden de elektrostatische interacties faciliteren om de negatief geladen lading te vangen, vindt de synthese van LNPs meestal plaats in een zure omgeving om het ioniseerbare lipide te protoneren. Recente studies hebben echter aangetoond dat een zure omgeving met pH onder 5,9 het Cas9-eiwit kan beschadigen. Daarom richt **hoofdstuk 3** zich op het optimaliseren van de syntheseparameters van LNPs voor het invangen van Cas9-eiwit samen met gRNA en ssDNA. Verschillende syntheseparameters en moleculaire verhoudingen tussen de betrokken moleculen zijn onderzocht. LNPs werden gesynthetiseerd in een pH-neutrale omgevingen en in citraatbuffer (pH 4), en aan beide omgevingen werd een kationisch lipide, DOTAP, aan de LNPs toegevoegd. DOTAP werd toegevoegd om de elektrostatische interactie met de negatief geladen CRISPR-Cas9 componenten te verzekeren. De resulterende LNPs werden gekarakteriseerd op basis van deeltjesgrootte, stabiliteit in menselijk plasma en uiteindelijk genmodificatiefunctionaliteit. Uit

de experimenten is gebleken dat HEPES buffer (pH 7.4) of nuclease vrij water de meeste genmodificatie in cellen geeft en beide zijn stabiel in menselijk plasma. Om het ssDNA mede af te leveren, vereiste de formulering dat DOTAP werd opgenomen tot 0.25% van de totale lipided en een molaire verhouding van 2:1 tussen ssDNA en gRNA.

In **hoofdstuk 3** werden LNPs geoptimaliseerd voor de directe levering van Cas9-eiwit in plaats van Cas9 als mRNA, zoals hierboven beschreven. Voordeel van de directe levering van het eiwit is dat het na levering niet eerst in het cytosol hoeft te worden vertaald. Het heeft daarom ook een kortere halfwaardetijd en is onderzocht om daarom minder off-targets te riskeren. Nadelen zijn echter dat het Cas9-eiwit als complex is ingekapseld met het gRNA. Dit Cas9-gRNA complex, ribonucleoprotein complex (RNP) genaamd, is een groot molecuul. Bovendien heeft het Cas9-eiwit zelf een positieve lading. Alleen in complex met het gRNA heeft het een netto-negatieve lading en is het dan niet gelijkmatig verdeeld over het oppervlak can het complex. Dit zou de efficiënte insluiting in LNPs kunnen verstoren. We waren daarom nieuwsgierig om LNPs te vergelijken die het eiwit of direct insluiten of als een mRNA molecuul. LNPs werden geformuleerd gebaseerd op de best functionerende formulatie uit **hoofdstuk 3**. In het geval van LNPs die mRNA leveren, werd het mRNA aan de formulering toegevoegd in een molaire verhouding van 4:1 tot het gRNA. **Hoofdstuk 4** concludeerde overtuigend dat mRNA Cas9 een betere vorm is voor de levering van CRISPR-Cas9 via LNPs. mRNA LNPs resulteerden in kleinere nanodeeltjes en meer genmodificatie op cellen in kweek vergeleken met LNPs die RNP leveren. Verrassend genoeg veroorzaakten de mRNA Cas9 LNPs ook sneller genmodificatie dan Cas9 RNPs, ondanks dat ze eerst moesten worden vertaald naar een eiwit in het cytosol van cellen. Mogelijk is dit te verklaren door een betere opname van deze LNPs, of het mRNA vertaalt zich intracellulair naar hogere Cas9 concentraties dan directe levering van het eiwit. Verder beschrijft **hoofdstuk 4** een proefdierstudie waarbij muizen werden geïnjecteerd met de twee verschillende LNPs om de lokalisatie van deeltjes in

organen en functionaliteit te bepalen. Schokkend genoeg stierven alle muizen waaraan LNPs met RNP waren toegediend binnen 20 uur na injectie van de LNPs. Muizen die mRNA LNPs toegediend kregen vertoonden geen tekenen van ongemak, en er is vastgesteld dat de LNPs efficiënt CRISPR-Cas9 aan de hepatocyten afleverden. Dit resulteerde in 60% genmodificatie. Het blijft een open vraag waarom LNPs die het Cas9-eiwit afleverden de dood tot gevolg hadden. Dit moet verder worden onderzocht alvorens directe levering van de RNP voor therapeutische toepassingen te overwegen.

CRISPR-Cas9 is afkomstig van bacteriën, waardoor mensen hier al aan zijn- blootgesteld. Om binnendringende bacteriën te bestrijden, wordt het immuunsysteem van de mens geactiveerd en daarom tonen onderzoeken aan dat er reeds bestaande immuunresponses bestaan, specifiek tegen CRISPR-Cas9. Voor de levering van CRISPR-Cas9 via LNPs aan patiënten met een genetische ziekte vormen deze reeds bestaande immuunresponsen een risico om CRISPR-Cas9 te elimineren voordat het het DNA kan knippen of bewerkte cellen kan verwijderen. Daarom rapporteert **hoofdstuk 5** over een aanpak om een immuunrespons te voorkomen en in plaats daarvan tolerantie voor CRISPR-Cas9 te induceren. De sleutel tot het mediëren van tolerantie of immuunrespons zijn dendritische cellen. Dendritische cellen kunnen een tolerogeen fenotype verkrijgen, tolerogene dendritische cellen (tolDCs) gekenmerkt door verminderde expressieniveaus van oppervlaktemarkers en scheiden ontstekingsremmende cytokines af. TolDCs rekruteren geen cytotoxische T-cellen maar regulatoire T-cellen. Regulatoire T-cellen (Tregs), vredeshandhavers van ons immuunsysteem, voorkomen een aanval van het immuunsysteem op moleculen die het niet zou moeten aanvallen. Een medicijn genaamd dexamethason kan een tolerogeen fenotype stimuleren. Door dexamethason of zijn prodrug dexamethasonfosfaat samen met Cas9-eiwit in te kapselen in nanodeeltjes die gericht zijn op dendritische cellen, kan Cas9-specifieke tolerantie worden geïnduceerd. **Hoofdstuk 5** beschrijft de formulering van liposomen, een vehikel voor medicijnafgifte dat ook bestaat uit lipiden, maar

gesynthetiseerd via een andere methodologie en met een andere structuur, die de prodrug dexamethasonfosfaat samen met het Cas9-eiwit inkapselt. Deze liposomen werden gekarakteriseerd om efficiënt een tolerogeen fenotype van dendritische cellen in kweek te induceren. Verder werden de liposomen in een muizenstudie voornamelijk opgenomen door de milt en lever, organen die betrokken zijn bij tolerantie en immuunresponsen. Echter, de muizen waarbij dexamethasonfosfaat-Cas9-liposomen werden toegediend, produceerden slechts marginaal minder Cas9-specifieke antilichamen na introductie van Cas9-eiwit vergeleken met de controlegroep. Er kon geen verschil in expressie van Tregs worden gedetecteerd tussen muizen die liposomen kregen toegediend en controlemuizen.

Dit proefschrift laat veelbelovende resultaten zien om LNPs te formuleren die op efficiënte wijze CRISPR-Cas9 samen met een ssDNA kunnen afleveren voor specifiek herstel en voortijdige klaring kunnen omzeilen door reeds bestaande immuunresponsen op het bacteriële hulpmiddel voor uiteindelijke behandeling van genetische ziekten.

About the author

Johanna Walther was born in Heidelberg, Germany on October 8th 1993. After finishing high school with the German Abitur at the German-American John F. Kennedy School, Berlin, she did an internship at the German Institute of Human Nutrition in Potsdam-Rehbrücke, Germany for a year, where she studied the distribution of bitter receptors within mice. Afterwards she moved to Halle (Saale), Germany for her bachelor's in biochemistry at the Martin-Luther-University, Halle (Saale), Germany. In 2016 Johanna did a project as junior scientist with Cristal Therapeutics in collaboration with Department of Pharmaceutics, UIPS, Utrecht University in The Netherlands. This project focused on the cellular delivery of CriPec nanoparticles via *in vitro* assays. The internship introduced her to the master's program Drug Innovation at Utrecht University which she then started in 2017. During her master's Johanna performed a 9 month internship on delivery vehicles for CRISPR-Cas9 for gene therapy at the Department of Pharmaceutics, UIPS, Utrecht University supervised by prof. dr. Enrico Mastrobattista. Within her master's program Johanna also performed a 6 month internship on *in silico* determination of the effect of thrombocyte transfusion on organ transplantations at the Department of Biology and Bioinformatics, Utrecht University under supervision of by dr. Can Kezmir. She received her MSc. Diploma in 2019 and continued the research on delivery vehicles for CRISPR-Cas9 for therapeutic gene correction as her PhD project at Department of Pharmaceutics together with Enrico Mastrobattista. The results of this work are presented in this thesis.

List of Publications

Beztsinna, N., De Matos, M. B. C., **Walther, J.**, Heyder, C., Hildebrandt, E., Leneweit, G., ... & Kok, R. J. (2018). Quantitative analysis of receptor-mediated uptake and pro-apoptotic activity of mistletoe lectin-1 by high content imaging. Scientific Reports, 8(1), 2768

Wilbie, D., **Walther, J.**, & Mastrobattista, E. (2019). Delivery aspects of CRISPR/Cas for in vivo genome editing. Accounts of chemical research, 52(6), 1555-1564

Walther, J., Wilbie, D., Tissingh, V. S., Öktem, M., Van Der Veen, H., Lou, B., & Mastrobattista, E. (2022). Impact of formulation conditions on lipid nanoparticle characteristics and functional delivery of CRISPR RNP for gene knock-out and correction. Pharmaceutics, 14(1), 213.

Hebels, E. R., Bindt, F., **Walther, J.**, van Geijn, M., Weterings, J., Hu, Q., ... & Vermonden, T. (2022). Orthogonal Covalent Entrapment of Cargo into Biodegradable Polymeric Micelles via Native Chemical Ligation. Biomacromolecules.

Douka, S., Brandenburg, L. E., Casadidio, C., **Walther, J.**, Garcia, B. B. M., Spanholtz, J., ... & Caiazzo, M. (2023). Lipid nanoparticle-mediated messenger RNA delivery for ex vivo engineering of natural killer cells. Journal of Controlled Release, 361, 455-469

Acknowledgements

Enrico, we have known each other now for almost 7 years. I am grateful to Cristal Therapeutics and you for my gap year project as this really opened up the world of pharmaceutical sciences for me! And my life in The Netherlands. Thank you for supporting and supervising me during my master's thesis and I am especially grateful to you for offering me the PhD project. I am thankful for all of these opportunities and your guidance throughout each phase. You were always available for help even with a full schedule. I truly appreciate that you provide an open and safe space to talk about challenges in the lab but also about mental health. Thank you for trusting in my capabilities and helping me to be a better scientist. Thank you for checking in after presentations and conferences. I have learned a tremendous amount from you, but especially hope to one day be a mentor to others with the same patience and fairness as you have shown us. En bedankt voor het oefenen van Nederlands!

Piter, thank you for being my co-promoter. I enjoyed working together with you and your team on PFIC organoids! Thank you for your guidance, support, and feedback on my scientific writing. (And thank you for your courier service between DDW and Tytgat Institute.)

To my lovely paranymphs: **Bárbara**, Bárbarita, you are an inspiring friend and colleague, and you are a fighter! I am in awe of your energy, of your devotion. I am grateful to you for your help in the lab and brainstorming on our projects, but I am especially grateful for the emotional support, motivation and encouragement! **Danny**, together we embarked on the VICI CRISPR-Cas9 project and it has been great to get to know you! Your fascination of science and scientific capabilities have inspired me many times. Thank you for being a supporting colleague.

Erik, as one of my first friends in The Netherlands, I want to thank you for your friendship! I am grateful that we ended up doing PhDs in the same lab as your aid throughout these last 4 years have kept me going and it was truly wonderful to share the days with a friend!

I am thankful to all of the other fellow PhD candidates and Post-Docs at Department of Pharmaceutics that I have got to know and work with in the last years. I especially want to thank **Stefania, Deja, Lucas, Martina, Blessing, Cristina, Karina, Yan, Boning, Angela, Matthijs, & Masha**.

Thank you, **Olivier**, for your brainstorming and answering any questions I had on molecular biology, reporter cells and CRISPR-Cas9! Your feedback has been received with great gratitude and your detailed look at my scientific writing definitely let me learn tremendously.

Marcel, you have always been a motivating colleague with your positive attitude and jokes. I truly appreciate your help in designing the *in vivo* studies and your help in the lab!

Barbara, dank je wel voor jouw steun met administratieve zaken maar vooral bedankt voor de praatjes in jouw kantoor! Ik ga jouw enthousiasme voor karaoke missen! Hopelijk gaan we weer ergens naar de karaoke bar!

I would like to thank the research technicians of Department of Pharmaceutics for their aid in technical questions, ordering supplies, but especially for making our labs safe and functional during the COVID-19 pandemic. Thank you, **Mies**, for always being available for questions even if it meant calling in off-hours. I am grateful to you, **Antoinette**, for taking over the AF4 studies for me. **Jaimie**, thank you for your "let's do it attitude" and organized approach to helping with the *in vivo* studies.

I would also like to thank my students that I have supervised over the course of the last four years: **Maarten, Heleen, Thomas, Bonne, & Billy**. I am grateful for your hard work on the projects during my PhD trajectory! I have learned a great amount while supervising you.

Thank you for giving me your feedback. I wish you all the best for your future in the field of life sciences.

I learned a lot on immunology during my collaboration with Department of Infectious Diseases and Immunology. Thank you **Femke** for your critical feedback and comments during meetings and writing. **Daniëlle**, I am grateful for your efforts and willpower to move our tolerance project forward. Thank you for helping with supervising Bonne und Billy. And for our lovely meetings to just generally catch up on our PhD trajectories. **Naomi**, thank you for your help on designing experiments, handling the mice in our *in vivo* studies, and your feedback on my scientific writing. I enjoyed our time at CRS Annual in Montreal together and our talks on work-life balance/scientific working!

I am thankful for my collaboration with UMCU. **Zhiyong**, I truly appreciate your help with the *in vivo* study in Ai9 mice. Thank you for handling the mice, but especially thank you for your feedback on the design of the study, help with experiment protocols and feedback on my writing. Thank you **Qiangbing** for synthesizing mRNA Cas9 for me and thank you **Cornelis** for performing cryo-TEM on liposomes and lipid nanoparticles for me. **Sander**, I really appreciate that you took time for meetings and looking at protocols with me on single cell flow cytometry! Your knowledge on the theory and hands-on lab experience was treasured and essential for those studies. Thanks also to you, **Dan** and **Martijn**, for helping out across the streets!

Lysbeth and **Yue**, your experience and hands-on help with the studies on lipid nanoparticles on PFIC organoids is truly appreciated. Thank you for performing those assays! Thank you for always receiving me with a warm welcome in your lab at the Tytgat Institute.

To my friends:
I am grateful for the support and for the incredibly fun times I have with my friends! **Julia B.**, mein Biochemie-buddy! Danke für die Unterstüztung seit unserem Bachelor und die wunderbaren Wochenenden zusammen! **Julia E.E.**, I am so glad that our masters and House Hess brought us together! You made our home in De Bilt a place of

comfort and place of support! Thank you for being there for me! Only Sheldon knows the troubles we've seen. **Gesa**, du warst mein Zuhause in Halle! Ich bin dir so dankbar und ich vermisse dich in den Niederlanden. Ich bin unendlich froh dich als Freundin zu habe! Danke, dass wir gemeinsam die Ups und Downs im Leben erleben! **Victoria**, ich schätze es sehr, dass wir uns schon seit Schulzeiten kennen und nach wie vor gute Freundinnen sind. Danke dass du eine aufmerksame und fürsorgliche Freundin bist! **Mariona**, I am very grateful to you for being an encouraging and supportive friend! You always brighten up any space with your energy and joyful aura. Thank you **Haley** for introducing me to our wonderful friends **Amy, Elle, Maaike, & Luan**. Thank you all for our day and weekend trips and vacations! They have always given me strength!

To my family:
An meine lieben Eltern, **Sabine** und **Dirk**: Eure Zuversicht und eure Vertrauen in mir hat mich schon immer gestärkt! Ich habe von Euch gelernt, dass wenn ich etwas wirklich will und wirklich anpacke, ich es auch schaffen kann. Und dabei wusste ich immer, dass ich eure Unterstützung habe! Danke, dass ihr bei allem was ich tue für mich da seid! Ich bin euch sehr dankbar für die liebe, zugewandte und offene Familie, die ihr gebildet habt.

My dearest sisters, **Lena** and **Clara**: I could never have asked for better sisters! I am so grateful for our bond! Thank you for always, always having my back! And thank you for bringing Gina and Shahab into our family.

Dear **Gina**, dear **Shahab**: I am so happy to get to call you family. Thank you for checking in on me and my PhD project, but especially thank you for looking out for my sisters!

Liebe **Oma Renate** und lieber **Opa Hans-Georg**, liebe **Oma Monika** und lieber **Opa Walter**, ich staune immer wieder was ihr alles erlebt habt/erleben musstet. Und was für einen Lebenslauf ihr bereits hattet! Opa Hans-Georg, Opa Walther, ich vermisse euch. Ich bin sehr froh liebevolle Großeltern zu haben, bei denen ich mich geborgen fühle.

Das gibt mir viel Energie und Zuversicht, dass ich als eure Enkelin auch Dinge anpacken und Herausforderungen schaffen kann!

Danke an meine erweiterte Familie **Anka**, **Donald** und **Daniel** für unser Familienleben!

Dank jullie wel, **Lidy**, **Jaap** en **Thomas** voor jullie steun en voor jullie warm welkom in jouw familie. Bedankt voor de mooie weekendje weg. Hopelijk gaan we dit verder doen omdat ik de tijd om jullie beter kenen te leren en samen avonturen hebben te kunnen zo leuk vind!

Joppe, I am especially grateful to you! You are an incredible and thoughtful support. Thank you for encouraging me, thank you for comforting me, and thank you for looking out for me. I adore your calm and your patience. I am truly looking forward to our future together.

Your,
Johanna